Disturbance legacies and post-disturbance trajectories of belowground carbon dynamics in peatland

Keunbae KIM

Promotor:
prof.dr. Karen Vancampenhout, KU Leuven

Co-Promotor:
prof.dr. Boris Jansen, University of Amsterdam
prof.dr. María J. I. Briones, University of Vigo
prof.dr. Willem-Jan Emsens, University of Antwerp

Members of the examination committee:
prof.dr. Karel Kellens (chair), KU Leuven
prof.dr. Ellen Desie, KU Leuven
prof.dr. Gert Verstraeten, KU Leuven
dr. Bas Van der Veken, Regionaal Lanschap Kleine en Grote Nete
prof.em.dr. Rudy van Diggelen, University of Antwerp
prof.dr. Ben Aernouts, KU Leuven

Dissertation presented
in partial fulfilment of
the requirement of the
degree of Doctor
of Engineering Technology
(PhD)

May 2026

Doctoraatsproefschrift aan de Faculteit Industriële Ingenieurswetenschappen van de KU Leuven.

© 2026 KU Leuven, Sicence, Engineering & Technology

Uitgegeven in eigen beheer, KEUNBAE KIM, Leuven, Belgium

Alle rechten voorbehouden. Niets uit deze uitgave mag worden vermenigvuldigd en/of openbaar gemaakt worden door middel van druk, fotokopie, microfilm, elektronisch of op welke andere wijze ook zonder voorafgaandelijke schriftelijke toestemming van de uitgever.

All rights reserved. No part.of the publication may be reproduced in any form by print, photoprint, microfilm, electronic or any other means without written permission from the publisher.

Acknowledgements

I would like to express my sincere gratitude to my main promoter, *Karen Vancampenhout*, for opening the door to the fascinating field of peatland carbon dynamics. Your guidance allowed me to broaden my research perspective and develop a wide range of scientific interests. You created an environment in which I could grow independently, encouraging a proactive attitude and a strong problem-solving mindset. Although this journey was challenging, it was an immensely rewarding and formative experience in my life. I am truly grateful to have undertaken this path under your supervision. Beyond research, I deeply appreciate the many interdisciplinary skills I have learnt from you: how to collaborate across diver backgrounds, how to consistently reflect on feedback to scientific thinking and writing, and how to approach research with creativity and broader perspective. Your way of communicating science−through engaging storytelling and strong public speaking−has been especially inspiring. Your openness, patience, and humanity have shaped not only my development as a researcher but also as a person. Without your support, I would not have discovered the direction in which I wish to grow in my future career and life.

I also warmly thank my co-supervisors, *Boris Jansen, María J. I. Briones, and Willem-Jan Emsens*, for your continuous support and guidance throughout my PhD journey. Your feedback and discussions were invaluable from beginning to close end. *Boris*, I am deeply grateful for introducing me to molecular world and for hosting me at University of Amsterdam. Your expertise, sharp insights and occasional with wits−especially in responding to reviewers−have greatly strengthen my confident in my work and made my work delightful. *María*, I sincerely appreciate your thoughtful guidance and introducing me to soil ecology as a way of understanding ecosystem functioning. Your perspective has enriched my research in meaningful way. *Willem-Jan*, I would like to express my appreciation for your critical feedback. Over time, I came to recognize the care and dedication behind your comments. Your advice has been instrumental in helping me navigate interdisciplinary research and strengthen my scientific reasoning.

I would also like to thank my former co-promoter, *Judith Schellekens*. Although we could not collaborate throughout the entire my PhD journey. I greatly value your expertise in molecular work, your detailed interpretation, and your thoughtful advice. I feel grateful for your kind words and for the opportunity to learn from you.

My sincere thanks also go to my assessors, *Ben Aernouts*, *Ellen Desie,* and *Gert Verstraeten*, for your critical insights and constructive feedback. Your ability to refine research questions and provide practical guidance has been invaluable. While your comments often challenged me, they eventually led to stronger results and a deeper understanding of my work. I truly appreciate your time, your thoughtful engagement, and your willingness to listen when I need guidance. I also extend my gratitude to my external committee *Rudy van Diggelen*, your valuable advice on data interpretation and for generously sharing your expertise.

I would like to express my appreciation to *Bas Van der Veken* and *Toon Deswert* for the opportunities to participate in field excursions in such beautiful and fascinating natural environments. Your dedication to protecting nature and your deep care for the reserves were truly inspiring. I hope to carry forward these values in my future work. I also warmly thank *Maarten Goosens, Pieter Dierckx,* and *Ward Royens* for hosting and supporting fieldwork and experimental setup, and for generously sharing extensive field knowledge.

To all colleagues in Team FNL and Campus Geel, I am grateful for the opportunity to work in such a dynamics environment. Although being part of two groups was sometimes challenging, it eventually provided a unique and enriching experience. I have learned a great deal from your diverse expertise, and I will always cherish the small conversations and shared laughter during coffee breaks and lunchtime. To my colleagues in EDAPHOS and my office mates in 03.222, thank you for creating a warm and supportive environment. You made everyday work more enjoyable and gave me a strong sense of belonging.

Now, I would like to express my deepest gratitude to my beloved family, my mom, my dad, and my brother. Your unwavering support from afar, your encouragement, and your constant presence in my life have been essential throughout this journey. Your happiness is my happiness, I hope we will continue to share many joyful moments together.

Finally, I would like to give my heartfelt thanks to my beloved partner, *Hye-In Yang*. You have enriched my life in countless ways and have been a constant source of strength and motivation. You inspire me to grow and become a better person. I am confident that we will continue to grow together and face whatever comes next with laughter and love. Thank you for always being by my side!

This research was supported by the Research Foundation Flanders (FWO) under grant agreement no. FWO-G060721N.



Table of Content

Acknowledgements i

Table of Content iv

Summary viii

Samenvatting xi

List of Figures xiv

List of Tables xviii

1. Introduction 1

1.1. Peatlands and their role in soil carbon 2

1.2. Peatland degradation and disturbance from drainage, climate change, and fire 3

1.3. Soil carbon stability in peatlands 6

1.4. Threats of non-linear belowground responses to disturbance 9

1.5. Peatland restoration and recovery of belowground C stability and storage from disturbance 12

1.6. Importance of legacy effect on belowground soil organic matter and C stability 14

1.7. Research objectives & thesis outline 14

2. Limited recovery of soil organic matter composition in fen peatlands after rewetting ... 17

Abstract 18

2.1. Introduction 20

2.2. Materials and Methods 22

2.2.1. Site description 22

2.2.2. Soil sampling and bulk analysis 24

2.2.3. Pyrolysis-gas chromatography/mass spectrometry (Py-GC/MS) 25

2.2.4. Statistical analyses 27

2.3. Results 28

2.3.1 Changes in bulk density, carbon and nitrogen contents and isotopic ratio across hydrological status 28

2.3.2 Changes in SOM molecular composition across hydrological status 30

2.3.3 Changes in individual pyrolysis product across hydrological status 36

2.3.5. Correlation between peat molecular composition vs. physicochemical properties and estimated year since rewetting 38

2.4. Discussion 40

2.4.1 Fens have a distinct molecular composition, reflecting ecosystem characteristics 40
2.4.2. Drainage effects on belowground processes differ along the peat profile in fens 41
2.4.3. Rewetting can only partly restore fen below-ground processes over time, and restoration trajectories differ among sites 44
2.5. Conclusion 46
Acknowledgements 47
3. Mid-infrared spectroscopy as a tool to monitor molecular changes in fens upon restoration 48
Abstract 49
3.1. Introduction 51
3.2. Materials and methods 55
3.2.1 Site description and peat sampling 55
3.2.2. Pyrolysis-gas chromatography/mass spectroscopy (py-GC/MS) 55
3.2.3. Basal respiration CO_2 and SOC decomposability 56
3.2.4. Mid-infrared spectroscopy 57
3.2.5. Statistical analyses and modelling 58
3.3. Results 61
3.3.1. Raw spectra of mid-infrared spectroscopy 61
3.3.2. Pyrolysis GC-MS derived molecular composition prediction using MIR spectroscopy 66
3.3.3. Peat SOC degradability prediction using MIR spectroscopy 69
3.3.4. Spectral differences across restoration status 73
3.4. Discussion 78
3.4.1. Model performance for predicting molecular composition and stability 78
3.4.2 MIR spectroscopy as a tool to evaluate restoration success in fens 79
3.5. Conclusions 81
Acknowledgements 82
4. Peat collapse as a new threat to fen ecological stability: the case of Nature reserve De Zegge, Belgium 83
Abstract 84
4.1. Introduction 86
4.2. Materials and Methods 90
4.2.1 Field study 90

4.2.2. Mesocosm study 96
4.2.3 Statistical analyses 99
4.3. Results 101
4.3.1 Elevation, C stock, and functional domains in response to peat collapse obtained from field data 101
4.3.2 GHG measurement and their stability metrics from mesocosm experiments 106
4.3.3 Chemical properties from the mesocosm experiment 109
4.3.4 Direct and indirect effects of drainage and solution addition treatments on GHG fluxes 110
4.4. Discussion 112
4.4.1 Fen peat collapse causes persistent, multi-dimensional changes in ecosystem structure and functions 112
4.4.2. Potential mechanisms contributing to fen peat collapse at De Zegge 114
4.4.3. Early warning signals 119
4.5. Conclusions 120
Acknowledgements 122
5. No legacy effect of wildfire on peat carbon stability in a Belgian peatland 123
Abstract 124
5.1. Introduction 126
5.2. Materials and methods 129
5.2.1 Study site and experimental design 129
5.2.2. Data collection 131
2.2.3. Estimated SOM functional groups and SOC decomposability 133
5.2.3. Statistical analyses and modelling approach 134
5.3. Results 135
5.3.1. NDVI and physicochemical properties in intact vs. burnt plots 135
5.3.2 SOM molecular composition and SOC decomposability in intact vs. burnt plots 138
5.4. Discussion 142
5.4.1. Peatland's resilience to low-severity fire and recovery towards the pre-fire state 143
5.4.2. Drought stress does not accelerate peat degradation of fire-disturbed peats 145
5.5. Conclusions 146

Acknowledgements 148
6. Synthesis 149
6.1. Main findings 150
6.1.1. Potential catastrophic effects of disturbances on peat C stability 151
6.1.2. Potential ecosystem alternative states and their distinct basins of attraction 152
6.1.3. Mid infrared spectroscopy as a tool to monitor molecular changes in fens upon restoration 154
6.1.4 The contentious nature of peatland legacy-effects 154
6.2. Limitation of research 156
6.3. Valorization: New insights on peat decomposition processes under disturbance 159
7. References 162
8. Appendix 188
Appendix A 189
Appendix B 203
Appendix C 215
Appendix D 224
Statement on the use of Generative AI 226
List of publications 227

Summary

Peatlands play an important role in global carbon (C) cycling, hydrological regulation, and provision of biodiversity across continents. Yet, these unique ecosystems have been substantially degraded by human activities and are increasingly threatened by climate change. Major disturbances encompass drainage for agriculture, forestry, and peat extraction, as well as climate-driven droughts, floods, and fires. Such disturbances can shift peatlands from long-term C sink to net C sources, thereby amplifying climate change. With growing recognition of their ecological and societal value, extensive restoration and management initiatives have been implemented to rehabilitate degraded peatlands and restore their ecological functions. Nevertheless, how disturbances with ongoing climate stressors alter peatland stability and the extent to which different degradation levels constrain or prolong recovery trajectories remain insufficiently understood. Therefore, assessing disturbance effects and post-disturbance dynamics under interacting climate stressors is essential for understanding peatland resilience.

Belowground soil organic matter (SOM) composition is central to uncovering the mechanisms underlying C storage and stability, as it reflects decomposition processes, plant-microbial interactions, and vegetation inputs. Despite its fundamental role, the molecular-level dynamics of SOM in response to disturbance, and during restoration or natural recovery, have not yet been comprehensively explored. This dissertation aims to enhance our understanding of how disturbances and post-disturbance trajectories influence C dynamics and stability through changes in belowground SOM at molecular level, considering their legacy effects across degradation gradients. This dissertation is structured into two main sections. The first section comprises three empirical studies investigating how belowground processes respond to hydrological changes from drainage to rewetting in fens, how belowground processes respond to fire, and the non-linear peat collapse dynamics. The second section focuses on developing time- and cost-efficient tools to facilitate peatland degradation monitoring, which were subsequently applied within empirical studies as analytical approaches.

After the General Introduction (Chapter 1), Chapter 2 explores the hydrological responses to drainage and rewetting by examining molecular-level changes in European fen peat under contrasting hydrological conditions. Rewetting partially reversed drainage-induced degradation, with some fens −particularly those rewetted for longer periods− exhibiting shifts toward undrained conditions. However, significant differences remained between rewetted and undrained fens. These findings suggest that although rewetting can lead to partial recovery of carbon dynamics over time, the legacy of drainage persists in the belowground system for at least several decades.

In Chapter 3, we developed a mid-infrared (MIR) spectroscopy-based predictive model to reproduce molecular information obtained from pyrolysis-gas chromatography/mass spectroscopy (Py-GC/MS). This approach enables efficient and scalable assessment of peat SOM composition and carbon stability. MIR spectroscopy therefore represents a cost- and time-efficient tool for supporting data-driven peatland monitoring and restoration strategies.

In Chapter 4, we investigated the non-linear peat collapse dynamics, focusing on the mechanisms that drive tipping behavior and strategies to prevent further spatial propagation. Collapsed fen peatlands exhibited substantial surface subsidence and carbon losses, alongside structural and functional shifts across mesofaunal, vegetation, physiochemical and molecular characteristics. In a mesocosm experiment, hydrological perturbation reduced peat stability, particularly in regulating greenhouse gases fluxes. Sulfate (SO_4^{2-}) emerged as a key stressor, exerting system-wide pressure on stability, with high spatial variability. Collectively, this chapter offers new insights into long-term pedological shifts affecting peat integrity and function in fen ecosystems.

In Chapter 5, we examined fire disturbance and post-fire recovery trajectories by assessing how fire alters SOM molecular composition and evaluating whether the system returns to its pre-disturbance state. Three years after the fire, belowground fire effects were no longer

detectable, and fire-disturbed peat did not exhibit differential responses to an additional drought stressor. This case study further indicates the absence of persistent fire legacy effects on soil molecular composition and carbon stability.

In summary, this dissertation shows how disturbance and subsequent restoration or recovery trajectories shape carbon stability in peatlands. Prolonged or severe disturbances can trigger cascading and potentially irreversible changes, delaying or preventing return to pre-disturbance state. These findings underscore the urgency of preserving peatlands and implementing continuous monitoring surveys to mitigate further peatland degradation and associated climate impacts.

Samenvatting

Veengebieden spelen een belangrijke rol in de wereldwijde koolstofcyclus (C), de hydrologische regulatie en het behoud van biodiversiteit op verschillende continenten. Toch zijn deze unieke ecosystemen in sterke mate aangetast door menselijke activiteiten en worden zij in toenemende mate bedreigd door klimaatverandering. Belangrijke verstoringen omvatten ontwatering voor landbouw, bosbouw en veenwinning, evenals klimaatgedreven droogtes, overstromingen en branden. Dergelijke verstoringen kunnen veengebieden doen verschuiven van een langdurige koolstofsink naar een netto koolstofbron, waardoor klimaatverandering verder wordt versterkt. Met de groeiende erkenning van hun ecologische en maatschappelijke waarde zijn er omvangrijke herstel- en beheerinitiatieven opgezet om aangetaste veengebieden te rehabiliteren en hun ecologische functies te herstellen. Desondanks blijft het onvoldoende begrepen hoe verstoringen, in combinatie met aanhoudende klimaatstressoren, de stabiliteit van veengebieden beïnvloeden en in hoeverre verschillende niveaus van degradatie hersteltrajecten beperken of vertragen. Daarom is het essentieel om de effecten van verstoringen en de dynamiek na verstoring onder interacterende klimaatstressoren te onderzoeken om de veerkracht van veengebieden beter te begrijpen.

De samenstelling van organische stof in de bodem (SOM) in de ondergrond is cruciaal om de mechanismen achter koolstofopslag en -stabiliteit te ontrafelen, aangezien deze de afbraakprocessen, plant-microbe-interacties en vegetatie-inputs weerspiegelt. Ondanks deze fundamentele rol zijn de moleculaire dynamieken van SOM als reactie op verstoring, en tijdens herstel of natuurlijke regeneratie, nog niet uitgebreid onderzocht. Dit proefschrift heeft als doel ons begrip te vergroten van hoe verstoringen en post-verstoringstrajecten de koolstofdynamiek en -stabiliteit beïnvloeden via veranderingen in SOM in de ondergrond op moleculair niveau, rekening houdend met hun nalatigheidseffecten langs degradatiegradiënten. Dit proefschrift is opgebouwd uit twee hoofdonderdelen. Het eerste deel omvat drie empirische studies die onderzoeken hoe processen in de ondergrond reageren op hydrologische veranderingen van

ontwatering tot hervernatting in venen, hoe zij reageren op brand, en de niet-lineaire dynamiek van veeninklinking. Het tweede deel richt zich op de ontwikkeling van tijd- en kostenefficiënte instrumenten om de monitoring van veendegradatie te faciliteren, die vervolgens in empirische studies als analytische benaderingen zijn toegepast.

Na de algemene introductie (hoofdstuk 1) onderzoekt hoofdstuk 2 de hydrologische respons op ontwatering en hervernatting door moleculaire veranderingen in Europees venveen onder contrasterende hydrologische omstandigheden te analyseren. Hernatten keerde de door ontwatering veroorzaakte degradatie gedeeltelijk om, waarbij sommige venen—met name die langer hervernat waren—verschuivingen vertoonden richting niet-ontwaterde omstandigheden. Er bleven echter significante verschillen bestaan tussen hervernatte en niet-ontwaterde venen. Deze bevindingen suggereren dat, hoewel hervernatting op termijn kan leiden tot gedeeltelijk herstel van koolstofdynamiek, de nalatenschap van ontwatering in het ondergrondse systeem minstens meerdere decennia aanwezig blijft.

In hoofdstuk 3 ontwikkelden we een voorspellend model op basis van midden-infraroodspectroscopie (MIR) om moleculaire informatie, verkregen via pyrolyse-gaschromatografie/massaspectrometrie (Py-GC/MS), te reproduceren. Deze benadering maakt een efficiënte en schaalbare beoordeling van de samenstelling van SOM en koolstofstabiliteit in veen mogelijk. MIR-spectroscopie vormt daarmee een tijd- en kostenefficiënt hulpmiddel ter ondersteuning van datagestuurde monitoring en herstelstrategieën voor veengebieden.

In hoofdstuk 4 onderzochten we de niet-lineaire dynamiek van veeninklinking, met focus op de mechanismen die omslaggedrag (tipping behavior) aandrijven en strategieën om verdere ruimtelijke verspreiding te voorkomen. Ingeklonken venveengebieden vertoonden aanzienlijke maaivelddaling en koolstofverliezen, evenals structurele en functionele veranderingen in mesofauna, vegetatie, fysisch-chemische en moleculaire kenmerken. In een mesocosm-experiment verminderde hydrologische verstoring de stabiliteit van veen, met name in

de regulatie van broeikasgasfluxen. Sulfaat (SO_4^{2-}) kwam naar voren als een belangrijke stressfactor die systeemwijd druk uitoefent op de stabiliteit, met een hoge ruimtelijke variabiliteit. Gezamenlijk biedt dit hoofdstuk nieuwe inzichten in langetermijn pedologische veranderingen die de integriteit en functie van veen in venecosystemen beïnvloeden.

In hoofdstuk 5 onderzochten we brandverstoring en post-brand hersteltrajecten door te analyseren hoe brand de moleculaire samenstelling van SOM verandert en of het systeem terugkeert naar de toestand van vóór de verstoring. Drie jaar na de brand waren de effecten in de ondergrond niet langer detecteerbaar en vertoonde brandverstoord veen geen afwijkende respons op een extra droogtestressor. Deze casestudy wijst erop dat er geen blijvende nalatenschapseffecten van brand zijn op de moleculaire samenstelling van de bodem en de koolstofstabiliteit.

Samenvattend toont dit proefschrift aan hoe verstoringen en daaropvolgende herstel- of regeneratietrajecten de koolstofstabiliteit in veengebieden vormgeven. Langdurige of ernstige verstoringen kunnen cascade-effecten en mogelijk onomkeerbare veranderingen veroorzaken, waardoor terugkeer naar de oorspronkelijke toestand wordt vertraagd of verhinderd. Deze bevindingen onderstrepen de urgentie van het behoud van veengebieden en het implementeren van continue monitoring om verdere degradatie en de daarmee samenhangende klimaateffecten te beperken.

List of Figures

Fig. 1.1. Outline of the structure of this Ph.D. thesis. Chapters 2 and 3 focus on developing a general understanding of peat molecular composition at the European scale. The broader perspective is then used as a foundation to investigate context-dependent responses at the local scales. Chapter 4 investigates the characteristics and potential drivers of peat collapse whereas Chapter 5 examines the effects of fire disturbance and peatland natural recovery at ecosystem level. 15

Fig. 2.1. Top: 13 study fen regions across Europe, overlaid on a biogeographic and peatland map. Bottom: Study and sampling design. A total of 39 fen sites (13 fen regions × 3 types of drainage status) were sampled in three different peat layers (Map data ©OSM). 24

Fig. 2.2. Average composition of peat molecular functional group (pyrolysis products) from 13 study fen regions, analyzed across three drainage status (undrained, drained, and rewetted) and three peat layers (0−5 cm, 15−20 cm, and 45−50 cm).....31

Fig. 2.3. Nonmetric multidimensional scaling (NMDS, stress = 0.112) showing sample coordinates based on the Bray-Curtis dissimilarity of soil organic matter (SOM) molecular compositions across three drainage stages (undrained, drained, and rewetted) and three different depths (0−5 cm, 15−20 cm, and 45−50 cm). The ordination includes samples from undrained, drained, and rewetted fens at three depths. To illustrate sequential changes in SOM molecular composition due to drainage and rewetting, each panel is colored by depth for a specific drainage stage: undrained (A), drained (B), and rewetted (C). 33

Fig. 2.4. Nonmetric multidimensional scaling (NMDS, stress = 0.112) showing vector fitting analysis of soil organic matter (SOM) molecular composition and enviromental variables based on the ordination in Fig. 3. Compound vectors represent correlations between individual compound abundances and the NMDS axes. Blue arrows indicate fitted enviromental vectors, illustrating the direction and strength with the ordination space. These vectors reflect how compounds and environmental variable are associated with the NMDS axes. 34

Fig. 2.5. Volcano plots of pyrolysates (i.e., molecular composition) as per differential abundance test: (A) undrained vs. drained; (B) undrained vs. rewetted; (C) drained vs. rewetted. The volcano plot depicts log2 fold change on x-axis and statistical significance on the y-axis. Pyrolysis products are coloured red when false discovery rate (i.e., adjusted *P*-value) is less than 0.05. The codes for pyrolysates are given in Supplementary Table 2.2. ..37

Fig. 2.6. Pearson correlations between changes in peat physicochemical properties and dissimilarity (between undrained to drained fens; red & triangle), and dissimilarity (between undrained to rewetted fens; green & circle). Bray−Curtis dissimilarity were computed from molecular composition obtained by pyrolysis-GC/MS.Pearson's correlation coefficients (R) and significance (P) are given in each plot. 39

Fig. 2.7. Time since rewetting vs. dissimilarity in peat molecular composition between undrained and rewetted at 15−20 cm depth, along with dissimilarity values within undrained fens. The left panel shows the Bray−Curtis dissimilarity between undrained and rewetted fens as function of time since rewetting. The blue line represents the fitted linear relationship, with the shaded grey area indicating the 95% confidence interval. The right panel presents a box plot of dissimilarity values within undrained fens, serving as a reference to estimate the timeframe at which rewetted fens begin to resemble undrained fens in terms of peat molecular composition recovery. 40

Fig. 3.1. Mid-infrared spectra of peat samples collected at three different depths from 13 regions under three restoration status. Spectra were pre-processed using Savitzky−Golay smoothing followed by standard normal variate transformation (n = 117).....64
Fig. 3.2. Performance and coefficients of partial least square regression (PLSR) model for SOC decomposability. (A): Measured versus PLSR-predicted cumulative fluxes (i.e., SOC decomposability) at day 105 based on group-wise cross-validation (CV) predictions. Black dots represent individual samples, and the black line shows regression fit. Model performance metrics include n (number of samples), n_latent (number of PLS latent variables), Rsq (coefficient of determination), RMSE (root mean squared error), and MAE (mean absolute error). (B): Regression coefficients obtained for the PLSR model based on mid-infrared spectroscopy for SOC decomposability.....70
Fig. 3.3. Cumulative basal respiration per SOC (i.e., SOC decomposability) across restoration status (undrained, drained and rewetted) measured at two peat layers of 0−5 cm and 45−50 cm, with predicted values for the second peat layer of 15−20 cm.....72
Fig. 3.4. Nonmetric multidimensional scaling (NMDS, stress = 0.089, 0.060, and 0.067, respectively) score plots of peat molecular composition based on the Euclidean distance at three drainage stages (undrained, drained, and rewetted) at three different depths (A: 0−5 cm; B: 15−20 cm; and C: 45−50 cm), in 13 fens across Europe. 95 % confidence ellipses are shown for each group. PERMANOVA indicates significant difference across restoration status for the first tow depths (0−5 cm: R^2 = 0.139, F =2.913, P = 0.024; 15−20 cm: R^2 = 0.134, F = 2.773, P = 0.017), but not for the deepest layer (45−50 cm: R^2 = 0.008, F = 0.153, P = 0.971; 999 permutation). 74
Fig. 3.5. Coefficients of the partial least squares discriminate analysis (PLS-DA) model based on three depth specific models (0−5 cm, 15−20 cm, and 45−50 cm) from mid-infrared spectra. 77

Fig. 4.1. Study region with visible signs of what is referred to in this study as to peat collapse. (A) Aerial photograph of study region within the nature conservation area “De Zegge” (province of Antwerp). Based on distinctive changes in vegetation community composition and surface elevation, three and four collapsed plots were established in site 1 (panel B) and site 2 (panel C), respectively. Non-collapsed adjacent (NCA) plots (controls) were established at four points in close proximity to each collapsed (C) plot. Sites 3−7 served as distant non-collapsed plots. Photo credits: K. Kim, T. Deswert91
Fig. 4.2. Mesocosm experimental setup for greenhouse gas (GHGs) flux measurements and peat porewater sampling. (A) Configuration of peat cores in a water bath, with water table manipulation achieved through punctured holes on the lateral sides of the PVC cores, allowing equilibration between bath water and peat core water levels. (B) GHGs fluxes (CO_2 CH_4 and N_2O) were measured using LICOR-7810 and -7820 gas analyzers, connected to a smart chamber placed over individual peat cores. 97
Fig. 4.3. Orthophotos (A,C) and elevation difference maps (B,D) illustrating changes between 2015 and 2025 at two sites affected by peat collapse. Elevation differences were derived from light detection and ranging (Li−DAR) data and indicate surface subsidence or accumulation over the 10-year period. The scale bars represent distance in meters (m). 102
Fig. 4.4. Non-metric Multidimensional Scaling (NMDS) ordination plot depicting the variation in (A) mesofauna community composition, (B) vegetation community composition, (C) physiochemical properties, and (D) soil organic matter molecular composition at the three treatments: collapsed, non-collapsed adjacent, and non-collapsed distant plots. Permutational multivariate analysis of variance (PERMANOVA) with its respective R^2, F, and P value provide in the figures. Dissimilarity is measured as Bray-Curtis distance for (A), (B), and Euclidean distance for (C), (D). In panels (A), and (C), blue-labeled

text indicates variable loadings on the ordination. The number of sample size in mesofauna is double as measured twice in a year. 104
Fig. 4.5. Relative responses of solution addition treatments (control, ditch, and SO_4^{2-} addition) to hydrological pulse perturbation over time on CO_2, CH_4 and N_2O fluxes. Dense dots represent mean log response ratio (n=4), faint dots represent individual data points, and error bars show standard error of the means. Lager dense dots denote statistically significant effects of the perturbation (P <0.05), based on one-way ANOVA for fluxes responses. 108
Fig. 4.6. Structural equation model illustrating the effects of key environmental drivers on greenhouse gas emissions (CO_2, CH_4, and N_2O) under (A) drawdown and (B) re-saturation phases. Arrows represent hypothesized causal relationships; only significant pathways are shown with values indicating standardized path coefficients. 111
Fig. 4.7. Conceptual representation of the impact of chronic and acute stressors on peat stability. Left: key redox reactions influenced by the presence of pyrite and by inputs of labile carbon and nitrogen via ditch water. Right: the interaction between chronic and acute stressors can trigger peat collapse, representing a state from which no reversed pathway is possible.....118

Fig. 5.1. Study site, twin-plot design and fire effects on vegetation cover index (NDVI): (A) Map of Landschap De Liereman nature reserve showing twin-plot established along the fire scar, based on difference in NDVI values between pre- and post-fire periods (two-week difference). The twin plots correspond to areas of burn severity. (B) Landscape photograph of the study site. (C) mean NDVI values at each sampling plot from 2017 to 2024, highlighting a significant difference between intact and burnt plots observed in 2020 (P <0.01, **).....130
Fig. 5.2. Elemental analysis results between intact and burnt plots over four consecutive years. Red asterisks (*) denotes statistically significant difference at $\alpha < 0.05$. 136
Fig. 5.3. Molecular composition changes between intact and burnt peat. (A) Coefficients from partial least squares discriminate analysis (PLS−DA) models highlighting molecular vibration differences between treatments. The PLS−DA model was developed using the 2020 dataset to maximize variance in mid-infrared spectral data between intact and burnt plots, reflecting pronounced fire-induced compositional changes. Positive coefficients indicate higher abundance of molecular vibrations in intact peat, whereas negative coefficients indicate higher abundance in burnt peat. (B) Estimates of functional groups of soil organic matter (SOM) molecular composition derived from mid-infrared spectroscopy, compared between intact and burnt plots across four consecutive years. Red asterisks (*) denote statistically significant differences (*, $P < 0.05$; **, $P < 0.01$; ***, $P < 0.001$).....139
Fig. 5.4. Measured cumulative and daily fluxes of basal respiration (A, B) and estimated cumulative flux via MIRs (C) between intact and burnt plots. No significant differences in measured cumulative CO_2 fluxes were observed between intact and burnt plots in 2021 and 2023 ($Ps > 0.05$). The estimated cumulative flux was significantly different between treatments only in 2020 (P <0.05).....141
Fig. 5.5. Pearson correlation coefficients (r) for the relationship between changes in environmental variables between intact and burnt plots. The color gradient represents the correlation strength and direction (from blue to red; $-1 \leq r \leq 1$). Statistical significance is indicated by asterisks: *** P <0.001, ** P <0.01, * P <0.05. Meas means measured, and Est refers to estimated. 142

Fig. 6.1.External conditions affect the resilience of multi-stable ecosystem to perturbation. The bottom plane shows the equilibrium curve. The stability landscapes depict the equilibria

and their basins of attraction at five different conditions. Stable equilibria correspond to valley; the unstable middle section of olde equilibrium curve corresponds to a hill. If the size of the attraction basin is small, resilience is small and even a moderate perturbation may bring the system into the alternative basin of attraction (Scheffer et al., 2001).153

List of Tables

Table 2.1. Bulk density, total organic carbon and nitrogen, C/N ratios and isotopic composition across the drainage status and depth.....29
Table 2.2. Permutational multivariate analysis of variance (PERMANOVA) of peat molecular composition across drainage status and depths, as well as pairwise comparisons..35

Table 3.1. Conventional absorption band assignment of mid-infrared spectroscopy to functional groups or soil component based on the literature. ν indicates stretching vibration, while δ denotes bending vibration (adapted from Peltre et al., (2014); reproduction permitted as documented in supplementary material). 65
Table 3.2. Root mean squared error (RMSE), R squared (R^2) and mean absolute error (MAE) results for proportion of chemical group in peat, as determined by partial least squares regression models for calibration (C), cross-validation (CV), and validation dataset (P). 68

Table 4.1. Least squares means of mesofauna, vegetation community composition, and physiochemistry across collapsed (n= 7), adjacent non-collapsed (n= 7), and distant non-collapsed plots (n= 5) in study area.....105
Table 4. 2. Least squares means under different solution addition treatments (control, ditchwater, and SO_4^{2-} addition) and water drawdown condition (no drainage, drainage) across consecutive four phases (baseline, treatment-loading, drawdown, and re-saturation) and in total 107

Table 5.1. Elementary analysis of intact and burnt peat samples.....137

1

Introduction

1.1. Peatlands and their role in soil carbon

Intact peatlands provide a wide range of ecosystem functions, including carbon (C) storage, support of biodiversity for both fauna and flora, regulation and maintenance of the hydrological cycle, and cultural and recreational benefits that contribute to human well-being (Yu et al., 2010; Leifeld and Menichetti, 2018). Peatlands cover about 3 % of the global land surface, yet they store a disproportionately large amount of terrestrial carbon in their soil profile (Joosten et al., 2017; Loisel et al., 2017; Xu et al., 2018). Globally, peatlands are estimated to contain about 612 Gt C, of which approximately 562 Gt C is stored in northern boreal and temperate peatlands and around 50 Gt C in tropical peatlands. Together, these C stocks account for roughly 25 % of global soil C, highlighting peatlands as critical components of the global C cycle.

Peatland soils are allocated to the Histosol reference soil group in WRB (https://wrb.isric.org). They are defined as consisting of organic materials, typically with ≥ 30% organic carbon soil content, accumulated to a sufficient thickness of ≥ 30 cm peat layer (Leifeld et al., 2012; Klingenfuß et al., 2014). These soils contain diagnostic histic or folic horizons, depending on the duration that the soil is saturated with water (Turetsky et al., 2011; Upton et al., 2018). Their morphologies can be further described as fibric, hemic and sapric, depending on the degree of decomposition of the organic materials, approximated by their color, amount of recognizable plant materials, bulk density and chemical and physical properties (Bauriegel et al., 2024). Peatlands are commonly classified into rainwater-fed peatlands (ombrotrophic bogs) and groundwater-fed peatlands (minerotrophic fens; Apori et al., 2022). Compared with bogs, fens typically exhibit distinct vegetation composition, including low abundance or absence of *Sphagnum* spp. and higher abundance of brown mosses and vascular plants (Joosten et al., 2017). In bogs and blanket peats, the Histosol profile is sometimes subdivided in an upper, living and aerobic layer (acrotelm) and a lower water-logged and compacted layer (catotelm; Ingram, 1978) but this distinction is not made in fen ecosystems (Emsens et al., 2020).

Carbon sequestration in peatland soils begins with peat accumulation (Rydin and Jeglum, 2006). Peat accumulation occurs when inputs of plant litter input exceed rates of organic matter decomposition (Ribeiro et al., 2021; Gaffney et al., 2024). This imbalance primarily results from the distinct hydrological conditions as well as from the biochemical characteristics of peat-forming vegetation (Rupp et al., 2019; Drollinger et al., 2020). Persistent waterlogged and anaerobic conditions limit oxygen availability and are often associated with relatively cool local temperature, thereby constraining microbial activity and slowing aerobic microbial decomposition processes (Gorham, 1991; Olefeldt et al., 2013; Dieleman et al., 2015). Concurrently, peat-forming plants produce and release structural plant polymers or components with a low nominal oxidation state, including cross-linked phenolic structures (e.g., lignin) and pectin-like polysaccharides (e.g., sphagnan), which further inhibit microbial decomposition (Boye et al., 2017; Barel et al., 2021). These hydrological and biochemical characteristics reinforce a positive feedback loop (i.e., amplified process) in which saturated, cold conditions promote the accumulation of recalcitrant plant materials, which in turn enhances peat formation and sustains the environmental conditions necessary for long-tern carbon storage over decadal to millennial timescales (Cao et al., 2022). Consequently, intact peatlands play a crucial role in global carbon dynamics and climate change mitigation by exerting a net cooling effect on global climate system (Moomaw et al., 2018; Korn et al., 2024).

1.2. Peatland degradation and disturbance from drainage, climate change, and fire

The unique peatland ecosystems have historically been overlooked and extensively degraded by anthropogenic disturbances such as drainage, land use change, and peat extraction for agriculture, forestry, and infrastructure development. More recently, climate change and climate-induced wildfire have further intensified peatland degradation (Peltoniemi et al., 2012; Xue et al., 2025). Such unprecedented environmental changes have become a global concern, because they alter fundamental biogeochemical processes and may further lead to detrimental

effects on peatland functioning and services provision (Salimi et al., 2021; Briones et al., 2022; Mursyid et al., 2025).

Drainage is one of the primary drivers of peatland degradation (Knox et al., 2015). Since the medieval period−and increasingly during and after the Industrial Revolution−peatlands have been intensively drained for agriculture, forestry, and energy production (IPCC, 2018). Globally, an estimated 10−15 % of the current peatlands (500,000 km^2) worldwide have been drained, with the majority of drainage occurring in Europe (Greifswald Mire Centre, 2015). Consequently, approximately 46 % of the European peatlands are now degraded to the extent that active peat formation has halted (Swenson et al., 2019). Drainage enhances soil aeration and hence, oxygen availability, accelerating organic matter decomposition and increasing CO_2 emissions, which are estimated at about 2 Gt of CO_2eq annually (Leifeld and Menichetti, 2018; Kitson and Bell, 2020). By disrupting the ecohydrological feedback that sustains peat accumulation (see also 1.4), drainage can shift peatlands from long-term C sinks to net sources of greenhouse gases (GHGs) emissions, thereby reinforcing a climate-carbon feedback.

Drainage has been predominantly carried out in fens due to their rapid release of nutrients after drainage, and greater productivity after land conversion in the past (Piayda et al., 2020). Despite being the dominant peatland type in the temperate climatic zone and highly vulnerable to anthropogenic disturbances, fens remain comparatively underrepresented in peatland research and long-term monitoring relative to bogs.

Climate change acts as a major compounding stressor that further disrupts the hydrological stability in peatlands (Olefeldt et al., 2017; Barel et al., 2021; Gaffney et al., 2025). In northern temperate regions, warming temperatures of approximately 0.2 ºC per decade, irregular precipitation patterns, more frequent freeze-thaw cycles, and increased occurrence of extreme events such as droughts and floods are becoming more common (IPCC, 2018). These hydroclimatic regimes, combined with rising temperatures, drive greater water-table fluctuations

and prolonged groundwater drawdowns (Kane et al., 2021). Such disturbances facilitate deeper oxygen penetration and alter the vertical distribution and activity of the microbial communities, thereby promoting oxidative decomposition and releasing substantial amounts of C to the atmosphere (Radu and Duval, 2018; Fenner and Freeman, 2020; Hapsari et al., 2022). Subsequently, climate change disrupts biogeochemical cycling and may ultimately transform essential ecosystem services into ecosystem disservices (Chiang et al., 2021; Salimi et al., 2021; Mander et al., 2024).

Peat fires have also emerged as an increasingly important disturbance factor in peatland ecosystems, since climate change enhances fire frequency and severity and expands the fire-prone landscape (Ackley et al., 2021; Feurdean et al., 2022; Wilkinson et al., 2023). Wildfire can accelerate climate warming through reductions in land-surface albedo, which increases radiative energy absorption, as well as through the combustion of aboveground biomass and peat. This combustion releases large amounts of C into the atmosphere, with peat fires contributing 2 Gt CO_2 loss annually−about 5% of all anthropogenic GHG emissions−while smoldering belowground fires may account for up to 15% of annual GHG emissions (Rein, 2015). The net effect of fire on GHG emissions reinforces climate-carbon feedback and introduces substantial uncertainty in earth-system long-term feedbacks.

Overall, the net effect of major disturbances−drainage, climate change, and fire−on peat C storage and persistence is substantial. Their impacts are further complicated by variability in disturbance intensity and duration, site-specific environmental condition, and legacy effects (Harris et al., 2022). However, our understanding of resulting C dynamics and post-disturbance trajectories towards recovery remains limited. It is therefore essential to investigate how these disturbances alter C dynamics and post-fire recovery pathways to mitigate the impacts of ongoing climate change and anthropogenic disturbances, and to sustain key peatland ecosystem functions and services.

1.3. Soil carbon stability in peatlands

While the aboveground aspects of peatland functioning have been intensely studied (Austin and Cooper, 2016; Kreyling et al., 2021; Guêné-Nanchen et al., 2022), the belowground compartment remains comparatively less understood. More than in many soil environments, the functioning of Histosols is primarily governed by soil C dynamics (Bauriegel et al., 2024). In particular, the capacity of peatland soils to accumulate and stabilize soil C over long timescales underpins their ecosystem functioning and associated services (González de Andrés et al., 2022). Soil organic matter (SOM) dynamics reflect the interplay between plant inputs, edaphic conditions (pH, water table, temperature, and nutrient availability), and decomposer community dynamics (Schellekens et al., 2009; Vancampenhout et al., 2009). Through biological, chemical, and physical interactions, SOM quantity and quality further regulate C sequestration capacity and long-term C stability (Gholizadeh et al., 2013; Jamaluddin et al., 2024). More fundamentally, C stability reflects the balance between persistence, turnover, and vulnerability. These processes are governed by a combination of chemical properties (e.g., molecular composition and recalcitrance), physical protection mechanisms (e.g., occlusion and organo-mineral associations), and environmental conditions (e.g., nutrient limitations or low temperature; Kaiser and Guggenberger, 2003; Kögel-Knabner et al., 2008; Dungait et al., 2012). Understanding C stability and persistence in peatlands under global environmental change is therefore imperative. Traditionally, C stability has often been inferred indirectly, using proxies such as C stocks (accumulation) or C fluxes (mineralization rate under controlled conditions). However, these approaches capture only limited aspects of soil C dynamics.

The prevailing paradigm *sensu* Lehmann and Kleber (2015) conceptualizes soil C stability mainly based on physical protection mechanisms. Accordingly, intrinsic recalcitrance and nutrient limitations are considered to exert only short-term controls, as no SOM component is inherently resistant to microbial decomposition (Schmidt et al., 2011). Instead, SOM persistence depends on the extent to which SOM is protected from microbial access. This protection occurs

mainly through occlusion within soil aggregates, associated with intermediate turnover times, or through association with mineral surfaces, which can confer longer-term stabilization (Schmidt et al., 2011).

Following this paradigm, SOM is often operationally fractionated into distinct pools: particulate organic matter (POM) and particulate organic matter occluded in aggregates (oPOM), which are considered labile with the latter being temporarily stabilized, and mineral-associated organic matter (MAOM) pool, which is regarded as relatively stable (Kögel-Knabner et al., 2008). Within this conceptual framework, the microbial C pump (Liang et al., 2017) has the crucial role in stimulating the formation of MAOM. In contrast, the role of soil fauna remains largely underrepresented, often reduced to their contribution to aggregate formation, particularly by earthworms (Grandy et al., 2016; Briones et al., 2022).

This paradigm is heavily biased towards well-buffered, well-drained, temperate agricultural soils without litter layers (Kögel-Knabner et al., 2008), and a growing body of literature suggests that this physical defined, pool-based framework may be overly simplistic (Lehmann et al., 2020; Kleber et al., 2021; Angst et al., 2023). In Histosols, aggregates and mineral surfaces are largely absent or occur only in a limited extent (Kan et al., 2025), and the majority of organic matter resides in the POM fraction. Nevertheless, turnover times of peatland POM can exceed millennia under persistent waterlogged conditions (Dargie et al., 2017). This highlights the need for an alternate view of the mechanisms regulating C stability in peatlands, where low oxidative conditions constrain decomposition processes.

Freeman et al (2001) proposed an enzymatic ‘latch’ mechanism, whereby the activity of the enzyme phenol oxidase is suppressed under low-oxygen conditions, because the energetic returns are insufficient to justify the production of costly enzymes. Subsequent studies have identified additional compounds that may impede decomposition, including molecules with a low nominal oxidative state or complex carbohydrates (e.g., sphagnan; Bengtsson et al., 2018). Certain

compounds can inhibit microbial activity or extracellular enzymes, and in some cases exert toxic effects (Wang et al., 2017). This suggests a more context-dependent view of recalcitrance, in which decomposition is constrained not only by substrate properties but also by environmental conditions and energetic limitations. Under oxygen-limited conditions, microorganisms may refrain from decomposing certain components when energy yield is low, as they have to rely on less efficient alternative electron acceptors (Ivanova et al., 2016; Bengtsson et al., 2018; Juan-Ovejero et al., 2019).

In addition, an alternative form of "occlusion" has been proposed for peat soils where labile organic components in plant cells are shielded not only by mineral associations, as in the classical oPOM concept, but through encapsulation inside the cell walls composed of lignin and complex polysaccharides that are relatively resistant to microbial attack under anoxic conditions (Hájek et al., 2011; Säurich et al., 2019). According to this theory, peat decomposition upon drainage may become a self-amplifying process: periodic drying progressively weakens these structural barriers (i.e., "coffin" structure), increasing microbial access to previously protected labile substrates.

The role of soil fauna further amplifies these processes. For instance, increased abundance of enchytraeids has been linked to enhanced mineralization of 'old' C pools (Briones et al., 2010), potentially by disrupting physical barriers and increasing substrate accessibility. However, alternative models do not invoke spatial separation between decomposers and substrates and assume preferential consumption of the most labile compounds. In such cases, C losses are highest during initial stages of decomposition and decline over time as more recalcitrant material remains available.

Quantifying C persistence and vulnerability of soil organic carbon (SOC) is therefore much more challenging in peat soils, as conventional pool-based fractionation into POM, oPOM in aggregates and MAOM does not adequately capture the context-dependent mechanisms

governing SOC stability in peatlands. While overall turnover can be assessed using radiocarbon dating (Wang et al., 2026), this technique is less suited for resolving dynamics on annual to decadal timescales, which are most relevant for effective management and restoration (Emsens et al., 2020; Kreyling et al., 2021; Groß-Schmölders et al., 2022). The vulnerability of SOC to environmental perturbation, such as drought, can be evaluated using biological methods, including incubation-based assessments of basal respiration (Säurich et al., 2019) or through field-based assessments of GHG emissions. However, the latter are often characterized by high spatial and temporal variability (Tersago et al., 2025). The overall degree of degradation can be assessed by isotopic approaches (Schellekens et al., 2015b), while more detailed insight into SOM composition and transformation process can be obtained through molecular-level techniques. These include spectroscopic methods, such as Fourier-transformed infrared (FTIR) or mid-infrared spectroscopy (MIR) as well as ^{13}C nuclear magnetic resonance (NMR), which resolve broad functional groups, and more advanced techniques such as pyrolysis-gas chromatography mass-spectroscopy (py-GCMS, Schellekens et al., 2009; Vancampenhout et al., 2009).

These approaches that assess the molecular composition of peat soil also give a mechanistic insight into C dynamics by encompassing information on organic matter sources, degree of decomposition, and potential biochemical pathways (Schellekens et al., 2015b). However, such detailed biogeochemical assessments remain technically demanding and are therefore relatively scarce and to date, they are particularly lacking for fen systems.

1.4. Threats of non-linear belowground responses to disturbance

Growing empirical evidence indicates that structural, compositional, and functional traits of ecosystems can exhibit non-linear responses to disturbance, rather than exhibiting a gradual change (Scheffer et al., 2001; Dakos et al., 2012; Keith et al., 2023). Such abrupt transitions are often attributed to ecological thresholds, especially when key components that exert disproportionate control over ecosystem functioning are lost or replaced under the stressors

(Hagerthey et al., 2008; Jassey et al., 2018; Rupp et al., 2019). Several of these thresholds have been proposed for peatland ecosystems. One of them is a state shift between a moss-dominated state versus a vascular plant dominated state, often associated with a depth-to-water table and bulk density thresholds proposed for bogs, where the tree line can advance when bulk density increases above ca. 0.3 and the depth-to-water-table drops below 7-22 cm (Dragoni et al., 2007; Draga et al., 2025). Trees and larger plants will subsequently outcompete vegetation of mosses and sedges for light, heighten evaporation and stimulate decomposition by root exudates, tipping the system from an open peatland to a swamp forest (Temmink et al., 2026). Increased nutrient loads in fens have also been shown to contribute to a process referred to as 'helophytisation', where smaller plant species (bryophytes, sedges) are replaced by taller plants (Emsens et al., 2020). The WRB soil classification system describes this shift as a transition from a histic to a folic belowground horizon (https://wrb.isric.org).

Similarly, Dieleman et al (2015) proposed that climate change can initiate a transition from bogs to fens, accompanied by the loss of the keystone genus *Sphagnum*, that may shift peatlands towards conditions favorable for organic matter decomposition. The decline of keystone vegetation alters litter quality−from polyphenolic-rich, recalcitrant compounds to more labile C input−and modifies soil chemistry through increased pH and nutrient availability (Dieleman et al., 2015). These changes can drastically stimulate microbial activity and decomposition processes, thereby exacerbating the loss of long-term C sequestration capacity, and amplifying climate-C feedback loops (Belyea and Baird, 2006; Dieleman et al., 2015). Tahvanainen (2011) also describes the reverse trajectory, i.e. ombrotrophication, in boreal mires that switched from minerogenous to an ombrogenous hydrology, within two decades after hydrological disturbances in the catchment. Finally, observational studies have documented abrupt shifts from marshes to mudflats in a very short time span, which highlights the potential for rapid state shifts in peatlands (referred to as peat collapse; Chambers et al., 2019).

Understanding degradation effects on soil processes and C dynamics therefore plays a pivotal role in preventing cascading effects and emergent feedbacks on peatland ecosystem functioning (Milner et al., 2021; Keith et al., 2023; Temmink et al., 2026). Such abrupt transitions between contrasting ecosystems states, e.g. from short to tall vegetation or forest, from bog to fen or from marsh to mudflat −often referred to as regime shifts− reflect the existence of certain boundary conditions, beyond which recovery of the peatland ecosystem can be difficult or irreversible (Scheffer et al., 2001). Regime shift theory underscores the importance of identifying potential threshold situations at landscape level, since this enables the detection of vulnerable systems that require close monitoring to avoid rapid transitions and, ultimately, functional collapse (Folke et al., 2004). To date, this concept has been well established in the context of aboveground vegetation dynamics (Dieleman et al., 2015; Mander et al., 2024). In contrast, its application to belowground processes remains comparatively limited (Desie et al., 2019). While there is a broad consensus that soils are complex systems (Young and Crawford, 2004; Vogel et al., 2018), our understanding of how contemporary stressors −such as drainage, climate change, and fire− regulate C cycle dynamics and potential threshold behavior in in fens is still incomplete (Rupp et al., 2019; Zeh et al., 2020; Apori et al., 2022; Määttä and Malhotra, 2024). Several metrics have been proposed to investigate changes in ecosystem stability in peatlands, yet the existence of alternate (stable) states can be notoriously difficult to prove conclusively (Scheffer et al., 2001; Folke et al., 2004) and many of the metrics are not straightforwardly applicable (Scheffer et al., 2001; Folke et al., 2004; Orwin and Ostle, 2012; White et al., 2020; Van Meerbeek et al., 2021).

Nevertheless, the potential abrupt overall biotic and abiotic changes and threshold behavior described above, as well as hysteresis and differing responses after disturbance or recovery (memory or legacy effects) could be indicative elements of the existence of alternate states in peatland ecosystems. Temmink et al. (2026) reviewed potential emergent self-amplifying and self-dampening feedbacks associated with a transition from a peat moss-dominated state to a vascular plant-dominated state in bogs and some fens. While multiple chemical, physical and

biological processes have been reviewed, detailed process-based information on how soil C dynamics are responding to such shifts, and whether they can contribute to self-amplification or self-dampening, remains scarce (Temmink et al., 2026).

Therefore, investigating degradation effects (or degradation legacy effects) on soil C dynamics is essential not only for elucidating peatland soil C stability, but also for contributing to our understanding of the vulnerability of peatland ecosystems to environmental perturbations as well as for identifying critical processes potentially affecting the results of peatland restoration efforts (Mahdiyasa et al., 2023; Dean et al., 2024).

1.5. Peatland restoration and recovery of belowground C stability and storage from disturbance

With increasing global recognition of the ecological and climate-regulating importance of peatlands, multiple peatland restoration and management initiatives have been implemented to halt degradation, promote recovery toward pre-disturbed conditions, and focus on a cost-effective, nature-based solution for climate change mitigation and adaptation (Moomaw et al., 2018; Swenson et al., 2019; Mursyid et al., 2025). Despite these efforts, limited consensus to standardized restoration and management practices remains (Zak and McInnes, 2022). Restoration success rates are frequently lower and costs are often higher than those associated with many other ecosystem types (Andersen et al., 2017). Particularly, site-specific environmental conditions and the inherent complexity of peatland systems make it difficult to develop universally effective restoration strategies (Kane et al., 2021; Smolders et al., 2024).

Rewetting drained peatlands to re-establish near-natural hydrological conditions is the primary and most widely applied restoration intervention (Andersen et al., 2017; Loisel and Gallego-Sala, 2022; EU Parliament, 2024). This is typically achieved through ditch blocking, dam installation, refilling drainage channels, pumping water into peatlands, or facilitating natural hydrological recovery via ecosystem engineers (e.g., beavers; Tanneberger et al., 2021). Rewetting

is widely regarded as a foundational step because restoring high water tables can immediately reduce GHG emissions by suppressing aerobic decomposition and promoting the re-establishment of peat-forming vegetation (Bragazza et al., 2013; Günther et al., 2020). Beyond hydrological restoration, complementary strategies−including revegetation, ecosystem revitalization, adaptive management, and stakeholder engagement−are increasingly recognized as essential for long-term restoration success (Zak and McInnes, 2022; Mursyid et al., 2025). Nevertheless, restoration effectiveness is often strongly mediated by site-specific degradation (e.g., drainage, drought, and fire intensity and durations) and historical land legacies (e.g., vegetations type and edaphic characteristics), and duration and type of restoration practices (Urbanová et al., 2018; Emsens et al., 2020; Kreyling et al., 2021). These interacting factors remain insufficiently evaluated, particularly with respect to belowground C storage and stability, which are central to peatland climate-regulating functions (Kitson and Bell, 2020; Negassa et al., 2021).

Another important limitation in peatland restoration research is the scarcity of spatiotemporal datasets (Peltre et al., 2014; Kunarso et al., 2025). Field-based studies in peatlands are costly because they are labor-intensive and peatlands are often sited in remote locations and accessible during short periods of time (Brown et al., 2023). Furthermore, many assessments remain largely qualitative and reliant on expert judgement, which limits reproducibility and increases susceptibility to subjective bias (Schmidt et al., 2011; Brown et al., 2023). There is therefore a growing need for a standardized, quantitative, and process-based monitoring approach (Hodgkins et al., 2018; Ng et al., 2022). To disentangle management effects from complex, interacting environmental factors, and to separate biotic and abiotic drivers of soil C dynamics, cost-effective technical tools that enable regular monitoring of belowground processes are needed (Brosens et al., 2021). Such methods would provide new avenues to link soil ecological processes with management outcomes, enhancing the applicability of peatland research through interdisciplinary integration (Ninnes et al., 2023).

1.6. Importance of legacy effect on belowground soil organic matter and C stability

With increasing recognition that C storage and stability may show non-linear responses to disturbances, a growing attention has been directed toward research on degradation and recovery trajectories such as post-disturbance dynamics and post-restoration dynamics on SOM quantity and composition (Forouzangohar et al., 2015; Heller et al., 2015; Günther et al., 2020; Baysinger et al., 2022). Disturbance-induced legacy effects in SOM can persist for longer than expected, potentially constraining recovery trajectories even after external pressures are reduced (Groß-Schmölders et al., 2022; Antonijević et al., 2023). Because SOM is intrinsically linked to nutrient cycling, microbial community structure, and physicochemical conditions, such legacy effects may affect the re-establishment of critical biota and reactivation of peat accumulation processes (Loisel and Gallego-Sala, 2022).

However, the mechanisms by which disturbances, such as drainage, climate change, and fire, alter belowground SOM quantity and composition, and the extent to which these changes may trigger deviating restoration trajectories and potentially irreversible shifts, remain insufficiently understood (Cécillon et al., 2012). Moreover, how disturbance-driven alteration in SOM translates into long-term changes in C sequestration functioning and stability remains unresolved (Olefeldt et al., 2013; Jackson et al., 2017). Addressing these knowledge gaps requires a comprehensive assessment of SOM at both quantitative and compositional levels to elucidate the mechanism governing C stability in peatland systems.

1.7. Research objectives & thesis outline

The overarching goal of this dissertation is to assess and elucidate the impact of concurrent peatland disturbances −such as drainage, climate change and fire− on soil C dynamics by using molecular techniques (py-GC/MS and MIRs). To our knowledge, detailed assessments of belowground C responses in fen ecosystems, particularly in relation to drainage and restoration and potential disturbance legacy effects, remain insufficiently explored. This knowledge gap is

especially pronounced for belowground process, despite the global importance of peatlands for C sequestration and ecosystem service provision. To address this gap, this dissertation is structured into two main parts, each targeting a critical aspect of fen C dynamics at two different spatial scales (Fig. 1.1).

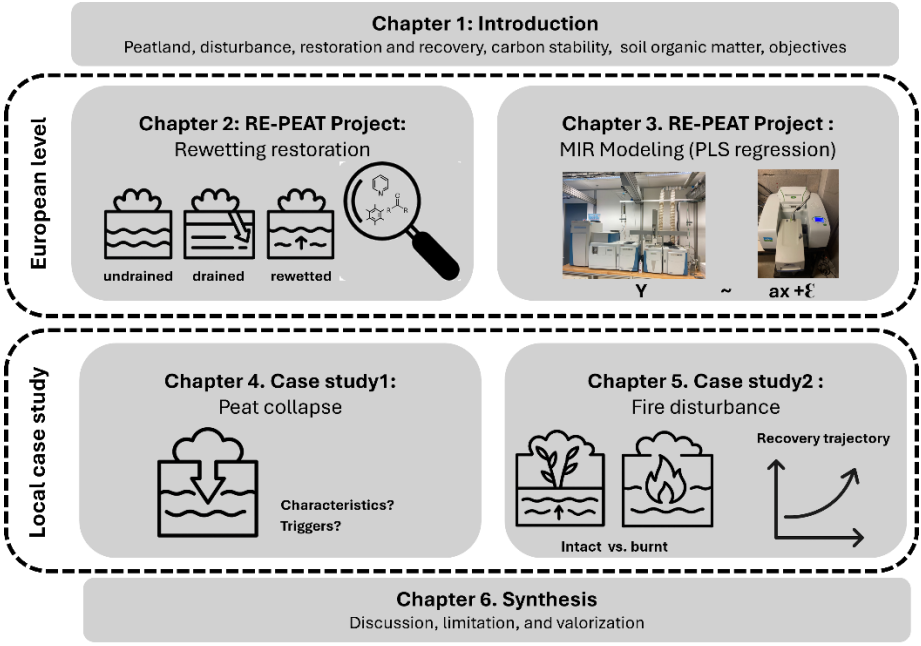


Fig. 1.1. Outline of the structure of this Ph.D. thesis. Chapters 2 and 3 focus on developing a general understanding of peat molecular composition at the European scale. The broader perspective is then used as a foundation to investigate context-dependent responses at the local scales. Chapter 4 investigates the characteristics and potential drivers of peat collapse whereas Chapter 5 examines the effects of fire disturbance and peatland natural recovery at ecosystem level.

In Part 1, we address the critical lack of detailed molecular data on fen SOM by using a well-documented, large-scale European dataset. **Chapter 2** investigates how belowground SOM molecular composition responds to drainage and whether it returns toward pre-drainage state following rewetting. This chapter not only provides information on changes in SOM molecular composition with a high analytical resolution using pyrolysis-gas chromatogram/mass spectroscopy (py-GC/MS), but it also evaluates the success of rewetting restoration across

hydrological degradation gradients. Building on the same dataset, **Chapter 3** develops an upscaling framework by applying statistical (chemometric) models that relate mid-infrared spectral data to molecular composition derived from py-GC/MS from Chapter 2. This approach responds to the increasing demand for advancing monitoring tools that improve spatial and temporal resolution with high analytical resolution that helps in capturing belowground dynamics across degradation and restoration. The results described in this chapter improve monitoring efficiency and scalability for assessing SOM composition across broader spatial scales.

Part 2 applies the insights and molecular tools developed in Part1 at a scale that is directly relevant for ecosystem management. This part focuses on two ecologically valuable and highly protected fen sites−De Zegge and Landschap De Liereman−which have been significantly impacted by anthropogenic pressures. These studies provide a unique opportunity to investigate potential nonlinear ecosystem responses and regime shifts under ongoing and future disturbance.

Chapter 4 examines the causes of an observed abrupt fen peat collapse, interpreted as a nonlinear response to disturbance. Using a mesocosm experiment combined with field observations, this chapter investigates the potential drivers and underlying mechanisms responsible for fen peat collapse. **Chapter 5** applies the modelling framework developed in Chapter 3 to assess fire perturbation effects, evaluating C dynamics from a molecular SOM perspective. The findings from **Chapter 2**−**5** are synthesized and integrated in **Chapter 6**, where broader implications and limitations for peatland disturbance dynamics, restoration trajectories, and C stability are thoroughly discussed.

2

Limited recovery of soil organic matter composition in fen peatlands after rewetting

Based on : Kim, K., Schellekens, J., Emsens, W.-J., van Diggelen, R., Aggenbach, C., Verbruggen, E., Liczner, Y., Klimkowska, A., Tanneberger, F., Kotowski, W., Iglesias Briones, M.J., Jansen, B., Vancampenhout, K., 2026. Limited recovery of soil organic matter composition in fen peatlands after rewetting. Geoderma 465, 117646. https://doi.org/10.1016/j.geoderma.2025.117646

Abstract

Approximately half of Europe's peatlands have been extensively drained for agriculture, forestry, and peat extraction, with lowland fens disproportionately affected due to their high nutrient availability and productivity post-drainage. Peatland rewetting has gained importance as a strategy to mitigate carbon losses and restore biodiversity; however, its effectiveness in reestablishing below-ground processes remains uncertain. Soil organic matter (SOM) dynamics play a crucial role in peatland restoration outcomes, influencing peat structural integrity and hydrological properties, as well as the availability of substrates and nutrients for microbial and plant communities. Here, we present a Europe-wide assessment of the effects of fen drainage and rewetting on SOM molecular composition, analyzing fens with contrasting hydrological status (undrained, drained, and rewetted) across three depths (0−5, 15−20, and 45−50 cm) using pyrolysis-gas chromatography/mass spectrometry (Py-GC/MS). Despite considerable variability induced by site-specific heterogeneity, the molecular composition of undrained fens clearly reflected the dominant contributions of sedges, grasses, and brown mosses to peat formation in fens, with characteristic stratification. Drainage consistently led to a decline in components from plant biopolymers (carbohydrates and lignins) across sites, and an increase in microbially altered compounds (N-compounds, benzenes, and aliphatics), with the most pronounced effects at intermediate depths (15−20 cm). Rewetting partially reversed these alterations, with some fens exhibiting a shift in molecular composition reverting toward undrained conditions, particularly in sites rewetted for longer periods. However, significant differences remained between rewetted and undrained fens. Our findings suggest that while rewetting over time can facilitate partial recovery of carbon dynamics, the below-ground legacy of drainage-induced alterations can persist, at least for a timescale of several decades.

Key words: peatlands, fens, Pyrolysis GC/MS, soil organic matter, restoration

Highlights

- Distinct patterns in SOM molecular composition for undrained, drained and rewetted fens were found across 13 regions in Europe
- The extent of drainage-induced decomposition varies with level of depth.
- Rewetting can induce a partial recovery in soil carbon dynamics, but the extent of this recovery is time and context dependent

2.1. Introduction

Intact peatlands provide multiple ecosystem services, including carbon (C) storage and water buffering and purification, and provide habitats for highly specialized and often rare biota (Yu et al., 2010; Leifeld and Menichetti, 2018). Despite covering only about 3% of the land surface, peatlands contain approximately 30% of terrestrial C stocks, or around 600 Gt, globally (Batjes, 1996; Yu et al., 2010; Xu et al., 2018). Peatlands are also important reservoirs of archaeological remains and contain information on past environmental conditions (Dieleman et al., 2015; Andersen et al., 2017). The prevalent anoxic environment in intact peatlands restricts the degradation of structural plant polymers or components with a low nominal oxidation state, including cross-linked phenolic structures (e.g., lignin) and pectin-like polysaccharides (e.g., sphagnan; (Painter, 1991; Schmidt et al., 2011; Hájek et al., 2011; Boye et al., 2017). Consequently, intact peatland soils consist mainly of plant remains, and the quantity and quality of this soil organic matter (SOM) play a key role in ecosystem functioning (Hoyos-Santillan et al., 2016; Emsens et al., 2020).

An estimated 10−15 % of the current peatland area (i.e. 500,000 km^2) worldwide and 50 % of peatlands in the EU have been subjected to drainage for agriculture, peat extraction or forestry (Tanneberger et al., 2021). These practices turn peatlands from carbon sinks into sources, releasing an estimated 2 Gt of CO_2eq to the atmosphere annually (McClymont et al., 2011; Leifeld and Menichetti, 2018; Chen et al., 2020; Kitson and Bell, 2020), an effect likely to be accelerated by positive feedback loops between peat degradation and climate change (Bridgham et al., 2008; Bragazza et al., 2013; Fenner and Freeman, 2020; Zeh et al., 2020). While drainage effects on SOM quantity and C stocks have been intensively studied (Krüger et al., 2021; Liu et al., 2021), much less is known about effects of drainage on the molecular composition of SOM, which is indicative for below-ground processes of organic matter input, decomposition dynamics as well as peat structural integrity (Schellekens et al., 2009; McClymont et al., 2011; Abbott et al., 2013; Schellekens et al., 2015b; Lopes-Mazzetto et al., 2018; Klein et al., 2022). Most research focused

on rainwater-fed peatlands (bogs), which are predominantly present in northern boreal ecosystems (Biester et al., 2014; Schellekens et al., 2015b; Klein et al., 2022). In contrast, SOM composition of groundwater-fed peatlands (fen peatlands or fens) has been seldom studied (Säurich et al., 2019), even though fens are the dominant peatland type in the temperate climatic zone (Joosten et al., 2017). Compared to bogs, fens exhibit a strong depth stratification of microbial processes (Emsens et al., 2020), and often feature a distinct vegetation composition, with absence or a low abundance of Sphagnum spp. and a higher abundance of brown mosses and vascular plants (Väliranta et al., 2017). These differences have been shown to affect the organic matter decomposition rate (Straková et al., 2011). Because of their rapid release of nutrients after drainage and higher productivity, many temperate fens have been heavily affected by drainage in the past (Emsens et al., 2020; Kreyling et al., 2021; Groß-Schmölders et al., 2022) and drainage effects on microbial decay could be stronger in fens (Urbanová and Bárta, 2016).

To reduce losses of carbon and to restore ecosystem functions, rewetting of drained peatlands has become increasingly important in Europe and worldwide, with a global aim to restore 500 000 km^2 of drained peatland under the COP26 (Andersen et al., 2017; Tanneberger et al., 2021; Loisel and Gallego-Sala, 2022; EU Parliament, 2024). Reestablishment of waterlogged anoxic conditions can reduce drainage-induced SOM losses (Bragazza et al., 2013; Günther et al., 2020) yet may not always be successful in reviving peatland carbon and water cycles, and therefore in restoring biotic communities and peatland functioning, especially in fens (Emsens et al., 2020; Kreyling et al., 2021; Loisel and Gallego-Sala, 2022; Groß-Schmölders et al., 2022). The molecular composition of the peat upon rewetting may influence restoration success: plant biopolymers contribute to peat structure, microtopography and hydraulic properties, while changes in substrate quality may affect nutrient cycles and microbial communities, also affecting the re-establishment of critical plant species (Emsens et al., 2020; Loisel and Gallego-Sala, 2022). Nevertheless, studies that investigate rewetting effects on belowground carbon dynamics and SOM molecular composition in peatlands remain scarce. Furthermore, the typical belowground

vertical depth stratification of peatland ecosystems adds additional complexity (Säurich et al., 2019; Zeh et al., 2020; Negassa et al., 2021; Klein et al., 2022). To the best of our knowledge, no studies exist that discuss how drainage- and rewetting-induced shifts in inputs and decomposition affect the molecular properties of SOM in surface peat of European fens, and how that could affect restoration targets and outcomes.

Our study thus aims to unravel the influence of drainage and rewetting on soil carbon dynamics in fen peatlands, by providing a comprehensive assessment of SOM molecular composition in European fens. We used a space-for-time substitution approach by selecting triplets of undrained, drained and rewetted plots in 13 representative fen areas belonging to the REPEAT EU BiodivERsA project (https://www.biodiversa.eu/2022/10/31/repeat/; Supplementary Table 1). The selected regions represent a longitudinal gradient (i.e. Atlantic, continental and nemoral-sub-meridional biogeographic regions). At each region, soils from undrained, drained and rewetted plots were sampled at three different depths and their molecular composition was analysed using pyrolysis gas chromatography–mass spectrometry (Py-GC/MS) complemented with isotopic (^{13}C, and ^{15}N) and stoichiometric (C:N) analyses.

We hypothesize that (1) drainage and rewetting affects fen belowground functioning through changes in input composition and shifts between anaerobic and aerobic decay; that (2) the nature and magnitude of these changes vary with peat depth; and that (3) degradation and restoration may follow different trajectories depending on context and time since rewetting.

2.2. Materials and Methods

2.2.1. Site description

Peat samples were collected in June 2017 in 13 lowland fen regions that span a longitudinal gradient (> 1500 km;

Fig. 2.1) from a temperate Atlantic to a continental climate (United Kingdom, Belgium, the Netherlands, Germany, and Poland) (Emsens et al., 2020; Groß-Schmölders et al., 2022). In each region, three distinct fen sites with different hydrological status (undrained, drained and rewetted) were selected. For details on the sites as well as on the site selection procedure, we refer to Emsens et al., (2020); A brief description of the vegetation at each site is given in Supplementary Table 2.1. Although species composition varied considerably between regions, the undrained fen sites were typically dominated by typical fen species (e.g., Carex spp., brown mosses) and had a groundwater table near the peat surface for most of the year. In drained fen sites, groundwater levels often dropped deeper than 50 cm below the peat surface, typically in summer, and the vegetation mainly consisted of wet grassland species. Rewetted fen sites had similar water table dynamics to undrained fens sites due to active restoration projects or dam building by beavers, which is subsequently followed by re-emerge of fens species (Carex spp., and brown mosses; Supplementary Table 2.1). A full analysis of the effects of drainage and rewetting on vegetation for these European fens can be found in Emsens et al., (2020). The time-since-rewetting ranged from less than 15 years (Peene Mouth, Drentse Aa, Suwalszczyna and Kiel) to more than 50 years (for Arlon) prior to our sampling campaign (Supplementary Table 2.1).

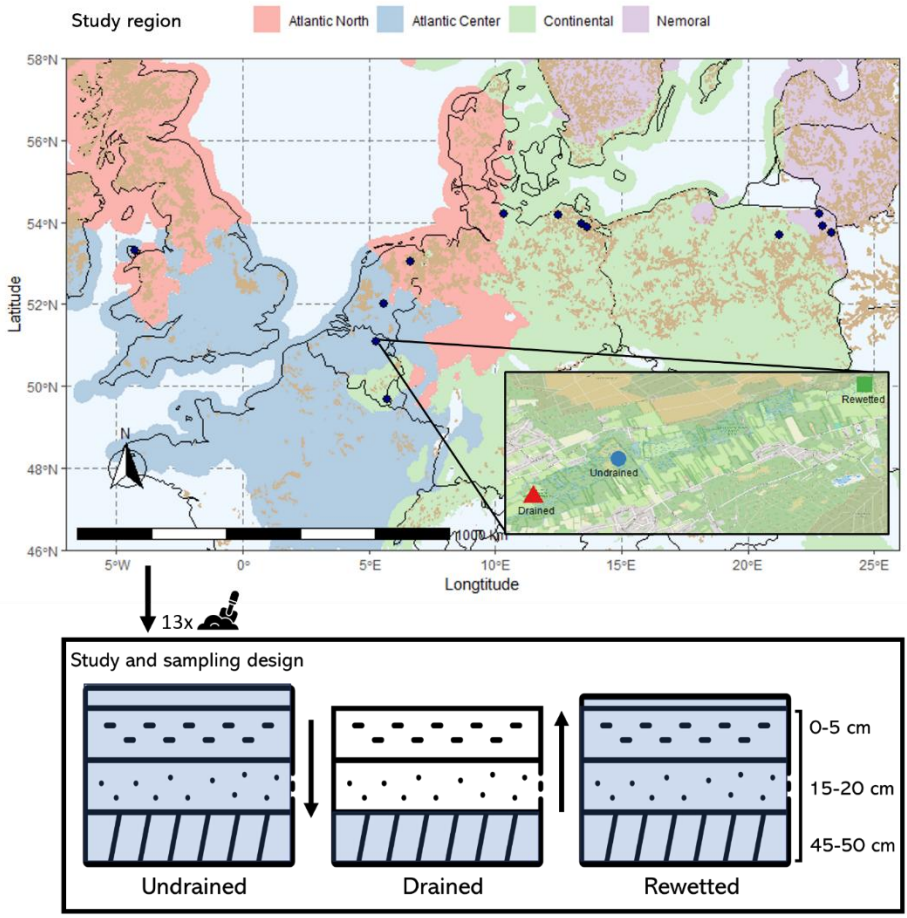


Fig. 2.1. Top: 13 study fen regions across Europe, overlaid on a biogeographic and peatland map. Bottom: Study and sampling design. A total of 39 fen sites (13 fen regions × 3 types of drainage status) were sampled in three different peat layers (Map data ©OSM).

2.2.2. Soil sampling and bulk analysis

At each of the 39 fen sites (i.e. 13 regions × 3 hydrological status), we mixed five soil subsamples into one composite sample, and also sampled at three different depths: 0−5 cm, 15−20 cm and 45−50 cm (making a total of 117 peat samples). These depths were chosen to reflect the impact of drainage on the peat along the soil profile, as the 0-5 layer is typically impacted by seasonality in all fens, the 15-20 cm layer remained below the water table for the undrained fens, was above the water table for the drained situation, and resubmerged for the rewetted samples.

The 45-50 cm depth remained largely submerged across treatments. Although differences in site history and potential subsidence may induce additional variability, sampling according to fixed depths typically is the best workable option in the field and is often used for relative comparison between sites with different drainage legacies (Smeds et al., 2025). Samples were all individually packed into plastic bags and transported in a sunproof cooler, and then deep-frozen (-18°C) until further analyses. Samples were oven-dried at 45 °C for 72 h, and homogenously ball-milled with a vibrating ball mill (MM400, Retsch, Germany). Total organic carbon (TOC), nitrogen and their isotopes were measured in an elemental analyzer (Thermo Flash HT/EA) equipped with an isotope ratio mass spectrometer (Thermo Delta V advantage; EA-IRMS; De Troyer et al., 2010). Stable isotope analysis was conducted in a single analytical run. Calibration was performed using certified standards including caffeine, tuna, and leucine. The analytical precision was ± 0.03‰ and ± 0.05‰ for $\delta^{13}C$ and $\delta^{15}N$, respectively. Bulk density was separately measured by oven drying (70 °C) a second batch of peat samples with known volume (Emsens et al., 2020).

2.2.3. Pyrolysis-gas chromatography/mass spectrometry (Py-GC/MS)

Bulk peat samples were pyrolyzed using a multi-shot furnace pyrolyser (EGA/Py-3030D; Frontier Lab, Japan) with an AS-1020E auto-sampler, coupled to a Thermo Scientific Trace 1300 gas chromatograph (GC; Milan, Italy) with an Rxi-1 ms fused silica column (Restek: 30m; 0.25 mm i.d.) at the IBED laboratory (University of Amsterdam; Nikolaus et al., 2023). The column was coated with di-methyl poly-siloxane (film thickness: 0.05 µm) and helium was used for carrier gas (constant flow: 1ml/min). The pyrolyser was set to 600 °C (0.8 min) and the interface temperature between pyrolyser and GC was set to 300 °C. The injection temperature to the GC (operated in 100:1 split mode) was 250 °C. The GC was stared at 40°C (hold time: 1min, heating rate: 7.0 °C/min) and the final temperature was 320 °C (hold time: 10 min). A Thermo Scientific ISQ 7000 Single Quadrupole MS (Milan, Italy)(mass to charge ratio (m/z): 47-500;

ionization energy: 70 eV) was coupled to the GC. Upon calibration with pilot samples, the amount of sample to be pyrolyzed was determined. Bulk samples were weighted up to 200 μg.

The processing of pyrolysis data was performed with untargeted GC-MS workflow in MZmine3 and NIST MS search v2.3 software (Schmid et al., 2023). Baseline correction was first performed on the raw data, afterwards mass detection was set up for each scan to build a chromatogram using an automated data analysis pipeline (ADAP) chromatogram builder (Boelens et al., 2005). Below the background noise level in the data, the detected signal of the scan was discarded. These built chromatograms were smoothed using the Loess smoothing module prior to construction of the extracted ion chromatogram, which were then resolved into individual features by the local minimum resolver algorithm provided by MZmine3 (Cleveland and Devlin, 1988; Du et al., 2006; Schmid et al., 2023). To identify analytes, similar features were combined, and their intensities were used to construct fragmentation mass spectra using hierarchical clustering spectral deconvolution (Pluskal et al., 2010; Smirnov et al., 2018). Isotopologues of the same chemical entity in the feature list were subsequently filtered out using the ^{13}C isotope filter module. In the ADAP aligner section, features were aligned and if a feature occurred in less than 30% of the samples it was removed. Missing values in the aligned feature table, possibly filtered out during data process, were back-filled using the gap-filling module (Jiang et al., 2010). The resulting list of 437 compounds was exported to the NIST MS library search for further downstream analysis. This NIST MS search was used for rapid compounds identification based on the cosine spectra similarity as compared against the NIST 2017 database and the MassBank of North America database (Horai et al., 2010). Peaks were visually inspected to ensure alignment, thereafter the full mass spectral profile of each compound was manually curated and confronted with additional literature (Schellekens et al., 2009, 2015b; Vancampenhout et al., 2016; Klein et al., 2022). These identified compounds from peat were grouped based on their probable origin and chemical characteristics (Schellekens et al., 2009, 2015a; Vancampenhout et al., 2016; Klein et al., 2022). The peaks were quantified by their characteristic fragment ions and then exported to R software,

and the batch effects were dealt with using the Combat batch correction (Supplementary Fig. 2.1; R 4.2.3). In line with the broader geographical scope of our research focussing on the overall effects of drainage and rewetting rather than localized variation, and to avoid our results being skewed by rare components occurring only in a few samples, and misaligned fragment ions due to batch effect, the final reduced dataset of 75 compounds were selected based on literature knowledge, relative abundance ranking and the criterion of occurrence in at least 30 % of the samples (Grace et al., 2016). Quantified abundances (i.e., peak areas) were normalized by percentage before following downstream analyses.

2.2.4. Statistical analyses

All analyses were conducted in R 4.2.4 and statistical significance was accepted at $P < 0.05$. The effects of hydrological status and depth (and their interactions) on peat physicochemical variables were tested using linear-mixed effect models ($P < 0.05$; main factors: drainage status × depth, random factor: site location). Normality and homoscedasticity of the model residuals were assessed using Shapiro-Wilk's and Levene's test, respectively (NLME package of 3.2.1), box-cox transformation was applied when the model assumptions were violated. Pairwise comparison was carried out after significant ANOVA with Tukey's Honest Significance Difference using agricolae package in R (Mendiburu, 2020).

Nonmetric multidimensional scaling (k = 2; NMDS) was performed based on Bray−Curtis dissimilarity distances to compare SOM molecular composition between the peat samples. The effects of drainage status, depth and their interactions on molecular composition were thereafter tested with a permutational multivariate analysis of variance (permanova) with 999 iterations by using site location as a random factor ('block' effect) (Andersen et al., 2017; Yang et al., 2023). Pairwise comparisons were additionally conducted using the anonis2 function from the vegan package in R. To investigate how the NMDS ordination space related to compounds abundances and environmental variables, a separate NMDS plot was generated.

Compound vectors were visualized in one ordination, while environmental variables that show significant correlations with SOM molecular composition were projected as arrows onto the ordination space. Significance was assessed using 999 permutations, follow the approach described by Dixon (2003). To find differences in the relative abundance of each pyrolysis product across hydrological status, a differential abundance test was performed by using a negative binominal generalized linear model from the edgeR package in R (Robinson et al., 2010). The model was adjusted for additional covariates such as site location and depth, and the test results were later used in volcano plots. Moreover, the magnitude of change related to drainage status were calculated by Bray-Curtis dissimilarity distances of SOM molecular composition between undrained fens as reference and corresponding rewetted and drained fens (Emsens et al., 2020). Concomitantly, the magnitude of depth-induced decomposition was calculated as mentioned above, but between the first layer as a reference and the third layer of the same fen. Thereafter, Pearson (R) correlations were consequently obtained by plotting the dissimilarity distances against physicochemical characteristics. Similarly, for each depth, restoration timeframe projection was also estimated using linear regression between years since rewetting and Bray-Curtis dissimilarity distance of molecular composition between rewetted and undrained fen sites.

2.3. Results

2.3.1 Changes in bulk density, carbon and nitrogen contents and isotopic ratio across hydrological status

Bulk density of peat in the investigated fen sites ranged between 0.036 and 0.900 g/cm^3 with an average of 0.208 g/cm^3 and was significantly altered by drainage status and depth ($Ps <$ 0.05; Table 2.1): undrained sites had the lowest average bulk density, followed by rewetted and drained sites. The bulk density of the 0−5 cm layer was significantly lower than that of other two layers. An interaction effect was present for the first two layers (0−5 cm, 15−20 cm), having significantly different bulk density between drainage statuses, but not for the deepest layer (45−50

cm, no difference across drainage status). Total organic carbon (TOC) content varied between 93.9 mg C g^{-1} soil and 531.5 mg C g^{-1} soil with an average of 372.9 mg C g^{-1} soil. Overall, the TOC content in the undrained sites was significantly higher than that in drained sites, but similar to that in rewetted sites (P <0.05; Table 2.1). Peat depth also had a significant effect on the TOC content, and it was significantly higher at the deepest peat layer (45−50 cm) than that of the upper two depth layers (0−5 cm, 15−20 cm). There was an interaction effect between drainage status and depth (Ps < 0.05; Table 2.1). The TOC content in undrained fens did not vary significantly with depth, in contrast to the drained and rewetted fens. The TOC of the first two layers (0−5 cm, 15−20 cm) differed significantly depending on drainage status, whereas the TOC content of the deepest layer (45−50 cm) showed no significant differences across drainage status (Table 2.1). Total organic nitrogen ranged between 4.4 and 38.8 mg N g^{-1} soil with an average of 22.8 mg N g^{-1} soil and did not show any significant differences across drainage status and depth (Ps > 0.05; Table 2.1). Drainage status and depth had a significant impact on C:N ratios (Ps < 0.05; Table 2.1). Particularly, $\delta^{13}C$ was significantly influenced by depth whereas $\delta^{15}N$ was significantly affected by drainage status (Ps < 0.05; Table 2.1).

Table 2.1. Bulk density, total organic carbon and nitrogen, C/N ratios and isotopic composition across the drainage status and depth.

	BD¶ (g/cm3)	TOC (mg C/g-1 soil)	TN (mg C/g-1 soil)	C/N	$\delta^{13}C$ (‰)	$\delta^{15}N$ (‰)
Undrained	0.12 a	398.15 b	21.89	17.67 c	-28.35	2.04 a
Drained	0.25 c	359.33 a	22.95	14.58 a	-28.12	4.09 b
Rewetted	0.17 b	391.22 ab	23.89	16.02 b	-28.20	3.47 b
0-5 cm	0.13 a	365.67 a	21.47	16.62 b	-28.73 a	3.12
15-20 cm	0.21 b	351.76 a	23.50	14.10 a	-28.00 b	3.29
45-50 cm	0.19 b	428.75 b	23.76	17.67 b	-27.73 b	3.07
Drainage	<0.001***	<0.05*	0.2455	<0.001***	0.1547	<0.001***
Depth	<0.001***	<0.001***	0.1146	<0.001***	<0.001***	0.792
Drainage: Depth	<0.001***	<0.001***	0.1326	<0.001***	0.4442	<0.001***

BD¶ indicates bulk density.

Least-squares means are shown as values in the table from a linear-mixed model afterwards two-way ANOVA.
*,**, and *** indicates statistical significance at $P < 0.05$, $P < 0.01$, $P < 0.001$, respectively.
Different lowercase exhibits significance between experimental treatment based on two-way ANOVA (n=13).

2.3.2 Changes in SOM molecular composition across hydrological status

A full list of quantified pyrolysis products is given in Supplementary Table 2. The reduced dataset contained three unspecified aliphatics (Al), five n-alkanes (C_{16}, C_{24}, C_{25}, C_{29}, and C_{31})), two n-alkenes ($C_{11:1}$, and $C_{26:1}$), two methyl ketones (MK), seven benzenes (B) containing benzene, indene, toluene, and styrene; fifteen carbohydrates (C) including furans, furaldehydes, and monomeric sugars; fifteen lignin components (Lg) including p-hydroxyphenyl, guaiacyl and syringyl moieties; seventeen N compounds (N) including benzonitriles, amides and pyrroles; six phenols (Ph) and three unidentified components (Fig. 2.2; Supplementary Table 2.2). In summed relative abundance, carbohydrates were most prevalent, followed by phenols, lignins, N compounds and benzene compounds. Aliphatic compounds (n-alkanes, n-alkenes, n-methyl ketones and unspecified aliphatic compounds) were relatively rare in this dataset (Fig. 2.2; Supplementary Table 2.3).

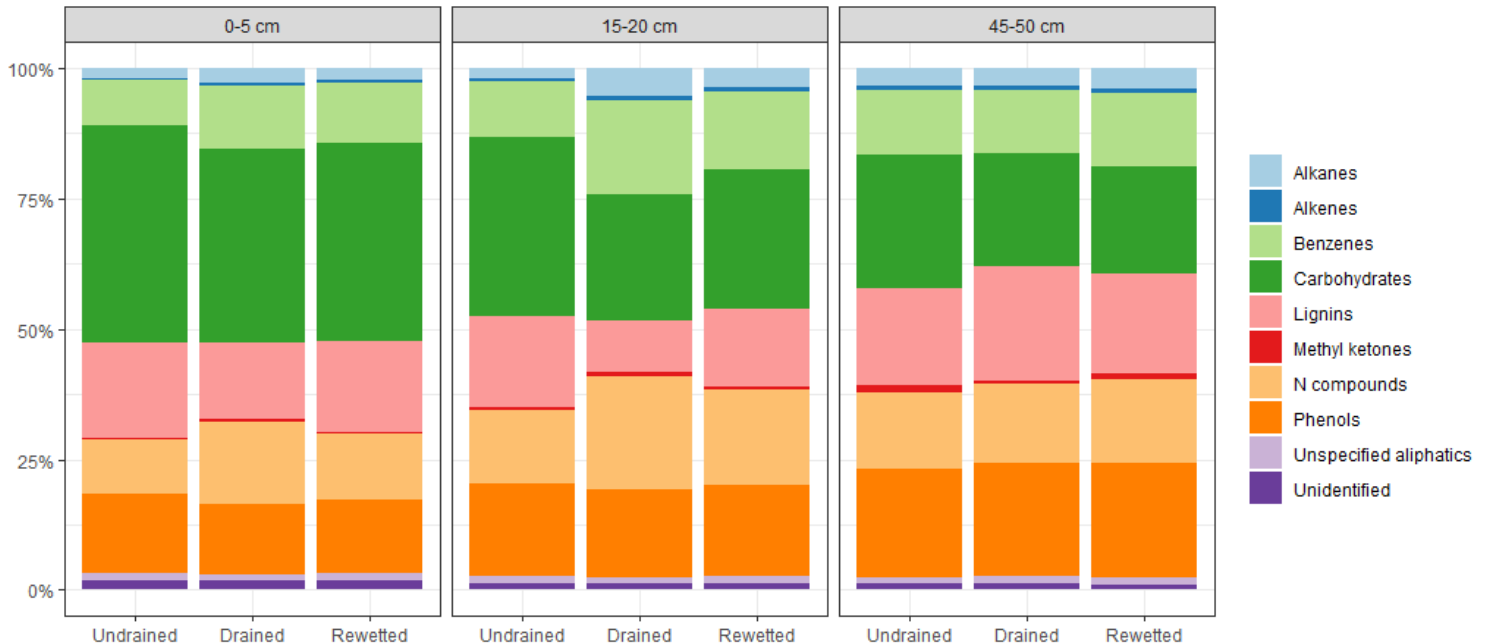


Fig. 2.2. Average composition of peat molecular functional group (pyrolysis products) from 13 study fen regions, analyzed across three drainage status (undrained, drained, and rewetted) and three peat layers (0−5 cm, 15−20 cm, and 45−50 cm).

The results of NMDS are represented in Fig. 2.3 (sample positions) and Figure 4 (component vectors). A shift of sample positions to more positive values along the first NMDS ordination axis indicates a shift in molecular composition with drainage status, in particular for the samples taken at 0−5 cm and 15−20 cm depth, while the deepest samples (45−50 cm) remained largely unaffected (Fig. 2.3). By comparing this shift to the vector fitting plot of the different components (Fig. 2.4), we can infer that differences in drainage status were mainly associated with changes in the relative abundance of lignin, carbohydrate vs. N compounds, benzenes and aliphatics. Sample positions in Fig. 2.3 also shift along the second ordination axis, where the samples from the upper layer (0−5 cm) have more positive positions, samples from the middle layer (15−20 cm) have intermediate positions, and samples from the deepest layer (45−50 cm) have the lowest positions (Fig. 2.3; Supplementary Fig. 2.2). The component vectors along the second NMDS axis (Fig. 2.3) reveal that the gradient of depth reflected a contrast between carbohydrates (positive sample positions, i.e. higher relative abundance less deep in the peat profile) vs. lignins (negative sample positions, i.e. higher relative abundance deeper in the profile). When analysed in more detail, fen sites from the western Atlantic region (i.e., Drentse Aa, Zwarte Beek, Binnenveld to some extend Anglesey), were affected by a somewhat larger relative accumulation of aliphatics (n-alkanes, unspecified alipahtics, and n-methyl ketones) as a result of drainage, as compared to the other sites where the relative accumulation of N compounds was most prominent (especially evidenced in the second layer; Supplementary Fig. 2.3).

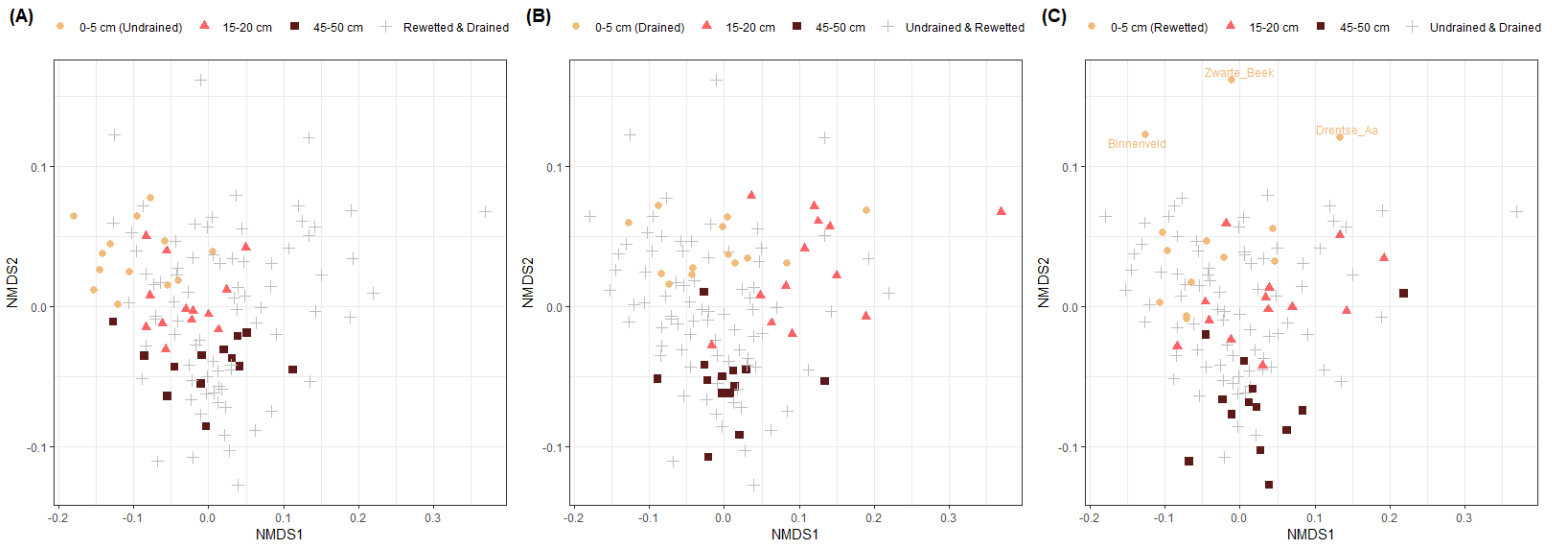


Fig. 2.3. Nonmetric multidimensional scaling (NMDS, stress = 0.112) showing sample coordinates based on the Bray-Curtis dissimilarity of soil organic matter (SOM) molecular compositions across three drainage stages (undrained, drained, and rewetted) and three different depths (0−5 cm, 15−20 cm, and 45−50 cm). The ordination includes samples from undrained, drained, and rewetted fens at three depths. To illustrate sequential changes in SOM molecular composition due to drainage and rewetting, each panel is colored by depth for a specific drainage stage: undrained (A), drained (B), and rewetted (C).

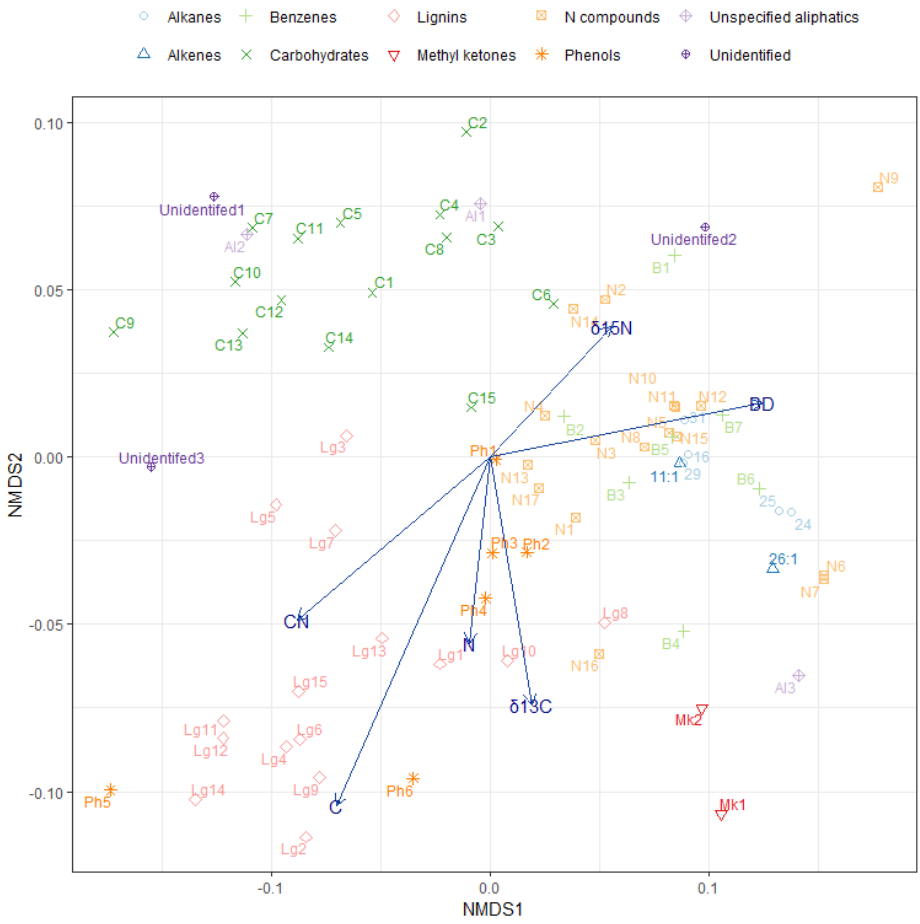


Fig. 2.4. Nonmetric multidimensional scaling (NMDS, stress = 0.112) showing vector fitting analysis of soil organic matter (SOM) molecular composition and enviromental variables based on the ordination in Fig. 3. Compound vectors represent correlations between individual compound abundances and the NMDS axes. Blue arrows indicate fitted enviromental vectors, illustrating the direction and strength with the ordination space. These vectors reflect how compounds and environmental variable are associated with the NMDS axes.

Rewetting resulted in an intermediate placement along the first axis for some but not all samples: for the 15−20 cm depth interval, mainly samples from Peene Mouth, Drentse Aa, Suwalszczyna and Kiel had continued high positive positions on NMDS1 after rewetting (Fig. 2.3). These sites have been rewetted fairly recently (estimated less than 15 years) and are richer fens with slightly higher relative abundances of N compounds even in their natural, undrained

state. Furthermore, the topsoil samples (0−5 cm) from the western Atlantic Region (i.e. Binnenveld, Zwarte Beek and Drentse Aa) diverge from the general rewetting-restoration trend and shift upward along NMSD2 upon rewetting (Fig. 2.3C), indicative for an increase in furaldehyde compounds (C2–C4, C8; Supplementary Table 2.2).

Permanova analysis confirmed that molecular composition significantly differed with drainage status (pseudo-F = 6.270, R^2 = 0.077, P <0.001) and depth (pseudo-F = 16.908,R^2 = 0.207 , P <0.001), with a significant interaction effect between fen drainage status and depth (pseudo-F = 2.320 ,R^2 = 0.057 , P <0.004,

Table 2.2). In detail, the differences in molecular composition that are associated with fen drainage status were significantly different in the first two layers (0−5 cm, 15−20 cm), but were not significantly different at a depth of 45−50 cm (Ps < 0.05; P = 0.061;

Table 2.2). In addition, these differences in molecular composition were most discernible in the second layer of peat (first layer R^2= 0.145, second layer R^2 = 0.255, third layer R^2 = 0.062;

Table 2.2). In pairwise comparisons, molecular composition differed between undrained and rewetted and between undrained and drained sites (P <0.003; P <0.001), but there was no significant difference between rewetted and drained sites (P = 0.212;

Table 2.2). For the pairwise comparison of depth, molecular composition exhibited significant differences across depths (Ps < 0.001,

Table 2.2).

Table 2.2. Permutational multivariate analysis of variance (PERMANOVA) of peat molecular composition across drainage status and depths, as well as pairwise comparisons.

	Drainage × Depth		
	R^2	F.model	P value
Drainage	0.077	6.270	0.001***
Depth	0.207	16.908	0.001***
Drainage: Depth	0.057	2.320	0.004**

	Pairwise comparison (P value)		
	Undrained	Rewetted	
Rewetted	0.003**		
Drained	0.001***	0.212	
	0-5 cm	15-20 cm	
15-20 cm	0.001***		
45-50 cm	0.001***	0.001***	
	Drainage effects along the depth		
	R^2	F.model	P value
0-5 cm	0.145	3.063	0.001***
15-20 cm	0.255	6.145	0.001***
45-50 cm	0.062	1.19	0.061

Signifiant codes : P <0.05,* ; P<0.01,** ; *P* <0.001,***.
P value is adjusted by false discovery rate (FDR), the number of permutations with 999 iterations.

Physicochemical properties were significantly correlated with sample positions along the ordination axes (Ps < 0.05; Fig. 2.4; Supplementary Table 2.4): Bulk density was primarily associated with the first ordination axis, which reflects variation due to drainage status. In contrast, N and $\delta^{13}C$ were mostly negatively correlated with second ordination axis, which corresponds to depth-related variation. C:N ratio, $\delta^{15}N$ and C showed correlations with both axes.

2.3.3 Changes in individual pyrolysis product across hydrological status

The volcano plot showed which individual compounds changed significantly in molecular composition between undrained and drained sites and the magnitude of the difference (*Ps* < 0.05, Fig. 2.5A): many carbohydrates (C1, C5, C7, C9, C10, C11, C12, C14), two aliphatics (Al2, MK1), lignins (Lg4, Lg14, Lg15; the lignins with C_3 side-chain (Lg9, Lg12) and the lignins with vinyl-side chains (Lg3, Lg5, Lg 11)), and one phenol (Ph5) are relatively more abundant in undrained sites, whereas N compounds (benzonitrile, furan, pyridine, acetamide, pyrrole and certain unspecified N-containing compounds: N2, N3, N4, N5, N6, N7, N8, N9, N10, N11, N12, and N15), benzenes (indene, most of the benzene, toluene and styrene: B1, B2, B3, B5, B6, and B7), the n-alkanes (C_{16}, C_{24}, C_{25}, C_{29}, and C_{31}) and n-alkenes ($C_{11:1}$, $C_{26:1}$) and one lignin containing an acetyl side chain (Lg8) were relatively more abundant in drained sites.

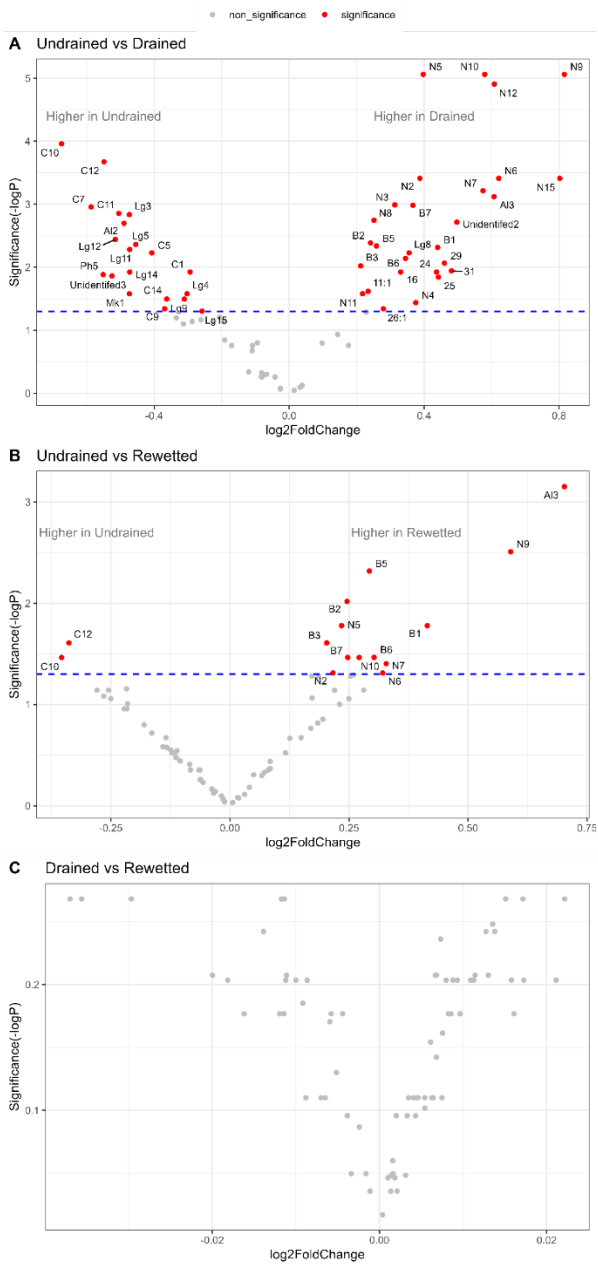


Fig. 2.5. Volcano plots of pyrolysates (i.e., molecular composition) as per differential abundance test: (A) undrained vs. drained; (B) undrained vs. rewetted; (C) drained vs. rewetted. The volcano plot depicts log2 fold change on x-axis and statistical significance on the y-axis. Pyrolysis products are coloured red when false discovery rate (i.e., adjusted *P*-value) is less than 0.05. The codes for pyrolysates are given in Supplementary Table 2.2.

In contrast, the difference in molecular composition between undrained and rewetted sites was less distinctive than the difference between undrained and drained sites (*Ps* < 0.05, Fig.

2.5B): two carbohydrates (C10, C12) had a higher relative abundance in undrained sites, while several N compounds (N2, N5, N6, N7, and N9, N10), benzenes (B1, B2, B3, B5, B6, and B7), and one unspecified aliphatic (Al3) were significantly more abundant in rewetted sites.

Not a single compound showed a statistically different relative abundance between drained and rewetted sites ($Ps > 0.05$, Fig. 2.5C).

2.3.5. Correlation between peat molecular composition vs. physicochemical properties and estimated year since rewetting

Dissimilarity distances were separately calculated as a function of drainage and depth, thereafter correlations were plotted between the dissimilarity distances and physicochemical properties (Fig. 2.6; Supplementary Fig. 2.4). The Bray-Curtis dissimilarity distance of SOM molecular composition between undrained vs. drained sites within corresponding layer was positively correlated with bulk density and $\delta^{15}N$, and negatively correlated with C and C:N ratio ($Ps < 0.05$; Fig. 2.6; Supplementary Fig. 2.4). In contrast, the Bray-Curtis dissimilarity distance of SOM molecular composition between undrained vs. rewetted sites increased with an increasing bulk density, but it was not significant correlated with other physicochemical properties ($Ps < 0.05$; Fig. 2.6; Supplementary Fig. 2.4). In addition, peat depth-induced decomposition in undrained and rewetted fens (i.e., Bray-Curtis dissimilarity distance of molecular composition between the first vs. deepest layer) was positively correlated with an increase of bulk density ($P < 0.05$; Supplementary Fig. 2.4). In the case of drained fens, no significant correlation between depth-induced decomposition and physicochemical properties was observed ($Ps > 0.05$; Supplementary Fig. 2.4).

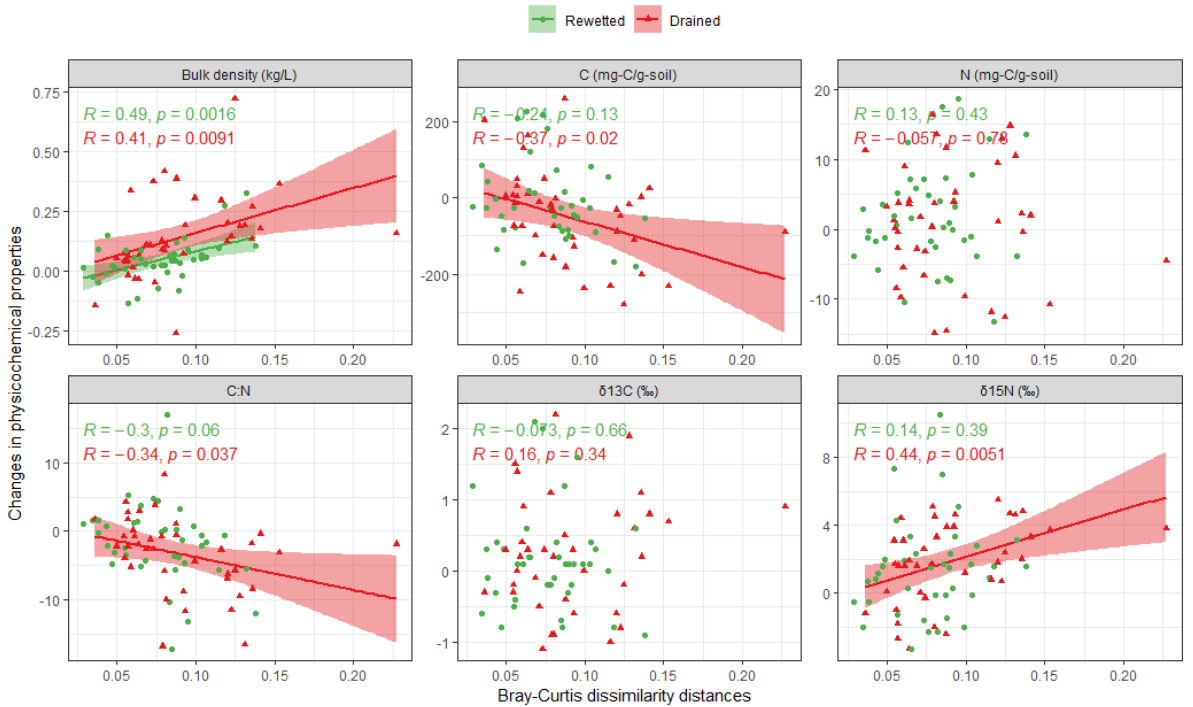


Fig. 2.6. Pearson correlations between changes in peat physicochemical properties and dissimilarity (between undrained to drained fens; red & triangle), and dissimilarity (between undrained to rewetted fens; green & circle). Bray−Curtis dissimilarity were computed from molecular composition obtained by pyrolysis-GC/MS.Pearson's correlation coefficients (R) and significance (P) are given in each plot.

Time since rewetting was significantly correlated with the dissimilarity in SOM molecular composition between undrained and rewetted fens in the second, most dynamic layer (15−20 cm) of the sites (linear model $P = 0.003$, Fig. 2.7). Yet, this pattern was not clearly observed in other two layers ($P > 0.05$, Supplementary Fig. 2.5).

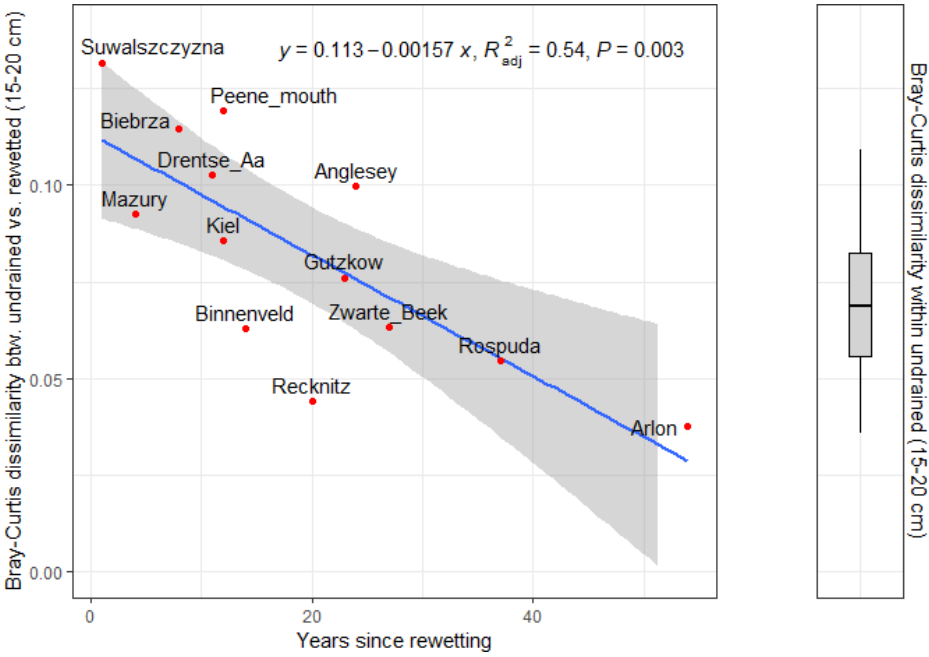


Fig. 2.7. Time since rewetting vs. dissimilarity in peat molecular composition between undrained and rewetted at 15−20 cm depth, along with dissimilarity values within undrained fens. The left panel shows the Bray−Curtis dissimilarity between undrained and rewetted fens as function of time since rewetting. The blue line represents the fitted linear relationship, with the shaded grey area indicating the 95% confidence interval. The right panel presents a box plot of dissimilarity values within undrained fens, serving as a reference to estimate the timeframe at which rewetted fens begin to resemble undrained fens in terms of peat molecular composition recovery.

2.4. Discussion

2.4.1 Fens have a distinct molecular composition, reflecting ecosystem characteristics

In general, we found the same dominance of carbohydrates (Fig. 2.2) with high levels of levoglucosan (C14) and phenols that are also commonly evidenced in bogs and attributed to vegetation inputs from Sphagnum mosses or grasses by most authors (Nierop et al., 2001; Biester

et al., 2014; Stricker et al., 2019; Klein et al., 2022). In contrast to what has been described for bogs however, our fen samples showed a more important relative abundance of lignins, benzenes, aliphatic compounds and organic N compounds (Schellekens et al., 2009; Säurich et al., 2019). Lignin components in soils originate from vascular plants and in bogs they are generally linked to higher shares of graminoids or woody vegetation (Schellekens et al., 2015a). The vegetation in the studied fens was dominated by brown mosses, wetland grasses and sedges (Emsens et al., 2020), which most likely explains the higher lignin share as compared to bogs dominated by Sphagnum species. Some of the carbohydrate pyrolysis products in our dataset, i.e. C9 (a pyrolysis product of xylose) and the higher relative share of other pentoses, could also point to a higher input of hemicelluloses abundant in grasses and sedges (Hoch, 2007; Pouwels et al., 1989; Biester et al., 2014; Schellekens et al., 2015a).

An accumulation of N compounds and benzenes is generally attributed to higher microbial alteration both in mineral soils and peatlands (Schellekens et al., 2009). In our study sites, the relatively higher abundance of N compounds and benzenes may be attributed to the nutrient-rich supply and greater N availability of fens compared to bogs, promoting enhanced microbial alteration (Li et al., 2019). This trend is particularly evident in Gutzkow, Peene mouth, Drentse Aa and Reckniz and to a lesser extent also Arlon, Kiel and Suwalszczyzna (data not shown). Nevertheless, despite the elevated presence of N compounds in some undrained sites, their contribution remains considerably lower than in their drained counterparts (vide infra, Supplementary Fig. 2.3). A higher share of vascular plants can also contribute to the abundance of benzenes encountered (Schellekens et al., 2009; Säurich et al., 2019; Zeh et al., 2020; Klein et al., 2022).

2.4.2. Drainage effects on belowground processes differ along the peat profile in fens

The natural variability in site-specific conditions across European fens and potential subsidence upon drainage imply substantial heterogeneity in soil carbon composition among them.

In our setup, we sampled a large number of locations (13 regions, 39 sites) to attenuate the influence of site-specific variability on our main factor of interest, i.e. hydrological status. As such, despite considerable variability, consistent effects of drainage and rewetting were indeed distinguishable in our results (Fig. 2.3).

Two types of SOM alterations upon drainage were evidenced in our dataset. A first was a natural alteration (or ageing) with depth, evidenced by a decrease in the relative abundance of carbohydrates and an increase in lignins with depth in all sites including the undrained ones (Fig. 2.3). This feature also is common in graminoid-dominated bogs and has been attributed to a preferential loss of vegetation-derived carbohydrates over lignins, as the decomposition of polyphenolic lignin is severely hampered by anoxic conditions (Schellekens et al., 2015a).

The second type of alteration is an accelerated, increasingly aerobic decomposition that occurs when peatlands are drained. In our dataset, the effects of drainage showed a strong interaction with depth: drainage had only little effect in the deepest layer (45−50 cm) as the organic matter at this depth remained permanently below the groundwater table in all drainage status (Emsens et al., 2020; Groß-Schmölders et al., 2022). In contrast, the 15-20 cm layer was below the groundwater table in undrained sites, above the groundwater table in drained sites, and was resubmerged after a period of drainage in the rewetted sites. Consequently, this peat layer showed the largest alterations of the entire dataset. Upon drainage, it is characterised by a relative depletion of lignocellulose (lignins and carbohydrates) and an increase in N-containing compounds, benzenes and aliphatics, which is consistent with an increased aerobic decomposition of the plant materials in the peat (Schellekens et al., 2014; Klein et al., 2022). Lignin mainly decomposes aerobically (Agosti et al., 1998), and its lower proportion in peat of the drained sites coincided with a higher relative abundance of benzenes and with stronger side-chain alterations of the lignins (increased abundance of lignin compounds with acetyl side-chain (Lg8), and decreased abundance of lignin components with vinyl side-chain (Lg3, Lg5, Lg11) and C_3 side-chain (Lg9, Lg12); (Schellekens et al., 2012; Biester et al., 2014; Schellekens et al., 2015a). Lignocelluloses

are important structural components in peatland SOM, and their loss can lower ecological resilience by affecting peat structural integrity, microtopography and hydrological conductivity (Loisel and Gallego-Sala, 2022). The increased relative abundance of N components in drained fens− particularly low molecular weight fragments – are likewise indicative for stronger decomposition and microbial alteration (Fig. 2.5; Schellekens et al., 2009; Xu et al., 2021).

Intriguingly, there was a separation between drained plots belonging to the West-Atlantic region (Drentse Aa, Zwarte Beek, Binnenveld and to a lesser extend also Anglesey) showing a more prominent relative accumulation of aliphatics as opposed to the typical relative accumulation in N-components in most of the other sites (Fig. 2.3; Supplementary Fig. 2.3). Such a differential accumulation of aliphatics is typical for higher root inputs from vascular plants (Schellekens et al., 2014), or – as evidenced in tropical peats and acid mineral soils – a preferential decomposition of lignin over highly resistant aliphatic biopolymers after polysaccharides are depleted (Vancampenhout et al., 2009; Schellekens et al., 2015a). Atlantic fen sites were typically richer in nutrients (Kreyling et al., 2021) and Drentse Aa, Binnenveld en Zwarte Beek were also rich in iron, which may have amplified effects of drainage, but more research is required to confirm on the importance of these potential contributing (Aggenbach et al., 2013; Emsens et al., 2016).

The upper layer of the peat profiles (0-5 cm) showed a similar increase in pyrolysis products indicative for increased aerobic decay (Fig. 2.3), although the effects were attenuated by the large share of (living) unaltered plant material typically observed in the upper strata of peatland profiles. As such, shifts in inputs caused by a changing vegetation composition will most likely be a dominant process in this layer (Dehmer, 1993; Biester et al., 2014; Klein et al., 2022).

In Fig. 2.6, changes in molecular composition following drainage are combined with environmental variables to further elaborate underlying processes. Dissimilarity distances were significantly positively correlated with bulk density, confirming that alteration of fen molecular

composition concurs with shrinkage, compaction, and consolidation upon peat drying (Sinclair et al., 2020). The positive correlation to $\delta^{15}N$ indicates that its enrichment relates to higher microbial degradation favoured by oxic conditions (Klein et al., 2022). Likewise, dissimilarity distances between undrained and drained fens were negatively correlated with C:N ratio, implying a typical increased carbon loss due to oxic respiration, but no correlation with $\delta^{13}C$. This implies that drainage-induced changes may have been affected by other factors such as temperature, humidity, water table and plant species, which could interrupt or obscure the signal of degradation process on such proxies (Biester et al., 2014; Schellekens et al., 2014; Zeh et al., 2020).

2.4.3. Rewetting can only partly restore fen below-ground processes over time, and restoration trajectories differ among sites

While undrained fens were significantly different in terms of molecular composition from drained and rewetted plots, the rewetted plots showed no significant differences from drained plots (

Table 2.2, Fig. 2.3), and no specific pyrolysis products differ rewetted from drained plots (Fig. 2.5C). This is in line with the formation and accumulation of peat being a very slow process (Rydin and Jeglum, 2006) and the statement postulated by Emsens et al., (2020), Kreyling et al., (2021), and Loisel and Gallego-Sala, (2022) that not all of the peatland ecosystem services and functions can easily be restored. Heterogeneity in the dataset due to site-specific factors, subsidence or different time-since-rewetting may further contribute to the lack of significance when the overall dataset is considered.

More specifically, the difference is largest in the second layer, where the shift from anaerobic to aerobic decay was most extreme upon drainage (see Fig. 2.3 and section 4.2). The molecular composition of this layer in the rewetted sites was intermediate between those of undrained and drained sites, showing that below-ground processes in at least some of the rewetted sites gradually shift back to those of the undrained sites, mainly the ones with the longer time

since rewetting (Fig. 2.3; Fig. 2.7). Indeed, subsequent correlative analyses revealed a converging of molecular dissimilarity in the second layer of fens that have been rewetted for over 30 years (Fig. 2.7). Rewetting caused contrasting responses in the 0-5 cm layer, with strong relative increases in certain carbohydrates in some sites from the western Atlantic regions, mainly Zwarte Beek, Binnenveld and Drentse Aa. This change is less evidenced for the other sites and may be to the high iron content or a strong growth of vascular plants upon rewetting in some sites (helophytisation, Kreyling et al., 2021). Intriguingly, the sites that deviate in the restoration trajectory of the upper layer also showed the unusual accumulation of aliphatics in the second layer upon drainage (see section 4.2), which supports the hypothesis of helophytisation, as necromass of increased vascular root systems would introduce isuberan-like structures that produce (predominantly even-numbered) mid-chain alipahtics upon pyrolysis (Nierop et al., 1999; Schellekens and Buurman, 2011), that alternate restoration trajectories may exist depending on site properties.

These results suggest that alternate restoration trajectories may exist depending on site properties, and that below-ground restoration can re-establish processes similar to the natural peat development occurring in undrained fens, however full recovery to the original state may not be achievable in all cases. In any case, below-ground restoration at molecular level requires considerable time, and strong hydrological legacy effects persist for several decades (Fig. 2.7). From the perspective of ecosystem stability, the greater variability observed in drained and rewetted sites compared to undrained sites in the ordination analyses (Fig. 2.3) moreover suggests reduced predictability in their responses to the external forces. This variability also implies a declining degree of self-regulation (Dakos and Kéfi, 2022). Consequently, the observed oscillation indicates that these two hydrological status not only exhibit lower stability, but also more susceptible to extreme climatic perturbances than undrained fen sites (Folke et al., 2004; Kreyling et al., 2021).

As such, our data evidence that rewetting can be considered an effective –albeit slow- restoration method for reviving belowground processes and carbon dynamics, but restoration outcomes may be context dependent. A detailed identification of tipping points or shifts between different belowground restoration trajectories and their implications for ecosystem stability is an important scope for further research, as it will help set restoration targets and monitoring needs and predict and improve future outcomes of fen rewetting (Scheffer and Carpenter, 2003).

2.5. Conclusion

This study provides empirical evidence of how SOM molecular composition shifts in response to hydrological status and, in turn, influences the trajectory of restoration in European fens. In particular, changes in molecular composition play a crucial role in ecological resilience by affecting peat structural integrity, microtopography, and hydrological conductivity. Rewetting drained fen peatlands to the original water level induces a positive dynamic; but does not achieve full restoration within a short timeframe and the restoration trajectory is context dependent. Hydrological legacies, such as aerobic decomposition and newly added vegetative compounds into the molecular composition, likely contribute to the observed irreversible changes at the molecular level within peat. Consequently, this study suggests that while rewetting is an effective restoration method for reviving belowground process and carbon dynamics, it requires clearly defined restoration targets and continuous monitoring as fen rewetting outcomes are time and context dependent.

Acknowledgements

The authors gratefully acknowledge the assistance of Yannick Stroobandt, Lore Fondu, Kim Vekemans, Eva de Rijke, Myrthe van der Kolk and Sascha Nijdam for their contribution to the sample handling procedure, equipment operation and training, and for sharing their expertise to enhance workflow. This research was funded by the Research Foundation Flanders (FWO-G060721N). Sample acquisition was supported by BiodivERsA COFUND, the Polish National Science Centre (NCN, 2016/22/Z/NZ8/00001), the Deutsche Forschungsgemeinschaft (DFG JO 332115) and Belspo (BR/175/A1/XXX-BE REPEAT).

3

Mid-infrared spectroscopy as a tool to monitor molecular changes in fens upon restoration

Based on : Kim, K., Aernouts, B., Emsens, W.-J., Schellekens, J., Van Diggelen, R., Aggenbach, C., Verbruggen, E., Jansen, B., Briones, M.J.I., Vancampenhout, K., 2026. Mid-infrared spectroscopy as a tool to monitor molecular changes in fens upon restoration. Organic Geochemistry 214, 105154. https://doi.org/10.1016/j.orggeochem.2026.105154

Abstract

Peatlands are crucial components of the global carbon (C) cycle but have been extensively degraded by drainage. Rewetting is a common practice to restore drained peatlands, yet its effectiveness and impacts on belowground soil organic carbon (SOC) dynamics remain uncertain. To effectively monitor restoration outcomes, affordable, time-efficient, and informative tools are essential. Pyrolysis-gas chromatography/mass spectrometry (py-GC/MS) provides detailed soil organic matter (SOM) characterization, but its high cost, time-intensive nature, and technical complexity limit its routine use. In contrast, mid infrared (MIR) spectroscopy, combined with chemometrics, can offer a promising alternative. This study evaluated the potential of MIR spectroscopy for: (1) reproducing the relative contribution of chemical groups as derived from py-GC/MS, (2) estimating SOC decomposability, and (3) monitoring belowground changes when undrained peatlands are drained or drained peatlands are rewetted. Our results indicated that MIR spectroscopy can effectively estimate specific chemical groups, including benzenes (R^2_P = 0.89), carbohydrates (R^2_P = 0.85), N-containing compounds (R^2_P = 0.76), and n-alkenes (R^2_P =0.74), with fair predictions for lignins (R^2_P = 0.68) and phenols (R^2_P = 0.64). SOC decomposability, expressed as basal respiration per SOC, was also reasonably estimated (R^2_{CV} = 0.74). MIR spectra significantly differed between undrained and drained fens (P <0.05), whereas rewetted fens did not differ from either condition (Ps > 0.05). Partial least squares−discriminant analysis further identified the functional groups most responsive to hydrological changes. Overall, MIR spectroscopy represents a cost- and time-efficient tool for assessing SOM composition and carbon stability in fens, supporting data-driven peatland restoration strategies.

Key words: Carbon persistence, Soil organic matter, Mid-infrared spectroscopy, Pyrolysis-GC/MS

Highlights

- MIR spectroscopy can predict the relative contributions of specific chemical groups.
- MIR spectroscopy can estimate peat and individual SOM functional group decomposability.
- MIR spectroscopy can detect belowground SOM changes following fen drainage and rewetting.
- MIR spectroscopy offers a cost- and time-efficient approach for monitoring fen restoration.

3.1. Introduction

Despite covering only 2−3 % of the Earth's land surface, peatland soils are estimated to contain 600−650 Gt C, approximately one-third of the world's soil carbon stock (Yu et al., 2010; Heller et al., 2015; Kreyling et al., 2021). Pristine peatlands act as net C sinks as the rate of soil organic matter (SOM) decomposition is slow relative to photosynthetic C inputs, which is primarily due to anoxic conditions, low temperature, low pH and high refractory content of plant remnants, which restricts microbial activity (Pengerud et al., 2013; Dieleman et al., 2015; Fenner and Freeman, 2020).

However, despite their crucial role in C sequestration at local and global scales, peatlands have been substantially degraded by anthropogenic activities and their coverage area has been rapidly diminishing over the last couple of centuries, with an estimated loss of about 80 % of current peatlands worldwide (Joosten and Clarke, 2002; McAnallen et al., 2017; Loisel and Gallego-Sala, 2022). Main contributors to this accelerated loss are drainage for agricultural use or forestry, and peat extraction (Meyer et al., 2014; Dieleman et al., 2015; Upton et al., 2018; Lehmann et al., 2020; Zak and McInnes, 2022). Drainage alters peat hydrology, aeration, vegetation cover, and organic decomposition rates, leading to an increased release of C into the atmosphere and into aquatic systems, thereby shifting peatlands from net C sinks to sources (Morris et al., 2011; Günther et al., 2020; Dean et al., 2024).

Therefore, peatland restoration, particularly through rewetting, is increasing, as part of biodiversity incentives and C trading initiatives under the Kyoto protocol (Kitson and Bell, 2020; Loisel and Gallego-Sala, 2022). Rewetting involves physical interventions such as ditch blocking and reprofiling to raise water levels, with the primary aim to restore pivotal ecological functions (Zak and McInnes, 2022). Restoration through rewetting significantly reduces net CO_2 emissions and could, in some cases, result in the reemergence of typical peatland species within a relatively short time span (Leifeld and Menichetti, 2018; Günther et al., 2020). The recovery of belowground

dynamics, including edaphic properties, processes and soil biota, however, is much slower and rewetting results are more variable (Lai, 2009; Rodriguez et al., 2021; Groß-Schmölders et al., 2022). The quality of SOM substrates, along with their physicochemical properties, play a crucial role in regulating microbial activity and abundance, subsequently influencing soil organic carbon (SOC) decomposability and microbial processes related to carbon sequestration and greenhouse gas emissions (Gholizadeh et al., 2013; Urbanová and Bárta, 2016; Jamaluddin et al., 2024). Despite these insights, the post-drainage and post-rewetting C dynamics largely remain enigmatic and difficult to assess, yet they may significantly impact restoration outcomes and determine the vulnerability of peatlands to future disturbance (Forouzangohar et al., 2015; Heller et al., 2015; Matamala et al., 2017; Günther et al., 2020; Baysinger et al., 2022). Hence, to evaluate the long-term success and sustainability of peatland restoration, it is important to closely monitor and quantify below-ground C dynamics, peat vulnerability, and overall soil functioning in response to restoration strategies.

Pyrolysis-gas chromatography/mass spectroscopy (py-GC/MS) is a reliable technique to obtain the molecular composition of SOM with high analytical detail (Klein et al., 2022; Abdelhady et al., 2024). It has been widely used to elucidate SOM decomposition process and belowground dynamics upon peatland drainage and rewetting (Schellekens et al., 2009; Ninnes et al., 2023; Kim, 2026). Vulnerability of peatlands to future damage can moreover be assessed through chemical methods, such as SOM molecular composition via py-GC/MS, or biological methods, such as CO_2−C evolution during laboratory incubations (Schmidt et al., 2011). However, the use of py-GC/MS and incubation studies is technically demanding and costly, limiting their potential for large-scale monitoring (Ng et al., 2022; Ninnes et al., 2023). Furthermore, as the number of samples that can be processed is limited, our knowledge of peatland C dynamics is based on a very limited number of researched sites, potentially yielding biased results that may not accurately reflect reality at a regional or landscape scale (Brosens et al., 2021). Consequently, advances in peatland carbon dynamics' research face fundamental challenges in balancing the cost

of powerful analytical tools against the high temporal and spatial sampling resolution needed for designing and monitoring peatland conservation and restoration efforts (Ninnes et al., 2023).

As an alternative, Fourier transformed infrared spectroscopy in the mid-infrared region (4000−400 cm^{-1}), also referred to as MIR spectroscopy, is a high-throughput, low-cost, non-destructive, and reproducible analytical method for assessing soil carbon stocks (Forouzangohar et al., 2015; Kunarso et al., 2025). By analysing the reflected wavelengths corresponding to vibrations of specific molecular bonds in a soil sample, MIR can be used to deduct SOM functional groups and thus offers a potentially scalable alternative for studying molecular dynamics in soils (Peltre et al., 2014; Moinet and Millard, 2020; Ng et al., 2022). However, the interpretation of highly resolved spectra from MIR spectra is complex as vibrations of different functional groups and bonds may overlap in the same wavenumber region, especially when mineral material is present in the samples (Peltre et al., 2014).

Combining MIR spectra with chemometric methods, such as multivariate regression and classification models, can overcome these challenges by providing both high sampling resolution with analytical details, while addressing spectral overlap issues (Rumpel et al., 2001; Aernouts et al., 2020). This approach has been widely used as a screening tool for examining several soil characteristics in mineral soils (Forouzangohar et al., 2015; Ma et al., 2024). However, its applicability to peat samples remains uncertain, as peat is characterised by high C content (typically > 40−50 % C on a dry-mass basis) and a distinct chemical composition that may not be directly transferable to existing models developed for mineral soils (Teickner and Knorr, 2022). Moreover, the effectiveness of MIR spectra in assessing the relative contribution of chemical groups and C stability is still unclear, which raises questions about its efficiency as a monitoring tool for peat restoration (Heller et al., 2015; Helfenstein et al., 2021; Martínez Cortizas et al., 2021). Therefore, further evaluation of the integration of MIR spectra with advanced chemometric analyses is essential for its effective application in peatland recovery monitoring, as it may offer

high sampling resolutions together with detailed analytical insights into peatland vulnerability (Peltre et al., 2014; Barthès and Chotte, 2021; Ng et al., 2022).

In this study, we assessed the potential of MIR spectroscopy combined with chemometric modelling as a rapid yet reliable technique for peatland research and monitoring. To achieve this, we compared MIR spectra with molecular data obtained via py-GC/MS for the same samples (Kim et al., 2026b) alongside indicators of peat decomposability derived from lab incubations. This study encompassed samples from undrained, drained and rewetted sites from 13 fen peatlands across Europe. As such, we evaluated if MIR spectra could provide an avenue to (1) assess the relative contribution of chemical groups in fen samples, (2) predict the vulnerability of fen samples to decomposition and if so, infer information about labile functional groups, and (3) detect belowground changes in fen SOM composition upon drainage or rewetting of fen peatlands.

3.2. Materials and methods

3.2.1 Site description and peat sampling

Peat soils were sampled in 13 lowland groundwater-fed fen regions across a longitudinal transect from western to eastern Europe−United Kingdom (Anglesey), Belgium (Arlon, Zwarte Beek), The Netherlands (Binnenveld, Drentse Aa), Germany (Gützkow, Peene Mouth, Kiel, Recknitz) and Poland (Biebrza, Rospuda, Suwalszczyzna, Mazury)−in June 2017, as described in detail elsewhere (Emsens et al., 2020; Groß-Schmölders et al., 2022). Briefly, three fen sites with different restoration status (undrained, drained, and rewetted fens) were selected in each of the 13 regions, resulting in a total of 39 sites. Site identification of restoration status was determined based on field observations (e.g. water level data and current/present vegetation), information by the management and historical archives (Emsens et al., 2020; Groß-Schmölders et al., 2022). At each site, five peat subsamples were collected using an auger and homogenised into a single composite sample. This process was repeated at three depths (0−5 cm, 15−20 cm, and 45−50 cm), resulting in a total of 117 composite peat samples. Freshly collected peat samples were stored deep-frozen to prevent biogeochemical or molecular changes. For subsequent analyses, the frozen peat samples were oven-dried at 55 °C for 72 hours.

3.2.2. Pyrolysis-gas chromatography/mass spectroscopy (py-GC/MS)

The py-GC/MS method and results are described in detail in Kim et al., (2026). In brief, samples were pyrolyzed without prior solvent extraction, as to avoid potential biases in the relative abundances of key compound classes (Schellekens et al., 2009; Jansen and Wiesenberg, 2017). Upon calibration with pilot samples to determine the appropriate sample mass, dried bulk samples were weighted up to 200 µg for pyrolysis. The samples were then processed using a multi-shot furnace pyrolizer (EGA/Py-3030D; Frontier Lab, Japan) with an AS-1020E auto-sampler, coupled to a Thermo Scientific Trace 1300 gas chromatograph (GC; Milan, Italy) with an Rxi-1 ms fused silica column (Restek: 30m; 0.25 mm i.d.) at the IBED laboratory (University of Amsterdam, The

Netherlands). The processing of pyrolysis data was performed with untargeted GC-MS workflow in MZmine3 and NIST MS search v2.3 software (Schmid et al., 2023). Quantified pyrolysate abundances (i.e., peak areas) were normalized by percentage before following downstream analyses, and used here according to percentages of chemical groups, including n-alkanes, n-alkenes, benzenes, carbohydrates, lignin products, methyl ketones, N compounds, phenols, unspecified aliphatics, and unidentified compounds.

3.2.3. Basal respiration CO_2 and SOC decomposability

The method presented here follows the procedure described by Dettmann et al., (2021). Two grams of peat were aerobically incubated in 250 ml jars at 21 °C for 105 days (15 weeks), with four replicates per composite sample. Water filled pore space (WFPS) was adjusted to 60%. Peat weight and WFPS were determined through a preliminary test where various peat weight and WFPS were tested to ensure maximal microbial activity. The necessary amount of water, the porosity (Φ) of the dry sample was calculated as follows:

$$\Phi = 1 - \frac{\rho_{loose}}{\rho_s}$$

Where ρ_{loose} (g cm^{-3}) is the bulk density of the loose sample (i.e., dry sample) and ρ_s (g cm^{-3}) is the particle density (Säurich et al., 2019). The ρ_s for organic soils was estimated by formula given by Bohne (2005):

$$\rho_s = 0.086 \times AC + 1.44$$

where AC (%) is the ash content of the sample. Ash content was determined by igniting dried samples in a muffle furnace at 550 ºC until complete combustion of organic matter. The remaining inorganic residue was then weighted, and ash content was calculated as a percentage of the initial dry mass. The amount of CO_2 emitted was measured using a gas analyser (PBI Dansensor; Checkpoint II Portable Gas Analyser, Ringsted, Denmark). Carbon degradability was calculated using the following equation:

$$F = \left(\frac{dC}{dt}\right) \times \left(\frac{P \times V}{R \times T \times m}\right) \times 1M \times k \times \left(\frac{1}{SOC}\right)$$

where F is the CO_2 flux (SOC degradability; μg CO_2−C g SOC^{-1} day^{-1}), dC/dt is the slope of a simple linear regression (μm^3 m^{-3} h^{-1}), P is the pressure of the gas (Pa), V is the headspace volume of the jar (m^3), R is the gas constant (m^3 Pa K^{-1} mol^{-1}), T is the temperature of the gas (K), m is the peat mass (g $peat^{-1}$), M is the atomic mass of C (12.01 g mol^{-1}), SOC is the fraction of peat organic carbon per peat (g SOC^{-1} g $peat^{-1}$) and k is a conversion factor for the flux unit (from g CO_2−C g SOC^{-1} h^{-1} to μg CO_2−C g SOC^{-1} day^{-1}). The cumulative of CO_2 basal respiration divided by SOC was used as an indicator of the fraction of labile SOC (SOC decomposability; Supplementary Fig. 3.1; Supplementary Fig. 3.2). Based on the assumption that the SOC decomposition at a depth of 15−20 cm would be intermediate between that at 0−5 cm and 45−50 cm, only samples from two depths (0−5 cm and 45−50 cm) were selectively monitored throughout the incubation period.

3.2.4. Mid-infrared spectroscopy

MIR spectra were used to predict py-GC/MS-derived chemical groups by multivariate regression models and extract detailed information on peat molecular structure. Dry peat samples were finely ground using ball-mill machine (Pulverisette 7, FRITSCH, Germany). The ground samples were re-dried prior to scanning in the mid-infrared region (FrontierTM with auto-sampler from PerkinElmer, Waltham, MA, USA) to minimize spectral interfere from residual moisture. Spectra were obtained in % reflectance mode between 4000 and 400 cm^{-1} (wavenumber) at a resolution of 1 cm^{-1} with 32 accumulations, and four replicate scans were averaged for each spectrum. To prevent signal drift, the reflectance of the scanned samples was divided by the average of the background samples (Brosens et al., 2021). The spectra were firstly converted from reflectance (R) to absorbance (A) unit by A=log(1/R).

3.2.5. Statistical analyses and modelling

MIR spectral preprocessing, which is commonly used to improve spectral quality for multivariate analysis, was applied differently depending on the necessity for interpreting model (Supplementary Fig. 3.3; Aernouts et al., 2020). For the first research question, extensive spectral preprocessing, including wavenumber selection, was applied to improve the accuracy of the predictive model (Aernouts et al., 2020; Brosens et al., 2021). In contrast, for the last two research questions, minimal spectral preprocessing was applied to preserve interpretability for spectra as excessive preprocessing can complicate the interpretation of model coefficients. Here, for minimal preprocessing, spectra were smoothed using the Savitzky−Golay algorithm with a window size of twenty-one, followed by mean-centering across entire spectral range (Savitzky and Golay, 1964; Peltre et al., 2014). All statistical analyses and visualization were performed using R 4.2.3, and significance for statistical tests was accepted at $P < 0.05$ (R Development Core Team, 2025). We uploaded all code and data used in this study via Zenodo and GitHub, where they are openly available (Kim, 2025).

3.2.5.1 PLS regression on MIR spectra to predict py-GC/MS outcomes

PLS regression models were developed to predict the py-GC/MS-derived SOM molecular composition using the MIR spectra (Supplementary Fig. 3.4). Spectra and paired py-GC/MS-derived SOM molecular composition datasets were split into calibration and independent validation datasets in a ratio of 80:20 (calibration, n = 91; independent validation, n= 26) based on balanced group indices (restoration status × depth; Supplementary Fig. 3.3). The spectral preprocessing of the MIR spectra was: (1) moving average with a window size of twenty-one; (2) average of the first derivative; (3) average of the second derivative; (4) a first-, (5) second-, and (6) no-derivative Savitzky-Golay with a second order polynomial filter and twenty-one window length; (7) multiplicative scatter correction; (8) standard normal variate; (9) standard normal variate – detrend; (10) raw spectra (mean-centered). Thereafter, orthogonal signal correction (OSC)

was applied in two conditions−once with OSC and once without−resulting in a total of 20 distinct preprocessing combinations. With MIR preprocessed spectra, PLS regression with up to 20 latent variables was built to predict the fraction of each summed chemical group derived from py-GC/MS. The best performing preprocessing was selected based on the root mean square error of cross-validation ($RMSE_{CV}$) of the PLS regression models in a group-wise (nested) cross-validation at the region level to prevent information leakage. Moreover, the preprocessing that produced the most parsimonious model (i.e., lowest number of latent variables) was selected, provided it was not significantly different than the model with the lowest $RMSE_{CV}$. The significance test was performed with a one-tailed paired T-test ($\alpha = 0.05$) on the squared residuals of the cross-validation predictions. The selected best preprocessing methods for each compound further applied on 4 different variable selection methods: (1) variable importance in projection; (2) jack-knife; (3) forward interval PLS; and (4) reversed interval PLS. The performances of these 4 PLS regression models were compared mutually and with the model that used all wavenumber, and the most parsimonious model but equivalent to the model (one-tailed T-test, $\alpha = 0.05$) with the lowest $RMSE_{CV}$ was selected under the same group-wise cross validation criterion. The selected combination model was further evaluated using permutation testing with 999 iterations to avoid overfitting. The final prediction model, together with the selected combination of spectral preprocessing techniques and the selected set of wavenumbers, was then applied to predict molecular composition in the independent validation set. Thereafter, the root mean square error of prediction ($RMSE_P$) was calculated for the validation set.

3.2.5.2 Partial least squares (PLS) regression on MIR spectra to predict SOC decomposability

A SOC decomposability model was developed with PLS regression using the MIR spectra of all 117 samples. As before, the number of latent variables was selected using a group-wise (nested) cross-validation with a region-level, based on a one-tailed test ($\alpha = 0.05$). The final

model was the one with the lowest latent variables whose $RMSE_{CV}$ was statistically equivalent to that of the model with the lowest $RMSE_{CV}$. The regression coefficients of the final model were used to study the effect of the labile or recalcitrant components in the MIR spectra. For instance, spectra with positive model coefficients represent more labile C characteristics (Peltre et al., 2014). The final model was used to predict the SOC decomposability for peat samples of the second peat layer, which were not measured during the incubation experiment. The effects of restoration status and depths on predicted and measured SOC decomposability were further tested by applying a linear mixed model with restoration regime and depth as fixed factors and the site as a random factor.

3.2.5.3. Spectra difference across restoration status

3.2.5.3.1. Permutational analysis of variance (PERMANOVA)

To examine the differences of SOM composition across restoration status × depth, MIR spectra based on Bray−Curtis dissimilarity indices were tested with permutation analysis of variance (PERMANOVA) with 999 iterations, using the function 'adonis' in R which included plot location as a blocking factor ('strata') to take into account for within-plot dependence of the three depths. For pairwise comparisons, P values were further adjusted using the false discovery rate procedure. Data visualizations were thereafter performed with nonmetric multidimensional scaling (k=2).

3.2.5.3.2 Partial least squares discriminant analysis (PLS-DA) across restoration status

To better differentiate spectra across restoration status, we applied PLS-DA. This is because unsupervised techniques such as principal component analysis (PCA; Supplementary Fig. 3.5) and nonmetric multidimensional scaling (NMDS) only highlight variation among the spectra, whereas PLS-DA maximizes the covariance between spectra and explanatory variables (i.e., restoration status), thereby improving classification. For the PLS-DA model, four models were

established: one for the full-depth, and a single model for each of the three individual depths: 0−5 cm, 15−20 cm, and 45−50 cm. To determine the optimal number of latent variables, a group-wise cross-validation approach was used, testing between 1 to 20 latent variables. The region was assigned as the group in the group-wise cross-validation. The final selection of model complexity was made by highest accuracy (lowest $RMSE_{CV}$), but the smallest number of latent variables, within the range of a one-tailed paired T-test ($\alpha = 0.05$) on the squared residuals of the cross-validation predictions. The classification performance of the model was further assessed using class-wise metrics (precision/recall, macro-F1) from confusion matrices, as well as receiver operating characteristic (ROC) curves and the area under the curve (AUC). A 95 % confidence interval (CI) for the ROC and AUC were calculated using 10,000 bootstrap replicates to achieve a fair estimate for the second significant digit (Fawcett, 2006). The regression coefficients of each final models for classification were, thereafter, studied to differentiate spectra across restoration status.

3.3. Results

3.3.1. Raw spectra of mid-infrared spectroscopy

The MIR spectra of all 117 peat samples showed similar absorption peaks with varying intensities (Fig. 3.1). A visual assessment of MIR spectra (peak identifications based on Peltre et al., (2014) revealed a completely different signal to most mineral soil samples (Fig. 3.1; Table 3.1). As expected for peat with a high organic matter content, our sample showed minimal mineral interference. Indeed, the sharp peak near 3620 cm^{-1}–typically attributed to the stretching vibration (ν) of O−H in clay minerals–was largely missing. Similarly, the triplet of quartz overtones usually found near 1990, 1870 and 1795 cm^{-1} was either absent or present at very low intensities, and only clearly observed in those samples collected from the deeper layers of Arlon, Binnenveld, and Zwarte beek. The broad peak between 3600 and 2800 cm^{-1}−attributed to ν_{O-H} of various origins, including water, alcohols, carboxylic acids, and phenols, as well as the ν_{N-H} from amide−was

visually comparable across samples. Its absorbance was the lowest in deeper samples, where quartz-related peaks were more prominent, particularly in the profiles from Arlon and Zwarte beek. The superimposed twin peaks at 2920 and 2850 cm^{-1} were visually found in all samples and attributed to the ν_{C-H} of methyl and methylene groups. The absence of the typical peak near 2500 cm^{-1} in all but three samples (originating from Gutzkow) confirms the high organic matter content of the majority of the samples investigated here. All samples had high absorbance between 1750 and 1210 cm^{-1}, a region referred to as the 'double bond region', where high absorbance is largely associated with organic matter (Le Guillou et al., 2015). Our samples also showed a broad band between 1750−1540 cm^{-1} representing overlapping vibrations of $\nu_{C=O}$ from carboxylic acids (1720−1710 cm^{-1}) and amides (1690−1570 cm^{-1}), and $\nu_{C=C}$ from aromatics or ν_{COO}- from carboxyl groups (1660−1570 cm^{-1}), that show more variability with hydrological changes. Signals in this region also include several amide bands attributed to N−H bending vibration (δ) at 1610 cm^{-1}, and N−H and C−H stretching vibrations at 1570–1540 cm^{-1}, with a shoulder around 1515 cm^{-1} assigned to aromatic $\nu_{C=C}$ vibrations. The region between 1470 and 1200 cm^{-1} generally shows high absorbance in both mineral and organic samples. This is due to ν_{C-H} of aliphatic or organo-clay complexes as well as methyl (1465 cm^{-1}, 1445–1350 cm^{-1}). Superimposed on these were distinct signals from carboxylates (1373 cm^{-1}), a third amide band (1320–1230 cm^{-1}), and a shoulder at 1295–1220 cm^{-1} attributed to ν_{C-OH} from phenols and to the C−H in-plane from aromatics. This region consistently showed high absorption values in the case of the topsoil samples of undrained peat, while exhibiting great variability in the rest. Organic samples also had high absorbance in the region between 1170 and 1030 cm^{-1}, as organic samples usually have high ν_{C-O} from polysaccharides (1170−1060 cm^{-1}), nucleic acids and proteins as well as δ_{C-O} from carbohydrates at 1050 cm^{-1}. A ν_{Si-O} band from quartz was also found around 1100−1000 cm^{-1}, but this was typically lower and much sharper in mineral samples. Below 975 cm^{-1}, the region is dominated by mineral vibrations associated with clay, kaolinite, smectite, carbonates, quartz, and

iron oxides. This region also includes δ_{C-H} out-of-plane from aromatics and N−H wag frequencies of amine.

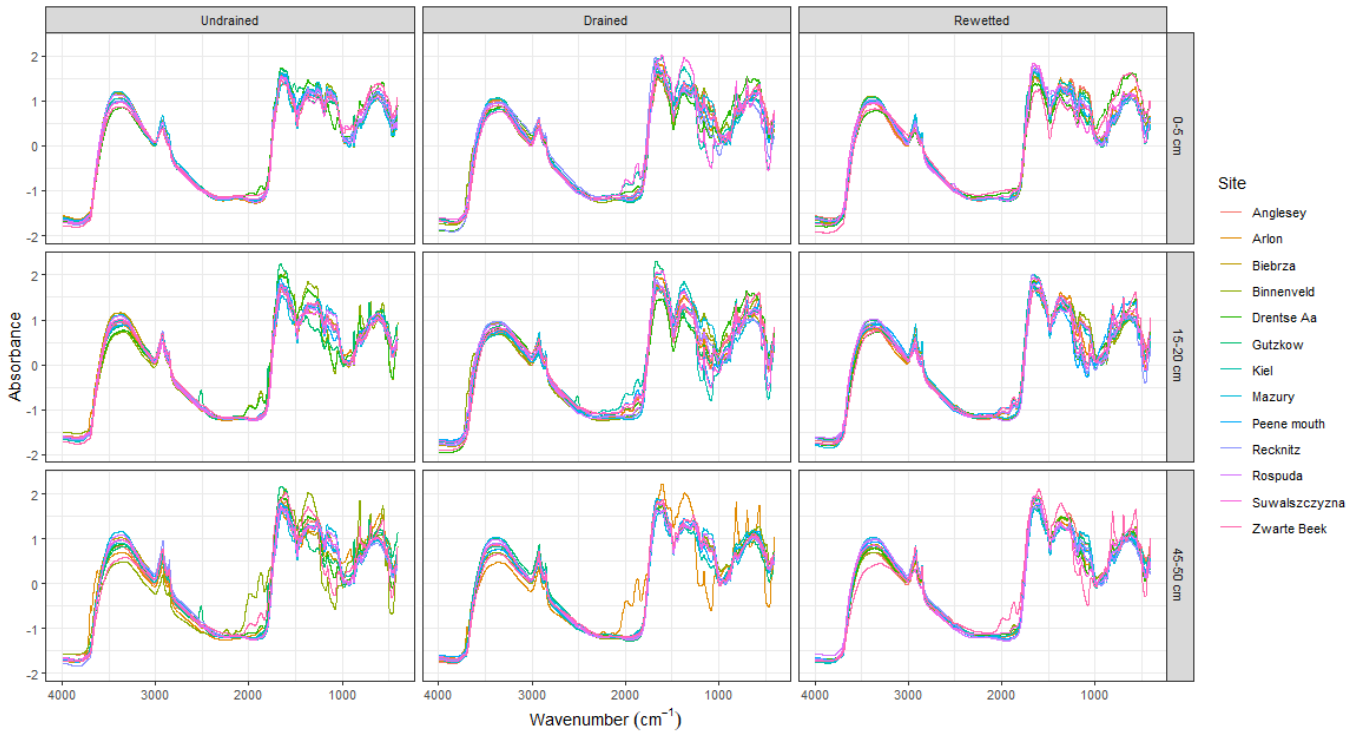


Fig. 3.1. Mid-infrared spectra of peat samples collected at three different depths from 13 regions under three restoration status. Spectra were pre-processed using Savitzky−Golay smoothing followed by standard normal variate transformation (n = 117).

Table 3.1. Conventional absorption band assignment of mid-infrared spectroscopy to functional groups or soil component based on the literature. ν indicates stretching vibration, while δ denotes bending vibration (adapted from Peltre et al., (2014); reproduction permitted as documented in supplementary material).

Wavenumber (cm^{-1})	Vibration	Functional group or component
3720−3580	νO−H	Clay minerals[a–e]
3600−2800	νO−H, νN−H	Water, alcohols and phenols; carboxyl and hydroxyl groups, amides[f–t]
3000−2800	νC−H	Aliphatic methyl and methylene group[f–t]
2560−2480	νCO_3^{2-}	Carbonates[f,k,o]
2200−2000	Overtone νCOH	Carbohydrates[n]
2000−1790		Quartz overtones[e]
1780−1710	νC=O	Carboxylic acids[f,j,l,n]
1690−1570	νC=O	Amides[d,l,n,o]
1660−1600	νC=C	Aromatics[i,j,m,o]
1630	νH−O−H	Clay-bound water[d,f]
1610	δN−H	Amine[d]
1600−1570	νC=C, νCOO^-	Aromatics[f,k,o], carboxylate[l]
1570−1540	νN−H and νC−H in plane	Amid II[i,l,o]
1515	νC=C	Aromatics[i,o]
1465	νC−H	Aliphatics[d], organo-clay complex[s]
1445−1350	νC−H	Methyls[d,n]
1430(1300−1500)	νCO_3^{2-}	Carbonates[d,f,r]
1373	νCOO^-	Carboxylate[n] (associated with BC in soil)
1320−1230	νC−N	Amid III[i,o]
1295−1220	νC−OH, C−H in plane	Phenols, aromatics[d,i,n,q]
1170−1060	νC−O	Polysaccharides[i], nucleic acids, proteins[i,m]
1100−1000	νSi−O	Silicates (quartz)[e,f,j,o]
1050	δC−O	Carbohydrate[d,i,n]
1030−950	νSi−O	Clay minerals[o,s]
975−675	δC−H out of plane	Aromatics[l,p,q,t]
915	δAl−H	Kaolinite and smectite[a,b,d]
875	C−O out of plane	Carbonates[o]
850−750	NH_2 out of plane	Primary amine[o]
800	Si−O	Quartz[e]
750−700	N−H wag	Secondary amine[o]
700	Si−O	Quartz[e]
700−600		Iron oxides[f]

([a]Madejová and Komadel, 2001; [b]Nayak and Singh, 2007; [c]Nguyen et al., 1991; [d]Rossel and Behrens, 2010; [e]Churchman et al., 2010; [f]Soriano-Disla et al., 2014; [g]Ellerbrock and Gerke, 2004; [h]Haberhauer and Gerzabek, 1999; [i]Calderón et al., 2013; [j]Pedersen et al., 2011; [k]Bernier et al., 2013; [l]Leifeld, 2006; [m]Movasaghi et al., 2008; [n]Janik et al., 2007; [o]Smidt and Meissl, 2007; [p]Niemeyer et al., 1992; [q]D'Acqui et al., 1999; [r]Du and Zhou, 2011; [s]Madejová, 2003; [t]Coates, 2006)

3.3.2. Pyrolysis GC-MS derived molecular composition prediction using MIR spectroscopy

Table 3.2 shows the performance metrics for the best models fitted for chemical groups as derived from py-GC/MS. Different spectral preprocessing methods (e.g., sgFirstDer sgSeconDer, snv_dt) and wavenumber selection (e.g., var.jack, ipls_forward, ipls_backward) were evaluated to achieve a high accuracy and robustness for the prediction of each chemical group. Permutation testing of the final models produced *P*-values < 0.001, confirming that the PLS models were statistically robust and not overfitted. Models were grouped into two categories based on performance in cross-validation and independent validation set (

Table 3.2;Supplementary Fig. 3.6; Supplementary Fig. 3.7). The first group had an R^2 values over 0.70 for both cross-validation and the independent validation set: n-alkenes, benzenes, carbohydrates, N compounds, and a group of two that showed an R^2 value < 0.70 for either cross-validation or independent validation: n-alkanes, lignin products, methyl ketones, phenols, unspecified aliphatics, and unidentified compounds. Detailed performance metrics values for MIR spectra prediction of pyrolysis chemical group proportions in both cross-validation and independent validation sets are presented in

Table 3.2, with visualization provided in Supplementary Fig. 3.6& Supplementary Fig. 3.7. In addition, to identify the spectral region contributing to each functional group, the model coefficients were projected and illustrated in Supplementary Fig. 3.8Supplementary Fig. 3.8.

Compounds	Pre-processing‖	OSC applied λ	Variable selection Φ	# of latent variables	Calibration (C)			Cross-validation (CV)			Validation (P)		
					$RMSE_C$ (%)	R^2_C	MAE_C (%)	$RMSE_{CV}$ (%)	R^2_{CV}	MAE_{CV} (%)	$RMSE_P$ (%)	R^2_P	MAE_P (%)
n-alkanes	sgSecondDer	-	ipls_forward	1	1.46	0.39	1.13	1.46	0.33	1.17	2.80	0.19	1.59
n-alkenes	snv_dt	-	ipls_forward	4	0.16	0.76	0.12	0.16	0.73	0.13	0.17	0.74	0.13
Benzenes	sgFirstDer	-	var_jack	2	1.86	0.83	1.28	1.89	0.81	1.43	2.17	0.89	1.70
Carbohydrates	snv_dt	-	var_jack	5	4.04	0.84	3.08	4.30	0.86	3.47	4.31	0.85	3.25
Lignins	sgFirstDer	-	ipls_backward	6	1.74	0.88	1.41	2.37	0.79	1.92	3.30	0.68	2.70
Methyl ketones	sgFirstDer	+	ipls_forward	1	0.47	0.41	0.36	0.47	0.47	0.38	0.53	0.24	0.44
N.compounds	snv_dt	-	ipls_forward	2	2.00	0.84	1.58	2.10	0.77	1.70	2.91	0.76	2.55
Phenols	sgFirstDer	-	var_jack	1	2.35	0.69	1.94	2.37	0.75	1.99	2.29	0.64	1.78
Unspecified aliphatics	sgFirstDer	+	var_jack	1	0.33	0.17	0.23	0.29	0.29	0.24	0.45	-0.07	0.34
Unidentified	sgFirstDer	+	ipls_forward	1	0.38	0.53	0.29	0.38	0.60	0.30	0.37	0.41	0.32

Table 3.2. Root mean squared error (RMSE), R squared (R^2) and mean absolute error (MAE) results for proportion of chemical group in peat, as determined by partial least squares regression models for calibration (C), cross-validation (CV), and validation dataset (P).

⁋ sgSecondDer, sgfirstDer, and, snv_dt stand for Savitzky-Golay second derivative, Savitzky-Golay first derivative, and standard normal variate−detrend, respectively

λ OSC denotes orthogonal signal correction; '+' indicates that OSC applied and '-' indicates that it was not.

Φ var_jack, ipls_forward, and ipls_backward mean jack-knife, forward interval PLS, and reversed interval PLS, respectively.

3.3.3. Peat SOC degradability prediction using MIR spectroscopy

Cumulative and daily SOC decomposability from raw data for two depths (0−5 cm and 45−50 cm) is presented in Supplementary Fig. 3.2. Cumulative CO_2 fluxes ranged from 0 to 547.9 μg CO_2−C g SOC^{-1} day^{-1}. Restoration status and depth significantly influenced cumulative CO_2 fluxes, with a significant interaction effect ($Ps < 0.05$). The cumulative CO_2 flux at a depth of 0−5 cm was significantly higher than that at the depth of 45−50 cm ($P < 0.05$; on average: 290.2 and 40.4 μg CO_2−C g $soil^{-1}$, respectively). In the first layer, undrained and rewetted fens exhibited significantly higher cumulative basal respiration compared to drained fens ($P < 0.05$; on average: 368.7 ,314.8, and 187.2 μg CO_2−C g $soil^{-1}$, respectively), However, at a depth of 45−50 cm, no significant differences were observed ($P > 0.05$).

The PLS regression model for SOC degradability yielded fair models using the two-depths dataset (R^2_{CV} = 0.74, $RMSE_{CV}$ =78.00 μg CO_2−C g SOC^{-1}, MAE_{CV} =59.07 μg CO_2−C g SOC^{-1}, Fig. 3.2A). The regression coefficients in Fig. 3.2B exhibited that the labile fraction of SOC was positively correlated with a broad band at 3600−3100 cm^1, ascribed to carboxyl and hydroxy groups of $\nu_{O–H}$ and amides of $\nu_{N–H}$. SOC decomposability was also positively correlated with a band at 1160, 1050 cm^{-1} attributed to ν_{C-O} cm^{-1} from polysaccharide, nucleic acids, protein. Conversely, the labile fraction of SOC was negatively correlated with aliphatic methyl and methylene groups of $\nu_{C–H}$ at 2920 and 2850 cm^{-1}, with carboxylic acid group of $\nu_{C=O}$ at 1700 cm^{-1}, with aromatics and carboxylate group of $\nu_{C=C}$, ν_{COO-} at 1570 and 1505 cm^{-1}, and with phenols and aromatics group of ν_{C-OH}, C−H in-plane at 1295 cm^{-1}.

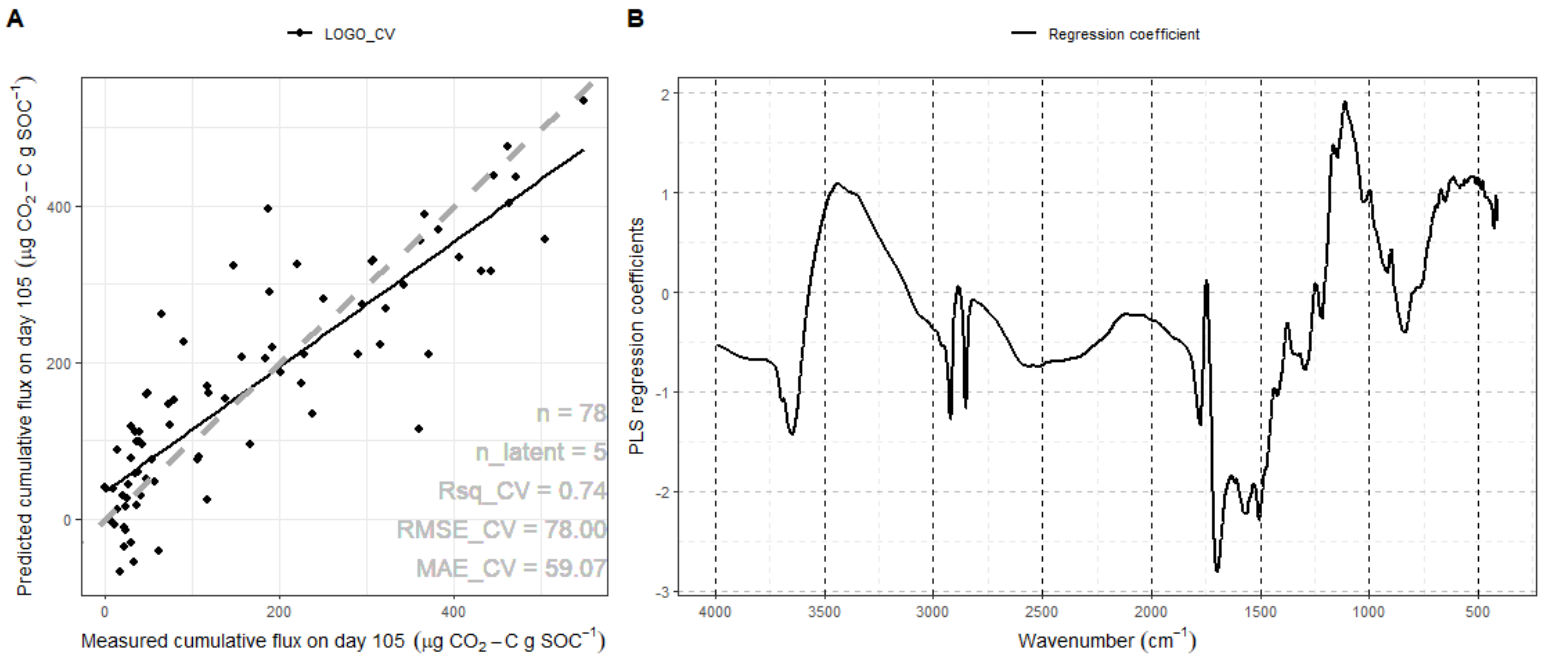


Fig. 3.2. Performance and coefficients of partial least square regression (PLSR) model for SOC decomposability. (A): Measured versus PLSR-predicted cumulative fluxes (i.e., SOC decomposability) at day 105 based on group-wise cross-validation (CV) predictions. Black dots represent individual samples, and the black line shows regression fit. Model performance metrics include n (number of samples), n_latent (number of PLS latent variables), Rsq (coefficient of determination), RMSE (root mean squared error), and MAE (mean absolute error). (B): Regression coefficients obtained for the PLSR model based on mid-infrared spectroscopy for SOC decomposability.

In the case of the intermediate peat layer (15−20 cm), predicted cumulative CO_2 fluxes from the PLS regression model did not differ significantly across restoration status ($P > 0.05$; Fig. 3.3). However, when integrating all peat layers, undrained and rewetted fens had a significantly higher cumulative basal respiration compared to drained fens ($P < 0.05$; on average: 160.2, 140.5, and 105.3 μg CO_2−C g $soil^{-1}$, respectively). The 0−5 cm peat layer showed the highest cumulative CO_2 flux followed by the 15−20 cm and 45−50 cm ones ($P < 0.05$; on average: 286.0, 132.3 and 52.3 μg CO_2−C g $soil^{-1}$, respectively).

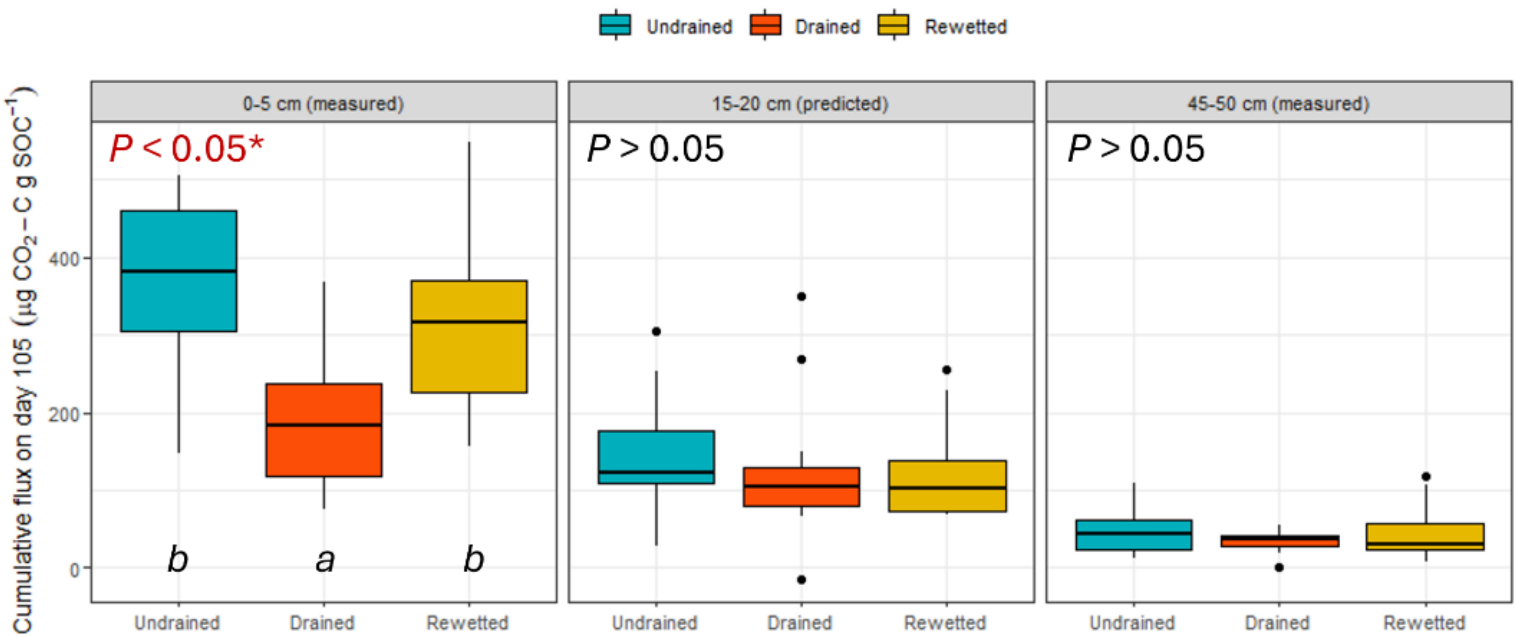


Fig. 3.3. Cumulative basal respiration per SOC (i.e., SOC decomposability) across restoration status (undrained, drained and rewetted) measured at two peat layers of 0−5 cm and 45−50 cm, with predicted values for the second peat layer of 15−20 cm.

3.3.4. Spectral differences across restoration status

The PERMANOVA analyses of the MIR spectra showed significant differences with restoration status ($R^2 = 0.047$, $F = 3.079$, $P < 0.05$) and peat depth ($R^2 = 0.082$, $F = 5.345$, $P < 0.05$), whereas their interaction between the two factors was not significant ($R^2 = 0.034$, $F = 1.110$, $P > 0.05$; Fig. 3.4; Supplementary Table 3.1). Differences across restoration status were most predominant in the top 0−5 cm layer ($R^2 = 0.139$, $F = 2.913$, $P < 0.05$), less so in the middle 15−20 cm layer ($R^2 = 0.134$, $F = 2.773$, $P < 0.05$), and nonsignificant in the deepest 45−50 cm layer ($R^2 = 0.008$, $F = 0.153$, $P > 0.05$). On average, the MIR spectra from rewetted fens did not differ from those of the undrained and drained fens ($Ps > 0.05$), while the spectra from undrained and drained fens were significantly different ($P < 0.05$; Supplementary Table 3.1).

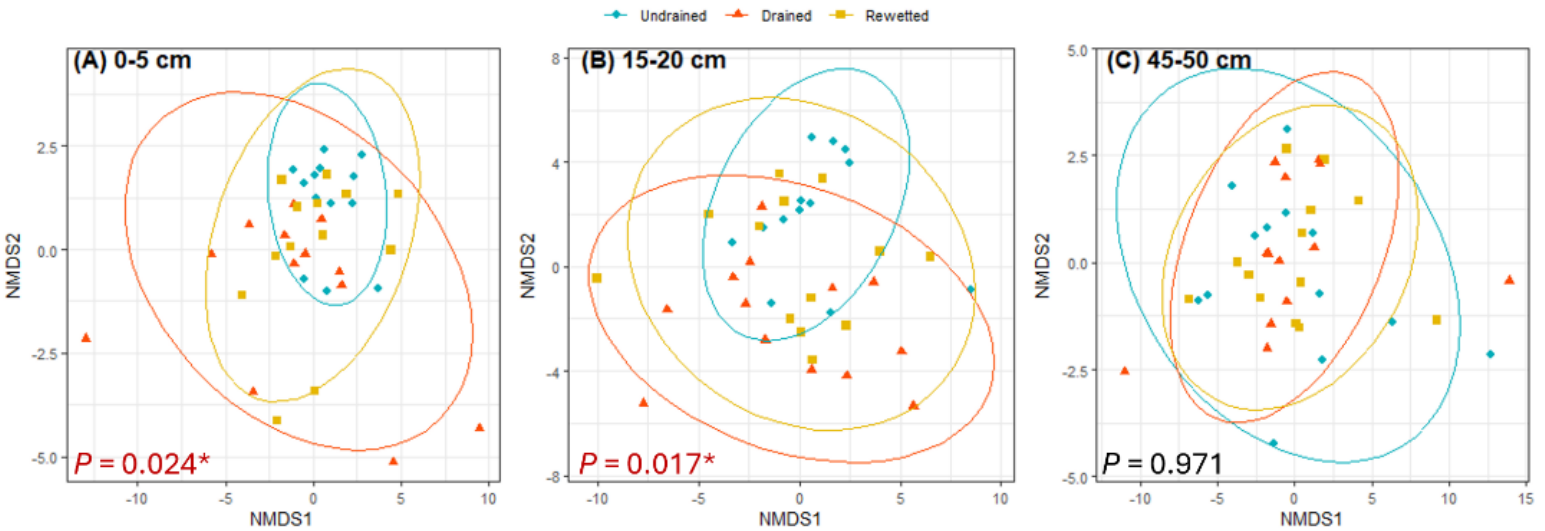


Fig. 3.4. Nonmetric multidimensional scaling (NMDS, stress = 0.089, 0.060, and 0.067, respectively) score plots of peat molecular composition based on the Euclidean distance at three drainage stages (undrained, drained, and rewetted) at three different depths (A: 0−5 cm; B: 15−20 cm; and C: 45−50 cm), in 13 fens across Europe. 95 % confidence ellipses are shown for each group. PERMANOVA indicates significant difference across restoration status for the first tow depths (0−5 cm: $R^2 = 0.139$, F =2.913, P = 0.024; 15−20 cm: $R^2 = 0.134$, F = 2.773, P = 0.017), but not for the deepest layer (45−50 cm: $R^2 = 0.008$, F = 0.153, P = 0.971; 999 permutation).

To identify spectral differences between undrained, drained and rewetted sites, PLS-DA was performed to maximize covariance between explanatory variables (restoration status) and response variables (MIR spectra). The PLS-DA with the optimal number of latent variables was finally selected for each depth models (A). The models produced a fair predictive accuracy for classification in a group-wise cross-validation: 0.53 for full-depth, 0.67 for the 0−5 cm layer, 0.59 for the 15−20 cm layer and 0.67 for the 45−50 cm layer, respectively (Supplementary Fig. 3.9A). The confusion matrix with class-wise metrics is provided in the Supplementary Table 2. Smoothed ROC curves and their AUC values for restoration status classification based on each model are shown in Supplementary Fig. 3.9B, with separate smoothed ROC curves for undrained, drained, and rewetted fens, respectively. For full depth, the AUC were 0.66 (95% CI: 0.55-0.76), 0.72 (0.63-0.80), and 0.58 (0.48-0.68); for 0−5 cm, 0.89 (0.79-0.95), 0.94 (0.89-0.97), and 0.60 (0.43-0.73); for 15−20 cm, 0.82 (0.68-0.94), 0.84 (0.73-0.93), and 0.46 (0.28-0.63); and for 45−50 cm, 0.82 (0.69-0.93), 0.81 (0.67-0.93), and 0.77 (0.61-0.88) for undrained, drained, and rewetted fens, respectively.

Since the separate peat depth models outperformed the full-depth model in terms of accuracy, the coefficients of each depth model will be described separately (Fig. 3.5). For the first two depths, the undrained fens were positively correlated with a broad band spanning 3500−3000 cm^{-1} that can be attributed to ν_{O-H} from water, alcohols, carboxylic acids, phenols and ν_{N-H} from amides, and two bands at 2850 and 2925 cm^{-1} attributed to ν_{C-H} from aliphatic, at 1225 cm^{-1} attributed to ν_{C-OH}, $_{C-H}$ in-plane from phenols, aromatics, at 1170 and 1080 cm^{-1} attributed to ν_{C-O} cm^{-1} from polysaccharide, nucleic acids, protein. In contrast, the undrained fens were negatively correlated with an absorption band at 3695 cm^{-1} likely attributed to ν_{O-H} from clay minerals, with a band at 1775 cm^{-1} linked to $\nu_{C=O}$ from carboxylic acids, and a band at 815 cm^{-1} linked to Si-O from quartz or NH_2 out of plane from primary amines. The drained fens showed the inverse relationship to those observed for the undrained fens. However, rewetted fens did not show distinctive coefficient values compared to the other two restoration treatments, likely due to the

model's low predictive accuracy for rewetted fens. The model for the deepest layer was complex, with rewetted fens being characterized by distinctive coefficient values below 500 cm^{-1}, corresponding to metal-O stretching from metal-oxygen (Fe-O, Al-O, Ti-O etc.). These bands were also dominant in drained fens. To verify whether the peat assignment may have been influenced by mineral content, we carefully examined the regression coefficient of the PLS model between ash content and MIR spectra (Supplementary Fig. 3.10).

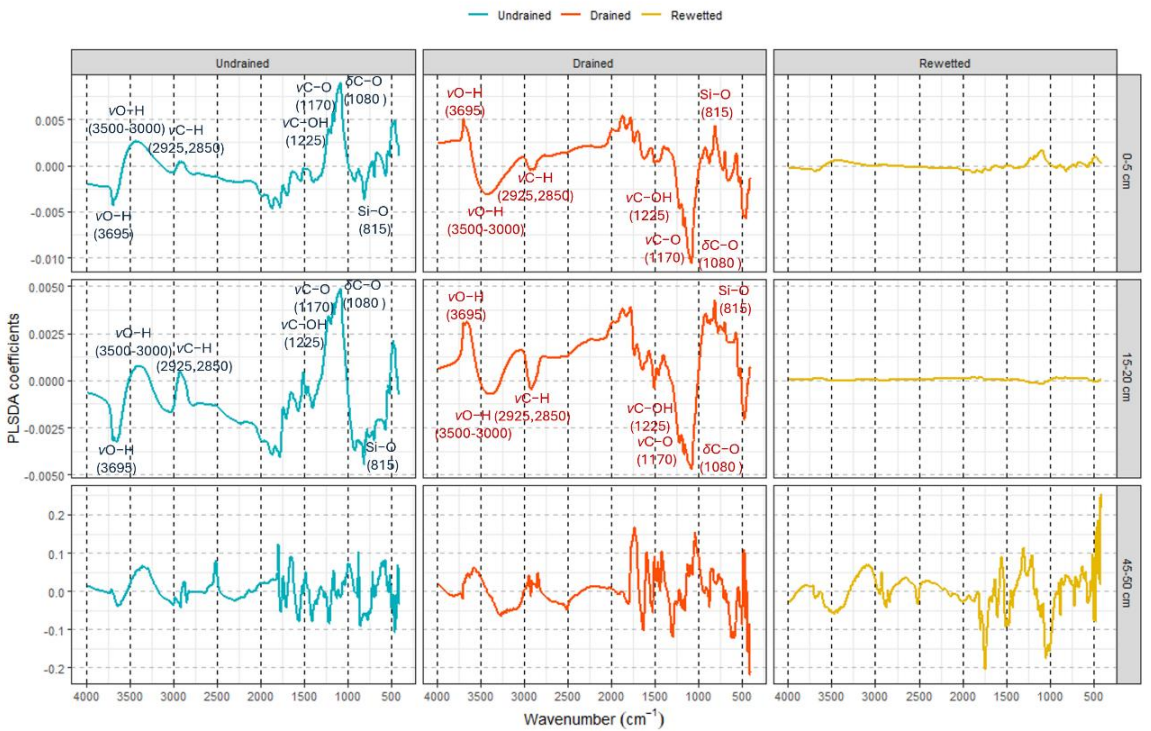


Fig. 3.5. Coefficients of the partial least squares discriminate analysis (PLS-DA) model based on three depth specific models (0−5 cm, 15−20 cm, and 45−50 cm) from mid-infrared spectra.

3.4. Discussion

3.4.1. Model performance for predicting molecular composition and stability

Previous studies mainly used MIR spectroscopy in peatlands to infer broad soil properties, such as total carbon or nitrogen contents (e.g., Helfenstein et al., 2021; Kunarso et al., 2025). Ninnes et al. (2023) successfully predicted the percentage of chemical groups obtained with py-GC/MS using MIR spectroscopy combined with PCA applied to Holocene sediment samples. Their findings showed well-aligned predictions when compared to reference data. In our study, we employed PLS regression to build models that maximize covariance between explanatory and dependent variables, along with diverse spectral preprocessing and wavelength selection to enhance prediction accuracy and robustness of the models. Also, independent validation was conducted to thoroughly assess model performance. Our independent validations indicated that our methodological approach has high potential for effectively estimating specific chemical groups in organic soils from fens, including benzenes (R^2_P = 0.89), carbohydrates (R^2_P = 0.85), N-containing compounds (R^2_P = 0.76), and n-alkenes (R^2_P = 0.74), with fair predictions for lignins (R^2_P =0.68) and phenols (R^2_P = 0.64). MIR spectroscopy also performed as a reasonable proxy for SOC decomposability according to basal respiration per SOC (R^2_{CV} = 0.74).

However, our model did not perform well when predicting n-alkanes, methyl ketones, or unspecified aliphatics. This is most likely due to the nature of the used analytical methods, as in MIR spectra, n-alkane groups along other aliphatic compounds are identified from less specific C−H vibrations that also occur in other molecules, leading to a low signal-to-noise ratio (Wang et al., 2019). In py-GC/MS, aliphatic compounds often yield similar but slightly different dominant mass fragments across batches (e.g., 57 or 71 m/z for n-$C_{19:0}$; n-$C_{20:0}$; n-$C_{21:0,}$ and related homologues; Buurman et al., 2005; Schellekens et al., 2009), which can cause difficulties in alignment for different batches. This resulted in the exclusion of some aliphatic compounds (see Kim et al., 2026 for more details), which may have contributed to the weaker predictive

performance for the aliphatic group. Mineral interference in our samples was relatively low to moderate (mean ash content 23.8 %, and median 17.1 %), confirming that the peat in our samples consists predominantly of partially decomposed, organic-rich materials (Loisel and Gallego-Sala, 2022). The predictive PLS model we developed was capable of selecting the most informative spectral features and encompassed extensive spectral preprocessing to minimize the interference with additional confirmation provided by the model coefficients.

3.4.2 MIR spectroscopy as a tool to evaluate restoration success in fens

The PERMANOVA results from MIR spectra revealed that MIR spectroscopy could detect significant differences between drained and undrained fens (P <0.05) and that rewetting is an effective restoration practice for returning drained fens closer to their original state, particularly with regard to their SOM molecular composition and peat C decomposability (Fig. 3.3&Fig. 3.4). Another important finding was that the effects of restoration status on SOM molecular composition decreased with peat depth, suggesting that drainage effects did not extend to deep layers. Despite drainage-induced aerobic decomposition, the deeper peat layer appeared to remain predominantly anaerobic. This depth-dependent stratification of SOM molecular composition across restoration status aligns with previous findings on microbial community composition and geochemistry (Emsens et al., 2020; Groß-Schmölders et al., 2022; Kim et al., 2026b). However, rewetted fens have not fully returned to their original state, given nonsignificant difference between rewetted and drained fens (P > 0.05) and the deviations of some rewetted fens from the expected recovery trajectory (Fig. 3.5). In line with this, variability in restoration timelines and the lack of a clearly defined post-rewetting trajectory may explain the limited ability of the MIR-based classification model to differentiate rewetted fens from either undrained or drained fens (Fig. 3.5). Importantly, confirming the restoration of identical compounds remains challenging due to the coarse analytical resolution of MIR spectra, and high-resolution techniques such as py-GC/MS may be necessary to validate detailed compositional recovery.

Our MIR results also suggest that the effects of hydrological changes on SOM molecular composition can translate to peat C decomposability. Undrained fens exhibited stronger ν_{O-H}/ν_{N-H} bands at 3500−3000 cm^{-1} and ν_{C-O} bands at 1170 and 1080 cm^{-1}, along with a weaker $\nu_{C=O}$ band at 1775 cm^{-1}, compared to drained fens. This spectral pattern implies higher carbohydrate contents in undrained fens, likely due to higher relative abundance of root biomass, root exudates, and other plant material inputs (Emsens et al., 2021). Drained fens, on the other hand, contain relatively more carboxylic acids due to enhanced oxidation upon drainage (Fig. 3.5; Table 3.1; Baldock et al., 1997; Ernakovich et al., 2015). Carbohydrates, with a higher nominal oxidation state of C, are theoretically more reactive and thus decompose faster than other compounds (Verbeke et al., 2022). In contrast, in drained fens, the spectral pattern indicates a higher abundance of carboxylates that are more resistant to biodegradation. These MIR-based interpretations are consistent with previous py-GC/MS findings (Kim et al., 2026b), indicating that MIR can capture similar shifts in molecular composition and underlying process. Notably, the decomposability of the altered functional groups under drainage also aligned with decomposability of C functional group inferred from the coefficients of the PLS model for SOC decomposability (Fig. 3.2B). Additionally, our MIR results also indicate that decomposability in peat can vary between individual compounds within certain functional groups, both under aerobic and anoxic conditions. For example, undrained fens displayed higher ν_{C-H} bands at 3000−2800 cm^{-1} compared to drained fens, suggesting a slightly greater decomposability of aliphatic compounds upon drainage (Fig. 3.5). Interestingly, this band was assigned as recalcitrant in the PLS model for SOC decomposability, reflecting a dominant contribution of more stable substrates in the aliphatic group (Fig. 3.2). The model, which was developed using data both 0−5 cm and 45−50 cm depths, accounts for both aerobic and anoxic decomposition processes and may emphasize the recalcitrance of aliphatic materials accumulated in deeper layers, where SOC decomposability was significantly lower than in the superficial layer. In other words, this suggests that aliphatic compounds accumulate under anaerobic conditions exhibit relatively high resistance to decomposition (Calderón et al., 2013;

Peltre et al., 2014), whereas aerobic decomposition due to drainage decreases the relative abundance of aliphatic compounds. In support of this, the higher intensity of the $\nu_{C\text{-}OH}$ band at 1220 cm^{-1} in undrained fens (classified as recalcitrant band in the PLS regression coefficient) reflects that phenolic and aromatic bands are relatively resistant under anaerobic conditions. Conversely, the lower intensity of the band at 815 cm^{-1} in undrained fens (classified as labile by PLS regression) indicates that these compounds decompose more readily under anaerobically than aerobically (Zeh et al., 2020; Klein et al., 2022). These findings corroborate that aliphatic, phenolic, aromatic, and nitrogenous compound exhibit highly different levels of vulnerability to oxic-anoxic conditions in fens (Lopes-Mazzetto et al., 2018; Klein et al., 2022).

3.5. Conclusions

Our study demonstrates that MIR spectroscopy holds great potential as a standalone tool for large-scale monitoring of SOC stability in peatland research, offering valuable insight into SOC dynamics under hydrological changes within restoration contexts. Our result further indicates that rewetting is an effective restoration for returning drained fens closer to their original state. Our approach successfully reproduced the relative abundances of specific chemical groups derived from py-GC/MS and not only estimated soil C decomposability but also revealed differences in the vulnerability of individual C functional groups, thereby enhancing the interpretation of peat C stability. Although differences in restoration timelines and the lack of a clearly defined post-rewetting trajectory have limited our models' ability to characterize rewetted fens, the marked spectral differences between undrained and drained fens−captured effectively by our predictive models−provide an insight into which functional groups should be evaluated to assess restoration progress through changes in peat constituents. While MIR spectroscopy does not offer the same level of analytical resolution as py-GC/MS, it remains a cost-effective, time-efficient, and informative tool for assessing the effectiveness of peat restoration interventions. Overall, this study underscores the utility of MIR spectroscopy in advancing peat-carbon research.

Acknowledgements

The authors gratefully acknowledge the assistance of Yannick Stroobandt, Lore Fondu, Kim Vekemans, Eva de Rijke, Myrthe van der Kolk, Sascha Nijdam, and Michel Bechtold for their help with the sample handling procedure, equipment operation and training, and for sharing their expertise to enhance workflow. This research was funded by the Research Foundation Flanders (FWO-G060721N). Sample acquisition was supported by BiodivERsA COFUND, the Polish National Science Centre (NCN, 2016/22/Z/NZ8/00001), the Deutsche Forschungsgemeinschaft (DFG JO 332115), Belspo (BR/175/A1/XXX-BE REPEAT), and Dutch OBN Knowledge Network (OBN-2016-80-NZ).

4

Peat collapse as a new threat to fen ecological stability: the case of Nature reserve De Zegge, Belgium[1]

[1] Keunbae Kim, Willem-Jan Emsens, Sam Ottoy, Judith Schellekens, Toon Deswert, Ellen Desie, Bart Muys, María J. I. Briones, Boris Jansen, Karen Vancampenhout

Abstract

Pristine fens play a critical role in carbon (C) sequestration and hydrological regulation, despite their global extent. They are undergoing widespread degradation, thereby potentially turning their function from C sink to source. Here, we investigated the drivers of the rapid peat collapse observed in several locations at the oldest Flemish nature reserve 'De Zegge', which represents an unheard form of fen deterioration, and an environmental warning signal. To assess how peat collapse may shift the system beyond an irreversible threshold, we (1) documented the extend of the phenomenon using e a light detection and ranging (LiDAR) digital terrain model; (2) compared mesofaunal, vegetative, physicochemical, and molecular characteristics across collapsed, adjacent non-collapsed and distant non-collapsed areas; and (3) conducted a mesocosm experiment to test potential collapse triggers−hydrological disturbances and hydro-chemical additions (control, ditchwater, and sulfate [SO_4^{2-}])−by calculating ecological stability metrics based on greenhouse gas (GHG) emissions. Peat collapse led to a rapid surface lowering and mudflat development in affected areas, alongside structural and functional shifts in mesofaunal, vegetation, physiochemical and molecular variables ($Ps < 0.05$). Both field observations and mesocosm results suggest that ecological stability can be compromised by the interaction between acute hydrological perturbation and increased sulfate concentrations as chronic stressors. These conditions stimulate peat decomposition by promoting microbially favorable environments, inducing shifts in the redox regime, increasing the availability of alternative electron acceptors, increasing pH, and enhancing nutrient release. This cascade of processes also led to increased spatial variability of stability metrics in mesocosm experiments and indirectly promoted CO_2 and N_2O emissions. Overall, this study provides new insights into long-term pedological shifts that compromise peat structural integrity and function in fens. Documenting these processes provides valuable guidance for site managers and policy makers to develop more targeted restoration strategies.

Keywords: Fens, Peat degradation, Sulfate, Greenhouse gas emissions, Sudden collapse

Highlights

- First documented case of peat collapse in a fen ecosystem in Western Europe.
- Peat collapse caused land flattening, losses in C stocks, and shifts in multiple peat properties.
- Molecular composition of soil organic matter can be an early warning signal for peat collapse
- Hydrological disturbance reduced peat stability through increased variation in GHG emissions.
- Sulfate released by bedrock weathering, most likely triggered by high N depositions upstreaming, decreases peat resilience to dry spells via rises in pH and nutrients
- High spatial variability under sulfate addition highlights the need for regular sulfate monitoring.

4.1. Introduction

Peatlands contain approximately one-third of the terrestrial soil carbon (C), estimated to be 600 ± 100 Gt, despite covering only c. 3% of the Earth's land surface (Gorham, 1991; Yu, 2012; Kirpotin et al., 2021). They play a critical role in the global C cycles and, when intact, function as net C sinks because rates of organic matter accumulation exceed those of decomposition (Dong et al., 2025). However, peatland integrity and functioning are increasingly threatened by anthropogenic disturbances and extreme climatic events (Campeau et al., 2017; Cadigan et al., 2022; Euskirchen et al., 2024). Prolonged drainage and more frequent drought events promote aerobic conditions, accelerating organic matter decomposition through oxidative processes (Freeman et al., 2001; Keiluweit et al., 2016). These perturbations typically result in gradual and relatively continuous peat C loss accompanied by surface subsidence (Leifeld et al., 2011).

Nevertheless, abrupt losses of soil strength and structural integrity have also been documented, leading to non-linear declines in surface elevation over the course of only a few months to a few years (Chambers et al., 2019). In contrast to gradual subsidence, this 'peat collapse' involves fragmentation of the wetland platform and the development of shallow dotted ponds or mudflats that progressively coalesce over time (DeLaune et al., 1994; Cahoon et al., 2003; Chambers et al., 2019). Such collapse events can trigger disproportionately large C emissions, loss of habitat, elevation changes and establishment of conditions beyond the lower limit of natural recovery. Peat collapse has therefore been considered as an emerging phenomenon indicative of a potential pedogenic regime shift, leading to an alternative stable state (Chambers et al., 2019).

To date, this specific type of shallow subsidence in organic soils leading to a loss of structural integrity and a decline in elevation over the cause of a few months or years (Chambers et al. 2019), and associated with biogeochemical changes rather than with erosion, permafrost

melt (Loiko et al., 2017) or the loss of the dome shape following logging or drainage (Kool et al., 2006), has been reported only in coastal marsh environments and mangroves, where it represents major mechanism of coastal peatland degradation (Cahoon et al., 2003; Radabaugh et al., 2021; Cadigan et al., 2022). To the best of our knowledge, no previous cases of sudden peat collapse have been reported in temperate inland fen systems.

Nevertheless, albeit being situated ca. 100 km from the nearest coastline, a break-up of the wetland platform and the emergence of small ponds was observed at two locations in the 'De Zegge' over the course of only a few months following a drought in 2018. De Zegge is an inland temperate groundwater-fed peatland ("fen") of 120 ha in the Campine area of Flanders belonging to the European Natura 2000 network (https://natura2000.eea.europa.eu); and one of the oldest, most important and highly protected conservation areas in Belgium (Fig. 1). This study, therefore, provides a critical opportunity to document the first occurrence of peat collapse in an inland fen, and investigate potential causes and underlying mechanisms, as to identify other inland fen areas that may be at risk as well as inform strategies aimed at curbing this rapid degradation. To date, land managers and scientists are often unaware that a system is progressing towards peat collapse until it has occurred (Lewis et al., 2016), making the identification of key diagnostic indicators of vulnerability for collapse an urgent knowledge gap (Chambers et al., 2019).

In marshes, several plausible drivers for peat collapse have been identified, including acute disturbances (e.g., hurricane activity, vegetation death or fire) and chronic stressors (e.g., sea level rise, hydrological changes, increased nutrient loads) or the combination of both, suggesting that peat collapse may not be a single process, yet may be a series of sequential or co-occurring, self-reinforcing processes, depending on context-specific conditions (Kool et al., 2006; Abbott and Jones, 2015; Chambers et al., 2019). In peatlands, the most common cause of peat loss are changes in hydrology, encompassing both (1) the lowering of the oxic-anoxic interface by drainage and (2) shifts in hydro-chemical properties by eutrophication or pollution (Radabaugh et

al., 2021; Laudon et al., 2023; Keith et al., 2023). Because peatland functioning is fundamentally influenced by hydrology, these changes strongly regulate decomposition processes. In particular, the intrusion of O_2 as an electron acceptor lifts important thermodynamic and enzymatic barriers (or 'latches', Freeman et al., 2001) to peat decomposition (Kool et al., 2006). O_2 intrusions are mainly linked to overall effects of drainage, droughts, or the intrusion of oxygen rich water, and generally lead to a wide peat subsidence rather than the local, rapid formation of small ponds associated to peat collapse, suggesting that other amplifying mechanisms may be at play (Robroek et al., 2024; Vindušková et al., 2025). In marshes, the most researched pathway is vegetation stress or death, causing elevation loss due to volumetric collapse of soil or aerenchyma pore spaces, and the loss of a living root network, reducing the structural strength of the peat (Chambers et al., 2019). Belowground changes in the SOM biogeochemical composition of the peat, and accelerated soil mineralization due to the addition of a limiting electron donor (in the form of labile, easy decomposable or dissolved organic matter), of an alternative electron acceptor (i.e. NO^{3-}, Fe^{3+} or SO_4^{2-}) or of a stoichiometrically limiting nutrient like N or P, have been proposed as alternative or auxiliary mechanisms compromising the structural integrity of the peat matrix, yet have been much less evidenced in the framework of peat collapse. Experimental evidence, underpinning the mechanisms of peat collapse suggested by observational studies, is scarce (Chambers et al., 2019).

In this study, we investigated the peat collapse event observed in De Zegge to identify potential drivers and underlying mechanisms by integrating field observations with a manipulative mesocosm experiment. Specifically, we (1) documented the area affected by extent of the peat loss based on elevation change in the collapsed areas using high-resolution unmanned aerial vehicle light detection and range (UAV-LiDAR) point clouds, and (2) assessed the belowground changes by comparing soil fauna communities, vegetation structure, physicochemical properties and molecular composition of soil organic matter between collapsed plots and the adjacent areas . We also sampled other, more distant locations across De Zegge to account for region-scale

heterogeneity. Moreover, we (3) experimentally evaluated the effects of hydrological alterations and potential hydro-chemical stressors (i.e., ditchwater as a source of labile DOC and nutrients, and sulfate [SO_4^{-2}] as an electron acceptor that is an important driver of eutrophication and pH changes) on greenhouse gas (GHG) emissions using mesocosm experiment from cores extracted near the collapsed plots.

Ditchwater treatment was selected because the affected area was subjected to recurrent winter flooding from surrounding ditches a few months before the collapse. Surface water, particularly from ditches, is often contaminated with sediments, fertilizers, and labile organic compounds (i.e., electron donors) originating from adjacent agricultural lands or wastewater inflows. These inputs disrupt plant-soil feedbacks, reduce belowground deep roots biomass development, and accelerate decomposition processes (Turner, 2011; Laudon et al., 2023).

Sulphate was selected as a treatment because it is considered a key driver of peat collapse in coastal marshes (Campeau et al., 2017). Although De Zegge does not have coastal influence, the region overlies marine sediments of the Diest formation (Houthuys et al., 2020). We therefore hypothesised that sulfates derived from those substrates may be mobilised by high soil nitrogen loading from upstream sources (Di and Cameron, 2002; Lamers et al., 2015), thereby inducing collapsed-related mechanisms typically associated with coastal systems (Reddy and DeLaune, 2008). Sulfates availability can enhance peat decomposability by serving an alternative electron acceptor, weaking peat structure even under anaerobic environments (van Dijk et al., 2019). Such changes significantly alter vegetation and microbial dynamics, suppress peat formation, and promote persistent anaerobic decomposition−ultimately leading to rapid peat subsidence (Cadigan et al., 2022; Middleton and David, 2022).

4.2. Materials and Methods

This study employed two complementary methodological approaches to address distinct research questions. First, a field investigation was carried out to find out which environmental conditions and mechanisms are responsible for what we refer to as tentative peat collapse. Secondly, a controlled mesocosm experiment was designed to evaluate the effect of hydrological and hydro-chemical stressors−specifically, intrusions of ditchwater and SO_4^{2-} on peat stability.

4.2.1 Field study

4.2.1.1 Study design, sampling and vegetation survey

Our study was conducted in the nature reserve "De Zegge", located within the floodplains of the Kleine Nete, in the Campine area of Flanders, Belgium (51°19'N, 4°93'E, **Error! Reference source not found.**A). De Zegge is one of the oldest nature conservation areas in Flanders and is currently recognised as a site of European importance under several frameworks, including the Natura 2000 Network and the Interreg Care-Peat project. The region has a temperate climate with mean annual precipitation of 755 mm and mean annual temperature of 11.1 °C (data from 2010 to 2022, Cruz-Alonso et al., 2023). The peat overlies highly glauconferous sandy deposits of the upper cycle of the Miocene Diest Formation (the so-called 'Kempen Diest sand'; Houthuys et al., 2020). Glauconite pellets of this formation are typically associated with pyrite formations (FeS_2; Bruneel et al., 2020).



Fig. 4.1. Study region with visible signs of what is referred to in this study as to peat collapse. (A) Aerial photograph of study region within the nature conservation area “De Zegge” (province of Antwerp). Based on distinctive changes in vegetation community composition and surface elevation, three and four collapsed plots were established in site 1 (panel B) and site 2 (panel C), respectively. Non-collapsed adjacent (NCA) plots (controls) were established at four points in close proximity to each collapsed (C) plot. Sites 3−7 served as distant non-collapsed plots. Photo credits: K. Kim, T. Deswert

The fen peatlands in this region are frequently subjected to altered hydrological conditions due to structural drainage and groundwater pumping from surrounding agricultural lands as well as irregular floodings. Small-scale abrupt peat fragmentation at two sites (hereafter, referred to as site 1 and site 2; **Error! Reference source not found.**A) appeared within a few weeks following the severe summer drought of 2018 and was subsequently accompanied by a slow but persistent decline in surface elevation over the following years. The collapsed area was further characterized by discolored, stagnant surface water, fragmented and fine-grained surficial peat texture, and low density of plant roots.

Within the two sites with clear signs of peat collapse, collapsed plots were identified based on consultations with local scientists and site managers, as well as visual inspection of the vegetation and surface elevation changes (**Error! Reference source not found.**B&C). We established three and four collapsed plots for site 1 and site 2 respectively, at the center of each visibly degraded, mudflat-like area. In addition, non-collapsed adjacent control plots were established near each collapsed plot, as illustrated in **Error! Reference source not found.**B&C. In this study, non-collapsed adjacent plots refer to area where peat degradation has potentially occurred but without abrupt changes, representing a transitional zone where collapse may be progressing as the collapsed areas expand over time. Furthermore, to effectively characterize and contrast peat properties between collapsed and non-collapsed plots, five non-collapsed sites located at least 150 m from the collapsed sites were selected across study region (site 3-7, **Error! Reference source not found.**A). These five sites were strategically chosen based on previous studies to accommodate spatial variability in vegetation composition and soil conditions in the entire conservation area and without any visual collapse-like features (Ottoy et al., 2019). Each site subsequently served as an individual plot. In total, the experimental design comprised seven collapsed plots (C), seven non-collapsed adjacent plots (NCA), and five non-collapsed distant plots (NCD), distributed across two sites with collapse (sites 1 &2) and five sites without collapse (sites 3-7; **Error! Reference source not found.**).

The field campaign was initiated on 27th Jul 2023 by collecting peat and fauna samples, with an additional fauna sampling conducted on 25th Sep 2023. From each plot, three peat subsamples were collected at a depth of 0−5 cm using an auger, then thoroughly mixed into a single composite sample. Similarly, two sets of three subsamples were collected from each plot using three kopecky rings with a volume of 100 cm^3 to accommodate two distinct extraction methods for soil fauna analysis: the Tullgren funnel extraction for microarthropods (mites and collembolans), and the Baermann funnel extraction for enchytraeids (O'connor, 1955). Each set of three kopecky rings were pooled into a single composite sample. All extruded composite samples were packed into Ziplock™ bags and transported to the laboratory in a cool box. Peat samples were stored at 4 °C until analysis, while fauna samples were immediately placed to fauna funnel extraction setup. Vegetation community composition was surveyed in the field in 2 × 2 m plots at the centre of each plot.

4.2.1.2 Peat analyses: Soil biota, physiochemistry, and molecular composition

Mesofauna specimen extracted from two distinct funnel techniques were preserved in 60 % ethanol and refrigerated at 7 °C until further counting (Bano and Roy, 2016), thereafter identification was performed in accordance with the Global Soil Biodiversity Atlas (Orgiazzi et al., 2016).

Soil bulk density (kg cm^{-3}) was determined by weighing oven-dried at 70 °C peat sample with known volumes. To carry out elemental analyses, peat samples were oven-dried at 50 °C and finely ground using a ball-mill (Pulverisette 7, FRITSCH, Germany). To eliminate potential interference from inorganic carbon, samples were pretreated with 30µL of 5% HCl, and then dried. Total organic carbon (TOC), total nitrogen (TN) and their isotopes were measured using an elementary analyser (Thermo Flash HT/EA, ThermoFischer Scientific, USA) equipped with an isotope ratio mass spectrometer (Thermo Delta V Advantage EA-IRMS, ThermoFischer Scientific, USA). Soil nitrate (NO_3^-) and ammonium (NH_4^+) were determined in salt extracts (after mixing

2.5 g fresh soil with 25 ml of 1M KCl solution) using a continuous flow analyzer. Soil pH was measured (1:1 soil-to-water suspension) using radiometer and a TIM840 pH meter. Total extractable cations −Ca^{2+}, Mg^{2+}, K^{+}, Na^{+}− and phosphorus (P) were analyzed by Inductively Coupled Plasma Optical Emission Spectroscopy (ICP-OES, Varian 720 ES).

For peat molecular characteristics, ground peat samples were scanned in the mid-infrared region (FrontierTM with auto-sampler from PerkinElmer, Waltham, MA, USA). Spectra were obtained in % reflectance mode between 4000 and 400 cm^{-1} (wavenumber) at a resolution of 1 cm^{-1} with 32 accumulations. Each sample was scanned in quadruplicate, and the resulting spectra were averaged. To prevent drift signal, the reflectance of the scanned samples was divided by the average of the background samples (Brosens et al., 2021). The spectra were then converted from reflectance (R) to absorbance (A) unit by A=log(1/R).

4.2.1.3 Terrain mapping and C loss estimation via RGB and Light detecting and Ranging (LiDAR)

To visualize the area affected by collapse-related peat loss in the Zegge, we quantified elevation changes and estimated C losses from collapsed plots. Baseline elevation data were obtained from the Digital Elevation Model Flanders II (https://www.vlaanderen.be) that comprises a Digital Terrain Model (DTM) with a resolution of 1 m. This raster dataset is based on aerial LiDAR point clouds with a minimal point density. This dataset was considered to be the reference baseline for detecting elevation changes over the 10-year period. The 2015 Li-DAR database was selected because it represents the most recent elevation survey available prior to the onset of peat collapse in the study region.

Two drone flight missions took place at each peat collapsed site on 17 July 2025. The first flight was conducted with a DJI Mavic 3T (M3T) system with an RGB camera, configured with 80 % forward and side image overlap to ensure photogrammetric accuracy. The collected RGB imagery was processed using the Pix4D software to generate an orthophoto mosaic. The

second flight employed a DJI M300RTK drone carrying a YellowSan's Survey Ultra (HeSAI XT32M2X) LiDAR system, flown with 50 % overlap and at a speed of 3 m/s to optimize point cloud density. The trajectory was postprocessed with the Applanix' POSPac MMS software and included the determination of the Smooth Best Estimated Trajectory (SBET) based upon the sensor's lever arms and the local RTK network FLEPOS (Flemish Positioning Service). After SBET processing, strip adjustment was performed based on the integrated 'Robust' method, and the resulting point cloud was classified (ground vs. non-ground). The LiDAR point-could resolution has 16 points/m² for baseline public data prior to peat collapse, whereas +1000 points/m² for our post-collapse field survey.

Peat height changes were calculated by subtracting the 2015 elevation values from those obtained in 2025, following delineation of collapsed plots. The peat collapsed plot was defined as areas within a 2-meter radius of established collapse sampling points, with exclusion of anomalous height increase, potentially attributed to ground classification errors or laser occlusion caused by dense vegetation (Moudrý et al., 2020; MacDonell et al., 2023). For each delineated plot, average height loss was computed, and carbon loss was subsequently estimated using volumetric calculation based on a pixel size of 0.04 m^2, multiplied by bulk density and C concentration values derived from field samples as follows:

$$C\ stock\ loss = \frac{V \times BD\ \times C \times \gamma}{A}$$

where C stock loss is the amount of C being lost following abrupt change (kg−C m^{-2}); V is the volume loss of each plot (m^3); BD represents the bulk density of peat (kg cm^{-3}); C is the carbon concentration of peat (kg kg^{-1}); A present the delineated area of each plot (m^2); γ indicates the unit conversion factor to express the result in kg−C m^{-2}. In this study, negative values were used to indicate carbon loss. RGB-imagery and LiDAR-derived DTMs were processed using a R software to produce an orthophoto with a spatial resolution of 20 × 20 cm resolution, along with a map of elevation changes across the two peat collapsed sites.

4.2.2. Mesocosm study

4.2.2.1 Study design and peat monolith sampling

24 PVC tubes (Ø 12.5 cm, 25 cm depth) containing intact peat monoliths were extracted near site 1 within the "De Zegge" reserve on 13 Sep 2024 (**Error! Reference source not found.**A). To ensure peat material homogeneity for the mesocosm experiment, six peat monoliths were sampled from each of four distinct locations within the area. These four locations were subsequently treated as a random effect in statistical analysis. Prior to core extraction, aboveground vegetation on the sampling area was carefully cut to peat surface level and removed. The PVC tubes were sharpened on their downward-facing edge to facilitate insertion into the peat. When the depth of peat monolith reached 20 cm, the tube with peat monolith was carefully extracted from the peat soil. The bottom of the tube was immediately sealed with a lid to prevent aerobic decomposition and sample loss during transport.

For the mesocosm experiment, ditchwater and SO_4^{-2} additions were chosen as potential chronic stressors based on the site-specific observations: i.e. (1) the presence of irregular surface water inflows from adjacent agricultural ditches during a flooding event a few months prior to the collapse, and (2) elevated groundwater SO_4^{-2} concentration nearby collapsed sites, as indicated by local monitoring data (Supplementary Fig. 4.1; Moris, 2020). The experimental setup followed a two-factorial design (three levels of solution treatments × two levels of drainage perturbation, n = 4; **Error! Reference source not found.**A). Each PVC tube was placed inside a wider PVC tube (Ø 20 cm, 25 cm depth), and the between-space was filled with white sand to prevent hydraulic interference between cores within the same bath (**Error! Reference source not found.**A). Throughout the experiment, water tables were maintained at the peat surface (±1 cm). The solution addition treatments consisted of control (demineralized water), ditchwater, and 2000 µmol of SO_4^{-2}, while the drainage treatment consisted in lowering the water table 15 cm below the peat surface for 35 days. **Error! Reference source not found.**Water level manipulation was accomplished by

water level of the basin as the inner PCV tubes were punctuated to allow treatment solutions to infiltrate the peat cores.

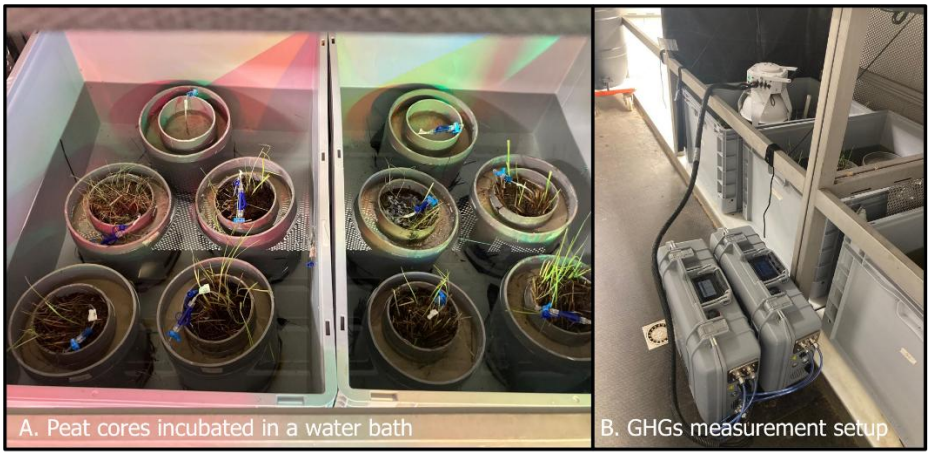


Fig. 4.2. Mesocosm experimental setup for greenhouse gas (GHGs) flux measurements and peat porewater sampling. (A) Configuration of peat cores in a water bath, with water table manipulation achieved through punctured holes on the lateral sides of the PVC cores, allowing equilibration between bath water and peat core water levels. (B) GHGs fluxes (CO_2 CH_4 and N_2O) were measured using LICOR-7810 and -7820 gas analyzers, connected to a smart chamber placed over individual peat cores.

The experiment was conducted over 120 days, from Sep 2024 to Jan 2025. The climate-controlled room was maintained at constant temperature regime of 23 °C during the day 18 °C at night, with a relative humidity of 75%. The peat monoliths were kept in dark conditions throughout the experiment to prevent vegetation establishment and radial oxygen loss (**Error! Reference source not found.**A).

4.2.2.2 Peat porewater sampling and analyses

Peat porewater was sampled during experimental phase (i.e., baseline, treatment-loading, drawdown, and re-saturation: four times in total). pH was measured using a pH electrode (radiometer and a TIM840 pH meter), and alkalinity was determined by titration to pH 4.2 with 0.01 M HCl. Electrical conductivity (EC), representing total dissolved ion content, was measured using a WTW-Retch conductivity meter. Prior to nutrients analysis, 20 mL of the aqueous samples

were acidified with 3mL 1M H_2SO_4 for analysis of NO_3^- and NH_4^+, and with 1.5 ml of 69 % HNO_3 for P analysis. The NH_4^+ and NO_3^- concentrations were quantified colorimetrically using a continuous-flow Auto Analyzer system. The phosphorous concentrations were measured using Inductively Coupled Plasma Optical Emission Spectroscopy (ICP-OES, Varian 720 ES).

4.2.2.3 Greenhouse gas (GHG) measurements and peat stability metrics

Three greenhouse gases (GHGs; CO_2, CH_4, and N_2O) were simultaneously measured using trace gas analyzers Li-COR 7810 and Li-COR 7820, equipped with a smart chamber in a closed loop (LI-COR Biosciences; Lincoln; NE, USA; **Error! Reference source not found.**B). GHG measurements were taken twice a week, with increased frequency during the onset of water drawdown and re-saturation phases to capture transient flux dynamics. Each measurement was conducted for a 100 second interval, with the chamber vented between measurements. GHG fluxes were calculated using the *R* package *goFlux*, which applied either linear or non-linear regression models to concentration data over time, selected based on goodness-of-fit criteria and visual inspection of diagnostic plot (Rheault et al., 2024). To ensure that GHG fluxes reflected ambient conditions, a control core filled with only white sand was monitored concurrently throughout the experiment.

The peat stability in response to the solution additions was assessed using four equilibrium components−temporal variability, spatial variability, resistance, and resilience−following the framework proposed by Orwin and Wardle (2004 and White et al. (2020). GHG fluxes served as indicator of functional stability, with contribution of each treatment quantified as the inverse of the stability response. This response was calculated using log response ratios (LRR) by comparing the fluxes between perturbed and unperturbed treatments following an experimental pulse perturbation (i.e., drainage event), as outlined by Hillebrand et al (2018). To calculate temporal and spatial variability, GHG fluxes were first detrended to remove potential

compounding effects associated with gradual changes over the duration of the experiment. The stability metrics were calculated as follows:

$$Temporal\ \&\ Spatial\ variabiltiy = \frac{Standard\ deviation_{unperturbed}}{Mean_{unpertubed}}$$

$$Resistance = |\overline{LRR}_{drawdown}|$$

$$Resilience = |\overline{LRR}_{drawdown} - \overline{LRR}_{resaturation}|$$

Temporal variability was quantified as the coefficient of variation (CV)−defined as the standard deviation divided by the mean− of GHG fluxes within each unperturbed experimental plot over time. Spatial variability was assessed using the CV among unperturbed plot within each treatment combination at each census point. Resistance was evaluated as the extent of change in GHG fluxes in response to perturbation, quantified by the mean absolute LRR of GHG fluxes during the drawdown phase. Resilience was evaluated as the recovery capacity of the peat following perturbation, quantified by the absolute difference in LRR between drawdown and re-saturation phase. In this setup, large values of temporal and spatial variability, as well as resistance, indicate lower peat stability. In contrast, higher resilience values reflect greater stability.

4.2.3 Statistical analyses

All statistical analyses were implemented in R 4.5.1 (R Development Core Team, 2025), and significance was accepted at $P < 0.05$ for all tests. To assess and visualize the ecological response in the field study, four response variables were analyzed: mesofauna, vegetation, physiochemical, and molecular compositions. Non-metrical multidimensional scaling (NMDS) ordination was performed by applying Bary−Curtis dissimilarity for mesofauna and vegetation, and Euclidean dissimilarity for physiochemistry and molecular composition. Prior to visualization, mesofauna data were log-transformed after adding a constant (+0.01), while vegetation data were log-transformed directly. Differences in community composition and spectral profiles across collapsed plots, non-collapsed adjacent plots, and non-collapsed distant plots were tested using

permutational analysis of variance (PERMANOVA) with 999 iterations, implemented via the 'adonis' function in the *vegan* package. In addition, the alpha diversity metrics−including richness, evenness, and the Shannon diversity index− were calculated for mesofauna and vegetation within each sample. In the NMDS ordination, loadings values overlaid within the same ordination space, illustrating the distribution of sample scores. To differentiate molecular composition characteristics between non-collapsed and collapsed sites, a classification model using partial least squares discriminant analysis (PLS-DA) was applied (Supplementary Fig. 4.2).

Next, linear models were used to test the difference among collapsed, non-collapsed adjacent, non-collapsed distant plots for individual components of mesofauna and vegetation diversity, as well as physicochemical variables. For fauna abundance, a generalized linear mixed model (GLMM) was fitted using *glmmTMB* package with a log link, accounting for seasonal variability. In the mesocosm experiment, linear mixed models were used to test: (1) the interaction effects of drainage perturbation × solution addition on porewater geochemistry; and (2) the effect of solution addition alone on multidimensional stability metrics by accounting for four sampling locations as random effects described in the peat monolith sampling procedure. Repeated measures were modeled to test (3) the interaction effects of drainage perturbation × solution addition on GHGs fluxes using individual cores and autoregressive correlation structure (corAR1), fitted separately for each experimental phase. Post hoc pairwise comparisons between drainage perturbation and solution addition treatment were conducted using the Tukey HSD test (Pinheiro et al., 2025). When assumptions of normality and homoscedasticity were violated, a Box-Cox transformation was applied to improve model fit.

To reduce complexity in the piecewise structural equation model (SEM), principal component analysis was used to derive composition gradients (Lefcheck, 2016). The first principal component (PC1) from EC and alkalinity was used to represent ionic strength, while the PC1 scores from NH_4^+, NO_4^- and P concentrations were used to represent the nutrient gradient. The

SEM was constructed to quantify relationships between categorical variables (hydrological perturbation × solution addition treatment), intermediate variables (nutrients, ionic strength, and pH), and final production (GHGs fluxes). We conceptualize that via an intermediate variable an indirect relationship exists between categorical variables and the final production. Akaike's Information Criterion (AIC) and the Bayesian Information Criterion (BIC) were used to facilitate model selection by comparing the fit of all model candidates (Shipley, 2013). The SEM Model fit was acceptable for both phases, with the water drawdown phase showing AIC = 94.30, BIC =146.14, Fisher's C = 6.30, *P* value = 0.18 and the re-saturation phases showing AIC = 90.42, BIC =142.26, Fisher's C = 2.42, *P* value = 0.66.

4.3. Results

4.3.1 Elevation, C stock, and functional domains in response to peat collapse obtained from field data

Field observations following the severe 2018 drought (Fig. 4.1B&C) show a break-up of the wetland platform and the emergence of small ponds filled with a reddish-brown to blackish, loose mud rather than peat, indicating an abrupt, rapid and non-linear elevation decline with time. Comparison of these images to the LiDAR-derived digital terrain models from 2025 (Fig. 4.3) moreover indicates that the collapsed area is expanding, as new ponds have appeared and ponds are coalescing, the latter especially at site C2. LiDAR-data indicated significant reductions of peat height between the 2015 reference and the 2025 assessment, amounting for-18.0 ± 2.2 cm and -8.9 ± 1.1 cm, for peat collapsed site 1 and site 2, respectively, with mean total elevation losses of -12.8 ± 2.3 cm at the collapsed plots (Fig. 4.3). . When comparing landscape photographs (Fig. 4.1B&C) with the LiDAR imagery (Fig. 4.3), it becomes more evident that the collapsed area is expanding. The corresponding C stock losses were -19.4 ± 9.1 kg−C m^{-2} and -23.3 ± 9.3 kg−C m^{-2}, for peat collapsed site 1 and 2, respectively (Fig. 4.3). On average, the two sites showed a C loss of -21.6 ± 6.1 kg−C m^{-2}.

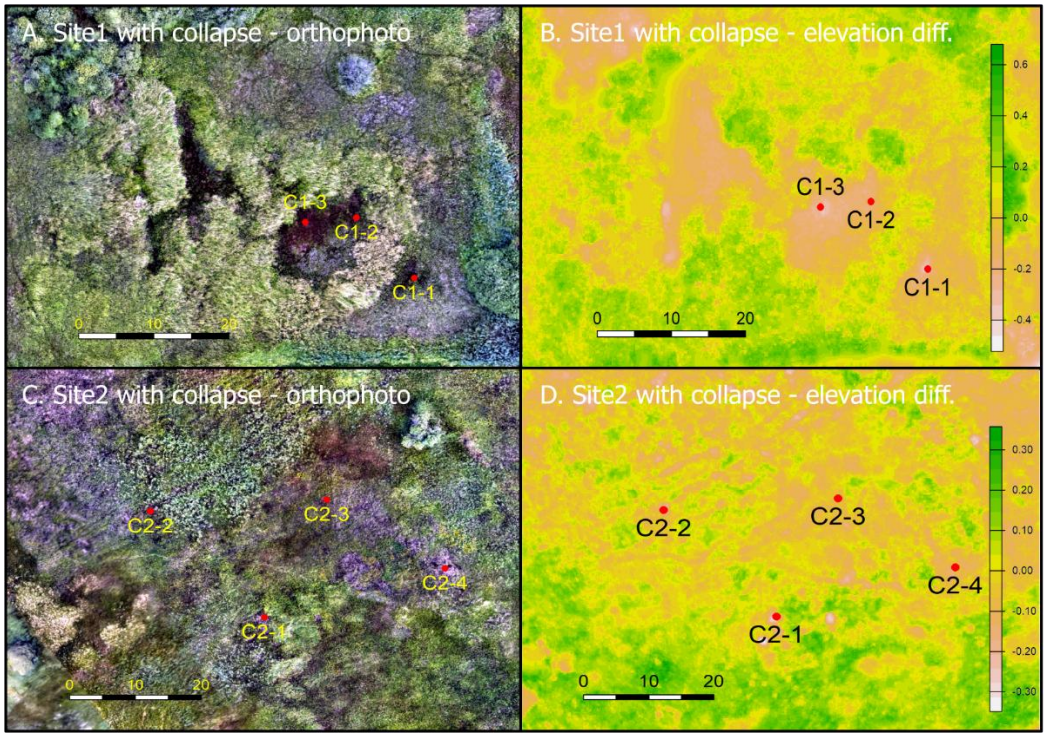


Fig. 4.3. Orthophotos (A,C) and elevation difference maps (B,D) illustrating changes between 2015 and 2025 at two sites affected by peat collapse. Elevation differences were derived from light detection and ranging (Li−DAR) data and indicate surface subsidence or accumulation over the 10-year period. The scale bars represent distance in meters (m).

Peat characteristics were significantly different across the collapsed plot, the non-collapsed adjacent plots, and the non-collapsed distant plots, particularly for the mesofauna and vegetation community composition, the physiochemistry, and the soil organic matter molecular composition ($Ps < 0.05$; Fig. 4.4; Supplementary Table 4.1). The collapsed plots consistently differed significantly from the non-collapsed distant plots across all ecological response components ($Ps < 0.05$; Fig. 4.4; Supplementary Table 4.1). In contrast, the non-collapsed adjacent plots exhibited intermediate characteristics between the collapsed and the non-collapsed distant plots, depending on the ecological variable tested. In the case of the mesofauna community, the non-collapsed adjacent plots significantly differed from collapsed plots ($P < 0.05$) but were similar to the non-collapsed distant plots. In addition, the non-collapsed distant plots had a significantly higher richness index in mesofauna communities compared to the collapsed plots, along with significantly higher abundances of mites and collembolans ($Ps < 0.05$; Table 4.1). Conversely, the vegetation community composition, diversity indices such as richness, evenness, and the Shannon diversity did not differ significantly between plots. However, the difference of the vegetation community composition showed a significant shift along the tentative degradation gradient, ranging from non-collapsed distant plots to collapsed plots ($P < 0.05$; Fig. 4.4).

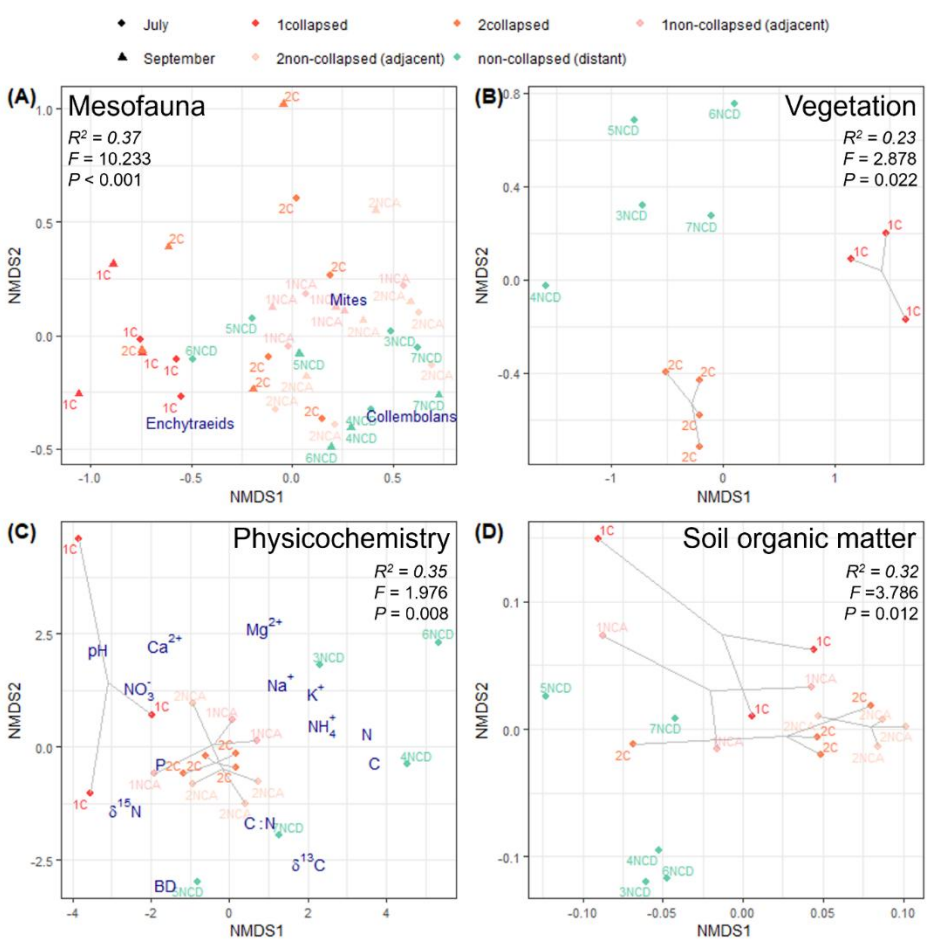


Fig. 4.4. Non-metric Multidimensional Scaling (NMDS) ordination plot depicting the variation in (A) mesofauna community composition, (B) vegetation community composition, (C) physiochemical properties, and (D) soil organic matter molecular composition at the three treatments: collapsed, non-collapsed adjacent, and non-collapsed distant plots. Permutational multivariate analysis of variance (PERMANOVA) with its respective R^2, F, and P value provide in the figures. Dissimilarity is measured as Bray-Curtis distance for (A), (B), and Euclidean distance for (C), (D). In panels (A), and (C), blue-labeled text indicates variable loadings on the ordination. The number of sample size in mesofauna is double as measured twice in a year.

Table 4.1. Least squares means of mesofauna, vegetation community composition, and physiochemistry across collapsed (n= 7), adjacent non-collapsed (n= 7), and distant non-collapsed plots (n= 5) in study area.

	unit	collapsed	non-collapsed (adjacent)	non-collapsed (distant)	P value
			Mesofauna		
Richness		2.07a	2.50ab	2.87b	<0.01**
Evenness		0.57	0.48	0.52	0.60
Shannon		0.38	0.45	0.54	0.35
Mites		33.2a	72.9ab	147.4b	<0.05*
Collembolans		0.5a	6.2b	16.7b	<0.0001***
Enchytraeids		18.9	7.7	22.7	0.12
			Vegetation		
Richness		8.63		9.97	0.40
Evenness		0.69		0.74	0.45
Shannon		1.54		1.74	0.33
			Physiochemistry		
BD	g/cm^3	0.11	0.13	0.14	0.54
C	%	20.5	23.4	30.9	0.07
N	%	1.22	1.33	1.76	0.12
CN		16.9	17.5	18.1	0.16
δC^{13}	‰	-29.2a	-28.8b	-28.8ab	<0.05*
δN^{15}	‰	-0.98	-0.74	-1.35	0.68
pH		4.54	4.25	4.10	0.06
NH_4	mg/g	0.09a	0.05a	8.45b	<0.01**
NO_3	mg/g	8.88	10.67	2.31	0.15
P	mg/kg	67.23	61.16	34.16	0.13
Ca	mg/kg	18.54	18.36	17.05	0.54
Mg	mg/kg	38.57	42.64	60.94	0.28
K	mg/kg	29.01	37.80	67.52	0.10
Na	mg/kg	29.13	29.50	49.63	0.17

* , **, and *** indicates statistical significance at $P < 0.05$, $P < 0.01$, $P < 0.001$.
Different lowercase letters indicate significance between peat condition based upon post hoc analysis after one-way ANOVA ($\alpha = 0.05$).

In the case of physiochemical properties and soil organic matter molecular composition, the non-collapsed adjacent plots significantly differed from the non-collapsed distant plots (*Ps* < 0.05; Fig. 4.4) but were similar to the collapsed plots. Accordingly, the ammonium (NH_4^+) concentration and the $\delta^{13}C$ values emerged as distinct factors along the degradation gradients (*Ps* < 0.05; Fig. 4.4; Table 4.1); the difference was marginally linked to the C concentration and the pH (*Ps* < 0.1; Fig. 4.4; Table 4.1). Collapsed and near-collapsed plots tended to have a higher pH, Ca and Mg contents as well as higher nutrient availability (P and nitrate) as did the 3NCD and

6NCD plots. Soil organic matter characteristics, i.e., mid infrared spectra, also differed between non-collapsed and collapsed sites (non-collapsed adjacent and collapsed plots), which were mainly caused by higher vibration of the organic matter signal encompassing *v*C−O from polysaccharides, *v*C=C from aromatics, *v*C=O from ester and carboxylic acids, *v*C−N from amides, and *v*C−H from aliphatic compounds (Fig. 4.4; Supplementary Fig. 4.3). A similar chemistry was seen in plots 5NCD and 7NCD.

4.3.2 GHG measurement and their stability metrics from mesocosm experiments

During the baseline phase (n = 7), GHG emissions ranged from 0.49 to 2.71 g−C m^{-2} day^{-1} for CO_2, 32.3 to 480 mg−C m^{-2} day^{-1} for CH_4, and -1.86 to 3.17 mg−N m^{-2} day^{-1} for N_2O (

	Baseline	Treatment-loading	Drawdown	Re-saturation	Total
			Daily CO_2 (g−C m^{-2} Day^{-1})		
Control (no drainage)	1.81	1.28	1.76a	1.14	1.19
Ditch	1.73	1.32	1.45a	1.25	1.24
SO_4	1.60	1.37	1.23a	1.05	1.07
Control (with drainage)	1.43	1.37	7.21b	0.97	1.31
Ditch	1.60	1.44	6.36b	0.97	1.30
SO_4	1.51	1.77	8.31b	1.02	1.41
Treatment	0.6686	0.5610	0.4095	0.8286	0.9544
Drainage	0.0601	0.1369	<0.0001***	0.1341	0.1653
Treatment: Drainage	0.4775	0.2670	0.1001	0.6547	0.6205
			Daily CH_4(mg−C m^{-2} Day^{-1})		
Control (no drainage)	140	169	128	68	92
Ditch	162	187	163	114	133
SO_4	132	137	158	93	109
Control (with drainage)	166	211	54	52	73
Ditch	194	216	68	56	84
SO_4	193	194	87	61	91
Treatment	0.7042	0.4848	0.8336	0.5619	0.3914
Drainage	0.1189	0.0542	0.0937	0.0737	0.0750
Treatment: Drainage	0.8267	0.8308	0.9710	0.7037	0.7200
			Daily N_2O (mg−N m^{-2} Day^{-1})		
Control (no drainage)	0.178	0.049	-0.231	0.116	0.039
Ditch	-0.018	-0.036	0.192	0.171	0.116
SO_4	0.015	0.000	0.303	0.994	0.600
Control (with drainage)	0.065	0.231	-0.065	0.407	0.249
Ditch	0.040	0.013	-0.053	0.322	0.159
SO_4	0.111	0.052	-0.134	0.334	0.190
Treatment	0.4427	0.0734	0.4049	0.3428	0.3011
Drainage	0.8415	0.0857	0.2714	0.9246	0.7651

Treatment: Drainage	0.4452	0.7146	0.2786	0.2672	0.2211

; Supplementary Fig. 4.4). During the treatment-loading phase (n =5), fluxes remained within similar ranges: 0.430 − 2.41 g−C m^{-2} day^{-1} for CO_2, 38.7 − 450 mg−C m^{-2} day^{-1} for CH_4, and 0.21 − 1.26 mg−N m^{-2} day^{-1} for N_2O (

	Baseline	Treatment-loading	Drawdown	Re-saturation	Total
		Daily CO_2 (g−C m^{-2} Day^{-1})			
Control (no drainage)	1.81	1.28	1.76a	1.14	1.19
Ditch	1.73	1.32	1.45a	1.25	1.24
SO_4	1.60	1.37	1.23a	1.05	1.07
Control (with drainage)	1.43	1.37	7.21b	0.97	1.31
Ditch	1.60	1.44	6.36b	0.97	1.30
SO_4	1.51	1.77	8.31b	1.02	1.41
Treatment	0.6686	0.5610	0.4095	0.8286	0.9544
Drainage	0.0601	0.1369	<0.0001***	0.1341	0.1653
Treatment: Drainage	0.4775	0.2670	0.1001	0.6547	0.6205
		Daily CH_4(mg−C m^{-2} Day^{-1})			
Control (no drainage)	140	169	128	68	92
Ditch	162	187	163	114	133
SO_4	132	137	158	93	109
Control (with drainage)	166	211	54	52	73
Ditch	194	216	68	56	84
SO_4	193	194	87	61	91
Treatment	0.7042	0.4848	0.8336	0.5619	0.3914
Drainage	0.1189	0.0542	0.0937	0.0737	0.0750
Treatment: Drainage	0.8267	0.8308	0.9710	0.7037	0.7200
		Daily N_2O (mg−N m^{-2} Day^{-1})			
Control (no drainage)	0.178	0.049	-0.231	0.116	0.039
Ditch	-0.018	-0.036	0.192	0.171	0.116
SO_4	0.015	0.000	0.303	0.994	0.600
Control (with drainage)	0.065	0.231	-0.065	0.407	0.249
Ditch	0.040	0.013	-0.053	0.322	0.159
SO_4	0.111	0.052	-0.134	0.334	0.190
Treatment	0.4427	0.0734	0.4049	0.3428	0.3011
Drainage	0.8415	0.0857	0.2714	0.9246	0.7651
Treatment: Drainage	0.4452	0.7146	0.2786	0.2672	0.2211

; Supplementary Fig. 4.4). In both baseline and treatment-loading phases, no significant differences in fluxes and LRR were observed among peat monoliths with respect to solution addition or drainage treatments (

	Baseline	Treatment-loading	Drawdown	Re-saturation	Total
		Daily CO_2 (g−C m^{-2} Day^{-1})			
Control (no drainage)	1.81	1.28	1.76a	1.14	1.19

Ditch	1.73	1.32	1.45a	1.25	1.24
SO_4	1.60	1.37	1.23a	1.05	1.07
Control (with drainage)	1.43	1.37	7.21b	0.97	1.31
Ditch	1.60	1.44	6.36b	0.97	1.30
SO_4	1.51	1.77	8.31b	1.02	1.41
Treatment	0.6686	0.5610	0.4095	0.8286	0.9544
Drainage	0.0601	0.1369	<0.0001***	0.1341	0.1653
Treatment: Drainage	0.4775	0.2670	0.1001	0.6547	0.6205
Daily CH_4(mg−C m^{-2} Day^{-1})					
Control (no drainage)	140	169	128	68	92
Ditch	162	187	163	114	133
SO_4	132	137	158	93	109
Control (with drainage)	166	211	54	52	73
Ditch	194	216	68	56	84
SO_4	193	194	87	61	91
Treatment	0.7042	0.4848	0.8336	0.5619	0.3914
Drainage	0.1189	0.0542	0.0937	0.0737	0.0750
Treatment: Drainage	0.8267	0.8308	0.9710	0.7037	0.7200
Daily N_2O (mg−N m^{-2} Day^{-1})					
Control (no drainage)	0.178	0.049	-0.231	0.116	0.039
Ditch	-0.018	-0.036	0.192	0.171	0.116
SO_4	0.015	0.000	0.303	0.994	0.600
Control (with drainage)	0.065	0.231	-0.065	0.407	0.249
Ditch	0.040	0.013	-0.053	0.322	0.159
SO_4	0.111	0.052	-0.134	0.334	0.190
Treatment	0.4427	0.0734	0.4049	0.3428	0.3011
Drainage	0.8415	0.0857	0.2714	0.9246	0.7651
Treatment: Drainage	0.4452	0.7146	0.2786	0.2672	0.2211

; Supplementary Fig. 4.4). During the water drawdown phase (n = 11), CO_2 and CH_4 fluxes in the drainage treatment increased immediately following the onset of water drawdown, although CH_4 fluxes subsequently declined (Supplementary Fig. 4.4). N_2O fluxes showed a slight downward trend, but no consistent pattern was evident (Supplementary Fig. 4.4). CO_2 fluxes were significantly enhanced under drainage conditions ($P < 0.05$), whereas the effect of solution addition on CO_2 fluxes was not significant (

	Baseline	Treatment-loading	Drawdown	Re-saturation	Total
Daily CO_2 (g−C m^{-2} Day^{-1})					
Control (no drainage)	1.81	1.28	1.76a	1.14	1.19
Ditch	1.73	1.32	1.45a	1.25	1.24
SO_4	1.60	1.37	1.23a	1.05	1.07
Control (with drainage)	1.43	1.37	7.21b	0.97	1.31
Ditch	1.60	1.44	6.36b	0.97	1.30
SO_4	1.51	1.77	8.31b	1.02	1.41
Treatment	0.6686	0.5610	0.4095	0.8286	0.9544

Drainage	0.0601	0.1369	<0.0001***	0.1341	0.1653
Treatment: Drainage	0.4775	0.2670	0.1001	0.6547	0.6205
Daily CH_4(mg−C m^{-2} Day^{-1})					
Control (no drainage)	140	169	128	68	92
Ditch	162	187	163	114	133
SO_4	132	137	158	93	109
Control (with drainage)	166	211	54	52	73
Ditch	194	216	68	56	84
SO_4	193	194	87	61	91
Treatment	0.7042	0.4848	0.8336	0.5619	0.3914
Drainage	0.1189	0.0542	0.0937	0.0737	0.0750
Treatment: Drainage	0.8267	0.8308	0.9710	0.7037	0.7200
Daily N_2O (mg−N m^{-2} Day^{-1})					
Control (no drainage)	0.178	0.049	-0.231	0.116	0.039
Ditch	-0.018	-0.036	0.192	0.171	0.116
SO_4	0.015	0.000	0.303	0.994	0.600
Control (with drainage)	0.065	0.231	-0.065	0.407	0.249
Ditch	0.040	0.013	-0.053	0.322	0.159
SO_4	0.111	0.052	-0.134	0.334	0.190
Treatment	0.4427	0.0734	0.4049	0.3428	0.3011
Drainage	0.8415	0.0857	0.2714	0.9246	0.7651
Treatment: Drainage	0.4452	0.7146	0.2786	0.2672	0.2211

). In addition, CH_4 and N_2O fluxes were not significantly affected by either drainage or solution addition (

	Baseline	Treatment-loading	Drawdown	Re-saturation	Total
Daily CO_2 (g−C m^{-2} Day^{-1})					
Control (no drainage)	1.81	1.28	1.76a	1.14	1.19
Ditch	1.73	1.32	1.45a	1.25	1.24
SO_4	1.60	1.37	1.23a	1.05	1.07
Control (with drainage)	1.43	1.37	7.21b	0.97	1.31
Ditch	1.60	1.44	6.36b	0.97	1.30
SO_4	1.51	1.77	8.31b	1.02	1.41
Treatment	0.6686	0.5610	0.4095	0.8286	0.9544
Drainage	0.0601	0.1369	<0.0001***	0.1341	0.1653
Treatment: Drainage	0.4775	0.2670	0.1001	0.6547	0.6205
Daily CH_4(mg−C m^{-2} Day^{-1})					
Control (no drainage)	140	169	128	68	92
Ditch	162	187	163	114	133
SO_4	132	137	158	93	109
Control (with drainage)	166	211	54	52	73
Ditch	194	216	68	56	84
SO_4	193	194	87	61	91
Treatment	0.7042	0.4848	0.8336	0.5619	0.3914
Drainage	0.1189	0.0542	0.0937	0.0737	0.0750
Treatment: Drainage	0.8267	0.8308	0.9710	0.7037	0.7200
Daily N_2O (mg−N m^{-2} Day^{-1})					
Control (no drainage)	0.178	0.049	-0.231	0.116	0.039

Ditch	-0.018	-0.036	0.192	0.171	0.116
SO_4	0.015	0.000	0.303	0.994	0.600
Control (with drainage)	0.065	0.231	-0.065	0.407	0.249
Ditch	0.040	0.013	-0.053	0.322	0.159
SO_4	0.111	0.052	-0.134	0.334	0.190
Treatment	0.4427	0.0734	0.4049	0.3428	0.3011
Drainage	0.8415	0.0857	0.2714	0.9246	0.7651
Treatment: Drainage	0.4452	0.7146	0.2786	0.2672	0.2211

). In this phase, LRR of all treatments to the drainage perturbation on CO_2 and CH_4 significantly changed over time (*Ps* < 0.05; Fig. 4.5). In addition, there were indications that CO_2 responded more strongly to SO_4^{2-} addition, but differences between solution treatments were not statistically significant; the same was true for the flux result (

	Baseline	Treatment-loading	Drawdown	Re-saturation	Total
		Daily CO_2 (g−C m^{-2} Day^{-1})			
Control (no drainage)	1.81	1.28	1.76a	1.14	1.19
Ditch	1.73	1.32	1.45a	1.25	1.24
SO_4	1.60	1.37	1.23a	1.05	1.07
Control (with drainage)	1.43	1.37	7.21b	0.97	1.31
Ditch	1.60	1.44	6.36b	0.97	1.30
SO_4	1.51	1.77	8.31b	1.02	1.41
Treatment	0.6686	0.5610	0.4095	0.8286	0.9544
Drainage	0.0601	0.1369	<0.0001***	0.1341	0.1653
Treatment: Drainage	0.4775	0.2670	0.1001	0.6547	0.6205
		Daily CH_4(mg−C m^{-2} Day^{-1})			
Control (no drainage)	140	169	128	68	92
Ditch	162	187	163	114	133
SO_4	132	137	158	93	109
Control (with drainage)	166	211	54	52	73
Ditch	194	216	68	56	84
SO_4	193	194	87	61	91
Treatment	0.7042	0.4848	0.8336	0.5619	0.3914
Drainage	0.1189	0.0542	0.0937	0.0737	0.0750
Treatment: Drainage	0.8267	0.8308	0.9710	0.7037	0.7200
		Daily N_2O (mg−N m^{-2} Day^{-1})			
Control (no drainage)	0.178	0.049	-0.231	0.116	0.039
Ditch	-0.018	-0.036	0.192	0.171	0.116
SO_4	0.015	0.000	0.303	0.994	0.600
Control (with drainage)	0.065	0.231	-0.065	0.407	0.249
Ditch	0.040	0.013	-0.053	0.322	0.159
SO_4	0.111	0.052	-0.134	0.334	0.190
Treatment	0.4427	0.0734	0.4049	0.3428	0.3011
Drainage	0.8415	0.0857	0.2714	0.9246	0.7651
Treatment: Drainage	0.4452	0.7146	0.2786	0.2672	0.2211

; Supplementary Fig. 4.4). Following re-saturation (n=17), CO_2 fluxes rapidly decreased, whereas CH_4 fluxes gradually increased. None of the solution addition treatments had a significant effect on any GHGs fluxes during this phase. Interestingly, in the absence of drainage, SO_4 addition led to a divergence in N_2O fluxes compared to other solution treatments (Supplementary Fig. 4.4).

Table 4. 2. Least squares means under different solution addition treatments (control, ditchwater, and SO_4^{2-} addition) and water drawdown condition (no drainage, drainage) across consecutive four phases (baseline, treatment-loading, drawdown, and re-saturation) and in total

	Baseline	Treatment-loading	Drawdown	Re-saturation	Total
			Daily CO_2 (g−C m^{-2} Day^{-1})		
Control (no drainage)	1.81	1.28	1.76a	1.14	1.19
Ditch	1.73	1.32	1.45a	1.25	1.24
SO_4	1.60	1.37	1.23a	1.05	1.07
Control (with drainage)	1.43	1.37	7.21b	0.97	1.31
Ditch	1.60	1.44	6.36b	0.97	1.30
SO_4	1.51	1.77	8.31b	1.02	1.41
Treatment	0.6686	0.5610	0.4095	0.8286	0.9544
Drainage	0.0601	0.1369	<0.0001***	0.1341	0.1653
Treatment: Drainage	0.4775	0.2670	0.1001	0.6547	0.6205
			Daily CH_4(mg−C m^{-2} Day^{-1})		
Control (no drainage)	140	169	128	68	92
Ditch	162	187	163	114	133
SO_4	132	137	158	93	109
Control (with drainage)	166	211	54	52	73
Ditch	194	216	68	56	84
SO_4	193	194	87	61	91
Treatment	0.7042	0.4848	0.8336	0.5619	0.3914
Drainage	0.1189	0.0542	0.0937	0.0737	0.0750
Treatment: Drainage	0.8267	0.8308	0.9710	0.7037	0.7200
			Daily N_2O (mg−N m^{-2} Day^{-1})		
Control (no drainage)	0.178	0.049	-0.231	0.116	0.039
Ditch	-0.018	-0.036	0.192	0.171	0.116
SO_4	0.015	0.000	0.303	0.994	0.600
Control (with drainage)	0.065	0.231	-0.065	0.407	0.249
Ditch	0.040	0.013	-0.053	0.322	0.159
SO_4	0.111	0.052	-0.134	0.334	0.190
Treatment	0.4427	0.0734	0.4049	0.3428	0.3011
Drainage	0.8415	0.0857	0.2714	0.9246	0.7651
Treatment: Drainage	0.4452	0.7146	0.2786	0.2672	0.2211

* , **, and *** indicates statistical significance at P <0.05, P <0.01, P <0.001.
Different lowercase letters indicate significance between treatments based upon post hoc analysis after two-ANOVA (α = 0.05).

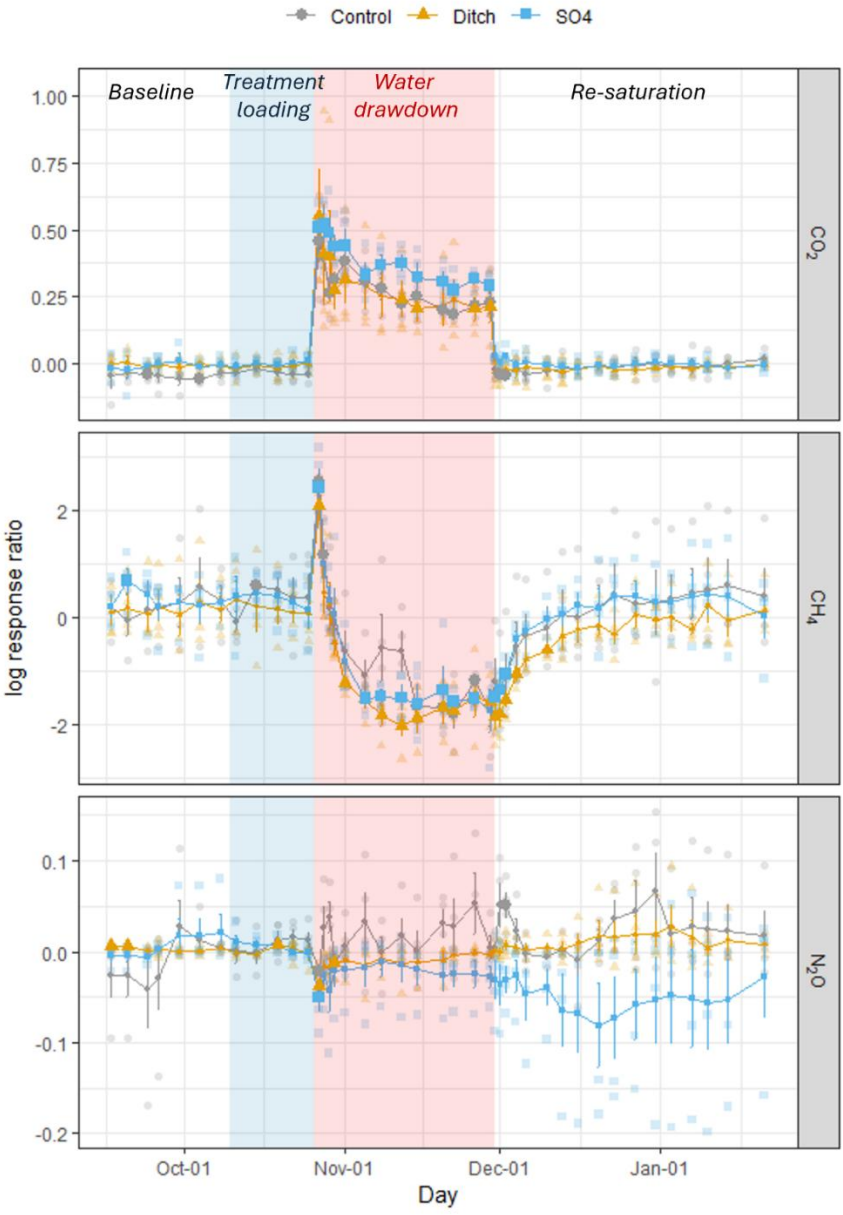


Fig. 4.5. Relative responses of solution addition treatments (control, ditch, and SO_4^{2-} addition) to hydrological pulse perturbation over time on CO_2, CH_4 and N_2O fluxes. Dense dots represent mean log response ratio (n=4), faint dots represent individual data points, and error bars show standard error of the means. Lager dense dots denote statistically significant effects of the perturbation (P <0.05), based on one-way ANOVA for fluxes responses.

Analyses of stability metrics−including temporal variability, resistance, and resilience−showed no significant difference in response to solution additions (Fig. 4.5; Supplementary Fig. 4.5). In contrast, the control (demineralized water) showed higher spatial variability in CO_2 and CH_4 fluxes ($Ps < 0.05$) than ditchwater and SO_4^{2-} addition, indicating that solution addition treatments are responsible for a greater stability of CO_2 and CH_4 emissions. For N_2O fluxes, SO_4^{2-} addition had the greatest spatial variability, followed by the control and ditchwater treatments, reflecting a pattern of peat destabilization ($P < 0.05$).

4.3.3 Chemical properties from the mesocosm experiment

During the baseline phase, EC, Alkalinity, and pH were not significantly different across drainage and solution addition treatments ($Ps > 0.05$; Supplementary Table 4.2). In the treatment-loading phase, EC, Alkalinity, and pH did not different significantly between drainage treatments ($Ps > 0.05$; Supplementary Table 4.2). However, alkalinity in the ditchwater addition treatment was significantly lower than in the control ($P < 0.05$), but similar to that of the SO_4^{-2} treatment. During the water drawdown phase, drainage significantly decreased EC, alkalinity, pH, and total P ($Ps < 0.05$). Among the solution treatments, SO_4^{2+} addition significantly increased pH compared to control and ditch treatments, whereas both ditchwater and SO_4^{2+} addition treatments had significantly lower NO_3^- concentrations than control treatment ($Ps < 0.05$). In the re-saturation phase, pH and alkalinity in SO_4^{2+} treatment were significantly higher than in other two solution treatments ($Ps < 0.05$). A significant interaction effect was observed for NO_3^- and total P ($Ps < 0.05$). In the control and ditchwater treatments, drainage had no effect on NO_3^-, whereas in the SO_4^{2+} addition treatment, the drained peat had significantly higher NO_3^- than the undrained peat. Total P in the control treatment was similar across the drainage treatment; however, in the ditch treatment, the drained peat had significantly lower total P than the undrained peat, while in the SO_4^{2+} addition treatment, the drained peat showed higher total P than the undrained peat.

4.3.4 Direct and indirect effects of drainage and solution addition treatments on GHG fluxes

The final piecewise SEM models revealed distinct phase-specific pathways linking environmental drivers to GHG emissions (Fig. 4.6). During the water drawdown phase, drainage significantly increased the CO_2 fluxes (coefficients: no-drainage = 1.22, drainage = 1.36) and decreased CH_4 fluxes (no-drainage = 2.33, drainage = 1.78) indicating a direct effect (*Ps* < 0.05; Fig. 4.6). In addition, drainage indirectly reduced the nutrient status via reduced ionic strength (*Ps* < 0.05; Fig. 4.6). The solution addition treatment significantly influenced nutrient status (control: 0.63, ditch: -0.45, SO_4^{2+} = -0.17) and pH (control: 6.18, Ditch: 6.10, SO_4^{2+} = 7.07), with pH further mediating the CO_2 flux (coefficient = 0.26; $P < 0.05$). Specifically, the highest pH values under SO_4^{2-} addition indirectly increased CO_2 fluxes through a positive pH−CO_2 relationship.

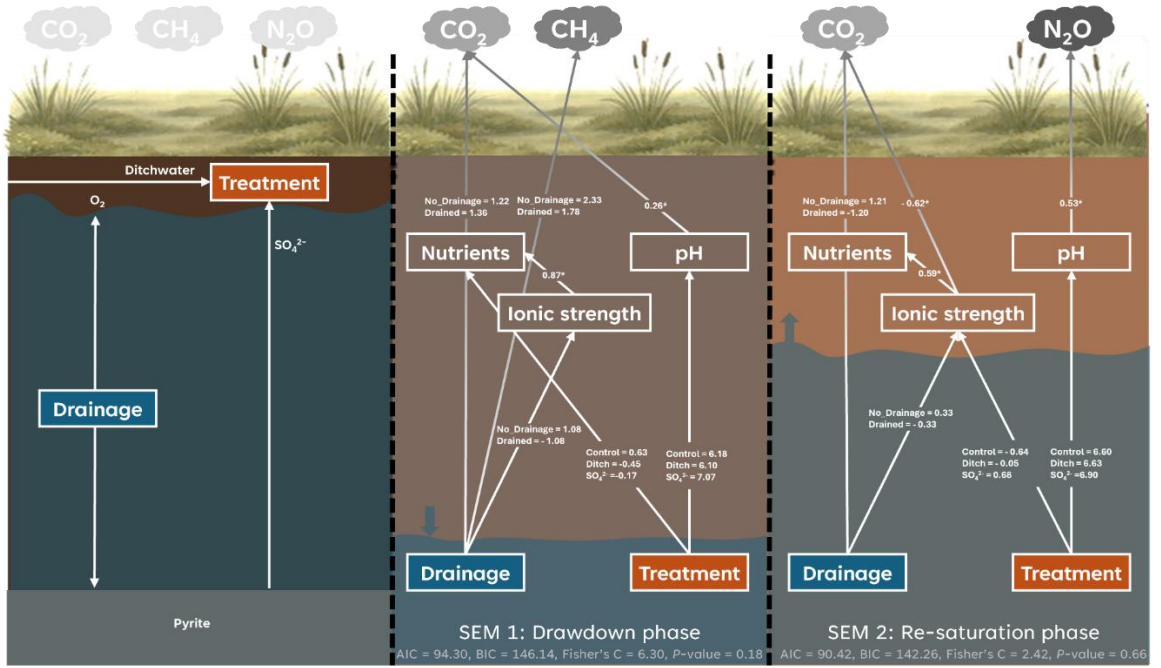


Fig. 4.6. Structural equation model illustrating the effects of key environmental drivers on greenhouse gas emissions (CO_2, CH_4, and N_2O) under (A) drawdown and (B) re-saturation phases. Arrows represent hypothesized causal relationships; only significant pathways are shown with values indicating standardized path coefficients.

In the re-saturation phase, legacy effects of prior drainage conditions remained evident, influencing the nutrient status, the ionic strength, and the CO_2 fluxes ($Ps < 0.05$; Fig. 4.6). Drainage significantly reduced CO_2 fluxes (coefficients: no-drainage = 1.21, drainage = 1.20) and indirectly reduced the nutrient status but increased the CO_2 fluxes via decreased ionic strength. The same drainage → ionic strength → nutrient pathway observed during drawdown phase persisted during re-saturation phase. Additionally, the solution addition treatment significantly affected the pH and the ionic strength, indirectly influencing the nutrient, and CO_2 and N_2O fluxes ($Ps < 0.05$; Fig. 4.6). Notably, SO_4^{2-} addition indirectly increased the N_2O fluxes (control: 6.60, ditch: 6.63, SO_4^{2-}: 6.90) via a positive pH−N_2O relationship (coefficient = 0.53; $P < 0.05$, Fig. 4.6), while also elevating ionic strength (control: -0.64, ditch: -0.05, SO_4^{2-}: 0.68), which positively affected nutrient release but negatively affected the CO_2 fluxes (coefficients: nutrient = 0.56, CO_2 flux = -0.62; $Ps < 0.05$).

4.4. Discussion

4.4.1 Fen peat collapse causes persistent, multi-dimensional changes in ecosystem structure and functions

Field observations, landscape photographs, and LiDAR-derived digital terrain models indicated abrupt and substantial reductions of surface height between 2015 and 2025, with mean total elevation losses of -12.8 ± 2.3 cm at the collapsed plots (Fig. 4.3). Although difference in LiDAR resolution between two surveys may introduce some uncertainty, the estimated annual rate of elevation loss is in line with previous reports of peat collapse in marshes (-1 to -7.5 cm yr^{-1}; Chambers et al., 2019). The collapsed area exhibited progressive expansion, characterized by the formation of new ponds or coalescence of existing ones−a pattern similarly also observed in marshland peat collapse (Chambers et al., 2019). Although it is challenging to infer exact carbon losses in the collapsed areas based on the LiDAR models, it is clear that losses were substantial (-

21.6 ± 6.1 kg−C m^{-2}) as compared to gradual peat subsidence in drained temperate fens (-0.8 to -1.6 cm yr^{-1} and -0.25 to -0.55 kg−C m^{-2} yr^{-1}; Leifeld et al., 2011).

The magnitude and abrupt nature of the fen collapse underline a rapid and critical alteration in ecosystem functioning, reflected in significant differences between collapsed and non-collapsed plots across all assessed ecological compartments (Fig. 4; Osland et al., 2020; Middleton and David, 2022). The observed elevation loss, together with shifts in soil chemical properties and biotic assemblages, indicates a transition from a lowland peat system toward a mudflat-like state (Cahoon et al., 2003). This transition was followed by significant vegetative shifts, including tentatively temporal reductions in plant biomass during the transition phase, as well as significant decline in mesofaunal abundance (Table 4.1). Mesofaunal communities shifted from collembolan-dominated assemblages to either mite- or enchytraeid-dominate assemblages in summer and early fall, with reduced richness. In addition to these biotic changes, soil organic matter molecular composition showed reductions in plant-derived structural components, such as carbohydrates, aliphatic compounds, and ester-linked moieties (Fig. 4.4; Supplementary Fig. 4.3), indicating substantial damage to the organic components scaffolding peat soil strength and structural integrity (Hagerthey et al., 2008; Schellekens et al., 2009; Flanagan et al., 2020; Cadigan et al., 2022).

Collectively, these results show that fen peat collapse is likely to restructure belowground ecological networks and their functional roles, as geochemical processes tightly regulate C release through feedback between soil chemistry and biological activity (Duhamel et al., 2019; Grudzinski et al., 2022; Laine et al., 2021; Milner et al., 2021; Reynaert et al., 2021). Shifts in soil mesofauna could alter soil C turnover through changes in burrowing and feeding activities (Juan-Ovejero et al., 2020), where mite-dominated communities near the collapsed areas may further accelerate peat decomposition (Seniczak et al., 2022). Vegetation changes may further influence soil C dynamics by modifying litter quality, root exudate patterns, and rhizosphere

transformations (Dieleman et al., 2015; Kreyling et al., 2021). Together, these biotic changes could reinforce a positive feedback loop, limiting plant biomass accumulation and limit natural recovery (Cahoon et al., 2003; Chambers et al., 2019).

4.4.2. Potential mechanisms contributing to fen peat collapse at De Zegge

Of the potential pathways for peat collapse suggested in literature (Chambers et al., 2019), the most researched pathway−where vegetation stress or mortality sets the conditions for collapse−is less evidenced in De Zegge. As corroborated by site managers, no obvious changes in vegetation were observed in the period leading to the collapse, despite frequent visual monitoring of the area (T. Deswert, personal communication, 2018). Our mesocosm experiment further highlights that hydrological perturbations remain the most important direct driver for oxidative losses of carbon (Fig. 4.6;

	Baseline	Treatment-loading	Drawdown	Re-saturation	Total
			Daily CO_2 (g−C m^{-2} Day^{-1})		
Control (no drainage)	1.81	1.28	1.76a	1.14	1.19
Ditch	1.73	1.32	1.45a	1.25	1.24
SO_4	1.60	1.37	1.23a	1.05	1.07
Control (with drainage)	1.43	1.37	7.21b	0.97	1.31
Ditch	1.60	1.44	6.36b	0.97	1.30
SO_4	1.51	1.77	8.31b	1.02	1.41
Treatment	0.6686	0.5610	0.4095	0.8286	0.9544
Drainage	0.0601	0.1369	<0.0001***	0.1341	0.1653
Treatment: Drainage	0.4775	0.2670	0.1001	0.6547	0.6205
			Daily CH_4(mg−C m^{-2} Day^{-1})		
Control (no drainage)	140	169	128	68	92
Ditch	162	187	163	114	133
SO_4	132	137	158	93	109
Control (with drainage)	166	211	54	52	73
Ditch	194	216	68	56	84
SO_4	193	194	87	61	91
Treatment	0.7042	0.4848	0.8336	0.5619	0.3914
Drainage	0.1189	0.0542	0.0937	0.0737	0.0750
Treatment: Drainage	0.8267	0.8308	0.9710	0.7037	0.7200
			Daily N_2O (mg−N m^{-2} Day^{-1})		
Control (no drainage)	0.178	0.049	-0.231	0.116	0.039
Ditch	-0.018	-0.036	0.192	0.171	0.116
SO_4	0.015	0.000	0.303	0.994	0.600
Control (with drainage)	0.065	0.231	-0.065	0.407	0.249

Ditch	0.040	0.013	-0.053	0.322	0.159
SO_4	0.111	0.052	-0.134	0.334	0.190
Treatment	0.4427	0.0734	0.4049	0.3428	0.3011
Drainage	0.8415	0.0857	0.2714	0.9246	0.7651
Treatment: Drainage	0.4452	0.7146	0.2786	0.2672	0.2211

; Table 2; Robinson and Moore, 1999; Radabaugh et al., 2021; Evans et al., 2021). However, drought events prior to 2018 did not cause peat collapses, nor have subsequent droughts so far triggered abrupt collapses elsewhere in the area. This suggests that drought alone is insufficient to initiate fen collapse. Evidence of preceding alteration in physicochemical and organic matter characteristics in the near-collapsed areas that collapsed in the following years (Fig. 4.4 C&D) further indicates that chronic stressors lower peatland resilience and modify biogeochemical properties, thereby preconditioning the system for collapse when drought occurs.

A key chronic stressor in this system appeared to be increased sulphate concentrations, likely originating from pyrite oxidation (FS_2). Site observations indicate higher Ca^{2+} and Mg^{2+} concentrations and soil pH near the collapsed sites (Fig. 4.4C), suggesting the presence of a groundwater recharge zone in the south-western part of De Zegge (including the collapsed sites C1 and C2 and non-collapsed sites NCD3 and NCD6) for at least part of the year. Groundwater samples from these locations (Supplementary Fig. 1; Moris, 2020) confirm sulphate enrichment. This enrichment is most plausibly explained by excessive nitrate leaching from upstreaming sources, which can lead to sulphate release from the pyrite present in the underlying marine sands (Bourceau et al., 2023), with subsequent upwards transport via recharged flow.

In a successional phase, higher sulphate concentrations appeared to act as chronic stressor, tentatively contributing to peat collapse through indirect effects via increasing pH rather than through immediate effects. Although sulfate can act as alternative electron acceptor for organic matter oxidation in waterlogged conditions (de Mars and Wassen, 1999), the commonly hypothesized mechanism of enhanced CO_2 production via sulfate reduction under anoxic conditions (Chambers et al., 2019; van Dijk et al., 2019) was not clearly observed in our flux measurements (

	Baseline	Treatment-loading	Drawdown	Re-saturation	Total
			Daily CO_2 (g−C m^{-2} Day^{-1})		
Control (no drainage)	1.81	1.28	1.76a	1.14	1.19
Ditch	1.73	1.32	1.45a	1.25	1.24
SO_4	1.60	1.37	1.23a	1.05	1.07
Control (with drainage)	1.43	1.37	7.21b	0.97	1.31
Ditch	1.60	1.44	6.36b	0.97	1.30
SO_4	1.51	1.77	8.31b	1.02	1.41
Treatment	0.6686	0.5610	0.4095	0.8286	0.9544
Drainage	0.0601	0.1369	<0.0001***	0.1341	0.1653
Treatment: Drainage	0.4775	0.2670	0.1001	0.6547	0.6205
			Daily CH_4(mg−C m^{-2} Day^{-1})		
Control (no drainage)	140	169	128	68	92
Ditch	162	187	163	114	133
SO_4	132	137	158	93	109
Control (with drainage)	166	211	54	52	73
Ditch	194	216	68	56	84
SO_4	193	194	87	61	91
Treatment	0.7042	0.4848	0.8336	0.5619	0.3914
Drainage	0.1189	0.0542	0.0937	0.0737	0.0750
Treatment: Drainage	0.8267	0.8308	0.9710	0.7037	0.7200
			Daily N_2O (mg−N m^{-2} Day^{-1})		
Control (no drainage)	0.178	0.049	-0.231	0.116	0.039
Ditch	-0.018	-0.036	0.192	0.171	0.116
SO_4	0.015	0.000	0.303	0.994	0.600
Control (with drainage)	0.065	0.231	-0.065	0.407	0.249
Ditch	0.040	0.013	-0.053	0.322	0.159
SO_4	0.111	0.052	-0.134	0.334	0.190
Treatment	0.4427	0.0734	0.4049	0.3428	0.3011
Drainage	0.8415	0.0857	0.2714	0.9246	0.7651
Treatment: Drainage	0.4452	0.7146	0.2786	0.2672	0.2211

), and its contribution appeared minor compared to the oxidative release of GHG in the mesocosm experiment (Fig. 4.5). Instead, the SEM revealed an indirect effect of SO_4^{-2} addition on peat decomposition via increased pH. Sulphate reduction consumes protons, thereby decreasing acidity and alleviating constraints on decomposition (Fig. 4.6; Anderson et al., 2017), and is consistent with the field observation of a higher pH in collapsed plots (Fig. 4.4C). The increase in pH may create a favorable environment for microbial activity or enzyme-mediated decomposition and increase nitrate availability (Frankenberger and Johanson, 1982), thereby enhancing CO_2 and N_2O emissions. This suggests that pH is a key mediator of peat stability, regulating CO_2 and N_2O release more strongly than sulfate-driven mineralization alone. However, the relatively low path coefficients between pH and CO_2 (0.26) and between pH and N_2O (0.53)

indicate that additional environmental factors could also play an important role (Vile and Novák, 2006; Bahram et al., 2022; AminiTabrizi et al., 2023).

Sulphate enrichment may further accelerate peat instability within sulphate-driven redox changes. Specifically, sulphates may lower stochiometric constraints on decomposition by (1) releasing phosphate previously bound in the form of vivianite ($Fe_3(PO_4)_2.8H_2O$) into the groundwater (Fig. 4.4C), and (2) indirectly enhancing nitrification (from NH^{4+} to NO^{3-}, Fig. 4.4C). Vivianite is common in fens, including De Zegge, and may become a major internal source of phosphorus under sulfate-rich conditions, a process linked to sulphate reduction that may intensify under future climate warming (Smolders et al., 2010; Han et al., 2023; Smolders et al., 2024). Relatively higher nitrate concentrations in collapsed plots (Fig. 4.4C), together with the indirect pathway in the SEM linking SO_4^{2-} addition to elevated N_2O fluxes, again mediated by increased pH, support the important role of this interaction between sulfates and nitrate availability for denitrification processes Fig. 4.6. In addition, SO_4^{2-} reduction produces hydrogen sulfide (H_2S), which may stimulate other denitrifying microbes capable of using H_2S as an electron donor (Helton et al., 2014).

Nevertheless, hydrological perturbation cannot be ruled out as a contributor to accelerating peat decomposition and to promoting the development of mudflat-like features. An increased frequency of drought−flood cycles may also reduce the stability of peatland functioning, particularly with respect to GHG emissions (Freeman et al., 2001). In addition to substantial CO_2 emissions, drainage induced pronounced peaks in the LRR of CH_4 and N_2O immediately following the perturbation, implying a transient instability in peat biogeochemical functioning (Fig. 4.5). Overall, the variability of GHG fluxes increased relative to the undisturbed peat monolith (Fig. 4.5), highlighting the critical role of hydrological perturbation in regulating peatland functioning as it has also been observed by other studies (e.g. Robroek et al., 2024; Jeewani et al., 2025).

Overall, elevated SO_4^{2-}–most likely released from ancient marine deposits- under present-day nitrate excesses may initiate a series of co-occurring, self-reinforcing processes, together with hydrological disturbances, that progressively destabilize the peat matrix and increase its vulnerability to peat collapse (Fig. 4.7). The indirect effects of increased pH on CO_2 and N_2O emissions, along with greater spatial variability observed under SO_4^{2-} addition, indicate that SO_4^{2-} intrusion could push the system toward ecological thresholds beyond which full recovery may no longer be achievable (Folke et al., 2004; Keith et al., 2023). Anthropogenic changes in climate and nitrate loading, interacting with the site's marine history dating back approximately 7-11 Ma ago, may therefore link the functioning of this lowland fen to processes currently observed in coastal marches (Chambers et al., 2019). This also highlights the need for close monitoring of fens where the peat is underlain by pyrite and exposed pollute intrusion and hydrological stressors, as these systems are likely vulnerable to abrupt peat collapse.

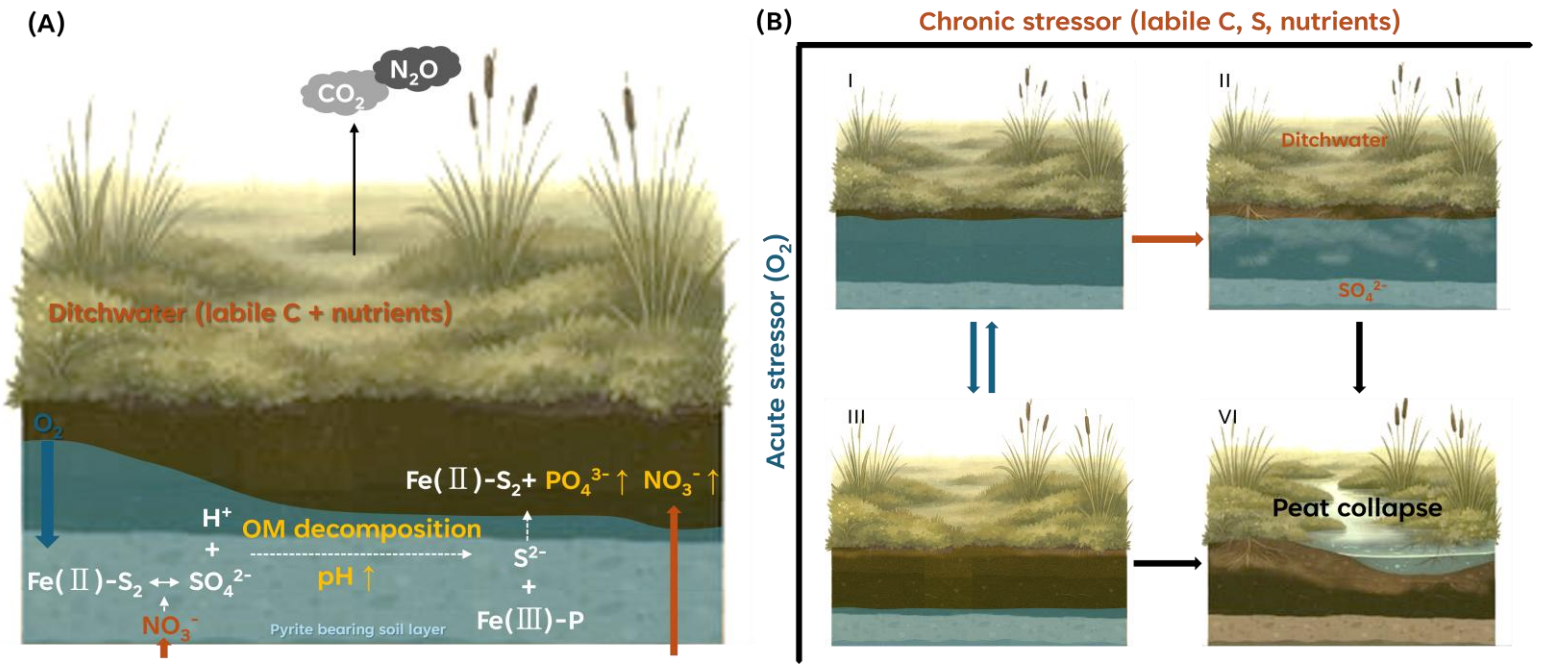


Fig. 4.7. Conceptual representation of the impact of chronic and acute stressors on peat stability. Left: key redox reactions influenced by the presence of pyrite and by inputs of labile carbon and nitrogen via ditch water. Right: the interaction between chronic and acute stressors can trigger peat collapse, representing a state from which no reversed pathway is possible.

4.4.3. Early warning signals

Early warning signals are critical to prevent abrupt losses of ecosystem functions and soil C stocks when a fen transitions to a mudflat-type of ecosystem (Andersen et al., 2009; Chambers et al., 2019). In our study, the ongoing expansion of the collapsed area (Fig. 4.3), coupled with evidence that peat damage and destabilization occur before visible changes at the surface or in the vegetation, corroborates the urgency of identifying reliable early warning indicators. Given that marine sediments and nitrate pollution are widespread in many lowland fens in Flanders (Khan et al., 2025), and that climatic extremes are becoming more frequent (Dai, 2013; Berg et al., 2016), such indicators would be valuable for assessing the vulnerability of other lowland fens to future perturbation. Nonetheless, observation at De Zegge suggests that the shift from gradual subsidence to sudden collapse is unlikely to result from a single driver. Instead, it appears to involve a series of transitional changes, underscoring the need for a multi-proxy approach to peat degradation assessment (Supplementary Fig. 6; Andersen et al., 2009).

Interestingly, while the mesofauna of plots adjacent to the collapsed plots resembled those of non-collapsed plots further away, their physiochemistry and soil organic matter molecular composition aligned more closely with the collapsed plots (Fig. 4.4), indicating that peat degradation precedes visible ecological changes. Li-DAR imagery from 2025 further confirms the lateral expansion of collapse into these plots. Two diagnostic pathways provide early-stage degradation: MIR spectra capture hydrologically induced degradation, while physicochemical measures reveal nutrient- and sulphate-induced stress. Collapse appears most likely when both pathways coincide. Site-level comparisons support why some site areas have not collapsed: for instance, NCD5 and NCD7 experience the largest hydrological fluctuations of the area and show similar peat compaction and molecular damage as the collapsed sites (Fig. 4.4C&D), yet are subjected to subsidence rather than collapse (Moris, 2020). In contrast, NCD 3 and NCD 6 are affected by recharge and have similar high base cations, nutrient availability, pH and SO_4^{2+}

availability (Moris, 2020) as the collapsed sites, but have the most stable water tables of the entire conservation area and the most intact molecular composition or sulphate alone, also stay stable as long as water table fluctuation remains moderate (Fig. 4.4C&D; Supplementary Fig. 4.1). These findings underscore that collapse happens only where chronic hydro-chemical stressors (S, nutrients and pH) and acute perturbations of water level drawdown coincide (Fig. 4.7). When combined, they create a greater risk for sudden and drastic changes. Thus, the areas most at risk for collapse are fens resting on pyrite-rich marine sediments affected by high nitrate pollution, a condition that occurs throughout the Nete valleys, an important hotspot for peat formation (Swinnen et al., 2023) that are affected by lowering water tables or increased incidence of severe or prolonged droughts. Restoring hydrological conditions and mitigating drought impacts are therefore crucial in avoiding subsidence and collapse in this catchment, and recognizing these two distinct early warning signals across degradation gradients is essential for timely intervention.

4.5. Conclusions

This study demonstrated that fen peatland collapse can lead to abrupt peat losses in fens, accompanied by structural and functional shifts in soil biota, vegetation, physicochemical properties and molecular composition. Such changes may critically undermine belowground stability and resistance to droughts and demand greater attention. Notably, asynchronous and variable-specific transitions highlight the need for multi-indicator approaches to effectively detect early warning signals of peat collapse. Based on combined field observations and mesocosm experiments, peat stability can be substantially compromised by the interaction between acute hydrological perturbation and elevated sulfate acting as chronic stressor. These conditions stimulate peat degradation by creating microbially favorable environments, inducing shifts in the redox regime, increasing the availability of alternative electron acceptors, prompting pH changes, and stimulating nutrient release. Collectively, our results advance our understanding of long-term impact of pedological regime shifts on fen peatland integrity. Given the rising climate variability

and the intrusion of SO_4^{2-} as derived from marine sediments (Shen et al., 2025), these stressors should be closely monitored to mitigate potentially severe consequences for peat structural integrity and ecosystem stability.

Acknowledgements

The authors gratefully acknowledge the assistance of Steven Bouillon, Yannick Stroobandt, Lore Fondu, Kim Vekemans, Toon Coolen, Caro Van Den Eynde, Michel van Son, and Ilié Storms for their contribution to the sample handling procedure, equipment operation and training, and for sharing their expertise to enhance workflow. We also thank the site managers Maarten Goossens, Pieter Dierckx, and Ward Royens for hosting and supporting filed excursions and experimental setup, and for their great willingness to share their extensive field knowledge. This research was funded by the Research Foundation Flanders (FWO-G060721N).

No legacy effect of wildfire on peat carbon stability in a Belgian peatland[2]

5

[2] Keunbae Kim, Willem-Jan Emsens, Judith Schellekens, Erik Verbruggen, Bas Van der Veken, Layla Maas, Rudy van Diggelen, María J. I. Briones, Boris Jansen, Karen Vancampenhout

Abstract

Ongoing climate change, particularly warmer and drier conditions, disrupts hydrological stability in peatland ecosystems and elevates wildfire risk. Higher burn severity and frequency are expected to accelerate carbon (C) losses and amplify climate-carbon feedback. In this study, we used an accidental and short-lived wildfire that occurred in 2020 at Landschap De Liereman (Belgium), a mosaic landscape ranging from poor-fen to bog-like peatlands, to investigate how belowground C dynamics respond to peatland fire in the subsequent four consecutive years under ongoing climatic pressures. A twin-plot design was established, consisting of burnt and nearby intact plots, and field measurements were integrated with model-based upscaling and remote sensing data. Burnt peatland patches were significantly altered during the first two years after the fire, evidenced by lower topsoil C:N ratios, reduced C and N isotopic values ($Ps < 0.05$), and shifts in soil organic matter (SOM) composition. Especially, carbohydrates declined whereas benzenes and N compounds increased ($P < 0.05$), indicating depletion of labile C and accumulation of recalcitrant aromatic C leading to lower soil organic carbon (SOC) decomposability (i.e., basal respiration per unit peat C, $P < 0.05$). These differences diminished within three years, with no smoldering fire and very little changes in bulk soil C and N contents between intact and burnt plots, suggesting a relatively high resilience to a low-severity fire. However, in 2022, abrupt changes in soil C and N concentrations, SOM composition, and SOC decomposability were observed in both burnt and intact plots that were likely related to drought stress, although a belated fire-effect cannot be excluded.

Keywords: Peatland fire, ecosystem recovery, soil carbon, and soil organic matter

Highlights

- A low-severity fire at Landschap De Liereman caused only transient variations in soil carbon composition and stability.
- Low-severity fire temporarily decreased labile C and increased recalcitrant aromatic C leading to increased C stability.
- Fire legacy did not aggravate the impact of a subsequent drought on soil carbon quantity or quality.

5.1. Introduction

Peatlands play a critical role in global carbon (C) sequestration and dynamics (Loisel et al., 2017). Despite covering only about 3 % of the Earth's land surface, peatlands store one-third of global terrestrial C pool−about 600 Pg of organic C (1 Pg = 10^{15} g). Environmental conditions (e.g., waterlogged conditions and low pH) and their structurally complex plant inputs (e.g., cross-linked phenolic lignin and pectin-like polysaccharides) restrict decomposition and have led to soil organic carbon (SOC) accumulation throughout the Holocene (Baird et al., 2009; Kim et al., 2026b). This persistence reflects a positive net ecosystem C balance, where continuous plant inputs outweigh oxidative losses (Andersen et al., 2013; Charman et al., 2013; Brown et al., 2023).

However, a warmer and drier climate −coupled with severe and more frequent droughts− disrupts the hydrological stability of peatlands, alters their vegetation composition, and disturbs the tight ecological interactions that typically maintain high water table levels in peatlands (Kettridge et al., 2015; Ledger et al., 2023). Such disturbances not only accelerate oxidative decomposition (Hapsari et al., 2022), releasing vast amounts of C to the atmosphere, but also make peatland ecosystems more prone to wildfires (Cong et al., 2020; Jones et al., 2024; Zhang et al., 2025).

Peat fires therefore represent a clear symptom of peatland vulnerability to climate change (Ackley et al., 2021). Burnt peatlands contribute an estimated 2 Pg CO_2 loss annually−about 5 % of all anthropogenic global greenhouse gas (GHG) emissions (Kettridge et al., 2015; Joosten et al., 2017)−with smoldering belowground fires accounting for up to 15 % of annual GHG emissions (Rein, 2015). When peat fires coincide with other anthropogenic pressures such as drainage for agriculture, forest plantation and peat extraction, fire severity can be amplified by one or more orders of magnitude, causing extensive damage to peat structure, vegetation changes, and alterations in microbial communities (Kettridge et al., 2015). Risk assessments have indicated that under ongoing climate change and human activities, fire-prone

landscape could expand by 29 % by end of the 21st century (Senande-Rivera et al., 2022). Consequently, fire intensity and frequency interacting with climate changes will significantly reinforce the climate−carbon feedback, introducing substantial uncertainty in future earth-system trajectories (Ballhorn et al., 2009; Wilkinson et al., 2023).

Despite the potentially disproportionate responses of peatlands to fire, very little is known about how fire affects their belowground C stability, or how these effects vary spatially and temporally during post-fire recovery . Apart from the immediate damage caused by the burning of organic material, peat fires can alter post-fire C dynamics through a number of contrasting mechanisms. On the one hand, fires can enhance C persistence by altering peat physicochemical properties: (i) structural changes such as increased bulk density and reduced porosity, which reduces microbial accessibility to organic matter (Guo et al., 2024); (ii) loss of labile compounds and the formation of pyrogenic and aromatic C compounds that are inherently recalcitrant to microbial decomposition (Singh et al., 2012; Hodgkins et al., 2018; Cong et al., 2020); (iii) deposition of ash that can suppress microbial and enzymatic activity, further slowing decomposition (Freeman et al., 2001; Pellegrini et al., 2015). On the other hand, peat fires can promote decomposition through changes that stimulate microbial process as a result of (i) increased nutrient availability and (ii) changes in labile C composition, which enhances microbial activities, thereby accelerating organic matter turnover . These opposite processes can cause peatland responses to follow divergent pathways in reaching post-fire C stability (Leifeld et al., 2012). The direction and magnitude will strongly depend on fire intensity, time since fire, and local climate and biota (Könönen et al., 2018; Gray et al., 2021; Harrison et al., 2024). These factors collectively reshape post-fire successional development, influencing peat habitat quality and ecosystem functioning (Davies et al., 2013; Dhandapani and Evers, 2020). Nonetheless, field studies integrating temporal and spatial post-fire trajectories with belowground dynamics, and including soil organic matter (SOM) as a key component of C stability, remain scarce.

In this study, we investigated the effects of an accidental peat fire without evidence of smoldering that occurred in 2020 at the Landschap De Liereman reserve, one of Belgium's oldest and protected conservation areas and an important site at the European level within the EU Natura 2000 network. This event provided a unique opportunity to evaluate *in situ* fire effects on belowground processes and post-fire ecosystem recovery, as well as to evaluate peatlands' response vulnerability in the context of concurrent climate threats. Particularly, the study aimed to: (i) assess the fire impacts on soil structure and integrity, including elemental composition and SOM components (ii) investigate temporal trajectories of C stability alongside soil physicochemical properties; and (iii) examine how soil functions and processes interplay with C stability after fire via remote sensing-based vegetation cover index, peat physiochemical properties, and SOM molecular composition. We hypothesized that this peatland would experience substantial soil C losses but little change in C stability due to the contrasting mechanisms described above, and that, given the assumed low-severity of the fire based on the absence of smoldering, recovery would be rapid toward the pre-fire state. Our experimental design consisted of nine twin-plots (intact and burnt) with repeated soil sampling conducted over four consecutive years to assess post-fire recovery and evaluate legacy effects to subsequent climate-related stressors, such as drought in 2022, over time.

5.2. Materials and methods

5.2.1 Study site and experimental design

Our study site was located at in the nature reserve “Landschap De Liereman” (51.32° N, 4.99° E) in Antwerp, Belgium (Fig. 5.1A). The nature reserve hosts a wide range of habitats ranging from wet heathlands to poor fen and bog-like peatlands. The region receives on average 804 mm of precipitation annually and has a mean temperature of 11.8 ºC (data from 2017 to 2024, Cruz-Alonso et al., 2023). To maintain a consistent experimental setup, our study focused on soils with histic horizons consisting of poorly aerated organic material (IUSS Working Group WRB, 2024). A fire incident occurred on April 22, 2020, affecting approximately 27 hectares. Rather than complete burning the site, patchy fire damage, likely influenced by strong easterly winds and spatial heterogeneity, allowed us to establish nine twin-plots (intact vs. burnt) along a topographical gradient rising approximately 1.3 m from west to east (Natuurpunt, 2020, Fig. 5.1A&B). Post-fire recovery was monitored over the four consecutive field campaigns conducted on July 29, 2020; September 6, 2021; July 28, 2022; and August 11, 2023.

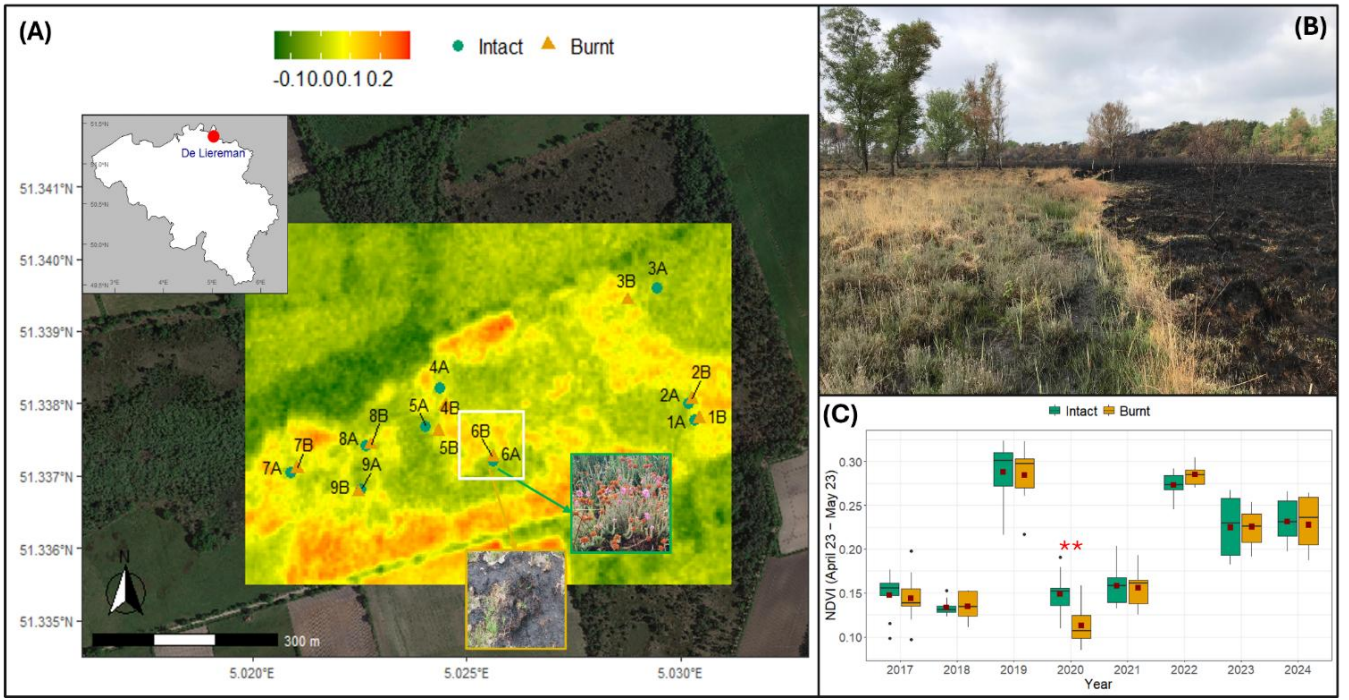


Fig. 5.1. Study site, twin-plot design and fire effects on vegetation cover index (NDVI): (A) Map of Landschap De Liereman nature reserve showing twin-plot established along the fire scar, based on difference in NDVI values between pre- and post-fire periods (two-week difference). The twin plots correspond to areas of burn severity. (B) Landscape photograph of the study site. (C) mean NDVI values at each sampling plot from 2017 to 2024, highlighting a significant difference between intact and burnt plots observed in 2020 (P <0.01, **).

5.2.2. Data collection

5.2.2.1. Satellite imagery for vegetation cover index

To assess fire severity and vegetation cover changes, and to quantify plot-based post-fire recovery, we used PlantScope multispectral satellite imagery (Planet labs Inc.). Its fine spatial resolution (3.5−4.1 m) enables a detailed tracking of vegetation dynamics over time. The imaginary consists of four bands: Red (590−682 nm), Green (500−585 nm), Blue (455−517 nm), and NIR (780−880 nm). Only images with cloud cover 0 % over the fire-affected area were retained. The normalized difference vegetation index (NDVI) was calculated as (NIR - Red) / (NIR + Red) using surface reflectance bands as used to compare conditions before and after the fire, and to track vegetation recovery over time. For annual monitoring, NDVI values were extracted for the April – May period for each year, using a 1-m buffer around each plot. More detailed field observations of vegetation changes can be found in (Maas et al (2026).

5.2.2.2. Field sampling and lab experiments

5.2.2.2.1 Peat depth and physicochemical properties

Peat depths in each plot were surveyed using an auger until the underlying mineral layer or bedrock was reached. Peat soil samples were collected from a depth of 0−5 cm using an auger and a knife. Four replicated subsamples from each plot were pooled into a single composite sample to represent each plot as one experimental unit. A total of 18 composite samples were collected annually during four consecutive years, resulting in 72 peat samples over the entire monitoring period. These samples were oven dried at 50 °C for 72 h and homogenously ball-milled with a vibration ball mill (MM400, Retsch, Germany). Total organic carbon and nitrogen contents, and their isotope values were measured in an elementary analyzer (Thermo Flash HT/EA; ISO 10694) equipped with an isotope ratio mass spectrometer (Thermo Delta V advantage; EA-IRMS). For dissolved organic carbon (DOC) analysis, dried samples were mixed with demineralized water at

a ratio of 1:10 and shaken for 48 h at 150 rpm. The suspensions were centrifuged for 20 mins at 3000 rpm and the supernatant was filtered through glass-fiber filter (0.7 µm pore size). These filtrates were acidified with HCl to pH 3.0 and stored until analysis. DOC and $DO^{13}C$ samples were subsequently measured using a wet oxidation TOC analyzer (IO analytical Aurora 1030W), coupled to an isotope ratio mass spectrometer (Thermo Finnigan Delta V Advantage). Ash content was determined by igniting dried samples in a muffle furnace at 550 ºC until complete combustion of organic matter. The remaining inorganic residues were expressed as a percentage of initial dry mass.

5.2.2.2.2 SOM molecular composition

SOM molecular composition in peat was determined using mid-infrared (MIR) spectroscopy (Frontier™ with auto-sampler from PerkinElmer, Waltham, MA, USA). Spectra were obtained in % transmittance mode over the wavenumber range of 4000 to 400 cm^{-1}, with a resolution of 1 cm^{-1} and 32 accumulations. Four replicate scans were averaged for each spectrum. To prevent drift signal, the reflectance of the scanned samples was divided by the average of the background samples (Brosens et al., 2021). The spectra were first converted from reflectance (R) to absorbance (A) unit by A=log(1/R) (Peltre et al., 2014).

5.2.2.2.3. Basal respiration incubation and SOC decomposability

The cumulative basal soil respiration divided by carbon contents is used as an indicator of the fraction of labile SOC, hereafter referred to as SOC decomposability. During the field campaigns in 2021 and 2023, four paired-replicated cores (100 cm^3, 5 cm height) were collected from each plot and one core from each pair was used to calculate bulk density and gravimetric water content, while the other core was retained for the incubation experiment. The aboveground litter layer was carefully removed using scissors prior to sampling.

The intact cores were immediately transferred to 250 ml jars and filled with field water to prevent any potential aerobic decomposition during transport. In the lab, water filled pore space (WFPS) of these cores was adjusted to 100 % and they were incubated at 21 °C for approximately 120 days throughout the incubation period. The volume of water required for saturation was calculated from porosity (Φ) of the sample:

$$\Phi = 1 - \frac{\rho_{bulk}}{\rho_s} \quad (1)$$

where ρ_{bulk} (g cm^{-3}) is the bulk density of the bulk sample, and ρ_s (g cm^{-3}) is the particle density, set at 2.65 g cm^{-3} (Säurich et al., 2019). Basal respiration was measured using a gas analyser (PBI Dansensor; Checkpoint II Portable Gas Analyser, Ringsted, Denmark) and CO_2 flux (μg CO_2−C g SOC^{-1} day^{-1}) was calculated as:

$$F = \left(\frac{dC}{dt}\right) \times \left(\frac{P \times V}{R \times T \times m}\right) \times 1M \times k \times \left(\frac{1}{SOC}\right) \quad (2)$$

where $\frac{dC}{dt}$ is the slope of a simple linear regression (μm^3 m^{-3} h^{-1}), P is the pressure of the gas (Pa), V is the headspace volume of the jar (m^3), R is the gas constant (m^3 Pa K^{-1} mol^{-1}), T is the temperature of the gas (K), m is the peat mass (g $peat^{-1}$), M is the atomic mass of C (12.01 g mol^{-1}), SOC is the fraction of peat organic carbon per peat (g SOC^{-1} g $peat^{-1}$) and k is a conversion factor for the flux unit (from g CO_2−C g SOC^{-1} h^{-1} to μg CO_2−C g SOC^{-1} day^{-1}).

2.2.3. Estimated SOM functional groups and SOC decomposability

The relative abundance of six functional groups−alkenes, benzene, carbohydrates, lignins, N compounds and phenols− as well as SOC decomposability, were estimated using predictive models based on MIR spectroscopy (Kim et al., 2026a). This model, developed from a large-scale European dataset of SOM molecular composition (Kim et al., 2026b), was specifically designed to assess differences in SOM functional groups across a broad gradient of aerobic and

anaerobic decomposition under varying hydrological conditions, and it is openly available for peatland monitoring purposes.

5.2.3. Statistical analyses and modelling approach

Post-fire effects on the NDVI values, soil physicochemical properties, SOC decomposability, and the estimated relative abundances of SOM functional groups were assessed. These effects were evaluated using analysis of variance (ANOVA) implemented through linear mixed-effect models (n = 18; 9 paired plots; df =8), with fire treatment specified as a fixed effect and twin-plot included as a random effect to account for the paired study design. The model assumption of residual normality and homoscedasticity were evaluated using the Shapiro-Wilk test and diagnostic plots. When the assumptions were violated, a Box-Cox transformation was applied. All statistical analyses were performed in R (R Development Core Team, 2025).

To analyze SOM molecular composition based on spectral data, a permutational multivariate analysis of variance (PERMANVOA; Anderson, 2001) with 999 iterations was conducted using Euclidian dissimilarity distance and implemented in the vegan package. Thereafter, data visualizations were performed using non-metric multidimensional scaling (NMDS, k=2).

For the MIR spectra dataset, a partial least squared discriminate (PLS-DA) model was established to identify key functional groups of SOM molecular composition most influenced by fire. Prior to model construction, a multilevel multivariate approach was applied to separate fire effects within paired plots from the random variation between paired plots (Liquet et al., 2012). The optimal number of latent variables for the model was determined using group-wise cross validation, with twin-plot assigned as the group. The final model was selected as the one achieving the highest classification accuracy while retaining the smallest number of latent variables within the range supported by a one-tailed T-test ($\alpha = 0.05$). The coefficients of the final model were subsequently used to identify the key functional groups of SOM molecular composition.

5.3. Results

5.3.1. NDVI and physicochemical properties in intact vs. burnt plots

Remote sensing data based on NDVI clearly reflected fire severity in the disturbed area immediately after the fire incident (Fig. 5.1A). However, the mean NDVI of the burnt plots was significantly lower in 2020, the year of the fire ($P < 0.05$) and thereafter, no significant differences between the intact plots and the burnt plots were observed (Fig. 5.1C), which is in line with field observations (Maas et al., 2026).

Compared with the burnt plots, the intact plots did not show significant differences in peat C and N contents across the consecutive four years of monitoring (2020−2023; $Ps > 0.05$; Fig. 5.2; Table 5.1). Conversely, significant decreases in the C:N ratio, $\delta^{13}C$, and $\delta^{15}N$ values were observed during the first two years since the fire incident (2020−2021; $Ps < 0.05$), although these differences diminished over time, with no significant treatment effect in later years ($Ps > 0.05$). The burnt plots also showed slightly shallower peat depths than the intact plots, but this difference was not statistically significant ($P > 0.05$; Table 5.1). Similarly, dissolved organic carbon (DOC), $\delta^{13}DOC$, bulk density, and ash content (sampled in 2021 and 2023; i.e., one and three years since the fire) did not differ between the intact and the burnt plots ($Ps > 0.05$; Table 5.1). Interestingly, temporal trends indicated detectable decreases in soil C and C:N ratio between pre- and post-2022 (Table 5.1).

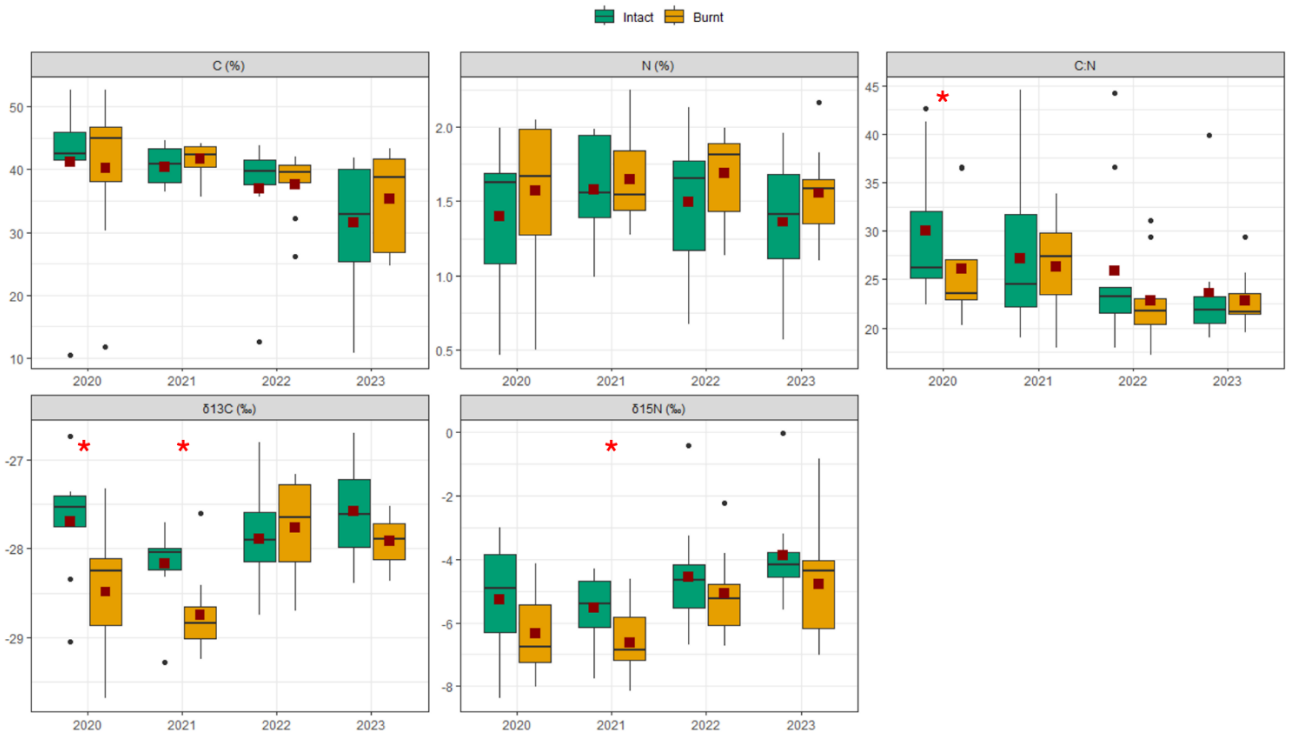


Fig. 5.2. Elemental analysis results between intact and burnt plots over four consecutive years. Red asterisks (*) denotes statistically significant difference at $\alpha < 0.05$.

Table 5.1. Elementary analysis of intact and burnt peat samples.

Year	Treatment	C (%)	N (%)	C:N	$\delta^{13}C$ (‰)	$\delta^{15}N$ (‰)	DOC (mg C L^{-1})	$\delta^{13}DOC$ (‰)	BD (g cm^{-3})	Ash content (%)	Peat depth (cm)
2020	Intact	41.2±4.1	1.4±0.2	30.0±2.4*	-27.7±0.2*	-5.3±0.6	-	-	-	-	-
	Burnt	40.3±4.1	1.6±0.2	26.2±2.1	-28.5±0.2	-6.3±0.4	-	-	-	-	-
2021	Intact	40.1±1.3	1.6±0.1	27.2±2.6	-28.2±0.2*	-5.5±0.4*	388.9±38.0	-27.1±0.5	0.1±0.0	-	-
	Burnt	41.1±1.2	1.6±0.1	26.3±1.8	-28.7±0.2	-6.6±0.4	388.4±33.4	-27.6±0.2	0.1±0.0	-	-
2022	Intact	37.0±3.2	1.5±0.2	25.9±2.9	-27.9±0.2	-4.6±0.6	-	-	-	-	-
	Burnt	37.7±1.7	1.7±0.1	22.8±1.5	-27.8±0.2	-5.1±0.5	-	-	-	-	-
2023	Intact	31.6±3.3	1.4±0.1	23.6±2.1	-27.6±0.2	-3.9±0.5	-	-	0.4±0.1	40.1±9.5	34.1±7.1
	Burnt	35.4±2.5	1.6±0.1	22.8±1.0	-27.9±0.1	-4.8±0.6	-	-	0.4±01	37.8±7.7	23.1±4.4

Symbols denoting intact and burnt treatment are significantly different at a given site (one-way ANOVA, n= 18, df =8, *P <0.05).

5.3.2 SOM molecular composition and SOC decomposability in intact vs. burnt plots

Changes in SOM molecular composition after the fire were evaluated using the MIR spectra, which revealed no significant differences between the intact and the burnt plots across any of the four consecutive years (2020−2023; PERMANOVA, *Ps* > 0.05; Supplementary Fig. 5.1). To further characterize fire effects on SOM molecular composition, a coefficient of PLS-DA model was used to identify the spectra regions explaining the main differences between intact and burned plots, based on samples collected later in 2020, immediately following the fire (Fig. 5.3A; for full model diagnostics please see Supplementary Fig. 5.2). The spectral peak assignments for molecular vibrations in SOM were adopted from the study of Peltre et al., 2014. The intact plots exhibited a positive correlation with the band at 3600−2800 cm^{-1}, ascribed to $_{\nu}$O−H from water, alcohols, and phenols as well as carboxyl and hydroxyl group; the band at 3000−2800 cm^{-1} corresponding to νC−H from aliphatic, methyl, and methylene groups; the band at 1160 cm^{-1}, attributed to $_{\nu}$C−O from polysaccharides, nucleic acids, and protein; and the band at 1050 cm^{-1}, corresponding to $_{\delta}$ C−O from carbohydrate (Fig. 5.3). In contrast, the burnt plots had a positive correlation with the band at 1565 cm^{-1}, attributed to νN−H and νC−N in-plane from amides; and the band at 1515 cm^{-1}, attributed to νC=C from aromatics compounds (Fig. 5.3A).

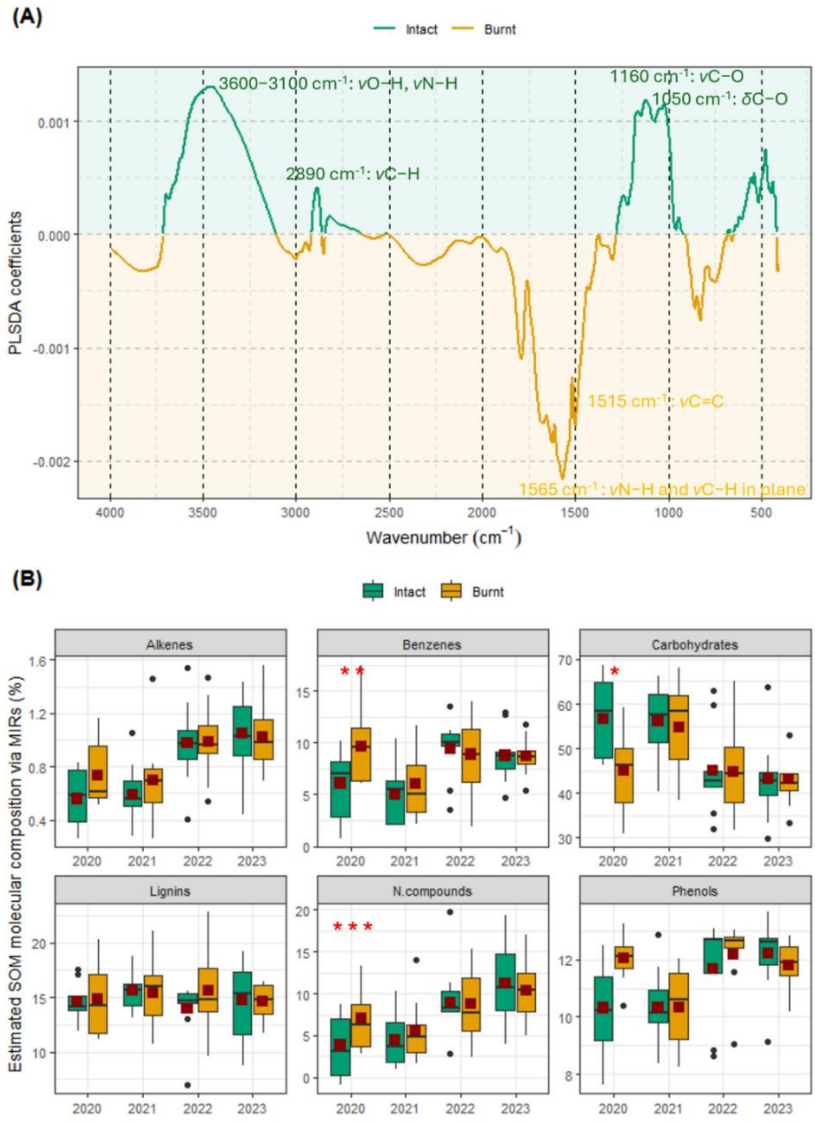


Fig. 5.3. Molecular composition changes between intact and burnt peat. (A) Coefficients from partial least squares discriminate analysis (PLS−DA) models highlighting molecular vibration differences between treatments. The PLS−DA model was developed using the 2020 dataset to maximize variance in mid-infrared spectral data between intact and burnt plots, reflecting pronounced fire-induced compositional changes. Positive coefficients indicate higher abundance of molecular vibrations in intact peat, whereas negative coefficients indicate higher abundance in burnt peat. (B) Estimates of functional groups of soil organic matter (SOM) molecular composition derived from mid-infrared spectroscopy, compared between intact and burnt plots across four consecutive years. Red asterisks (*) denote statistically significant differences (*, $P < 0.05$; **, $P < 0.01$; ***, $P < 0.001$).

The estimated relative abundances of the functional groups derived from the MIR-based predictive model showed clear treatment effects and temporal dynamics (Fig. 5.3B). In 2020, the same year as the fire, the burnt plots exhibited significantly higher relative abundances of benzene and N compounds, and significantly lower relative abundance of carbohydrates ($Ps < 0.05$; Fig. 5.3B). These differences disappeared from 2021 onwards ($Ps > 0.05$). Temporal trends also reveal pronounced compositional shifts between the pre- and post-2022, including decreased carbohydrate abundance and increased proportions of alkanes, N compounds, and phenols (Fig. 5.3B).

The measured cumulative CO_2 flux per C content, reflecting SOC decomposability, did not differ between the intact and the burnt plots in 2021 and 2023 ($Ps > 0.05$; Fig. 5.4A). However, the MIR-derived estimates of SOC decomposability indicated significantly lower decomposability in the burnt plots in 2020, the year of the fire ($P < 0.05$; Fig. 5.4B), with treatment differences diminishing in the subsequent years ($Ps > 0.05$). Notably, from 2022 onwards, several variables−including elemental composition, SOM components, and SOC decomposability–showed deviations from the consistent temporal trajectories (Fig. 5.2−Fig. 5.3Fig. 5.4).

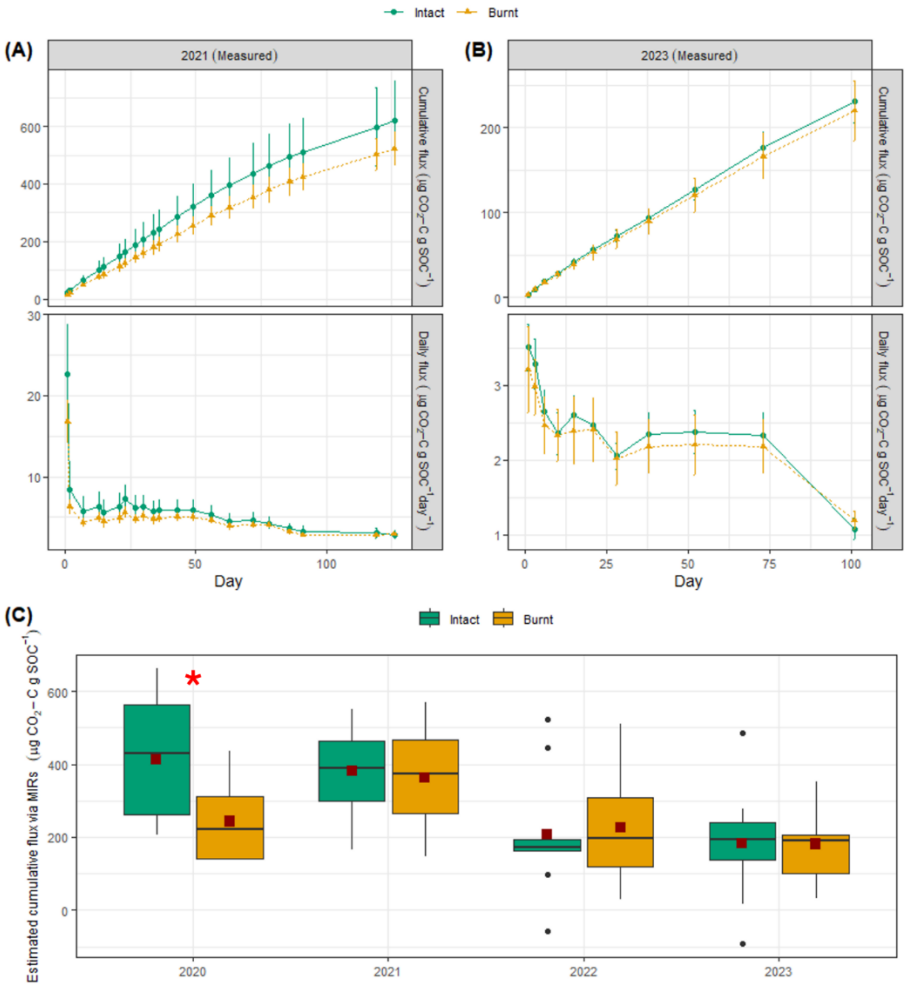


Fig. 5.4. Measured cumulative and daily fluxes of basal respiration (A, B) and estimated cumulative flux via MIRs (C) between intact and burnt plots. No significant differences in measured cumulative CO_2 fluxes were observed between intact and burnt plots in 2021 and 2023 ($Ps > 0.05$). The estimated cumulative flux was significantly different between treatments only in 2020 ($P < 0.05$).

The differences of the measured SOC decomposability between intact and burnt plots were positively correlated with the differences in C:N ratio, $DO^{13}C$, and relative carbohydrates abundance, whereas they were negatively correlated with the difference in N contents, DOC, and relative abundance of phenolic functional groups (Fig. 5.5; $Ps < 0.05$).

Similarly, the differences in the estimated SOC decomposability were positively correlated with differences in C content, C:N ratio, relative carbohydrate and lignin abundance, and NDVI, while they were negatively correlated with differences in $\delta^{15}N$, bulk density, relative abundance of N compounds, phenols, benzenes, alkenes (Fig. 5.5; *Ps* < 0.05).

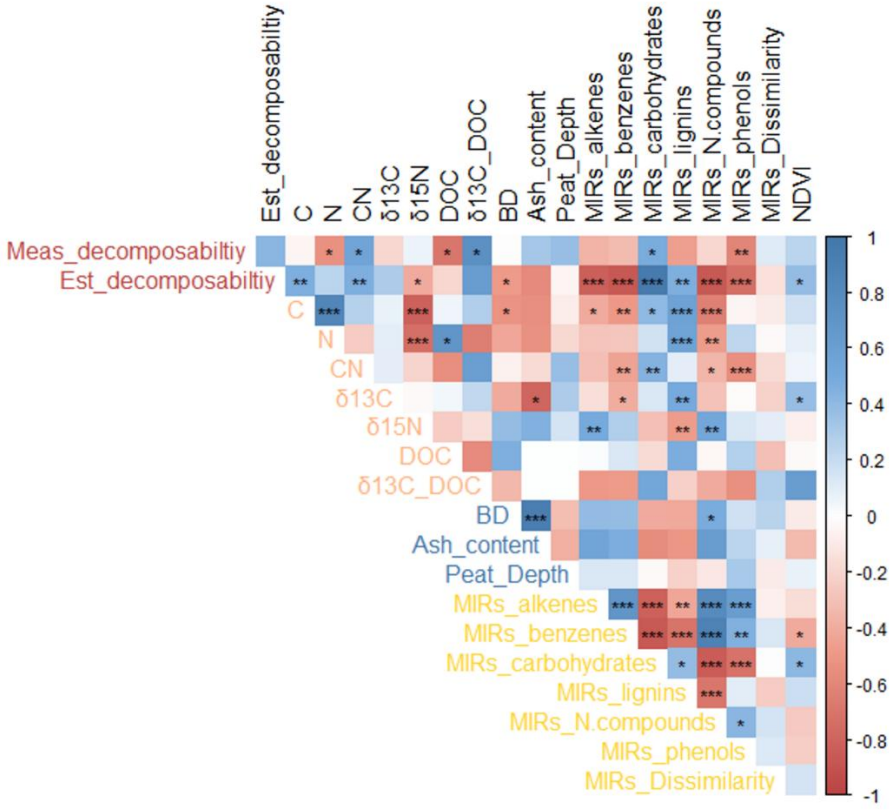


Fig. 5.5. Pearson correlation coefficients (r) for the relationship between changes in environmental variables between intact and burnt plots. The color gradient represents the correlation strength and direction (from blue to red; $-1 \leq r \leq 1$). Statistical significance is indicated by asterisks: *** P <0.001, ** P <0.01, * *P* <0.05. Meas means measured, and Est refers to estimated.

5.4. Discussion

Previous studies have typically assessed the effects of fire on physicochemical properties and C stocks either through qualitative, field-based evaluation at the local scale (e.g.,

Ackley et al., 2021; Whitehead et al., 2021; Blier-Langdeau et al., 2022) or through remote-sensing analyses at broader spatial scales (e.g., Jones et al., 2024; Vetrita et al., 2025). Here, the accidental peatland fire on 22 April 2020 at Landschap De Liereman reserve in Belgium created a mosaic pattern (i.e., adjacent intact and burnt patches). This patchy distribution allowed for the evaluation of *in situ* fire effects using a combination of repeated field measurements and up-scaling models for SOM composition (see Chapter 3) and C stability, together with a remote sensing approach to assess ecosystem responses across spatial and temporal scales (Fig. 5.1A&B).

5.4.1. Peatland's resilience to low-severity fire and recovery towards the pre-fire state

Our study suggests that the peatland ecosystem at Landschap De Liereman was rather resilient to the low-severity fire that occurred in 2020, with disturbed plots rapidly recovering and reaching soil C characteristics similar to those of intact plots within two years (Table 5.1; Fig. 5.1−Fig. 5.4). It is well known that fire-induced thermal degradation influences soil C dynamics through multiple pathways depending on fire intensity (Hirano et al., 2014; Könönen et al., 2018; Flanagan et al., 2020). At our study site, significant changes were observed in stable isotope signatures and SOM functional groups, whereas bulk soil C and N contents remained largely unchanged, and no signs of smoldering combustion or subsurface peat burning were observed (Table 5.1; Fig. 5.2Fig. 5.3). These results were also corroborated by changes in the NDVI index (Fig. 5.1C), as well as ongoing field surveys of vegetation and analyses of microbial community composition (Maas et al., 2026). This contrasts with high-severity fires, where smoldering combustion typically leads to severe declines in C concentration and enrichment in $\delta^{13}C$ and $\delta^{15}N$ due to preferential losses of the lighter isotopes (Fernandez et al., 2004; Flanagan et al., 2020; Agbeshie et al., 2022). Recovery following such high-severity fire often requires several decades (Volkova et al., 2023), whereas in our study ecological indicators in burnt plots converged toward those of intact plots within the first two years after the fire (Table 5.1; Fig. 5.1−Fig. 5.4). These findings suggest that the fire disturbance at our site corresponded to incomplete combustion

processes (i.e., a low-severity fire), to which this peatland showed a relatively high level of resilience.

However, this low-severity fire selectively altered the SOM molecular composition of surface peat, which likely contributed to the observed decrease in C isotopic signals. The increase in νC=C (Fig. 5.3A), indicative of enhanced aromatic bonds, together with higher relative abundance of benzenes as predicted by MIR-based model (Fig. 5.3B; $P < 0.05$) and, to some extent, phenols in burnt peat, are consistent with thermal condensation and aromatization under incomplete combustion (Flanagan et al., 2020). Such processes can introduce kinetic isotope fraction and produce relatively ^{13}C-depleted aromatic moieties (Olefeldt et al., 2013; Jiménez-Morillo et al., 2020), a mechanism further supported by the negative correlation between benzene abundance and $\delta^{13}C$ (R = -0.40; $P < 0.05$, Fig. 5.5). Conversely, the reductions in νC−O and νC−H functional groups (Fig. 5.3A), associated with polysaccharides and aliphatic C typical of fresh litter, as exhibited by the burnt peat, are consistent with the decline in estimated relative abundance of carbohydrates ($P < 0.05$, Fig. 5.3B), and their relationship with vegetation (Δcarbohydrate vs. ΔNDVI; R = 0.42; $P < 0.05$, Fig. 5.5). Preferential combustion of ^{13}C-enriched carbohydrate-like compounds may therefore have contributed to the declines in $\delta^{13}C$ following the fire (Pellegrini et al., 2015; Flanagan et al., 2020).

In contrast, the increases in νN−H and νC−N (Fig. 5.3A), together with the concurrent higher relative abundance of N compounds ($P < 0.05$, Fig. 5.3B), observed in burnt peat, were not accompanied by a corresponding negative relationship with the decline in $\delta^{15}N$ (Fig. 5.2&Fig. 5.5). This lack of association indicates that the post-fire reduction of $\delta^{15}N$ cannot directly be attributed to increases in nitrogenous pyrolysis products or microbially processed N compounds. Instead, the decline in $\delta^{15}N$ is more likely linked to the accumulation of ^{15}N-depleted ash (San-Emeterio et al., 2026) and to post-fire shifts in N cycles that increase ^{14}N in the soil, driven in part by reduced N isotope discrimination during plant uptake following vegetation mortality due to

fire (Tahmasbian et al., 2019). This implies that the observed shift in $\delta^{15}N$ reflects changes in isotopic partitioning within the soil N pool rather than alterations in SOM molecular composition per se.

The shifts in SOM molecular composition further indicate a reduction of labile carbohydrates and relative accumulation of aromatic and N compounds (Table 5.1; Fig. 5.3&Fig. 5.4), that lead to a lower basal respiration and therefore enhanced biological stability in the remaining peat after the fire. Increased aromaticity in burnt peats may enhance hydrophobicity by forming coating layers on peat particles, limiting microbial access and reducing evaporation and solubility (Kang et al., 2012; Flanagan et al., 2020). Similarly, the enrichment of N compounds further suggests increased molecular complexity and lower peat biodegradability (Schimel and Weintraub, 2003). These fire-induced changes in substrate quality and microbial accessibility may have contributed to a slowdown in microbial decomposition (Andersen et al., 2013; Li et al., 2025). This interpretation is further supported by reduction in SOC decomposability (both measured and model-estimates) and by lower C:N ratio, which indicates stoichiometric constraints on microbial activity (C:N ratio vs. measured flux; R= 0.55; $P < 0.05$, Fig. 5.5).

5.4.2. Drought stress does not accelerate peat degradation of fire-disturbed peats

Repeated sampling over four consecutive years revealed an abrupt variation in several ecological indicators−including physicochemical properties, SOM molecular composition, and SOC decomposability−in 2022 (Fig. 5.2Fig. 5.4). Based on field observation and experimental context, we propose three plausible mechanisms underlying this deviation. (i) Part of the variability likely reflects intra-seasonal differences in sampling timing (from July- to September; due to the need to wait for water levels to recede). (ii) A delayed, system-wide response following fire may have occurred, potentially related to priming effect or redistribution of nutrients that gradually spread across plots over subsequent years. (iii) The pronounced contrast with 2022−one of the driest years on record at the site (701.4 mm in 2022, 837.1 mm on average of 30 yrs) −

strongly suggests a climatic influence on peat structural and functional properties. We acknowledge that the current study design and available data do not allow to fully disentangle delayed fire effect from drought-driven response. Therefore, interpretations are primarily based on the most plausible climatic drivers while recognizing the potential confounding influence of delayed fire effects.

Among these mechanisms, climatic drought stress provides a particularly convincing explanation for the observed shifts. Such exceptionally dry condition may have accelerated peat degradation by stimulating oxidative enzyme activity, reducing substrate availability, and intensifying hydrological stress under marginal conditions for peat formation (Keith et al., 2023; Smolders et al., 2024). Despite this climate-related stress, fire-degraded peat (i.e., burnt peat) did not respond disproportionately to drought-associated stressors in terms of SOC stability (Fig. 5.4). This suggests that reinforcing feedback or ecosystem shifts (i.e., transitions toward an alternative stable state) were less evidenced under the combined fire and drought (Scheffer and Carpenter, 2003; Dakos et al., 2012). Instead, the burnt plots continued to follow recovery trajectories similar to intact plots, with no detectable fire legacy effects also on vegetation, soil physiochemical properties or SOM molecular composition under climatic stress. Overall, our findings indicate that the peatland at our study site exhibits high resilience to low-severity fire, with no exacerbation of SOC destabilization or ecosystem transition during the monitoring period.

5.5. Conclusions

Our study design provided new insights on how fire disturbance reshapes peatland C stability and stoichiometry across space and time. By combining high-resolution remote sensing with field measurement of soil C, this approach enabled assessment of post-fire dynamics at Landschap De Liereman. Ecosystem components responded strongly during the first two years after the fire, but these effects were mitigated over time. The low-severity fire with no smoldering induced depletion of labile C and accumulation of recalcitrant aromatic C in soil organic

mattertogether with shifts in carbon-isotope signatures. These shifts in substrate quality likely contributed to reduced SOC decomposability by restricting microbial accessibility. Overall, the peatland exhibited high resilience to low-severity fire, and fire legacy did not exacerbate drought-related stress on soil C stability.

Acknowledgements

The authors gratefully acknowledge the assistance of Yannick Stroobandt, Lore Fondu, Kim Vekemans, Toon Coolen, Caro Van Den Eynde, Michel van Son, and Kris Van der Steen for their contribution to the sample handling procedure, equipment operation and training, and for sharing their expertise to enhance workflow. We also thank the Natuurpunt for hosting and supporting field excursions and experimental setup, and for their great willingness to share their extensive field knowledge. This research was funded by the Research Foundation Flanders (FWO-G060721N).

6 Synthesis

6.1. Main findings

Peatlands are increasingly recognized for their critical ecosystem functions, including C sequestration, biodiversity support, and hydrological regulation (Yu et al., 2010; Leifeld and Menichetti, 2018). Yet, extensive drainage for agriculture, forestry, and peat extraction, together with ongoing climate change, threatens the functioning of these ecosystems (Joosten and Clarke, 2002; Loisel and Gallego-Sala, 2022; Temmink et al., 2022). Such disturbances may push peatlands across critical ecological thresholds, triggering abrupt shifts between multiple equilibrium states (i.e., alternative state) that are often difficult to reverse (Scheffer and Carpenter, 2003; Dieleman et al., 2015). Safeguarding peatland functions therefore requires a mechanistic understanding of degradation processes and disturbance legacy effects. This includes identifying ecological thresholds at which abrupt and potentially irreversible shifts occur, as well as examining post-disturbance response trajectories to assess the emergence of alternative states. Such knowledge is essential for anticipating regime shifts and preventing the loss of ecosystem functioning (Dakos et al., 2012; Van Meerbeek et al., 2021; Reed et al., 2025).

Particularly, soil organic matter (SOM) dynamics is a key indicator of belowground processes, as it influences peat structural integrity, SOC decomposability, and hydrological conductivity, thereby playing a key role in regulating C stability (Schellekens et al., 2009; Vancampenhout et al., 2009). However, field-based investigation of SOM dynamics and responses along disturbance-restoration or -recovery remain scarce. Likewise, disturbance legacy effects or post-disturbance trajectories are still insufficiently understood (Orwin and Wardle, 2004; Chambers et al., 2019). Moreover, methodological frameworks capable of capturing such complex processes and facilitating their upscaling to ecosystem or landscape levels remain underdeveloped (Kunarso et al., 2025).

This PhD dissertation evaluated how SOM molecular composition and belowground processes in peatlands respond to drainage, climate change, and fire disturbances, and the extent

of restoration and natural recovery that follow. In addition, it incorporated a modelling framework that enables the routinely useable molecular-level data acquisition tools, thereby supporting the upscaling of peat monitoring and management. The dissertation addressed these objectives through four research components: (1) estimation of the molecular responses to drainage and rewetting−examining molecular-level changes in European fen peat under contrasting hydrological conditions to improve our understanding of SOM responses to hydrological status; (2) development of a MIR-based predictive model to reproduce molecular information obtained from Py-GC/MS that enables a more efficient and scalable assessment of SOM composition and C stability; (3) description of the mechanisms causing peat surface collapse to identify critical thresholds that could help to develop better strategies for preventing further spatial propagation; and (4) assessment of fire disturbance and recovery trajectories and how fire alters SOM molecular composition .

By integrating field observations, molecular characterization, and modelling approaches, this dissertation contributed to a process-based understanding of peatland SOM dynamics under disturbances as well as during restoration and recovery phases. These insights are essential for predicting ecosystem responses to perturbation, and elucidating the mechanisms governing how, where, and when ecosystem functions may shift. This knowledge supports the development of science-based restoration and monitoring strategies.

6.1.1. Potential catastrophic effects of disturbances on peat C stability

Disturbances such as drainage, climate change, and fire, as well as peat collapse phenomena, significantly alter SOM at the molecular level, with direct shifts in peat C storage and stability. Rather than following a gradual and unidirectional degradation pathway, our findings reveal four key patterns: (1) divergent degradation trajectories, characterized by either aliphatic-dominant or N compound-dominant hydrologically degraded state; (2) peat collapse accompanied by substantial C loss during peat collapse; (3) greater dispersion in ordination space for rewetted

and drained fens compared to undrained fens and higher spatial variation of N_2O fluxes in SO_4^{2+} addition treatment in the mesocosm experiment, implying reduced ecosystem stability and a potential early warning signal of a regime shift; and (4) concurrent but asynchronous shifts across multiple system compartments−including vegetation, physicochemical properties, and soil mesofauna−under drainage, climate change, and fire disturbance, implying potentially cascading effects on ecosystem functioning and C stability.

6.1.2. Potential ecosystem alternative states and their distinct basins of attraction

Our findings further provide new insights into peatland ecological responses, as they exhibited contrasting restoration or recovery trajectories depending on their disturbance legacies. In particular, our study found clear signatures of hysteresis, indicating that recovery pathways do not simply reverse degradation processes. Rewetting drained fens restored water levels and reduced aerobic exposure but did not return to their pre-drainage conditions within the timeframe of the applied rewetting at our study sites. Drainage legacies−especially prolonged aerobic decomposition and incorporation of newly derived plant compounds in the topsoil−left lasting imprints on SOM molecular composition, indicating a strong hydrological legacy effect that may push the system toward an alternative state. These molecular shifts appear to constrain recovery, potentially driving nearly irreversible degradation trajectories that require extended timescales to reach approach pre-disturbance conditions.

In contrast, C dynamics following rewetting and post-fire recovery indicate presence of stabilizing processes consistent with a distinct attractor, defined as the set of initial condition in a dynamical system that evolve toward the same final (Fig. 6.1; Scheffer et al., 2001). These dynamics are further characterized by negative feedback mechanisms that gradually dampen disturbance effects and promote a return toward equilibrium. Recovery of SOM molecular composition over time was observed at a depth of 15−20 cm following rewetting, a layer relatively less influenced by newly added plant residues, indicating effectiveness of rewetting restoration.

Similarly, fire-disturbed peats did not display higher sensitivity to subsequent climate perturbation compared to intact peats. No accelerated or exponential shift in SOM composition were observed, indicating fire alone may be insufficient to push these peatlands beyond a tipping point toward a distinct alternative condition. This system appears to exhibit stabilizing processes that buffer ecosystems functioning against further perturbation.

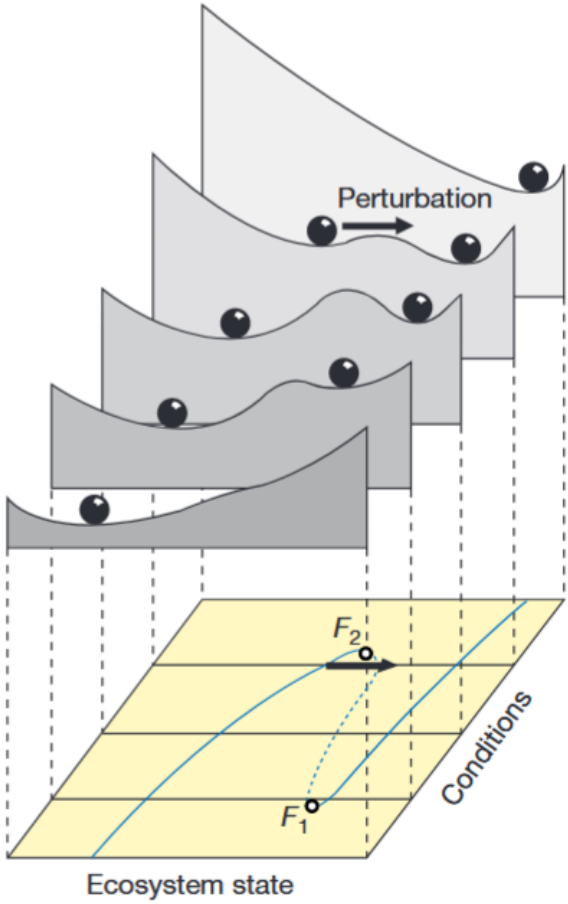


Fig. 6.1.External conditions affect the resilience of multi-stable ecosystem to perturbation. The bottom plane shows the equilibrium curve. The stability landscapes depict the equilibria and their basins of attraction at five different conditions. Stable equilibria correspond to valley; the unstable middle section of olde equilibrium curve corresponds to a hill. If the size of the attraction basin is small, resilience is small and even a moderate perturbation may bring the system into the alternative basin of attraction (Scheffer et al., 2001).

6.1.3. Mid infrared spectroscopy as a tool to monitor molecular changes in fens upon restoration

Given the time- and context-dependent outcomes of post-disturbance phases, clearly defined targets and sustained monitoring across spatial and temporal scales are essential to prevent irreversible effects on C stability upon legacy effects. Our findings demonstrated that MIR spectroscopy is a promising tool for tracking molecular-level changes in SOC stability under contrasting hydrological status. The MIR-based modelling approach successfully reproduced key chemical groups derived from Py-GC/MS and captured relevant indicators of C decomposability. Although MIR does not provide the same analytical resolution as Py-GC/MS, it offers substantial advantages regarding cost efficiency and scalability, making it particularly suitable for large-scale monitoring of restoration interventions.

Beyond hydrological variation, the model was also applied to a fire-disturbed system. Despite its relatively coarse resolution compared to py-GC/MS, the MIR-based approach effectively captured shifts in molecular composition and associated changes in C stability induced by fire disturbance. This suggests that the applicability of MIR-model can be extended to a broader range of disturbance factors. Overall, integrating molecular tools with spatially explicit and temporally resolved datasets strengthens the capacity to detect nonlinear ecosystem responses, evaluate restoration effectiveness, and predict long-term peatland C trajectories under changing environmental conditions. Such a model-based framework can then provide an avenue for an effort-efficient monitoring of the belowground processes in fens, that can then help guide restoration strategies and efforts.

6.1.4 The contentious nature of peatland legacy-effects

Throughout this dissertation, it became clear that legacy effects in peatlands are not driven by singular, unidirectional processes, but instead by complex interactions between different

factors and underlaying mechanisms across spatial scales of profiles or sites, over landscapes, and on time scales varying from months to millions of years.

In Chapters 2 and 3, we show how legacy effects induced by drainage can influence peatland recovery responses upon rewetting. In the European dataset, while many sites showed a decreasing dissimilarity between undrained and rewetted plots, several sites showed distinct shifts in organic matter cycling, with molecular changes veering towards compositions that are indicative for processes observed in more terrestrial systems, like the accumulation of aliphatic compounds. Our results therefore suggest that vegetation shifts from an open, moss-dominated state towards a more closed state dominated by larger vascular plants, i.e. helophytisation, may also have a molecular level dimension. The insights gained in Chapter 2 are the first step towards understanding why certain sites respond well to rewetting, while others may need more substantial restoration strategies such as species transplant or vegetation control to shift the system back to the open, moss dominated state. The model-based approach developed in Chapter 3 can provide an avenue for more efficient monitoring of the below-ground processes in fens, that can then help guide restoration strategies and efforts.

Chapter 4 shows a very different type of legacy, i.e. a million-years old legacy of marine deposits, that has been fundamentally altered by decades of nitrate pollution upstream. As fens occur at the lowest positions of the landscape, pollutants leaching from upper parts of the catchment can have an effect. Furthermore, the chapter shows that chronic stresses attributed to this marine legacy and current pollution, when combined to anthropogenically induced fluctuations of water tables worsened by climate change, can lead to rapid and unexpected shifts. Molecular data, combined to biogeochemical measurements and experimental valorisations, allowed us to gain insights into the mechanisms causing the peat collapse, and provided a crucial first step in identifying which other peatlands in Flanders and beyond may be a priority for collapse risk, i.e. that have a combination of marine legacies, upstream nitrogen pollution and are prone to increasing severity and duration of droughts due to drainage and climate change.

Finally, chapter 5 showed that the legacy of a dramatic event such as a fire should not distract us from the more occult but far more impactful effects of drought and drainage, as least if the fire can be quickly extinguished as was the case in Landschap De Liereman. The dramatic changes in C content, molecular composition and basal respiration would have gone undetected if not for the monitoring program to deal with post-fire effects, highlighting that there is an urgent need to better monitor the below-ground state of peatlands even in areas with no obvious above-ground damage.

This dissertation highlights the usefulness of molecular-level monitoring of fen ecosystem soil health in fen ecosystems. This approach not only serves as an academic exercise for gaining fundamental, process-based understanding, but when combined with a well-calibrated spectroscopy model, it can also be developed into practical tools for monitoring. Such an approach enables upscaling to assess peatland degradation under future disturbances at more extensive temporal and spatial scales. To enhance accessibility for practitioners and facilitate more detailed monitoring, near infrared spectra−capable of direct in situ measurements−has potential to be used as a proxy for chemical composition properties of peats. Further development of a user-friendly interface could support its wider adoption in applied settings.

In addition, our findings highlight that peat health is strongly influenced by context- and site-specific factors. This underscores the importance of continuous site-specific monitoring, and a holistic assessment framework to better understand the interacting biogeochemical processes within each system. Identifying the dominant stressors at each site is critical for designing effective monitoring and management strategies to avoid exacerbating peat degradation. Overall, this study contributes by providing a policy-relevant evidence base to support sustainable peatland management and climate adaptation strategies in conservation areas and beyond.

6.2. Limitation of research

Our overarching objective was to advance in the understanding of peatland below-ground C dynamics and stability in response to environmental disturbances, with a particular focus on abrupt shifts along degradation gradients using field-based studies. Peatland disturbances—such as drainage, climate change and fire—can leave persistent imprints on biogeochemical properties, preconditioning ecosystems to respond differently to subsequent perturbations (i.e., legacy effect). Within the framework of C dynamics and stability, such legacy effects may determine whether peatlands exhibit potential alternative stable states and ecological thresholds across degradation gradients. Based on the findings of our study, several recommendations emerge to guide future research.

First, a more holistic assessment of C dynamics and stability in disturbance—restoration and—recovery trajectories is needed to understand ecosystem vulnerability/resilience. While this work positioned SOM molecular composition as a central determinant of C dynamics, peatland C stability emerges from interactions between biological, chemical, and physical processes. A comprehensive framework should explicitly integrate: (1) microbial community composition and function, which regulates decomposition pathways and enzymatic capacity: (2) vegetation community dynamics, which influence litter input, root exudation, and rhizosphere processes, and (3) edaphic properties, including hydrological regimes, nutrient availability, and redox fluctuations. Linking these components within conceptual ecological feedback loops would provide a system-level understanding of C dynamics and stability.

Second, diversifying data resources can be considered to improve monitoring efficiency, particularly given the high logistical demands and costs of field campaigns and the need to better capture ecosystem behavior across spatial and temporal scales. Combining high-resolution analytical data (e.g., molecular-level SOM characterization) with predictive modelling and lower-cost monitoring approaches—such as remote sensing, automated measurement systems, and citizen science—can provide both detailed process-level insights and broader spatial and temporal coverage. Large-scale datasets help to minimize the influence of unnecessary covariates and reveal

generalizable patterns across degradation gradients, which is essential to disentangle transient responses from long-term shifts in ecosystem functioning. In this dissertation, a MIR-based model for molecular composition was developed; however, future applications could extend this approach by including additional parameters or achieve higher resolution through methodological improvements. Moreover, given the logistical and financial constraints of intensive field campaigns, diversifying additional datasets derived from remote sensing products, eddy covariance or stationary flux tower measurements, and citizen science or collaborative sampling networks would greatly enhance monitoring efficiency. When integrated with field measurements, such an approach can achieve better mechanistic interpretability while enabling restoration monitoring at broader spatial and temporal scales.

Third, identifying cost-effective and easy-to-use early warning indicators of abrupt shifts in peatland integrity is a priority for peatland monitoring and management. Temporal signals of instability −such as increased variances and critical slowing recovery rates− often require long-term temporal monitoring, which is missing in recently established monitoring sites. Warning signals of peatland degradation should be identified and used to detect ecological thresholds. For example, in this study mesofauna were investigated as low-cost early warning proxies, but their use is labor intensive and requires time to develop taxonomic expertise. In addition, identifying early warning proxies depends on the type of disturbance such as drought, flood, sulfate pollution or sea-level increase. Therefore, research on cost-effective, and easy-to-use disturbance-specific early-warning signals is necessary to predict and mitigate amplified disturbance effects.

In summary, advancing peatland research requires the integration of high-resolution sampling and analytical approach with modelling tools, the diversification of data sources, and identification of disturbance-dependent early-warning signals. Such a synthesis will enable a comprehensive assessment of C stability, the detection of tipping points, and the development of effective and cost-efficient restoration strategies undergoing environmental changes.

6.3. Valorization: New insights on peat decomposition processes under disturbance

A major challenge in peatland management and restoration is how to assess peat soil C stability and dynamics. Whereas above ground vegetation is often well monitored, the peat itself mostly remains −literally− an enigmatic 'black box' to managers and policy makers, with little options available to track damage or recovery other than crude measurements like C stocks. The FWO legacy project, of which this thesis is a part, was initiated after the management team of conservation area 'De Zegge' highlighted their difficulties in objectively and measurably evaluating the effect of environmental pressures and management actions on the belowground functioning, an important aspect also for prompting urgent hydrological restoration measures at catchment level by the relevant authorities. Conservation area 'Landschap De Liereman' faces a similar difficulty, complicated by a large fire in 2020. This dissertation therefore aimed at exploring more detailed data acquisition on the belowground state of these important landscapes, supporting managers and policy makers in their work to counteract climate change and other anthropogenic pressures on the system.

A first hurdle to this valorization goal was that a framework was lacking to benchmark the degradation state of fens. Most existing studies on peat quality focus on bogs rather than fens, are conducted at small scales, or lack convincing comparisons between favorable, unfavorable, and restored states. In chapter 2, we therefore used the European RePeat network of undisturbed, drained, and rewetted fens, to build the first detailed and European-scale dataset of SOM molecular composition assessment under different hydrological degradation. By separating drainage-induced degradation (aerobic decomposition) from long-term aging processes (anaerobic decomposition), this chapter established a mechanistic understanding of how hydrological degradation shapes below-ground peat biogeochemistry and further provided insights on what recovery trajectories emerge upon rewetting, contributing to better-evidenced diagnostic criteria for comprehensive assessment of peatland hydrological degradation at molecular level.

While py-GC/MS provided a very powerful technique to gain insights into the 'black box' that is fen belowground functioning, the technique is expensive, labor-intensive and requires specialized equipment and expertise that is rare even on a European level. Therefore, while highly insightful for establishing and benchmarking mechanisms, it is not a scalable tool that managers can use.

In chapter 3, we aimed at enhancing the scalability and applicability of the monitoring framework by developing a MIR-based model capable of reproducing the relative abundance of chemical groups that were identified as important for interpretability in C dynamics and stability in Chapter 2. MIR spectroscopy is more efficient and cost-effective, therefore applicable in large-scale monitoring of peatland degradation status and in the implementation of restoration and management programs. This technique can be transferred to a knowledge broker, e.g., the Soil Service of Belgium, that can do the measurements and translate them to the recommendation to the managers. The developed model is openly available for use by managers and researchers (Kim et al., 2026a) and has been applied in the empirical case studies in Chapter 4 and Chapter 5, which investigated changes in SOM composition of collapsed peatlands and fire-disturbed peatlands, respectively.

Our model proved to be effective in uncovering previous unknown dynamics in both 'De Zegge' and 'De Liereman' and already is used by local managers and authorities. In Chapter 4, we revealed the mechanisms behind peat collapse, serious damage to t peat integrity (in terms of substantial surface elevation and C losses accompanied by shifts in SOM composition) that needs urgent hydrological restoration and identified new indicator proxies that could serve as early warnings of potential alterations in ecological functioning.

Chapter 5 addressed the increasing vulnerability of peatlands to fire. The results showed that dramatic events, such as the 2020 fire, attracted a lot of attention yet in this case were much less damaging than the drought conditions that followed. This 'silent killer' is much more difficult

to assess yet provided to be pivotal in intensifying SOM transformations and C losses, which clearly showed in the molecular and respiration data and eventually also in total C measurement. These findings not only contributed to the scientific understanding of fire-affected peat system but also highlighted the growing urgency of climate change mitigation and political action to protect peatland ecosystems.

7

References

Abbott, B.W., Jones, J.B., 2015. Permafrost collapse alters soil carbon stocks, respiration, CH4 , and N2O in upland tundra. Glob Chang Biol 21, 4570–4587. https://doi.org/10.1111/gcb.13069
Abbott, G.D., Swain, E.Y., Muhammad, A.B., Allton, K., Belyea, L.R., Laing, C.G., Cowie, G.L., 2013. Effect of water-table fluctuations on the degradation of Sphagnum phenols in surficial peats. Geochimica et Cosmochimica Acta 106, 177–191. https://doi.org/10.1016/j.gca.2012.12.013
Abdelhady, A.A., Seuss, B., Jain, S., Fathy, D., Sami, M., Ali, A., Elsheikh, A., Ahmed, M.S., Elewa, A.M.T., Hussain, A.M., 2024. Molecular technology in paleontology and paleobiology: Applications and limitations. Quaternary International 685, 24–38. https://doi.org/10.1016/j.quaint.2024.01.006
Ackley, C., Tank, S.E., Haynes, K.M., Rezanezhad, F., McCarter, C., Quinton, W.L., 2021. Coupled hydrological and geochemical impacts of wildfire in peatland-dominated regions of discontinuous permafrost. Science of The Total Environment 782, 146841. https://doi.org/10.1016/j.scitotenv.2021.146841
Aernouts, B., Adriaens, I., Diaz-Olivares, J., Saeys, W., Mäntysaari, P., Kokkonen, T., Mehtiö, T., Kajava, S., Lidauer, P., Lidauer, M.H., Pastell, M., 2020. Mid-infrared spectroscopic analysis of raw milk to predict the blood nonesterified fatty acid concentrations in dairy cows. Journal of Dairy Science 103, 6422–6438. https://doi.org/10.3168/jds.2019-17952
Agbeshie, A.A., Abugre, S., Atta-Darkwa, T., Awuah, R., 2022. A review of the effects of forest fire on soil properties. J. For. Res. 33, 1419–1441. https://doi.org/10.1007/s11676-022-01475-4
Aggenbach, A.C.J., H, B., J, E.W., P, G.A., M, L.L.P., P, S.A.J., J, S.P., R, W.L.& V.D., 2013. Do high iron concentrations in rewetted rich fens hamper restoration? 85.
Agosti, D., Grimaldi, D., Carpenter, J.M., 1998. Oldest known ant fossils discovered. Nature 391, 447–447. https://doi.org/10.1038/35051
AminiTabrizi, R., Graf-Grachet, N., Chu, R.K., Toyoda, J.G., Hoyt, D.W., Hamdan, R., Wilson, R.M., Tfaily, M.M., 2023. Microbial sensitivity to temperature and sulfate deposition modulates greenhouse gas emissions from peat soils. Global Change Biology 29, 1951–1970. https://doi.org/10.1111/gcb.16614
Andersen, R., Chapman, S.J., Artz, R.R.E., 2013. Microbial communities in natural and disturbed peatlands: A review. Soil Biology and Biochemistry 57, 979–994. https://doi.org/10.1016/j.soilbio.2012.10.003
Andersen, R., Farrell, C., Graf, M., Muller, F., Calvar, E., Frankard, P., Caporn, S., Anderson, P., 2017. An overview of the progress and challenges of peatland restoration in Western Europe. Restoration Ecology 25, 271–282. https://doi.org/10.1111/rec.12415
Andersen, T., Carstensen, J., Hernández-García, E., Duarte, C.M., 2009. Ecological thresholds and regime shifts: approaches to identification. Trends in Ecology & Evolution 24, 49–57. https://doi.org/10.1016/j.tree.2008.07.014
Angst, G., Mueller, K.E., Castellano, M.J., Vogel, C., Wiesmeier, M., Mueller, C.W., 2023. Unlocking complex soil systems as carbon sinks: multi-pool management as the key. Nat Commun 14, 2967. https://doi.org/10.1038/s41467-023-38700-5
Antonijević, D., Hoffmann, M., Prochnow, A., Krabbe, K., Weituschat, M., Couwenberg, J., Ehlert, S., Zak, D., Augustin, J., 2023. The unexpected long period of elevated CH4 emissions from an inundated fen meadow ended only with the occurrence of cattail (Typha latifolia). Global Change Biology 29, 3678–3691. https://doi.org/10.1111/gcb.16713

Apori, S.O., Mcmillan, D., Giltrap, M., Tian, F., 2022. Mapping the restoration of degraded peatland as a research area: A scientometric review. Front. Environ. Sci. 10. https://doi.org/10.3389/fenvs.2022.942788

Austin, G., Cooper, D.J., 2016. Persistence of high elevation fens in the Southern Rocky Mountains, on Grand Mesa, Colorado, U.S.A. Wetlands Ecol Manage 24, 317–334. https://doi.org/10.1007/s11273-015-9458-7

Bahram, M., Espenberg, M., Pärn, J., Lehtovirta-Morley, L., Anslan, S., Kasak, K., Kõljalg, U., Liira, J., Maddison, M., Moora, M., Niinemets, Ü., Öpik, M., Pärtel, M., Soosaar, K., Zobel, M., Hildebrand, F., Tedersoo, L., Mander, Ü., 2022. Structure and function of the soil microbiome underlying N2O emissions from global wetlands. Nat Commun 13, 1430. https://doi.org/10.1038/s41467-022-29161-3

Baird, A.J., Comas, X., Slater, L.D., Belyea, L.R., Reeve, A.S., 2009. Understanding Carbon Cycling in Northern Peatlands: Recent Developments and Future Prospects, in: Carbon Cycling in Northern Peatlands. American Geophysical Union (AGU), pp. 1–3. https://doi.org/10.1029/2008GM000875

Baldock, J.A., Oades, J.M., Nelson, P.N., Skene, T.M., Golchin, A., Clarke, P., 1997. Assessing the extent of decomposition of natural organic materials using solid-state 13C NMR spectroscopy. Soil Res. 35, 1061–1084. https://doi.org/10.1071/s97004

Ballhorn, U., Siegert, F., Mason, M., Limin, S., 2009. Derivation of burn scar depths and estimation of carbon emissions with LIDAR in Indonesian peatlands. Proceedings of the National Academy of Sciences 106, 21213–21218. https://doi.org/10.1073/pnas.0906457106

Bano, R., Roy, S., 2016. Extraction of Soil Microarthropods: A low cost Berlese- Tullgren funnels extractor.

Barel, J.M., Moulia, V., Hamard, S., Sytiuk, A., Jassey, V.E.J., 2021. Come Rain, Come Shine: Peatland Carbon Dynamics Shift Under Extreme Precipitation. Front. Environ. Sci. 9. https://doi.org/10.3389/fenvs.2021.659953

Barthès, B.G., Chotte, J.-L., 2021. Infrared spectroscopy approaches support soil organic carbon estimations to evaluate land degradation. Land Degradation & Development 32, 310–322. https://doi.org/10.1002/ldr.3718

Batjes, N. h., 1996. Total carbon and nitrogen in the soils of the world. European Journal of Soil Science 47, 151–163. https://doi.org/10.1111/j.1365-2389.1996.tb01386.x

Bauriegel, A., Glina, B., Reintam, E., 2024. Histosol-Lecture-note.

Baysinger, M.R., Wilson, R.M., Hanson, P.J., Kostka, J.E., Chanton, J.P., 2022. Compositional stability of peat in ecosystem-scale warming mesocosms. PLOS ONE 17, e0263994. https://doi.org/10.1371/journal.pone.0263994

Belyea, L.R., Baird, A.J., 2006. Beyond "the Limits to Peat Bog Growth": Cross-Scale Feedback in Peatland Development. Ecological Monographs 76, 299–322. https://doi.org/10.1890/0012-9615(2006)076[0299:BTLTPB]2.0.CO;2

Bengtsson, F., Rydin, H., Hájek, T., 2018. Biochemical determinants of litter quality in 15 species of Sphagnum. Plant Soil 425, 161–176. https://doi.org/10.1007/s11104-018-3579-8

Berg, A., Findell, K., Lintner, B., Giannini, A., Seneviratne, S.I., van den Hurk, B., Lorenz, R., Pitman, A., Hagemann, S., Meier, A., Cheruy, F., Ducharne, A., Malyshev, S., Milly, P.C.D., 2016. Land–atmosphere feedbacks amplify aridity increase over land under global warming. Nature Clim Change 6, 869–874. https://doi.org/10.1038/nclimate3029

Bernier, M.-H., Levy, G.J., Fine, P., Borisover, M., 2013. Organic matter composition in soils irrigated with treated wastewater: FT-IR spectroscopic analysis of bulk soil samples. Geoderma 209–210, 233–240. https://doi.org/10.1016/j.geoderma.2013.06.017

Biester, H., Knorr, K.-H., Schellekens, J., Basler, A., Hermanns, Y.-M., 2014. Comparison of different methods to determine the degree of peat decomposition in peat bogs. Biogeosciences 11, 2691–2707. https://doi.org/10.5194/bg-11-2691-2014

Blier-Langdeau, A., Guêné-Nanchen, M., Hugron, S., Rochefort, L., 2022. The resistance and short-term resilience of a restored extracted peatland ecosystems post-fire: an opportunistic study after a wildfire. Restoration Ecology 30, e13545. https://doi.org/10.1111/rec.13545

Boelens, H.F.M., Eilers, P.H.C., Hankemeier, T., 2005. Sign constraints improve the detection of differences between complex spectral data sets: LC-IR as an example. Anal Chem 77, 7998–8007. https://doi.org/10.1021/ac051370e

Bohne, K., 2005. An Introduction Into Applied Soil Hydrology.

Bourceau, O.M., Ferdelman, T., Lavik, G., Mussmann, M., Kuypers, M.M.M., Marchant, H.K., 2023. Simultaneous sulfate and nitrate reduction in coastal sediments. ISME COMMUN. 3, 17. https://doi.org/10.1038/s43705-023-00222-y

Boye, K., Noël, V., Tfaily, M.M., Bone, S.E., Williams, K.H., Bargar, J.R., Fendorf, S., 2017. Thermodynamically controlled preservation of organic carbon in floodplains. Nature Geosci 10, 415–419. https://doi.org/10.1038/ngeo2940

Bragazza, L., Parisod, J., Buttler, A., Bardgett, R.D., 2013. Biogeochemical plant–soil microbe feedback in response to climate warming in peatlands. Nature Clim Change 3, 273–277. https://doi.org/10.1038/nclimate1781

Bridgham, S.D., Pastor, J., Dewey, B., Weltzin, J.F., Updegraff, K., 2008. Rapid Carbon Response of Peatlands to Climate Change. Ecology 89, 3041–3048. https://doi.org/10.1890/08-0279.1

Briones, M.J.I., Garnett, M.H., Ineson, P., 2010. Soil biology and warming play a key role in the release of 'old C' from organic soils. Soil Biology and Biochemistry 42, 960–967. https://doi.org/10.1016/j.soilbio.2010.02.013

Briones, M.J.I., Juan-Ovejero, R., McNamara, N.P., Ostle, N.J., 2022. Microbial "hotspots" of organic matter decomposition in temperate peatlands are driven by local spatial heterogeneity in abiotic conditions and not by vegetation structure. Soil Biology and Biochemistry 165, 108501. https://doi.org/10.1016/j.soilbio.2021.108501

Brosens, L., Robinet, J., Pelckmans, I., Ameijeiras-Mariño, Y., Govers, G., Opfergelt, S., Minella, J.P.G., Vanderborght, J., 2021. Have land use and land cover change affected soil thickness and weathering degree in a subtropical region in Southern Brazil? Insights from applied mid-infrared spectroscopy. CATENA 207, 105698. https://doi.org/10.1016/j.catena.2021.105698

Brown, C., Boyd, D.S., Sjögersten, S., Vane, C.H., 2023. Detecting tropical peatland degradation: Combining remote sensing and organic geochemistry. PLOS ONE 18, e0280187. https://doi.org/10.1371/journal.pone.0280187

Bruneel, Y., Van Laer, L., Brassinnes, S., Smolders, E., 2020. Radiocaesium sorption on natural glauconite sands is unexpectedly as strong as on Boom Clay. Science of The Total Environment 720, 137392. https://doi.org/10.1016/j.scitotenv.2020.137392

Buurman, P., Van Bergen, P.F., Jongmans, A.G., Meijer, E.L., Duran, B., Van Lagen, B., 2005. Spatial and temporal variation in podzol organic matter studied by pyrolysis-gas chromatography/mass spectrometry and micromorphology.

European Journal of Soil Science 56, 253–270. https://doi.org/10.1111/j.1365-2389.2004.00662.x
Cadigan, J.A., Jafari, N.H., Stagg, C.L., Laurenzano, C., Harris, B.D., Meselhe, A.E., Dugas, J., Couvillion, B., 2022. Characterization of vegetated and ponded wetlands with implications towards coastal wetland marsh collapse. Catena 218, 106547. https://doi.org/10.1016/j.catena.2022.106547
Cahoon, D.R., Hensel, P., Rybczyk, J., McKee, K.L., Proffitt, C.E., Perez, B.C., 2003. Mass tree mortality leads to mangrove peat collapse at Bay Islands, Honduras after Hurricane Mitch. Journal of Ecology 91, 1093–1105. https://doi.org/10.1046/j.1365-2745.2003.00841.x
Calderón, F., Haddix, M., Conant, R., Magrini-Bair, K., Paul, E., 2013. Diffuse-Reflectance Fourier-Transform Mid-Infrared Spectroscopy as a Method of Characterizing Changes in Soil Organic Matter. Soil Science Society of America Journal 77, 1591–1600. https://doi.org/10.2136/sssaj2013.04.0131
Campeau, A., Bishop, K.H., Billett, M.F., Garnett, M.H., Laudon, H., Leach, J.A., Nilsson, M.B., Öquist, M.G., Wallin, M.B., 2017. Aquatic export of young dissolved and gaseous carbon from a pristine boreal fen: Implications for peat carbon stock stability. Global Change Biology 23, 5523–5536. https://doi.org/10.1111/gcb.13815
Cao, C., Huang, J., Ge, L., Li, T., Bu, Z.-J., Wang, S., Wang, Z., Liu, Z., Liu, S., Wang, M., 2022. Does Shift in Vegetation Abundance After Nitrogen and Phosphorus Additions Play a Key Role in Regulating Fungal Community Structure in a Northern Peatland? Front. Microbiol. 13. https://doi.org/10.3389/fmicb.2022.920382
Cécillon, L., Certini, G., Lange, H., Forte, C., Strand, L.T., 2012. Spectral fingerprinting of soil organic matter composition. Organic Geochemistry 46, 127–136. https://doi.org/10.1016/j.orggeochem.2012.02.006
Chambers, L.G., Steinmuller, H.E., Breithaupt, J.L., 2019. Toward a mechanistic understanding of "peat collapse" and its potential contribution to coastal wetland loss. Ecology 100, e02720. https://doi.org/10.1002/ecy.2720
Charman, D.J., Beilman, D.W., Blaauw, M., Booth, R.K., Brewer, S., Chambers, F.M., Christen, J.A., Gallego-Sala, A., Harrison, S.P., Hughes, P.D.M., Jackson, S.T., Korhola, A., Mauquoy, D., Mitchell, F.J.G., Prentice, I.C., van der Linden, M., De Vleeschouwer, F., Yu, Z.C., Alm, J., Bauer, I.E., Corish, Y.M.C., Garneau, M., Hohl, V., Huang, Y., Karofeld, E., Le Roux, G., Loisel, J., Moschen, R., Nichols, J.E., Nieminen, T.M., MacDonald, G.M., Phadtare, N.R., Rausch, N., Sillasoo, Ü., Swindles, G.T., Tuittila, E.-S., Ukonmaanaho, L., Väliranta, M., van Bellen, S., van Geel, B., Vitt, D.H., Zhao, Y., 2013. Climate-related changes in peatland carbon accumulation during the last millennium. Biogeosciences 10, 929–944. https://doi.org/10.5194/bg-10-929-2013
Chen, H., Rhoades, C.C., Chow, A.T., 2020. Characteristics of soil organic matter 14 years after a wildfire: A pyrolysis-gas-chromatography mass spectrometry (Py-GC-MS) study. Journal of Analytical and Applied Pyrolysis 152, 104922. https://doi.org/10.1016/j.jaap.2020.104922
Chiang, F., Mazdiyasni, O., AghaKouchak, A., 2021. Evidence of anthropogenic impacts on global drought frequency, duration, and intensity. Nat Commun 12, 2754. https://doi.org/10.1038/s41467-021-22314-w
Churchman, G.J., Foster, R.C., D'Acqui, L.P., Janik, L.J., Skjemstad, J.O., Merry, R.H., Weissmann, D.A., 2010. Effect of land-use history on the potential for carbon sequestration in an Alfisol. Soil and Tillage Research 109, 23–35. https://doi.org/10.1016/j.still.2010.03.012

Cleveland, W.S., Devlin, S.J., 1988. Locally Weighted Regression: An Approach to Regression Analysis by Local Fitting. Journal of the American Statistical Association 83, 596–610. https://doi.org/10.1080/01621459.1988.10478639
Coates, J., 2006. Interpretation of Infrared Spectra, A Practical Approach, in: Encyclopedia of Analytical Chemistry. John Wiley & Sons, Ltd. https://doi.org/10.1002/9780470027318.a5606
Cong, J., Gao, C., Han, D., Li, Y., Wang, G., 2020. Stability of the permafrost peatlands carbon pool under climate change and wildfires during the last 150 years in the northern Great Khingan Mountains, China. Science of The Total Environment 712, 136476. https://doi.org/10.1016/j.scitotenv.2019.136476
Cruz-Alonso, V., Pucher, C., Ratcliffe, S., Ruiz-Benito, P., Astigarraga, J., Neumann, M., Hasenauer, H., Rodríguez-Sánchez, F., 2023. The easyclimate R package: Easy access to high-resolution daily climate data for Europe. Environmental Modelling & Software 161, 105627. https://doi.org/10.1016/j.envsoft.2023.105627
D'Acqui, L.P., Churchman, G.J., Janik, L.J., Ristori, G.G., Weissmann, D.A., 1999. Effect of organic matter removal by low-temperature ashing on dispersion of undisturbed aggregates from a tropical crusting soil. Geoderma 93, 311–324. https://doi.org/10.1016/S0016-7061(99)00073-7
Dai, A., 2013. Increasing drought under global warming in observations and models. Nature Clim Change 3, 52–58. https://doi.org/10.1038/nclimate1633
Dakos, V., Carpenter, S.R., Brock, W.A., Ellison, A.M., Guttal, V., Ives, A.R., Kéfi, S., Livina, V., Seekell, D.A., Nes, E.H. van, Scheffer, M., 2012. Methods for Detecting Early Warnings of Critical Transitions in Time Series Illustrated Using Simulated Ecological Data. PLOS ONE 7, e41010. https://doi.org/10.1371/journal.pone.0041010
Dakos, V., Kéfi, S., 2022. Ecological resilience: what to measure and how. Environ. Res. Lett. 17, 043003. https://doi.org/10.1088/1748-9326/ac5767
Dargie, G.C., Lewis, S.L., Lawson, I.T., Mitchard, E.T.A., Page, S.E., Bocko, Y.E., Ifo, S.A., 2017. Age, extent and carbon storage of the central Congo Basin peatland complex. Nature 542, 86–90. https://doi.org/10.1038/nature21048
Davies, G.M., Gray, A., Rein, G., Legg, C.J., 2013. Peat consumption and carbon loss due to smouldering wildfire in a temperate peatland. Forest Ecology and Management 308, 169–177. https://doi.org/10.1016/j.foreco.2013.07.051
de Mars, H., Wassen, M.J., 1999. Redox potentials in relation to water levels in different mire types in the Netherlands and Poland. Plant Ecology 140, 41–51. https://doi.org/10.1023/A:1009733113927
De Troyer, I., Bouillon, S., Barker, S., Perry, C., Coorevits, K., Merckx, R., 2010. Stable isotope analysis of dissolved organic carbon in soil solutions using a catalytic combustion total organic carbon analyzer-isotope ratio mass spectrometer with a cryofocusing interface. Rapid Communications in Mass Spectrometry 24, 365–374. https://doi.org/10.1002/rcm.4403
Dean, J.F., Billett, M.F., Turner, T.E., Garnett, M.H., Andersen, R., McKenzie, R.M., Dinsmore, K.J., Baird, A.J., Chapman, P.J., Holden, J., 2024. Peatland pools are tightly coupled to the contemporary carbon cycle. Global Change Biology 30, e16999. https://doi.org/10.1111/gcb.16999
Dehmer, J., 1993. Petrology and organic geochemistry of peat samples from a raised bog in Kalimantan (Borneo). Organic Geochemistry 20, 349–362. https://doi.org/10.1016/0146-6380(93)90125-U

DeLaune, R.D., Nyman, J.A., Jr., W.H.P., 1994. Peat Collapse, Ponding and Wetland Loss in a Rapidly Submerging Coastal Marsh. Journal of Coastal Research 10, 1021–1030.
Desie, E., Vancampenhout, K., Heyens, K., Hlava, J., Verheyen, K., Muys, B., 2019. Forest conversion to conifers induces a regime shift in soil process domain affecting carbon stability. Soil Biology and Biochemistry 136, 107540. https://doi.org/10.1016/j.soilbio.2019.107540
Dettmann, U., Kraft, N.N., Rech, R., Heidkamp, A., Tiemeyer, B., 2021. Analysis of peat soil organic carbon, total nitrogen, soil water content and basal respiration: Is there a 'best' drying temperature? Geoderma 403, 115231. https://doi.org/10.1016/j.geoderma.2021.115231
Dhandapani, S., Evers, S., 2020. Oil palm 'slash-and-burn' practice increases post-fire greenhouse gas emissions and nutrient concentrations in burnt regions of an agricultural tropical peatland. Science of The Total Environment 742, 140648. https://doi.org/10.1016/j.scitotenv.2020.140648
Di, H.J., Cameron, K.C., 2002. Nitrate leaching in temperate agroecosystems: sources, factors and mitigating strategies. Nutrient Cycling in Agroecosystems 64, 237–256. https://doi.org/10.1023/A:1021471531188
Dieleman, C.M., Branfireun, B.A., McLaughlin, J.W., Lindo, Z., 2015. Climate change drives a shift in peatland ecosystem plant community: Implications for ecosystem function and stability. Global Change Biology 21, 388–395. https://doi.org/10.1111/gcb.12643
Dixon, P., 2003. VEGAN, A Package of R Functions for Community Ecology. Journal of Vegetation Science 14, 927–930.
Dong, H., Qian, L., Yan, J., Gao, L., Fu, X., Wang, L., 2025. Biomarker analysis revealed tidal organic carbon input enhanced soil respiration and weakened carbon sequestration function of estuarine wetland: Field validation of the Jiuduansha Wetland in the Yangtze River estuary. Geoderma 453, 117134. https://doi.org/10.1016/j.geoderma.2024.117134
Draga, M., Gałka, M., Knorr, K.-H., Glatzel, S., Chojnicki, B.H., Fritz, C., Jassey, V.E.J., Juszczak, R., Meyer, H., Robroek, B.J.M., Thomas, C.L., Lamentowicz, M., 2025. Long-Term Ecological Baselines and Critical Thresholds in Ombrotrophic Peatlands of Europe: Implications for Restoration Strategies. Global Change Biology 31, e70629. https://doi.org/10.1111/gcb.70629
Dragoni, D., Schmid, H.P., Grimmond, C.S.B., Loescher, H.W., 2007. Uncertainty of annual net ecosystem productivity estimated using eddy covariance flux measurements. Journal of Geophysical Research: Atmospheres 112. https://doi.org/10.1029/2006JD008149
Drollinger, S., Knorr, K.-H., Knierzinger, W., Glatzel, S., 2020. Peat decomposition proxies of Alpine bogs along a degradation gradient. Geoderma 369, 114331. https://doi.org/10.1016/j.geoderma.2020.114331
Du, C., Zhou, J., 2011. Application of Infrared Photoacoustic Spectroscopy in Soil Analysis. Applied Spectroscopy Reviews 46, 405–422. https://doi.org/10.1080/05704928.2011.570837
Du, P., Kibbe, W.A., Lin, S.M., 2006. Improved peak detection in mass spectrum by incorporating continuous wavelet transform-based pattern matching. Bioinformatics 22, 2059–2065. https://doi.org/10.1093/bioinformatics/btl355
Duhamel, M., Wan, J., Bogar, L.M., Segnitz, R.M., Duncritts, N.C., Peay, K.G., 2019. Plant selection initiates alternative successional trajectories in the soil microbial community after disturbance. Ecological Monographs 89, e01367. https://doi.org/10.1002/ecm.1367

Dungait, J.A.J., Hopkins, D.W., Gregory, A.S., Whitmore, A.P., 2012. Soil organic matter turnover is governed by accessibility not recalcitrance. Global Change Biology 18, 1781–1796. https://doi.org/10.1111/j.1365-2486.2012.02665.x

Ellerbrock, R.H., Gerke, H.H., 2004. Characterizing organic matter of soil aggregate coatings and biopores by Fourier transform infrared spectroscopy. European Journal of Soil Science 55, 219–228. https://doi.org/10.1046/j.1365-2389.2004.00593.x

Emsens, W.-J., Aggenbach, C.J.S., Schoutens, K., Smolders, A.J.P., Zak, D., Diggelen, R. van, 2016. Soil Iron Content as a Predictor of Carbon and Nutrient Mobilization in Rewetted Fens. PLOS ONE 11, e0153166. https://doi.org/10.1371/journal.pone.0153166

Emsens, W.-J., van Diggelen, R., Aggenbach, C.J.S., Cajthaml, T., Frouz, J., Klimkowska, A., Kotowski, W., Kozub, L., Liczner, Y., Seeber, E., Silvennoinen, H., Tanneberger, F., Vicena, J., Wilk, M., Verbruggen, E., 2020. Recovery of fen peatland microbiomes and predicted functional profiles after rewetting. ISME J 14, 1701–1712. https://doi.org/10.1038/s41396-020-0639-x

Emsens, W.-J., Verbruggen, E., Shenk, P., Liczner, Y., van Roie, M., van Diggelen, R., 2021. Degradation legacy and current water levels as predictors of carbon emissions from two fen sites. Mires Peat 27, 1–15. https://doi.org/10.19189/MaP.2020.SNPG.StA.2149

Ernakovich, J.G., Wallenstein, M.D., Calderón, F. j., 2015. Chemical Indicators of Cryoturbation and Microbial Processing throughout an Alaskan Permafrost Soil Depth Profile. Soil Science Society of America Journal 79, 783–793. https://doi.org/10.2136/sssaj2014.10.0420

EU Parliament, 2024. European Parliament and of the Council on nature restoration and amending Regulation (EU) 2022/869 | TC1-COD(2022)0195 | European Parliament [WWW Document]. URL https://www.europarl.europa.eu/doceo/document/TC1-COD-2022-0195_EN.html (accessed 7.2.24).

Euskirchen, E.S., Edgar, C.W., Kane, E.S., Waldrop, M.P., Neumann, R.B., Manies, K.L., Douglas, T.A., Dieleman, C., Jones, M.C., Turetsky, M.R., 2024. Persistent net release of carbon dioxide and methane from an Alaskan lowland boreal peatland complex. Global Change Biology 30, e17139. https://doi.org/10.1111/gcb.17139

Evans, C.D., Peacock, M., Baird, A.J., Artz, R.R.E., Burden, A., Callaghan, N., Chapman, P.J., Cooper, H.M., Coyle, M., Craig, E., Cumming, A., Dixon, S., Gauci, V., Grayson, R.P., Helfter, C., Heppell, C.M., Holden, J., Jones, D.L., Kaduk, J., Levy, P., Matthews, R., McNamara, N.P., Misselbrook, T., Oakley, S., Page, S.E., Rayment, M., Ridley, L.M., Stanley, K.M., Williamson, J.L., Worrall, F., Morrison, R., 2021. Overriding water table control on managed peatland greenhouse gas emissions. Nature 593, 548–552. https://doi.org/10.1038/s41586-021-03523-1

Fawcett, T., 2006. An introduction to ROC analysis. Pattern Recognition Letters, ROC Analysis in Pattern Recognition 27, 861–874. https://doi.org/10.1016/j.patrec.2005.10.010

Fenner, N., Freeman, C., 2020. Woody litter protects peat carbon stocks during drought. Nat. Clim. Chang. 10, 363–369. https://doi.org/10.1038/s41558-020-0727-y

Fernandez, I., Cabaneiro, A., González-Prieto, S.J., 2004. Use of 13C to monitor soil organic matter transformations caused by a simulated forest fire. Rapid Communications in Mass Spectrometry 18, 435–442. https://doi.org/10.1002/rcm.1345

Feurdean, A., Diaconu, A.-C., Pfeiffer, M., Gałka, M., Hutchinson, S.M., Butiseaca, G., Gorina, N., Tonkov, S., Niamir, A., Tantau, I., Zhang, H., Kirpotin, S., 2022. Holocene wildfire regimes in western Siberia: interaction between peatland moisture conditions and the composition of plant functional types. Climate of the Past 18, 1255–1274. https://doi.org/10.5194/cp-18-1255-2022

Flanagan, N.E., Wang, H., Winton, S., Richardson, C.J., 2020. Low-severity fire as a mechanism of organic matter protection in global peatlands: Thermal alteration slows decomposition. Global Change Biology 26, 3930–3946. https://doi.org/10.1111/gcb.15102

Folke, C., Carpenter, S., Walker, B., Scheffer, M., Elmqvist, T., Gunderson, L., Holling, C.S., 2004. Regime Shifts, Resilience, and Biodiversity in Ecosystem Management. Annual Review of Ecology, Evolution, and Systematics 35, 557–581. https://doi.org/10.1146/annurev.ecolsys.35.021103.105711

Forouzangohar, M., Baldock, J.A., Smernik, R.J., Hawke, B., Bennett, L.T., 2015. Mid-infrared spectra predict nuclear magnetic resonance spectra of soil carbon. Geoderma 247–248, 65–72. https://doi.org/10.1016/j.geoderma.2015.02.006

Frankenberger, W.T., Johanson, J.B., 1982. Effect of pH on enzyme stability in soils. Soil Biology and Biochemistry 14, 433–437. https://doi.org/10.1016/0038-0717(82)90101-8

Freeman, C., Ostle, N., Kang, H., 2001. An enzymic "latch" on a global carbon store. Nature 409, 149–149. https://doi.org/10.1038/35051650

Gaffney, P.P.J., Tang, Q., Li, Q., Zhang, R., Pan, J., Xu, X., Li, Y., Niu, S., 2024. The impacts of land-use and climate change on the Zoige peatland carbon cycle: A review. WIREs Climate Change 15, e862. https://doi.org/10.1002/wcc.862

Gaffney, P.P.J., Tang, Q., Wang, J., Zhang, C., Xu, Ximeng, Xu, Xiangbo, Li, Y., Pap, S., Ratcliffe, J.L., Li, Q., Niu, S., 2025. The high-altitude peatland carbon cycle: A review of the impacts of climate change, human disturbance and management. Geography and Sustainability 6, 100353. https://doi.org/10.1016/j.geosus.2025.100353

Gholizadeh, A., Borůvka, L., Saberioon, M., Vašát, R., 2013. Visible, Near-Infrared, and Mid-Infrared Spectroscopy Applications for Soil Assessment with Emphasis on Soil Organic Matter Content and Quality: State-of-the-Art and Key Issues. Appl Spectrosc 67, 1349–1362. https://doi.org/10.1366/13-07288

González de Andrés, E., Shestakova, T.A., Scholten, R.C., Delcourt, C.J.F., Gorina, N.V., Camarero, J.J., 2022. Changes in tree growth synchrony and resilience in Siberian Pinus sylvestris forests are modulated by fire dynamics and ecohydrological conditions. Agricultural and Forest Meteorology 312, 108712. https://doi.org/10.1016/j.agrformet.2021.108712

Gorham, E., 1991. Northern Peatlands: Role in the Carbon Cycle and Probable Responses to Climatic Warming. Ecological Applications 1, 182–195. https://doi.org/10.2307/1941811

Grace, S.C., Hudson, D.A., Grace, S.C., Hudson, D.A., 2016. Processing and Visualization of Metabolomics Data Using R, in: Metabolomics - Fundamentals and Applications. IntechOpen. https://doi.org/10.5772/65405

Grandy, A.S., Wieder, W.R., Wickings, K., Kyker-Snowman, E., 2016. Beyond microbes: Are fauna the next frontier in soil biogeochemical models? Soil Biology and Biochemistry, Special issue: Food web interactions in the root zone: influences on community and ecosystem dynamics 102, 40–44. https://doi.org/10.1016/j.soilbio.2016.08.008

Gray, A., Davies, G.M., Domènech, R., Taylor, E., Levy, P.E., 2021. Peatland Wildfire Severity and Post-fire Gaseous Carbon Fluxes. Ecosystems 24, 713–725. https://doi.org/10.1007/s10021-020-00545-0
Greifswald Mire Centre, 2015. Home - Greifswald Mire Centre [WWW Document]. URL https://greifswaldmoor.de/home.html (accessed 2.18.26).
Groß-Schmölders, M., Klein, K., Emsens, W.-J., van Diggelen, R., Aggenbach, C.J.S., Liczner, Y., Frouz, J., Leifeld, J., Alewell, C., 2022. Stable isotopes (δ13C, δ15N) and biomarkers as indicators of the hydrological regime of fens in a European east–west transect. Science of The Total Environment 838, 156603. https://doi.org/10.1016/j.scitotenv.2022.156603
Grudzinski, B.P., Fritz, K., Golden, H.E., Newcomer-Johnson, T.A., Rech, J.A., Levy, J., Fain, J., McCarty, J.L., Johnson, B., Vang, T.K., Maurer, K., 2022. A global review of beaver dam impacts: Stream conservation implications across biomes. Global Ecology and Conservation 37, e02163. https://doi.org/10.1016/j.gecco.2022.e02163
Guêné-Nanchen, M., LeBlanc, M.-C., Rochefort, L., 2022. Post-fire peatland vegetation recovery: a case study in open rich fens of the Canadian boreal forest. Botany 100, 435–447. https://doi.org/10.1139/cjb-2021-0194
Günther, A., Barthelmes, A., Huth, V., Joosten, H., Jurasinski, G., Koebsch, F., Couwenberg, J., 2020. Prompt rewetting of drained peatlands reduces climate warming despite methane emissions. Nat Commun 11, 1–5. https://doi.org/10.1038/s41467-020-15499-z
Guo, J., Feng, H., Peng, C., Du, J., Wang, W., Kneeshaw, D., Pan, C., Roberge, G., Feng, L., Chen, A., 2024. Fire effects on soil CH4 and N2O fluxes across terrestrial ecosystems. Science of The Total Environment 948, 174708. https://doi.org/10.1016/j.scitotenv.2024.174708
Haberhauer, G., Gerzabek, M.H., 1999. Drift and transmission FT-IR spectroscopy of forest soils: an approach to determine decomposition processes of forest litter. Vibrational Spectroscopy 19, 413–417. https://doi.org/10.1016/S0924-2031(98)00046-0
Hagerthey, S.E., Newman, S., Rutchey, K., Smith, E.P., Godin, J., 2008. Multiple Regime Shifts in a Subtropical Peatland: Community-Specific Thresholds to Eutrophication. Ecological Monographs 78, 547–565. https://doi.org/10.1890/07-0538.1
Hájek, T., Ballance, S., Limpens, J., Zijlstra, M., Verhoeven, J.T.A., 2011. Cell-wall polysaccharides play an important role in decay resistance of Sphagnum and actively depressed decomposition in vitro. Biogeochemistry 103, 45–57. https://doi.org/10.1007/s10533-010-9444-3
Han, T., Zhou, K., Chao, J., Xu, X., Zhang, T., Wang, Y., Kong, M., 2023. Sulfate reduction promotes the release of organic phosphorus and iron-bound phosphorus in black-odor sediments in response to increased temperatures. J Soils Sediments 23, 3191–3200. https://doi.org/10.1007/s11368-023-03562-3
Hapsari, K.A., Jennerjahn, T., Nugroho, S.H., Yulianto, E., Behling, H., 2022. Sea level rise and climate change acting as interactive stressors on development and dynamics of tropical peatlands in coastal Sumatra and South Borneo since the Last Glacial Maximum. Global Change Biology 28, 3459–3479. https://doi.org/10.1111/gcb.16131
Harris, L.I., Richardson, K., Bona, K.A., Davidson, S.J., Finkelstein, S.A., Garneau, M., McLaughlin, J., Nwaishi, F., Olefeldt, D., Packalen, M., Roulet, N.T., Southee, F.M., Strack, M., Webster, K.L., Wilkinson, S.L., Ray, J.C., 2022. The essential

carbon service provided by northern peatlands. Frontiers in Ecology and the Environment 20, 222–230. https://doi.org/10.1002/fee.2437
Harrison, M.E., Deere, N.J., Imron, M.A., Nasir, D., Adul, Asti, H.A., Aragay Soler, J., Boyd, N.C., Cheyne, S.M., Collins, S.A., D'Arcy, L.J., Erb, W.M., Green, H., Healy, W., Hendri, Holly, B., Houlihan, P.R., Husson, S.J., Iwan, Jeffers, K.A., Kulu, I.P., Kusin, K., Marchant, N.C., Morrogh-Bernard, H.C., Page, S.E., Purwanto, A., Ripoll Capilla, B., de Rivera Ortega, O.R., Santiano, Spencer, K.L., Sugardjito, J., Supriatna, J., Thornton, S.A., Frank van Veen, F.J., Yulintine, Struebig, M.J., 2024. Impacts of fire and prospects for recovery in a tropical peat forest ecosystem. Proceedings of the National Academy of Sciences 121, e2307216121. https://doi.org/10.1073/pnas.2307216121
Helfenstein, A., Baumann, P., Viscarra Rossel, R., Gubler, A., Oechslin, S., Six, J., 2021. Quantifying soil carbon in temperate peatlands using a mid-IR soil spectral library. SOIL 7, 193–215. https://doi.org/10.5194/soil-7-193-2021
Heller, C., Ellerbrock, R.H., Roßkopf, N., Klingenfuß, C., Zeitz, J., 2015. Soil organic matter characterization of temperate peatland soil with FTIR-spectroscopy: effects of mire type and drainage intensity. European Journal of Soil Science 66, 847–858. https://doi.org/10.1111/ejss.12279
Helton, A.M., Bernhardt, E.S., Fedders, A., 2014. Biogeochemical regime shifts in coastal landscapes: the contrasting effects of saltwater incursion and agricultural pollution on greenhouse gas emissions from a freshwater wetland. Biogeochemistry 120, 133–147. https://doi.org/10.1007/s10533-014-9986-x
Hillebrand, H., Langenheder, S., Lebret, K., Lindström, E., Östman, Ö., Striebel, M., 2018. Decomposing multiple dimensions of stability in global change experiments. Ecol Lett 21, 21–30. https://doi.org/10.1111/ele.12867
Hirano, T., Kusin, K., Limin, S., Osaki, M., 2014. Carbon dioxide emissions through oxidative peat decomposition on a burnt tropical peatland. Global Change Biology 20, 555–565. https://doi.org/10.1111/gcb.12296
Hoch, G., 2007. Cell wall hemicelluloses as mobile carbon stores in non-reproductive plant tissues. Functional Ecology 21, 823–834. https://doi.org/10.1111/j.1365-2435.2007.01305.x
Hodgkins, S.B., Richardson, C.J., Dommain, R., Wang, H., Glaser, P.H., Verbeke, B., Winkler, B.R., Cobb, A.R., Rich, V.I., Missilmani, M., Flanagan, N., Ho, M., Hoyt, A.M., Harvey, C.F., Vining, S.R., Hough, M.A., Moore, T.R., Richard, P.J.H., De La Cruz, F.B., Toufaily, J., Hamdan, R., Cooper, W.T., Chanton, J.P., 2018. Tropical peatland carbon storage linked to global latitudinal trends in peat recalcitrance. Nat Commun 9, 3640. https://doi.org/10.1038/s41467-018-06050-2
Horai, H., Arita, M., Kanaya, S., Nihei, Y., Ikeda, T., Suwa, K., Ojima, Y., Tanaka, Kenichi, Tanaka, S., Aoshima, K., Oda, Y., Kakazu, Y., Kusano, M., Tohge, T., Matsuda, F., Sawada, Y., Hirai, M.Y., Nakanishi, H., Ikeda, K., Akimoto, N., Maoka, T., Takahashi, H., Ara, T., Sakurai, N., Suzuki, H., Shibata, D., Neumann, S., Iida, T., Tanaka, Ken, Funatsu, K., Matsuura, F., Soga, T., Taguchi, R., Saito, K., Nishioka, T., 2010. MassBank: a public repository for sharing mass spectral data for life sciences. J Mass Spectrom 45, 703–714. https://doi.org/10.1002/jms.1777
Houthuys, R., Adriaens, R., Goolaerts, S., Laga, P., Louwye, S., Matthijs, J., Vandenberghe, N., Verhaegen, J., 2020. The Diest Formation: a review of insights from the last decades. Geol. Belg. https://doi.org/10.20341/gb.2020.012
Hoyos-Santillan, J., Lomax, B.H., Large, D., Turner, B.L., Boom, A., Lopez, O.R., Sjoegersten, S., 2016. Quality not quantity: Organic matter composition controls

of CO_2 and CH_4 fluxes in neotropical peat profiles. Soil Biol. Biochem. 103, 86–96. https://doi.org/10.1016/j.soilbio.2016.08.017
Ingram, H. a. P., 1978. Soil Layers in Mires: Function and Terminology. Journal of Soil Science 29, 224–227. https://doi.org/10.1111/j.1365-2389.1978.tb02053.x
IPCC, 2018. Summary for Policymakers, IPCC Special Report on the Ocean and Cryosphere in a Changing Climate. Cambridge University Press.
Ivanova, A.A., Wegner, C.-E., Kim, Y., Liesack, W., Dedysh, S.N., 2016. Identification of microbial populations driving biopolymer degradation in acidic peatlands by metatranscriptomic analysis. Mol Ecol 25, 4818–4835. https://doi.org/10.1111/mec.13806
Jackson, R.B., Lajtha, K., Crow, S.E., Hugelius, G., Kramer, M.G., Piñeiro, G., 2017. The Ecology of Soil Carbon: Pools, Vulnerabilities, and Biotic and Abiotic Controls. Annual Review of Ecology, Evolution, and Systematics 48, 419–445. https://doi.org/10.1146/annurev-ecolsys-112414-054234
Jamaluddin, Schöpfer, K., Wagreich, M., Maria, Gier, S., Fathy, D., 2024. Effect of Depositional Environment and Climate on Organic Matter Enrichment in Sediments of the Upper Miocene—Pliocene Kampungbaru Formation, Lower Kutai Basin, Indonesia. Geosciences 14, 164. https://doi.org/10.3390/geosciences14060164
Janik, L.J., Skjemstad, J.O., Shepherd, K.D., Spouncer, L.R., 2007. The prediction of soil carbon fractions using mid-infrared-partial least square analysis. Soil Res. 45, 73–81. https://doi.org/10.1071/SR06083
Jansen, B., Wiesenberg, G.L.B., 2017. Opportunities and limitations related to the application of plant-derived lipid molecular proxies in soil science. SOIL 3, 211–234. https://doi.org/10.5194/soil-3-211-2017
Jassey, V.E.J., Reczuga, M.K., Zielińska, M., Słowińska, S., Robroek, B.J.M., Mariotte, P., Seppey, C.V.W., Lara, E., Barabach, J., Słowiński, M., Bragazza, L., Chojnicki, B.H., Lamentowicz, M., Mitchell, E.A.D., Buttler, A., 2018. Tipping point in plant–fungal interactions under severe drought causes abrupt rise in peatland ecosystem respiration. Global Change Biology 24, 972–986. https://doi.org/10.1111/gcb.13928
Jeewani, P.H., Brown, R.W., Evans, C.D., Cook, J., Roberts, B.P., Fraser, M.D., Chadwick, D.R., Jones, D.L., 2025. Rewetting alongside biochar and sulphate addition mitigates greenhouse gas emissions and retain carbon in degraded upland peatlands. Soil Biology and Biochemistry 207, 109814. https://doi.org/10.1016/j.soilbio.2025.109814
Jiang, W., Qiu, Y., Ni, Y., Su, M., Jia, W., Du, X., 2010. An automated data analysis pipeline for GC-TOF-MS metabonomics studies. J Proteome Res 9, 5974–5981. https://doi.org/10.1021/pr1007703
Jiménez-Morillo, N.T., Almendros, G., González-Vila, F.J., Jordán, A., Zavala, L.M., de la Rosa, J.M., González-Pérez, J.A., 2020. Fire effects on C and H isotopic composition in plant biomass and soil: Bulk and particle size fractions. Science of The Total Environment 749, 141417. https://doi.org/10.1016/j.scitotenv.2020.141417
Jones, E.A., Chasmer, L.E., Devito, K.J., Hopkinson, C.D., 2024. Shortening fire return interval predisposes west-central Canadian boreal peatlands to more rapid vegetation growth and transition to forest cover. Global Change Biology 30, e17185. https://doi.org/10.1111/gcb.17185
Joosten, H., Clarke, D., 2002. Wise use of mires and peatlands: background and principles including a framework for decision-making. Internat. Mire Conservation Group [u.a.], Totnes.

Joosten, H., Tanneberger, F., Moen, A., 2017. Mires and peatlands of Europe [WWW Document]. URL https://www.schweizerbart.de/publications/detail/isbn/9783510653836/Joosten_Tanneberger_Moen_Mires_and_peat (accessed 3.8.24).
Juan-Ovejero, R., Benito, E., Barreal, M.E., Rodeiro, J., Briones, M.J.I., 2019. Tolerance to fluctuating water regimes drives changes in mesofauna community structure and vertical stratification in peatlands. Pedobiologia 76, 150571. https://doi.org/10.1016/j.pedobi.2019.150571
Juan-Ovejero, R., Granjel, R.R., Ramil-Rego, P., Briones, M.J.I., 2020. The interplay between abiotic factors and below-ground biological interactions regulates carbon exports from peatlands. Geoderma 368, 114313. https://doi.org/10.1016/j.geoderma.2020.114313
Kaiser, K., Guggenberger, G., 2003. Mineral surfaces and soil organic matter. European Journal of Soil Science 54, 219–236. https://doi.org/10.1046/j.1365-2389.2003.00544.x
Kan, S., Yin, W., Li, Z., Guo, X., Ma, D., Yu, H., Zhao, Y., 2025. The “Iron Gate” Outcompetes the “Enzymic Latch” as the Dominant Soil Organic Carbon Stabilization Mechanism in Permafrost Peatlands of the Great Hing’an Mountains. Biology 14. https://doi.org/10.3390/biology14111504
Kane, E.S., Dieleman, C.M., Rupp, D., Wyatt, K.H., Rober, A.R., Turetsky, M.R., 2021. Consequences of Increased Variation in Peatland Hydrology for Carbon Storage: Legacy Effects of Drought and Flood in a Boreal Fen Ecosystem. Frontiers in Earth Science 8.
Kang, S., Li, X., Fan, J., Chang, J., 2012. Characterization of Hydrochars Produced by Hydrothermal Carbonization of Lignin, Cellulose, d-Xylose, and Wood Meal. Ind. Eng. Chem. Res. 51, 9023–9031. https://doi.org/10.1021/ie300565d
Keiluweit, M., Nico, P.S., Kleber, M., Fendorf, S., 2016. Are oxygen limitations under recognized regulators of organic carbon turnover in upland soils? Biogeochemistry 127, 157–171. https://doi.org/10.1007/s10533-015-0180-6
Keith, D.A., Benson, D.H., Baird, I.R.C., Watts, L., Simpson, C.C., Krogh, M., Gorissen, S., Ferrer-Paris, J.R., Mason, T.J., 2023. Effects of interactions between anthropogenic stressors and recurring perturbations on ecosystem resilience and collapse. Conservation Biology 37, e13995. https://doi.org/10.1111/cobi.13995
Kettridge, N., Turetsky, M.R., Sherwood, J.H., Thompson, D.K., Miller, C.A., Benscoter, B.W., Flannigan, M.D., Wotton, B.M., Waddington, J.M., 2015. Moderate drop in water table increases peatland vulnerability to post-fire regime shift. Sci Rep 5, 1–4. https://doi.org/10.1038/srep08063
Khan, A.H.A.N., Vanderborght, J., Smolders, E., Diels, J., 2025. Predicting denitrification in groundwater utilizing redoxcline depth and aquifer thickness. Science of The Total Environment 1004, 180775. https://doi.org/10.1016/j.scitotenv.2025.180775
Kim, K., 2026. Limited recovery of soil organic matter composition in fen peatlands after rewetting.
Kim, K., 2025. R script for pls and plsda model: Mid-infrared spectroscopy as a tool to assess oxidative signatures and monitor restoration trajectories in peatlands. https://doi.org/10.5281/zenodo.17857955
Kim, K., Aernouts, B., Emsens, W.-J., Schellekens, J., van Diggelen, R., Aggenbach, C., Verbruggen, E., Jansen, B., Briones, M.J.I., Vancampenhout, K., 2026a. Mid-infrared spectroscopy as a tool to monitor molecular changes in fens upon restoration. Organic Geochemistry 214, 105154. https://doi.org/10.1016/j.orggeochem.2026.105154

Kim, K., Schellekens, J., Emsens, W.-J., van Diggelen, R., Aggenbach, C., Verbruggen, E., Liczner, Y., Klimkowska, A., Tanneberger, F., Kotowski, W., Iglesias Briones, M.J., Jansen, B., Vancampenhout, K., 2026b. Limited recovery of soil organic matter composition in fen peatlands after rewetting. Geoderma 465, 117646. https://doi.org/10.1016/j.geoderma.2025.117646

Kirpotin, S.N., Antoshkina, O.A., Berezin, A.E., Elshehawi, S., Feurdean, A., Lapshina, E.D., Pokrovsky, O.S., Peregon, A.M., Semenova, N.M., Tanneberger, F., Volkov, I.V., Volkova, I.I., Joosten, H., 2021. Great Vasyugan Mire: How the world's largest peatland helps addressing the world's largest problems. Ambio 50, 2038–2049. https://doi.org/10.1007/s13280-021-01520-2

Kitson, E., Bell, N.G.A., 2020. The Response of Microbial Communities to Peatland Drainage and Rewetting. A Review. Frontiers in Microbiology 11.

Kleber, M., Bourg, I.C., Coward, E.K., Hansel, C.M., Myneni, S.C.B., Nunan, N., 2021. Dynamic interactions at the mineral–organic matter interface. Nat Rev Earth Environ 2, 402–421. https://doi.org/10.1038/s43017-021-00162-y

Klein, K., Schellekens, J., Groβ-Schmölders, M., von Sengbusch, P., Alewell, C., Leifeld, J., 2022. Characterizing ecosystem-driven chemical composition differences in natural and drained Finnish bogs using pyrolysis-GC/MS. Organic Geochemistry 165, 104351. https://doi.org/10.1016/j.orggeochem.2021.104351

Klingenfuß, C., Roßkopf, N., Walter, J., Heller, C., Zeitz, J., 2014. Soil organic matter to soil organic carbon ratios of peatland soil substrates. Geoderma 235–236, 410–417. https://doi.org/10.1016/j.geoderma.2014.07.010

Knox, S.H., Sturtevant, C., Matthes, J.H., Koteen, L., Verfaillie, J., Baldocchi, D., 2015. Agricultural peatland restoration: effects of land-use change on greenhouse gas (CO2 and CH4) fluxes in the Sacramento-San Joaquin Delta. Glob Chang Biol 21, 750–765. https://doi.org/10.1111/gcb.12745

Kögel-Knabner, I., Guggenberger, G., Kleber, M., Kandeler, E., Kalbitz, K., Scheu, S., Eusterhues, K., Leinweber, P., 2008. Organo-mineral associations in temperate soils: Integrating biology, mineralogy, and organic matter chemistry. Journal of Plant Nutrition and Soil Science 171, 61–82. https://doi.org/10.1002/jpln.200700048

Könönen, M., Jauhiainen, J., Straková, P., Heinonsalo, J., Laiho, R., Kusin, K., Limin, S., Vasander, H., 2018. Deforested and drained tropical peatland sites show poorer peat substrate quality and lower microbial biomass and activity than unmanaged swamp forest. Soil Biology and Biochemistry 123, 229–241. https://doi.org/10.1016/j.soilbio.2018.04.028

Kool, D.M., Buurman, P., Hoekman, D.H., 2006. Oxidation and compaction of a collapsed peat dome in Central Kalimantan. Geoderma 137, 217–225. https://doi.org/10.1016/j.geoderma.2006.08.021

Korn, R., Berg, C., Bersier, L.-F., Gray, S.M., Thallinger, G.G., 2024. Habitat conditions and not moss composition mediate microbial community structure in Swiss peatlands. Environmental Microbiology 26, e16631. https://doi.org/10.1111/1462-2920.16631

Kreyling, J., Tanneberger, F., Jansen, F., van der Linden, S., Aggenbach, C., Blüml, V., Couwenberg, J., Emsens, W.-J., Joosten, H., Klimkowska, A., Kotowski, W., Kozub, L., Lennartz, B., Liczner, Y., Liu, H., Michaelis, D., Oehmke, C., Parakenings, K., Pleyl, E., Poyda, A., Raabe, S., Röhl, M., Rücker, K., Schneider, A., Schrautzer, J., Schröder, C., Schug, F., Seeber, E., Thiel, F., Thiele, S., Tiemeyer, B., Timmermann, T., Urich, T., van Diggelen, R., Vegelin, K., Verbruggen, E., Wilmking, M., Wrage-Mönnig, N., Wołejko, L., Zak, D.,

Jurasinski, G., 2021. Rewetting does not return drained fen peatlands to their old selves. Nat Commun 12, 5693. https://doi.org/10.1038/s41467-021-25619-y
Krüger, J.P., Dotterweich, M., Seifert-Schäfer, A., Hoffmann, S., Kopf, C., Kneisel, C., Dotzler, S., Nink, S., Stoffels, J., Schüler, G., 2021. Carbon stocks and their spatial distribution in drained and rewetted peatland forests in a low mountain range area, Germany. Mires Peat 27, 1–18. https://doi.org/10.19189/MaP.2020.BG.StA.1991
Kunarso, A., Farquharson, R., Blanch, E.W., Grover, S., 2025. Mid-infrared spectroscopy as a potential tool for monitoring the success of tropical peatland restoration. Journal of Environmental Management 394, 127327. https://doi.org/10.1016/j.jenvman.2025.127327
Lai, D.Y.F., 2009. Methane Dynamics in Northern Peatlands: A Review. Pedosphere 19, 409–421. https://doi.org/10.1016/S1002-0160(09)00003-4
Laine, A.M., Lindholm, T., Nilsson, M., Kutznetsov, O., Jassey, V.E.J., Tuittila, E.-S., 2021. Functional diversity and trait composition of vascular plant and Sphagnum moss communities during peatland succession across land uplift regions. Journal of Ecology 109, 1774–1789. https://doi.org/10.1111/1365-2745.13601
Lamers, L.P.M., Vile, M.A., Grootjans, A.P., Acreman, M.C., van Diggelen, R., Evans, M.G., Richardson, C.J., Rochefort, L., Kooijman, A.M., Roelofs, J.G.M., Smolders, A.J.P., 2015. Ecological restoration of rich fens in Europe and North America: from trial and error to an evidence-based approach. Biological Reviews 90, 182–203. https://doi.org/10.1111/brv.12102
Laudon, H., Mosquera, V., Eklöf, K., Järveoja, J., Karimi, S., Krasnova, A., Peichl, M., Pinkwart, A., Tong, C.H.M., Wallin, M.B., Zannella, A., Hasselquist, E.M., 2023. Consequences of rewetting and ditch cleaning on hydrology, water quality and greenhouse gas balance in a drained northern landscape. Sci Rep 13, 20218. https://doi.org/10.1038/s41598-023-47528-4
Le Guillou, C., Dohmen, R., Rogalla, D., Müller, T., Vollmer, C., Becker, H.-W., 2015. New experimental approach to study aqueous alteration of amorphous silicates at low reaction rates. Chemical Geology 412, 179–192. https://doi.org/10.1016/j.chemgeo.2015.06.027
Ledger, M.J., Evans, C.D., Large, D.J., Evers, S., Brown, C., Jovani-Sancho, A.J., Callaghan, N., Vane, C.H., Marshall, C., Baskaran, A., Gan, J.Y., Sowter, A., Morrison, K., Sjögersten, S., 2023. Tropical peat surface oscillations are a function of peat condition at North Selangor peat swamp forest, Malaysia. Front. Environ. Sci. 11. https://doi.org/10.3389/fenvs.2023.1182100
Lefcheck, J.S., 2016. piecewiseSEM: Piecewise structural equation modelling in r for ecology, evolution, and systematics. Methods in Ecology and Evolution 7, 573–579. https://doi.org/10.1111/2041-210X.12512
Lehmann, J., Hansel, C.M., Kaiser, C., Kleber, M., Maher, K., Manzoni, S., Nunan, N., Reichstein, M., Schimel, J.P., Torn, M.S., Wieder, W.R., Kögel-Knabner, I., 2020. Persistence of soil organic carbon caused by functional complexity. Nat. Geosci. 13, 529–534. https://doi.org/10.1038/s41561-020-0612-3
Lehmann, J., Kleber, M., 2015. The contentious nature of soil organic matter. Nature 528, 60–68. https://doi.org/10.1038/nature16069
Leifeld, J., 2006. Application of diffuse reflectance FT-IR spectroscopy and partial least-squares regression to predict NMR properties of soil organic matter. European Journal of Soil Science 57, 846–857. https://doi.org/10.1111/j.1365-2389.2005.00776.x

Leifeld, J., Menichetti, L., 2018. The underappreciated potential of peatlands in global climate change mitigation strategies. Nat Commun 9, 1–7. https://doi.org/10.1038/s41467-018-03406-6
Leifeld, J., Müller, M., Fuhrer, J., 2011. Peatland subsidence and carbon loss from drained temperate fens. Soil Use and Management 27, 170–176. https://doi.org/10.1111/j.1475-2743.2011.00327.x
Leifeld, J., Steffens, M., Galego-Sala, A., 2012. Sensitivity of peatland carbon loss to organic matter quality. Geophysical Research Letters 39. https://doi.org/10.1029/2012GL051856
Lewis, R.R., Milbrandt, E.C., Brown, B., Krauss, K.W., Rovai, A.S., Beever, J.W., Flynn, L.L., 2016. Stress in mangrove forests: Early detection and preemptive rehabilitation are essential for future successful worldwide mangrove forest management. Marine Pollution Bulletin, Turning the tide on mangrove loss 109, 764–771. https://doi.org/10.1016/j.marpolbul.2016.03.006
Li, G., Sun, L., Ji, S., Li, X., Cong, J., Han, D., Wang, G., Gao, C., 2025. Low-severity fire promote carbon emissions in permafrost peatlands of the Great Khingan Mountains, Northeast China. CATENA 252, 108870. https://doi.org/10.1016/j.catena.2025.108870
Li, J., Nie, M., Pendall, E., 2019. An incubation study of temperature sensitivity of greenhouse gas fluxes in three land-cover types near Sydney, Australia. Sci. Total Environ. 688, 324–332. https://doi.org/10.1016/j.scitotenv.2019.06.206
Liang, C., Schimel, J.P., Jastrow, J.D., 2017. The importance of anabolism in microbial control over soil carbon storage. Nat Microbiol 2, 17105. https://doi.org/10.1038/nmicrobiol.2017.105
Liquet, B., Lê Cao, K.-A., Hocini, H., Thiébaut, R., 2012. A novel approach for biomarker selection and the integration of repeated measures experiments from two assays. BMC Bioinformatics 13, 325. https://doi.org/10.1186/1471-2105-13-325
Liu, C., Wang, S., Zhu, E., Jia, J., Zhao, Y., Feng, X., 2021. Long-term drainage induces divergent changes of soil organic carbon contents but enhances microbial carbon accumulation in fen and bog. Geoderma 404, 115343. https://doi.org/10.1016/j.geoderma.2021.115343
Loiko, S.V., Pokrovsky, O.S., Raudina, T.V., Lim, A., Kolesnichenko, L.G., Shirokova, L.S., Vorobyev, S.N., Kirpotin, S.N., 2017. Abrupt permafrost collapse enhances organic carbon, CO2, nutrient and metal release into surface waters. Chemical Geology 471, 153–165. https://doi.org/10.1016/j.chemgeo.2017.10.002
Loisel, J., Gallego-Sala, A., 2022. Ecological resilience of restored peatlands to climate change. Commun Earth Environ 3, 1–8. https://doi.org/10.1038/s43247-022-00547-x
Loisel, J., van Bellen, S., Pelletier, L., Talbot, J., Hugelius, G., Karran, D., Yu, Z., Nichols, J., Holmquist, J., 2017. Insights and issues with estimating northern peatland carbon stocks and fluxes since the Last Glacial Maximum. Earth-Science Reviews 165, 59–80. https://doi.org/10.1016/j.earscirev.2016.12.001
Lopes-Mazzetto, J.M., Schellekens, J., Vidal-Torrado, P., Buurman, P., 2018. Impact of drainage and soil hydrology on sources and degradation of organic matter in tropical coastal podzols. Geoderma 330, 79–90. https://doi.org/10.1016/j.geoderma.2018.05.015
Ma, Y., Minasny, B., Roudier, P., Theng, B.K.G., Carrick, S., 2024. Application of mid-infrared (MIR) spectroscopy to identify and quantify minerals in New Zealand soils. CATENA 242, 108115. https://doi.org/10.1016/j.catena.2024.108115
Maas, L., Verbruggen, E., Cosme, M., Ceulemans, T., Jacobs, S., Liczner, Y., Kim, K., Vancampenhout, K., Diggelen, R. van, Emsens, W.-J., 2026. Prolonged impact

of fire on peatland fungi despite rapid recovery of vegetation, prokaryotes, and soil physicochemistry. https://doi.org/10.64898/2026.02.20.707020
Määttä, T., Malhotra, A., 2024. The hidden roots of wetland methane emissions. Global Change Biology 30, e17127. https://doi.org/10.1111/gcb.17127
MacDonell, C.J., Williams, R.D., Maniatis, G., Roberts, K., Naylor, M., 2023. Consumer-grade UAV solid-state LiDAR accurately quantifies topography in a vegetated fluvial environment. Earth Surface Processes and Landforms 48, 2211–2229. https://doi.org/10.1002/esp.5608
Madejová, J., 2003. FTIR techniques in clay mineral studies. Vibrational Spectroscopy 31, 1–10. https://doi.org/10.1016/S0924-2031(02)00065-6
Madejová, J., Komadel, P., 2001. Baseline Studies of the Clay Minerals Society Source Clays: Infrared Methods. Clays and Clay Minerals 49, 410–432. https://doi.org/10.1346/CCMN.2001.0490508
Mahdiyasa, A.W., Large, D.J., Muljadi, B.P., Icardi, M., 2023. Modelling the influence of mechanical-ecohydrological feedback on the nonlinear dynamics of peatlands. Ecological Modelling 478, 110299. https://doi.org/10.1016/j.ecolmodel.2023.110299
Mander, Ü., Espenberg, M., Melling, L., Kull, A., 2024. Peatland restoration pathways to mitigate greenhouse gas emissions and retain peat carbon. Biogeochemistry 167, 523–543. https://doi.org/10.1007/s10533-023-01103-1
Martínez Cortizas, A., López-Merino, L., Silva-Sánchez, N., Sjöström, J.K., Kylander, M.E., 2021. Investigating the Mineral Composition of Peat by Combining FTIR-ATR and Multivariate Analysis. Minerals 11, 1084. https://doi.org/10.3390/min11101084
Matamala, R., Calderón, F.J., Jastrow, J.D., Fan, Z., Hofmann, S.M., Michaelson, G.J., Mishra, U., Ping, C.-L., 2017. Influence of site and soil properties on the DRIFT spectra of northern cold-region soils. Geoderma 305, 80–91. https://doi.org/10.1016/j.geoderma.2017.05.014
McAnallen, L., Doherty, R., Ogle, N., 2017. Organic composition and multiphase stable isotope analysis of active, degrading and restored blanket bog. Science of The Total Environment 599–600, 1779–1790. https://doi.org/10.1016/j.scitotenv.2017.05.064
McClymont, E.L., Bingham, E.M., Nott, C.J., Chambers, F.M., Pancost, R.D., Evershed, R.P., 2011. Pyrolysis GC–MS as a rapid screening tool for determination of peat-forming plant composition in cores from ombrotrophic peat. Organic Geochemistry 42, 1420–1435. https://doi.org/10.1016/j.orggeochem.2011.07.004
Mendiburu, F. de, 2020. agricolae: Statistical Procedures for Agricultural Research.
Meyer, L., Brinkman, S., van Kesteren, L., Leprince-Ringuet, N., van Boxmeer, F., 2014. Technical Support Unit for the Synthesis Report.
Middleton, B.A., David, J.L., 2022. Trends in vegetation and height of the topographic surface in a tidal freshwater swamp experiencing rooting zone saltwater intrusion. Ecological Indicators 145, 109637. https://doi.org/10.1016/j.ecolind.2022.109637
Milner, A.M., Baird, A.J., Green, S.M., Swindles, G.T., Young, D.M., Sanderson, N.K., Timmins, M.S.I., Gałka, M., 2021. A regime shift from erosion to carbon accumulation in a temperate northern peatland. Journal of Ecology 109, 125–138. https://doi.org/10.1111/1365-2745.13453
Moinet, G.Y.K., Millard, P., 2020. Temperature sensitivity of decomposition: Discrepancy between field and laboratory estimates is not due to sieving the soil. Geoderma 374, 114444. https://doi.org/10.1016/j.geoderma.2020.114444

Moomaw, W.R., Chmura, G.L., Davies, G.T., Finlayson, C.M., Middleton, B.A., Natali, S.M., Perry, J.E., Roulet, N., Sutton-Grier, A.E., 2018. Wetlands In a Changing Climate: Science, Policy and Management. Wetlands 38, 183–205. https://doi.org/10.1007/s13157-018-1023-8

Moris, V., 2020. Dynamiek van koolstof en nutriënten in veenbodems van natuurreservaat De Zegge. KU Leuven. Faculteit Industriële Ingenieurswetenschappen, Leuven.

Morris, P.J., Belyea, L.R., Baird, A.J., 2011. Ecohydrological feedbacks in peatland development: a theoretical modelling study. Journal of Ecology 99, 1190–1201. https://doi.org/10.1111/j.1365-2745.2011.01842.x

Moudrý, V., Klápště, P., Fogl, M., Gdulová, K., Barták, V., Urban, R., 2020. Assessment of LiDAR ground filtering algorithms for determining ground surface of non-natural terrain overgrown with forest and steppe vegetation. Measurement 150, 107047. https://doi.org/10.1016/j.measurement.2019.107047

Movasaghi, Z., Rehman, S., ur Rehman, Dr.I., 2008. Fourier Transform Infrared (FTIR) Spectroscopy of Biological Tissues. Applied Spectroscopy Reviews 43, 134–179. https://doi.org/10.1080/05704920701829043

Mursyid, H., Ramadhan, R., Irawan, A., Sadono, R., Susila Putra, E.T., Suryanto, P., 2025. A global development and dynamics of peatland restoration: a bibliometric analysis. Ecological Indicators 177, 113724. https://doi.org/10.1016/j.ecolind.2025.113724

Nayak, P.S., Singh, B.K., 2007. Instrumental characterization of clay by XRF, XRD and FTIR. Bull Mater Sci 30, 235–238. https://doi.org/10.1007/s12034-007-0042-5

Negassa, W., Eckhardt, K.-U., Regier, T., Leinweber, P., 2021. Dissolved organic matter concentration, molecular composition, and functional groups in contrasting management practices of peatlands. Journal of Environmental Quality 50, 1364–1380. https://doi.org/10.1002/jeq2.20284

Ng, W., Minasny, B., Jeon, S.H., McBratney, A., 2022. Mid-infrared spectroscopy for accurate measurement of an extensive set of soil properties for assessing soil functions. Soil Security 6, 100043. https://doi.org/10.1016/j.soisec.2022.100043

Nguyen, T.T., Janik, L.J., Raupach, M., 1991. Diffuse reflectance infrared fourier transform (DRIFT) spectroscopy in soil studies. Soil Res. 29, 49–67. https://doi.org/10.1071/sr9910049

Niemeyer, J., Chen, Y., Bollag, J.-M., 1992. Characterization of Humic Acids, Composts, and Peat by Diffuse Reflectance Fourier-Transform Infrared Spectroscopy. Soil Science Society of America Journal 56, 135–140. https://doi.org/10.2136/sssaj1992.03615995005600010021x

Nierop, K.G.J., Buurman, P., de Leeuw, J.W., 1999. Effect of vegetation on chemical composition of H horizons in incipient podzols as characterized by 13C<math><msup><mi></mi><mn>13</mn></msup><mtext>C</mtext></math> NMR and pyrolysis-GC/MS. Geoderma 90, 111–129. https://doi.org/10.1016/S0016-7061(98)00095-0

Nierop, K.G.J., van Lagen, B., Buurman, P., 2001. Composition of plant tissues and soil organic matter in the first stages of a vegetation succession. Geoderma 100, 1–24. https://doi.org/10.1016/S0016-7061(00)00078-1

Nikolaus, K., Schellekens, J., Mols, S., Jansen, B., Briones, M.J.I., Desie, E., Cornelis, J.-T., Absalah, S., Muys, B., Vancampenhout, K., 2023. Seeing the forest for the fractions – Comparing soil organic matter fractionation methods using molecular features after forest stand conversion. Geoderma 430, 116280. https://doi.org/10.1016/j.geoderma.2022.116280

Ninnes, S., Meyer-Jacob, C., Tolu, J., Bindler, R., Cortizas, A.M., 2023. Application of mid-infrared spectroscopy for the quantitative and qualitative analysis of organic

matter in Holocene sediment records. The Holocene 09596836231211872. https://doi.org/10.1177/09596836231211872
O'connor, F.B., 1955. Extraction of Enchytraeid Worms from a Coniferous Forest Soil. Nature 175, 815–816. https://doi.org/10.1038/175815b0
Olefeldt, D., Euskirchen, E.S., Harden, J., Kane, E., McGuire, A.D., Waldrop, M.P., Turetsky, M.R., 2017. A decade of boreal rich fen greenhouse gas fluxes in response to natural and experimental water table variability. Global Change Biology 23, 2428–2440. https://doi.org/10.1111/gcb.13612
Olefeldt, D., Turetsky, M.R., Blodau, C., 2013. Altered Composition and Microbial versus UV-Mediated Degradation of Dissolved Organic Matter in Boreal Soils Following Wildfire. Ecosystems 16, 1396–1412. https://doi.org/10.1007/s10021-013-9691-y
Orgiazzi, A., Bardgett, R.D., Barrios, E., Behan-Pelletier, V., Briones, M.J.I., Chotte, J.-L., De Deyn, G.B., Eggleton, P., Fierer, N., Fraser, T., Hedlund, K., Jeffery, S., Johnson, N.C., Jones, A., Kandeler, E., Kaneko, N., Lavelle, P., Lemanceau, P., Miko, L., Montanarella, L., Moreira, F.M.S., Ramirez, K.S., Scheu, S., Singh, B.K., Six, J., Putten, W.H. van der, Wall, D.H., European Commission (Eds.), 2016. Global soil biodiversity atlas. Publications Office, Luxembourg. https://doi.org/10.2788/799182
Orwin, K.H., Ostle, N.J., 2012. Moss species effects on peatland carbon cycling after fire. Functional Ecology 26, 829–836. https://doi.org/10.1111/j.1365-2435.2012.01991.x
Orwin, K.H., Wardle, D.A., 2004. New indices for quantifying the resistance and resilience of soil biota to exogenous disturbances. Soil Biology and Biochemistry 36, 1907–1912. https://doi.org/10.1016/j.soilbio.2004.04.036
Osland, M.J., Feher, L.C., Anderson, G.H., Vervaeke, W.C., Krauss, K.W., Whelan, K.R.T., Balentine, K.M., Tiling-Range, G., Smith, T.J., Cahoon, D.R., 2020. A Tropical Cyclone-Induced Ecological Regime Shift: Mangrove Forest Conversion to Mudflat in Everglades National Park (Florida, USA). Wetlands 40, 1445–1458. https://doi.org/10.1007/s13157-020-01291-8
Ottoy, S., Vanierschot, L., Dondeyne, S., Vancampenhout, K., Hermy, M., Van Orshoven, J., 2019. The devil is in the detail: Discrepancy between soil organic carbon stocks estimated from regional and local data sources in Flanders, Belgium. Soil Use and Management 35, 421–432. https://doi.org/10.1111/sum.12504
Painter, T.J., 1991. Lindow man, tollund man and other peat-bog bodies: The preservative and antimicrobial action of Sphagnan, a reactive glycuronoglycan with tanning and sequestering properties. Carbohydrate Polymers 15, 123–142. https://doi.org/10.1016/0144-8617(91)90028-B
Pedersen, J.A., Simpson, M.A., Bockheim, J.G., Kumar, K., 2011. Characterization of soil organic carbon in drained thaw-lake basins of Arctic Alaska using NMR and FTIR photoacoustic spectroscopy. Organic Geochemistry, Applications and developments of magnetic resonance techniques in Geosciences 42, 947–954. https://doi.org/10.1016/j.orggeochem.2011.04.003
Pellegrini, A.F.A., Hedin, L.O., Staver, A.C., Govender, N., 2015. Fire alters ecosystem carbon and nutrients but not plant nutrient stoichiometry or composition in tropical savanna. Ecology 96, 1275–1285. https://doi.org/10.1890/14-1158.1
Peltoniemi, K., Straková, P., Fritze, H., Iráizoz, P.A., Pennanen, T., Laiho, R., 2012. How water-level drawdown modifies litter-decomposing fungal and actinobacterial communities in boreal peatlands. Soil Biology and Biochemistry 51, 20–34. https://doi.org/10.1016/j.soilbio.2012.04.013

Peltre, C., Bruun, S., Du, C., Thomsen, I.K., Jensen, L.S., 2014. Assessing soil constituents and labile soil organic carbon by mid-infrared photoacoustic spectroscopy. Soil Biology and Biochemistry 77, 41–50. https://doi.org/10.1016/j.soilbio.2014.06.022

Pengerud, A., Cécillon, L., Johnsen, L.K., Rasse, D.P., Strand, L.T., 2013. Permafrost Distribution Drives Soil Organic Matter Stability in a Subarctic Palsa Peatland. Ecosystems 16, 934–947. https://doi.org/10.1007/s10021-013-9652-5

Piayda, A., Tiemeyer, B., Dettmann, U., Buschmann, C., Bechtold, M., Röder, N., 2020. Physical and chemical properties of fen peat soils under agricultural use across Europe. (No. EGU2020-13266). Presented at the EGU2020, Copernicus Meetings. https://doi.org/10.5194/egusphere-egu2020-13266

Pinheiro, J., Bates, D., R Core Team, 2025. nlme: Linear and Nonlinear Mixed Effects Models. https://doi.org/10.32614/CRAN.package.nlme

Pluskal, T., Castillo, S., Villar-Briones, A., Orešič, M., 2010. MZmine 2: Modular framework for processing, visualizing, and analyzing mass spectrometry-based molecular profile data. BMC Bioinformatics 11, 395. https://doi.org/10.1186/1471-2105-11-395

Pouwels, A.D., Eijkel, G.B., Boon, J.J., 1989. Curie-point pyrolysis-capillary gas chromatography-high-resolution mass spectrometry of microcrystalline cellulose. Journal of Analytical and Applied Pyrolysis 14, 237–280. https://doi.org/10.1016/0165-2370(89)80003-8

R Development Core Team, 2025. R: The R Project for Statistical Computing [WWW Document]. URL https://www.r-project.org/ (accessed 1.19.26).

Radabaugh, K.R., Dontis, E.E., Chappel, A.R., Russo, C.E., Moyer, R.P., 2021. Early indicators of stress in mangrove forests with altered hydrology in Tampa Bay, Florida, USA. Estuarine, Coastal and Shelf Science 254, 107324. https://doi.org/10.1016/j.ecss.2021.107324

Radu, D.D., Duval, T.P., 2018. Impact of rainfall regime on methane flux from a cool temperate fen depends on vegetation cover. Ecological Engineering, Wetlands and Carbon Revisited 114, 76–87. https://doi.org/10.1016/j.ecoleng.2017.06.047

Reddy, K.R., DeLaune, R.D., 2008. Biogeochemistry of Wetlands: Science and Applications. CRC Press, Boca Raton. https://doi.org/10.1201/9780203491454

Reed, D., Chavez, S., Castañeda-Moya, E., Oberbauer, S.F., Troxler, T., Malone, S., 2025. Resilience to Hurricanes Is High in Mangrove Blue Carbon Forests. Global Change Biology 31, e70124. https://doi.org/10.1111/gcb.70124

Rein, G. (Ed.), 2015. Smoldering-Peat Megafires: The Largest Fires on Earth, in: Coal and Peat Fires: A Global Perspective. Elsevier, Boston, pp. 1–11. https://doi.org/10.1016/B978-0-444-59510-2.00001-X

Reynaert, S., De Boeck, H.J., Verbruggen, E., Verlinden, M., Flowers, N., Nijs, I., 2021. Risk of short-term biodiversity loss under more persistent precipitation regimes. Global Change Biology 27, 1614–1626. https://doi.org/10.1111/gcb.15501

Rheault, K., Christiansen, J.R., Larsen, K.S., 2024. goFlux: A user-friendly way to calculate GHG fluxes yourself, regardless of user experience. Journal of Open Source Software 9, 6393. https://doi.org/10.21105/joss.06393

Ribeiro, K., Pacheco, F.S., Ferreira, J.W., de Sousa-Neto, E.R., Hastie, A., Krieger Filho, G.C., Alvalá, P.C., Forti, M.C., Ometto, J.P., 2021. Tropical peatlands and their contribution to the global carbon cycle and climate change. Global Change Biology 27, 489–505. https://doi.org/10.1111/gcb.15408

Robinson, M.D., McCarthy, D.J., Smyth, G.K., 2010. edgeR: a Bioconductor package for differential expression analysis of digital gene expression data. Bioinformatics 26, 139–140. https://doi.org/10.1093/bioinformatics/btp616

Robinson, S.D., Moore, T.R., 1999. Carbon and peat accumulation over the past 1200 years in a landscape with discontinuous permafrost, northwestern Canada. Global Biogeochemical Cycles 13, 591–601. https://doi.org/10.1029/1999GB900008
Robroek, B.J.M., Devilee, G., Telgenkamp, Y., Härlin, C., Steele, M.N., Barel, J.M., Lamers, L.P.M., 2024. More is not always better: peat moss mixtures slightly enhance peatland stability. Proceedings of the Royal Society B: Biological Sciences 291, 20232622. https://doi.org/10.1098/rspb.2023.2622
Rodriguez, A.F., Gerber, S., Inglett, P.W., Tran, N.T., Long, J.R., Daroub, S.H., 2021. Soil carbon characterization in a subtropical drained peatland. Geoderma 382, 114758. https://doi.org/10.1016/j.geoderma.2020.114758
Rossel, R.A.V., Behrens, T., 2010. Using data mining to model and interpret soil diffuse reflectance spectra. Geoderma, Diffuse reflectance spectroscopy in soil science and land resource assessment 158, 46–54. https://doi.org/10.1016/j.geoderma.2009.12.025
Rumpel, C., Janik, L.J., Skjemstad, J.O., Kögel-Knabner, I., 2001. Quantification of carbon derived from lignite in soils using mid-infrared spectroscopy and partial least squares. Organic Geochemistry 32, 831–839. https://doi.org/10.1016/S0146-6380(01)00029-8
Rupp, D., Kane, E.S., Dieleman, C., Keller, J.K., Turetsky, M., 2019. Plant functional group effects on peat carbon cycling in a boreal rich fen. Biogeochemistry 144, 305–327. https://doi.org/10.1007/s10533-019-00590-5
Rydin, H., Jeglum, J.K., 2006. The Biology of Peatlands. Oxford University Press. https://doi.org/10.1093/acprof:oso/9780198528722.001.0001
Salimi, S., Almuktar, S.A.A.A.N., Scholz, M., 2021. Impact of climate change on wetland ecosystems: A critical review of experimental wetlands. Journal of Environmental Management 286, 112160. https://doi.org/10.1016/j.jenvman.2021.112160
San-Emeterio, L.M., Jiménez-Morillo, N.T., Vega, J.A., Fernández, C., Fontúrbel, T., Almendros, G., González-Pérez, José.A., 2026. Effects of fire severity on soil organic matter: a multi-isotope (C, N, H, O) comparison of wildfires and experimental burns. CATENA 264, 109817. https://doi.org/10.1016/j.catena.2026.109817
Säurich, A., Tiemeyer, B., Don, A., Fiedler, S., Bechtold, M., Amelung, W., Freibauer, A., 2019. Drained organic soils under agriculture — The more degraded the soil the higher the specific basal respiration. Geoderma 355, 113911. https://doi.org/10.1016/j.geoderma.2019.113911
Savitzky, Abraham., Golay, M.J.E., 1964. Smoothing and Differentiation of Data by Simplified Least Squares Procedures. Anal. Chem. 36, 1627–1639. https://doi.org/10.1021/ac60214a047
Scheffer, M., Carpenter, S., Foley, J.A., Folke, C., Walker, B., 2001. Catastrophic shifts in ecosystems. Nature 413, 591–596. https://doi.org/10.1038/35098000
Scheffer, M., Carpenter, S.R., 2003. Catastrophic regime shifts in ecosystems: linking theory to observation. Trends in Ecology & Evolution 18, 648–656. https://doi.org/10.1016/j.tree.2003.09.002
Schellekens, J., Bindler, R., Martínez-Cortizas, A., McClymont, E.L., Abbott, G.D., Biester, H., Pontevedra-Pombal, X., Buurman, P., 2015a. Preferential degradation of polyphenols from Sphagnum – 4-Isopropenylphenol as a proxy for past hydrological conditions in Sphagnum-dominated peat. Geochimica et Cosmochimica Acta 150, 74–89. https://doi.org/10.1016/j.gca.2014.12.003

Schellekens, J., Bradley, J.A., Kuyper, T.W., Fraga, I., Pontevedra-Pombal, X., Vidal-Torrado, P., Abbott, G.D., Buurman, P., 2015b. The use of plant-specific pyrolysis products as biomarkers in peat deposits. Quaternary Science Reviews 123, 254–264. https://doi.org/10.1016/j.quascirev.2015.06.028
Schellekens, J., Buurman, P., 2011. *n*-Alkane distributions as palaeoclimatic proxies in ombrotrophic peat: The role of decomposition and dominant vegetation. Geoderma 164, 112–121. https://doi.org/10.1016/j.geoderma.2011.05.012
Schellekens, J., Buurman, P., Kuyper, T.W., 2012. Source and transformations of lignin in Carex-dominated peat. Soil Biology and Biochemistry 53, 32–42.
Schellekens, J., Buurman, P., Pontevedra-Pombal, X., 2009. Selecting parameters for the environmental interpretation of peat molecular chemistry – A pyrolysis-GC/MS study. Organic Geochemistry 40, 678–691. https://doi.org/10.1016/j.orggeochem.2009.03.006
Schellekens, J., Horák-Terra, I., Buurman, P., Silva, A.C., Vidal-Torrado, P., 2014. Holocene vegetation and fire dynamics in central-eastern Brazil: Molecular records from the Pau de Fruta peatland. Organic Geochemistry 77, 32–42. https://doi.org/10.1016/j.orggeochem.2014.08.011
Schimel, J.P., Weintraub, M.N., 2003. The implications of exoenzyme activity on microbial carbon and nitrogen limitation in soil: a theoretical model. Soil Biology and Biochemistry 35, 549–563. https://doi.org/10.1016/S0038-0717(03)00015-4
Schmid, R., Heuckeroth, S., Korf, A., Smirnov, A., Myers, O., Dyrlund, T.S., Bushuiev, R., Murray, K.J., Hoffmann, N., Lu, M., Sarvepalli, A., Zhang, Z., Fleischauer, M., Dührkop, K., Wesner, M., Hoogstra, S.J., Rudt, E., Mokshyna, O., Brungs, C., Ponomarov, K., Mutabdžija, L., Damiani, T., Pudney, C.J., Earll, M., Helmer, P.O., Fallon, T.R., Schulze, T., Rivas-Ubach, A., Bilbao, A., Richter, H., Nothias, L.-F., Wang, M., Orešič, M., Weng, J.-K., Böcker, S., Jeibmann, A., Hayen, H., Karst, U., Dorrestein, P.C., Petras, D., Du, X., Pluskal, T., 2023. Integrative analysis of multimodal mass spectrometry data in MZmine 3. Nat Biotechnol 41, 447–449. https://doi.org/10.1038/s41587-023-01690-2
Schmidt, M.W.I., Torn, M.S., Abiven, S., Dittmar, T., Guggenberger, G., Janssens, I.A., Kleber, M., Kögel-Knabner, I., Lehmann, J., Manning, D.A.C., Nannipieri, P., Rasse, D.P., Weiner, S., Trumbore, S.E., 2011. Persistence of soil organic matter as an ecosystem property. Nature 478, 49–56. https://doi.org/10.1038/nature10386
Senande-Rivera, M., Insua-Costa, D., Miguez-Macho, G., 2022. Spatial and temporal expansion of global wildland fire activity in response to climate change. Nat Commun 13, 1208. https://doi.org/10.1038/s41467-022-28835-2
Seniczak, A., Seniczak, S., Iturrondobeitia, J.C., Gwiazdowicz, D.J., Waldon-Rudzionek, B., Flatberg, K.I., Bolger, T., 2022. Mites (Oribatida and Mesostigmata) and vegetation as complementary bioindicators in peatlands. Science of The Total Environment 851, 158335. https://doi.org/10.1016/j.scitotenv.2022.158335
Shen, L., Peng, S., Zhang, Z., Tong, C., Lin, J., Li, Y., Zhong, H., Ma, S., Zhuang, M., Gauci, V., 2025. The large role of declining atmospheric sulfate deposition and rising CO2 concentrations in stimulating future wetland CH4 emissions. Science Advances 11, eadn1056. https://doi.org/10.1126/sciadv.adn1056
Shipley, B., 2013. The AIC model selection method applied to path analytic models compared using a d-separation test. Ecology 94, 560–564. https://doi.org/10.1890/12-0976.1
Sinclair, A.L., Graham, L.L.B., Putra, E.I., Saharjo, B.H., Applegate, G., Grover, S.P., Cochrane, M.A., 2020. Effects of distance from canal and degradation history on

peat bulk density in a degraded tropical peatland. Science of The Total Environment 699, 134199. https://doi.org/10.1016/j.scitotenv.2019.134199
Singh, N., Abiven, S., Torn, M.S., Schmidt, M.W.I., 2012. Fire-derived organic carbon in soil turns over on a centennial scale. Biogeosciences 9, 2847–2857. https://doi.org/10.5194/bg-9-2847-2012
Smeds, J., Ehnvall, B., Liu, T., Bertilsson, S., Björn, E., Nilsson, M.B., Bishop, K., Skyllberg, U., Öquist, M., 2025. Effect of Restoration on Physical and Chemical Peat Properties in Previously Drained Boreal Peatlands. Ecosystems 28, 45. https://doi.org/10.1007/s10021-025-00991-8
Smidt, E., Meissl, K., 2007. The applicability of Fourier transform infrared (FT-IR) spectroscopy in waste management. Waste Management 27, 268–276. https://doi.org/10.1016/j.wasman.2006.01.016
Smirnov, A., Jia, W., Walker, D.I., Jones, D.P., Du, X., 2018. ADAP-GC 3.2: Graphical Software Tool for Efficient Spectral Deconvolution of Gas Chromatography–High-Resolution Mass Spectrometry Metabolomics Data. J. Proteome Res. 17, 470–478. https://doi.org/10.1021/acs.jproteome.7b00633
Smolders, A.J.P., Lucassen, E.C.H.E.T., Bobbink, R., Roelofs, J.G.M., Lamers, L.P.M., 2010. How nitrate leaching from agricultural lands provokes phosphate eutrophication in groundwater fed wetlands: the sulphur bridge. Biogeochemistry 98, 1–7. https://doi.org/10.1007/s10533-009-9387-8
Smolders, A.J.P., Verstijnen, Y.J.M., Diggelen, J.M.H. van, Poelen, M.D.M., Lucassen, E.C.H.E.T., Dijk, G. van, 2024. Zwavelland. Sulfaat als obstakel voor het bereiken van de KRW-doelen. https://www.b-ware.eu/sites/default/files/publicaties/Landschap%202024-2-Zwavelland%2065-72.pdf.
Soriano-Disla, J.M., Janik, L.J., Viscarra Rossel, R.A., Macdonald, L.M., McLaughlin, M.J., 2014. The Performance of Visible, Near-, and Mid-Infrared Reflectance Spectroscopy for Prediction of Soil Physical, Chemical, and Biological Properties. Applied Spectroscopy Reviews 49, 139–186. https://doi.org/10.1080/05704928.2013.811081
Straková, P., Niemi, R.M., Freeman, C., Peltoniemi, K., Toberman, H., Heiskanen, I., Fritze, H., Laiho, R., 2011. Litter type affects the activity of aerobic decomposers in a boreal peatland more than site nutrient and water table regimes. Biogeosciences 8, 2741–2755. https://doi.org/10.5194/bg-8-2741-2011
Stricker, C.A., Drexler, J.Z., Thorn, K.A., Duberstein, J.A., Rossman, S., 2019. Carbon Chemistry of Intact Versus Chronically Drained Peatlands in the Southeastern USA. Journal of Geophysical Research: Biogeosciences 124, 2751–2767. https://doi.org/10.1029/2019JG005079
Swenson, M.M., Regan, S., Bremmers, D.T.H., Lawless, J., Saunders, M., Gill, L.W., 2019. Carbon balance of a restored and cutover raised bog: implications for restoration and comparison to global trends. Biogeosciences 16, 713–731. https://doi.org/10.5194/bg-16-713-2019
Swinnen, W., Ottoy, S., Vancampenhout, K., Verstraeten, G., 2023. Peat in Flemish soil and subsurface in relation to climate and above- and underground use of space.
Tahmasbian, I., Xu, Z., Nguyen, T.T.N., Che, R., Omidvar, N., Lambert, G., Bai, S.H., 2019. Short-term carbon and nitrogen dynamics in soil, litterfall and canopy of a suburban native forest subjected to prescribed burning in subtropical Australia. J Soils Sediments 19, 3969–3981. https://doi.org/10.1007/s11368-019-02430-3
Tahvanainen, T., 2011. Abrupt ombrotrophication of a boreal aapa mire triggered by hydrological disturbance in the catchment. Journal of Ecology 99, 404–415. https://doi.org/10.1111/j.1365-2745.2010.01778.x

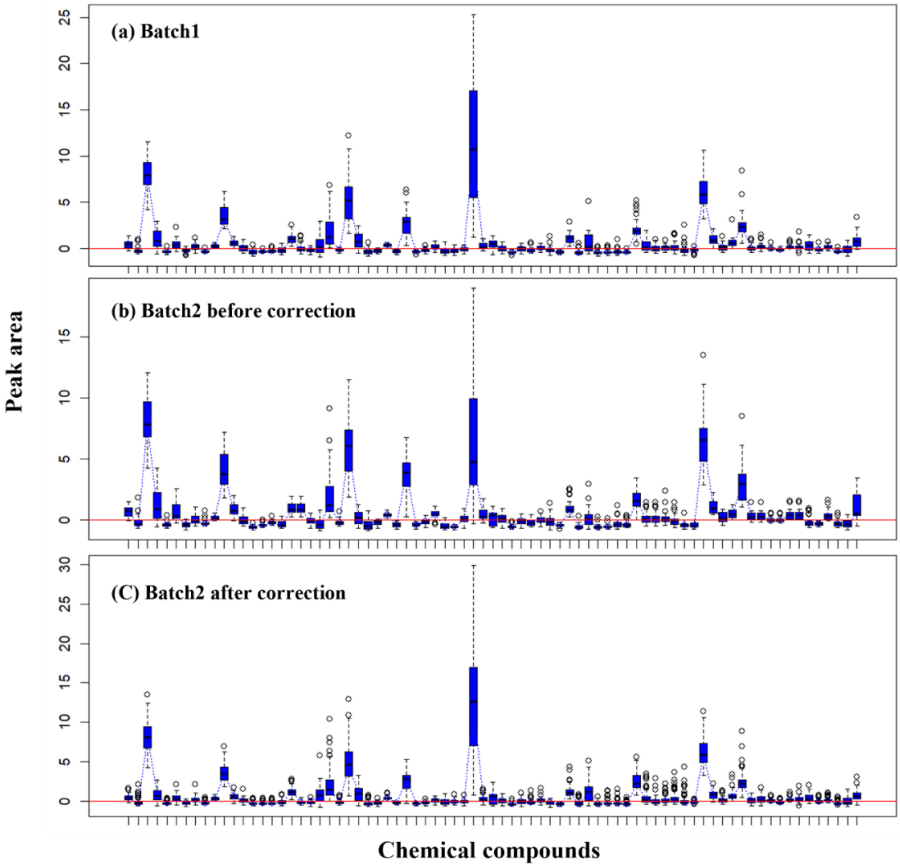
Tanneberger, F., Moen, A., Barthelmes, A., Lewis, E., Miles, L., Sirin, A., Tegetmeyer, C., Joosten, H., 2021. Mires in Europe—Regional Diversity, Condition and Protection. Diversity 13, 381. https://doi.org/10.3390/d13080381
Teickner, H., Knorr, K.-H., 2022. Improving models to predict holocellulose and Klason lignin contents for peat soil organic matter with mid-infrared spectra. SOIL 8, 699–715. https://doi.org/10.5194/soil-8-699-2022
Temmink, R.J.M., Delory, B.M., Rietkerk, M., Smolders, A.J.P., Lamers, L.P.M., Malhotra, A., Rochefort, L., Granath, G., Couwenberg, J., Koren, G., Robroek, B.J.M., 2026. Fostering Peat Moss Feedbacks to Accelerate Peatland Restoration. Global Change Biology 32, e70788. https://doi.org/10.1111/gcb.70788
Temmink, R.J.M., Lamers, L.P.M., Angelini, C., Bouma, T.J., Fritz, C., van de Koppel, J., Lexmond, R., Rietkerk, M., Silliman, B.R., Joosten, H., van der Heide, T., 2022. Recovering wetland biogeomorphic feedbacks to restore the world's biotic carbon hotspots. Science 376, eabn1479. https://doi.org/10.1126/science.abn1479
Tersago, R., Van Eupen, C., Meersmans, J., Aernouts, B., Truyers, E., Verstraeten, G., Desie, E., Vancampenhout, K., 2025. Spatial Variation in Carbon Effluxes Mediated by Grazing–Soil Interactions in a Semi-Natural Floodplain Grassland of North-Eastern Belgium. Soil Use and Management 41, e70159. https://doi.org/10.1111/sum.70159
Turetsky, M.R., Donahue, W.F., Benscoter, B.W., 2011. Experimental drying intensifies burning and carbon losses in a northern peatland. Nat Commun 2, 514. https://doi.org/10.1038/ncomms1523
Turner, R.E., 2011. Beneath the Salt Marsh Canopy: Loss of Soil Strength with Increasing Nutrient Loads. Estuaries and Coasts 34, 1084–1093. https://doi.org/10.1007/s12237-010-9341-y
Upton, A., Vane, C.H., Girkin, N., Turner, B.L., Sjögersten, S., 2018. Does litter input determine carbon storage and peat organic chemistry in tropical peatlands? Geoderma 326, 76–87. https://doi.org/10.1016/j.geoderma.2018.03.030
Urbanová, Z., Bárta, J., 2016. Effects of long-term drainage on microbial community composition vary between peatland types. Soil Biology and Biochemistry 92, 16–26. https://doi.org/10.1016/j.soilbio.2015.09.017
Urbanová, Z., Straková, P., Kaštovská, E., 2018. Response of peat biogeochemistry and soil organic matter quality to rewetting in bogs and spruce swamp forests. European Journal of Soil Biology 85, 12–22. https://doi.org/10.1016/j.ejsobi.2017.12.004
Väliranta, M., Salojärvi, N., Vuorsalo, A., Juutinen, S., Korhola, A., Luoto, M., Tuittila, E.-S., 2017. Holocene fen–bog transitions, current status in Finland and future perspectives. The Holocene 27, 752–764. https://doi.org/10.1177/0959683616670471
van Dijk, G., Wolters, J., Fritz, C., de Mars, H., van Duinen, G.J., Ettwig, K.F., Straathof, N., Grootjans, A.P., Smolders, A.J.P., 2019. Effects of Groundwater Nitrate and Sulphate Enrichment on Groundwater-Fed Mires: a Case Study. Water Air Soil Pollut 230, 122. https://doi.org/10.1007/s11270-019-4156-3
Van Meerbeek, K., Jucker, T., Svenning, J.-C., 2021. Unifying the concepts of stability and resilience in ecology. Journal of Ecology 109, 3114–3132. https://doi.org/10.1111/1365-2745.13651
Vancampenhout, K., Schellekens, J., Slaets, J., Hatté, C., Buurman, P., 2016. Fossil redox-conditions influence organic matter composition in loess paleosols. Quaternary International, Paleosols, polygenetic soils and soil chronosequences as archives

of landscape evolution 418, 105–115. https://doi.org/10.1016/j.quaint.2015.11.057
Vancampenhout, K., Wouters, K., De Vos, B., Buurman, P., Swennen, R., Deckers, J., 2009. Differences in chemical composition of soil organic matter in natural ecosystems from different climatic regions – A pyrolysis–GC/MS study. Soil Biology and Biochemistry 41, 568–579. https://doi.org/10.1016/j.soilbio.2008.12.023
Verbeke, B.A., Lamit, L.J., Lilleskov, E.A., Hodgkins, S.B., Basiliko, N., Kane, E.S., Andersen, R., Artz, R.R.E., Benavides, J.C., Benscoter, B.W., Borken, W., Bragazza, L., Brandt, S.M., Bräuer, S.L., Carson, M.A., Charman, D., Chen, X., Clarkson, B.R., Cobb, A.R., Convey, P., Pasquel, J. del Á., Enriquez, A.S., Griffiths, H., Grover, S.P., Harvey, C.F., Harris, L.I., Hazard, C., Hodgson, D., Hoyt, A.M., Hribljan, J., Jauhiainen, J., Juutinen, S., Knorr, K.-H., Kolka, R.K., Könönen, M., Larmola, T., McCalley, C.K., McLaughlin, J., Moore, T.R., Mykytczuk, N., Normand, A.E., Rich, V., Roulet, N., Royles, J., Rutherford, J., Smith, D.S., Svenning, M.M., Tedersoo, L., Thu, P.Q., Trettin, C.C., Tuittila, E.-S., Urbanová, Z., Varner, R.K., Wang, M., Wang, Z., Warren, M., Wiedermann, M.M., Williams, S., Yavitt, J.B., Yu, Z.-G., Yu, Z., Chanton, J.P., 2022. Latitude, Elevation, and Mean Annual Temperature Predict Peat Organic Matter Chemistry at a Global Scale. Global Biogeochemical Cycles 36, e2021GB007057. https://doi.org/10.1029/2021GB007057
Vetrita, Y., Diwyacitta, K., Sukarno, K.M., Albar, I., Usman, A.B., Ritonga, R.P., Santoso, I., Lestari, A.I., Kartika, T., Novresiandi, D.A., Prasasti, I., Ulfa, K., Novita, N., Siwi, S.E., Augusto, S., Prakoso, E.T., Rahmi, K.I.N., Nugroho, U.C., Widodo, J., Cochrane, M.A., 2025. Evaluating the capabilities of high-resolution PlanetScope and Sentinel-2 images for mapping burned area and vegetation regrowth in Indonesia's savannas. International Journal of Remote Sensing 46, 6803–6825. https://doi.org/10.1080/01431161.2025.2546154
Vile, M.A., Novák, M., 2006. Sulfur Cycling in Boreal Peatlands: from Acid Rain to Global Climate Change, in: Wieder, R.K., Vitt, D.H. (Eds.), Boreal Peatland Ecosystems. Springer, Berlin, Heidelberg, pp. 259–287. https://doi.org/10.1007/978-3-540-31913-9_12
Vindušková, O., Deckmyn, G., Reynaert, S., Vancampenhout, K., Schlüter, S., Frouz, J., De Boeck, H., Portillo-Estrada, M., Verbruggen, E., Asard, H., Beemster, G.T.S., Nijs, I., 2025. More persistent precipitation regimes induce soil degradation. Geoderma 455, 117230. https://doi.org/10.1016/j.geoderma.2025.117230
Vogel, H.-J., Bartke, S., Daedlow, K., Helming, K., Kögel-Knabner, I., Lang, B., Rabot, E., Russell, D., Stößel, B., Weller, U., Wiesmeier, M., Wollschläger, U., 2018. A systemic approach for modeling soil functions. SOIL 4, 83–92. https://doi.org/10.5194/soil-4-83-2018
Volkova, L., Krisnawati, H., Qirom, M.A., Adinugroho, W.C., Imanuddin, R., Hutapea, F.J., McCarthy, M.A., Di Stefano, J., Weston, C.J., 2023. Fire and tree species diversity in tropical peat swamp forests. For. Ecol. Manage. 529, 120704. https://doi.org/10.1016/j.foreco.2022.120704
Wang, H., Maestre, F.T., Lu, N., Zhao, G., Zhang, Y., Asensio, S., Bramble, D.S.E., Chen, W., Dippold, M.A., Eldridge, D.J., Gaitán, J.J., García-Gómez, M., Gozalo, B., Gross, N., Guirado, E., Le Bagousse-Pinguet, Y., Martínez-Valderrama, J., Mendoza, B.J., Ochoa, V., Plaza, C., Saiz, H., Schrumpf, M., Sierra, C.A., Tangarife-Escobar, A., Valencia, E., von Fromm, S.F., Wang, C., Wang, K., Wang, Y., Zaehle, S., Fu, B., Trumbore, S., Huang, J., 2026. Persistence and

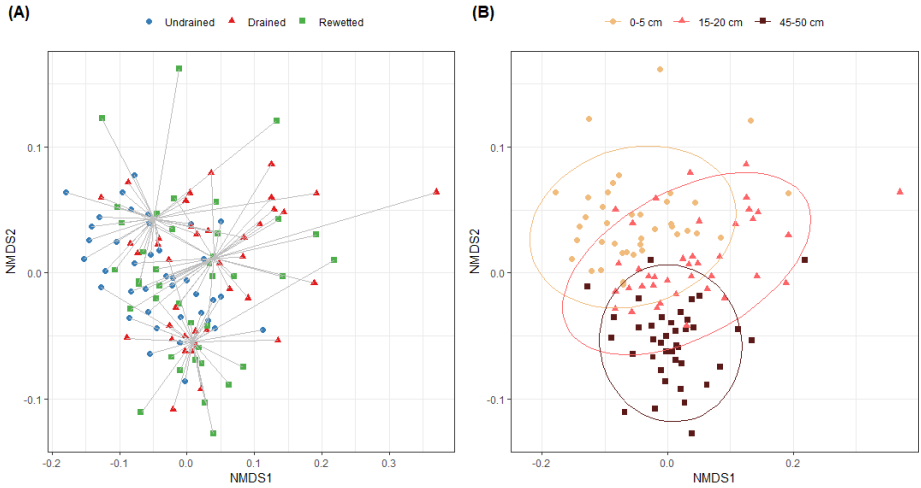
turnover of soil organic carbon in global drylands. Nat Commun 17, 3565. https://doi.org/10.1038/s41467-026-70623-9
Wang, L., Cheng, Y., Lamb, D., Dharmarajan, R., Chadalavada, S., Naidu, R., 2019. Application of infrared spectrum for rapid classification of dominant petroleum hydrocarbon fractions for contaminated site assessment. Spectrochimica Acta Part A: Molecular and Biomolecular Spectroscopy 207, 183–188. https://doi.org/10.1016/j.saa.2018.09.024
White, L., O'Connor, N.E., Yang, Q., Emmerson, M.C., Donohue, I., 2020. Individual species provide multifaceted contributions to the stability of ecosystems. Nat Ecol Evol 4, 1594–1601. https://doi.org/10.1038/s41559-020-01315-w
Whitehead, S., Weald, H., Baines, D., 2021. Post-burning responses by vegetation on blanket bog peatland sites on a Scottish grouse moor. Ecological Indicators 123, 107336. https://doi.org/10.1016/j.ecolind.2021.107336
Wilkinson, S.L., Andersen, R., Moore, P.A., Davidson, S.J., Granath, G., Waddington, J.M., 2023. Wildfire and degradation accelerate northern peatland carbon release. Nat. Clim. Chang. 13, 456–461. https://doi.org/10.1038/s41558-023-01657-w
Xu, J., Morris, P.J., Liu, J., Holden, J., 2018. PEATMAP: Refining estimates of global peatland distribution based on a meta-analysis. CATENA 160, 134–140. https://doi.org/10.1016/j.catena.2017.09.010
Xu, X., Lu, K., Wang, Z., Wang, M., Wang, S., 2021. Effects of drainage on dissolved organic carbon (DOC) characteristics of surface water from a mountain peatland. Science of The Total Environment 789, 147848. https://doi.org/10.1016/j.scitotenv.2021.147848
Xue, Z., Li, R., Jiang, M., Zou, Y., Wu, H., Lyu, X., Wang, Y., Tian, E., Zhang, R., 2025. Climate–human interactions influence widespread peatland subsidence and soil carbon stock vulnerability in China. Commun Earth Environ 6, 946. https://doi.org/10.1038/s43247-025-02896-9
Yang, Y., Geng, J., Cheng, S., Fang, H., Guo, Y., Li, Y., Zhou, Y., Shi, F., Vancampenhout, K., 2023. Linking soil microbial community to the chemical composition of dissolved organic matter in a boreal forest during freeze–thaw cycles. Geoderma 431, 116359. https://doi.org/10.1016/j.geoderma.2023.116359
Young, I.M., Crawford, J.W., 2004. Interactions and Self-Organization in the Soil-Microbe Complex. Science 304, 1634–1637. https://doi.org/10.1126/science.1097394
Yu, Z., Loisel, J., Brosseau, D.P., Beilman, D.W., Hunt, S.J., 2010. Global peatland dynamics since the Last Glacial Maximum. Geophysical Research Letters 37. https://doi.org/10.1029/2010GL043584
Yu, Z.C., 2012. Northern peatland carbon stocks and dynamics: a review. Biogeosciences 9, 4071. http://dx.doi.org/10.5194/bg-9-4071-2012
Zak, D., McInnes, R.J., 2022. A call for refining the peatland restoration strategy in Europe. Journal of Applied Ecology 59, 2698–2704. https://doi.org/10.1111/1365-2664.14261
Zeh, L., Igel, M.T., Schellekens, J., Limpens, J., Bragazza, L., Kalbitz, K., 2020. Vascular plants affect properties and decomposition of moss-dominated peat, particularly at elevated temperatures. Biogeosciences 17, 4797–4813. https://doi.org/10.5194/bg-17-4797-2020
Zhang, Y., Qin, Y., Chen, Y., Lin, S., Shu, Y., Huang, X., Zhou, M., 2025. Impact of underground wildfire on plant roots in peat soil. CATENA 259, 109371. https://doi.org/10.1016/j.catena.2025.109371

8 Appendix

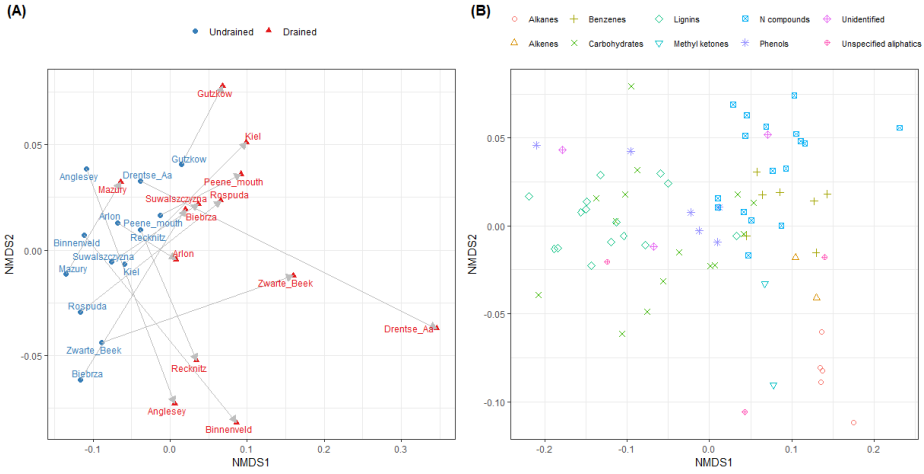
Appendix A



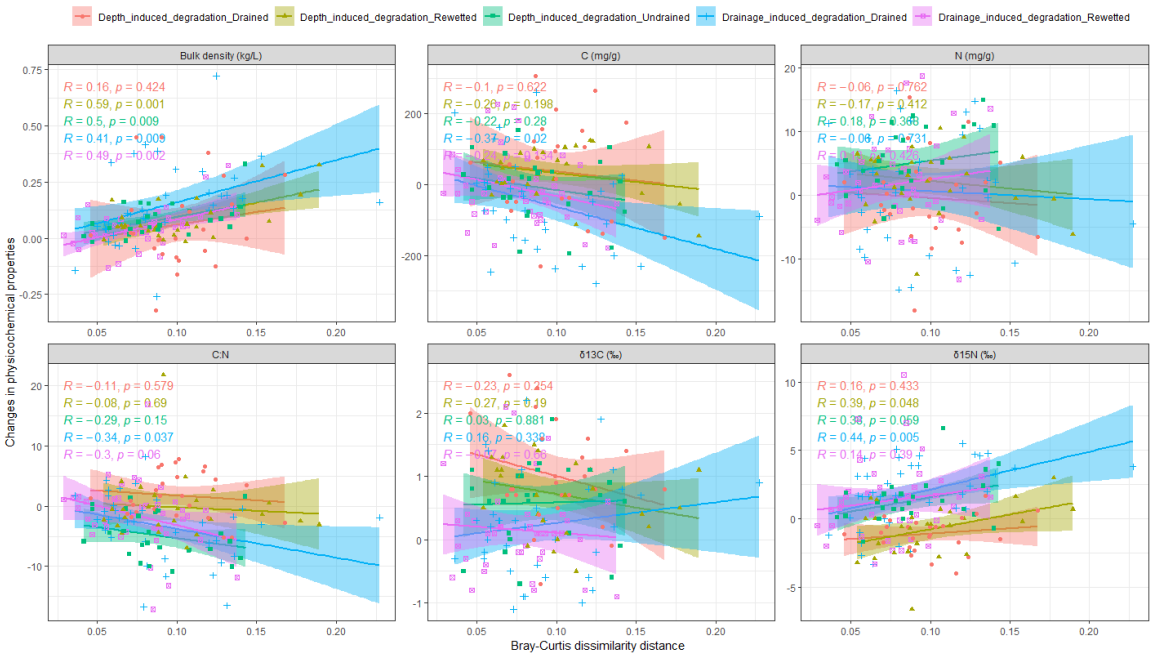
Supplementary Fig. 2.1. Batch effect correction to align molecular composition data from two separate analytical batches. Panel (A, B) represents the relative abundance of the 75 selected pyrolysates from peat samples analyzed in batch 1 and batch 2, respectively. Panel C illustrates the improved alignment of batch 2 data after batch effect correction using the Combat function from the sva package in R (Leek et al., 2012), enabling integration of both batches for consistent downstream analysis.



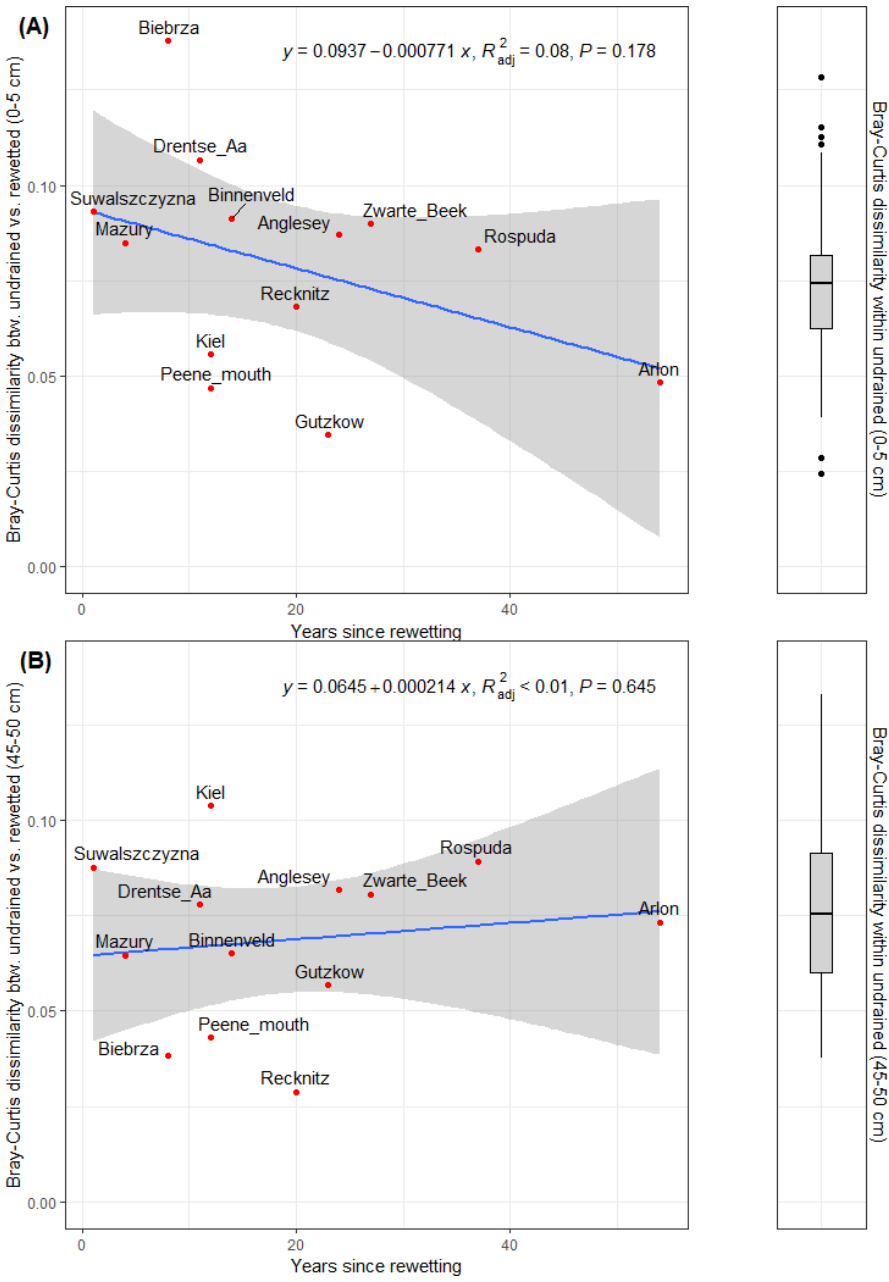
Supplementary Fig. 2.2. Nonmetric multidimensional scaling (NMDS, stress = 0.112) of soil organic matter (SOM) molecular composition across drainage stage and depth in 39 fen sites across Europe. NMDS was performed on pyrolysis-GC/MS data using Bray−Curtis dissimilarity to visualize variation in SOM molecular composition. The ordination includes three drainage stage (undrained, drained, and rewetted) and three depth layer (0−5 cm, 15−20 cm, and 45−50 cm). Panel (A) shows samples colored by drainage stage, with grey lines connecting samples to the centroid of their respective depth group. Panel (B) exhibits samples colored by depth, along with 95% confidence ellipses for each depth group. SOM molecular composition differed significantly by (A) drainage status (PERMANOVA, F=6.270, P <0.001) and (B) depth (PERMANOVA, F=16.908, P <0.001).



Supplementary Fig. 2.3. Nonmetric multidimensional scaling (NMDS) of soil organic matter (SOM) molecular composition in undrained and drained fens at 15−20 cm depth, based on Bray−Curtis dissimilarity. Panel (A) displays the ordination of paired samples from undrained and drained fens, with grey arrows indicating the directional shift in SOM molecular composition due to drainage. Panel (B) presents the results of vector fitting, where individual compound abundances are correlated with the NMDS axes from Panel A.



Supplementary Fig. 2.4. Pearson correlations between changes in peat physicochemical properties and dissimilarity (drainage- and depth-induced degradation) across drainage status. To evaluate how molecular degradation physiochemical changes, we quantified shifts in molecular composition using Bray−Curtis dissimilarity based on pyrolysis-GC/MS data. Two types of degradation were considered. Drainage-induced degradation was calculated as the dissimilarity between undrained and drained peat at corresponding depths, whereas depth-induced degradation was computed as the dissimilarity between the top (0−5 cm) and bottom (45−50 cm) layer within same treatment. Pearson's correlation coefficients (R) and significance (P) are given for each plot.



Supplementary Fig. 2.5. Time since rewetting restoration as a function of pairwise SOM molecular composition dissimilarity between undrained sites and rewetted counterparts based on Bray-Curtis dissimilarity at a depth of 0−5 cm and 45−50 cm. Blue line shows the linear relationship as predicted, its 95% confidence interval is shaded in grey. These two regression models do not show significant slopes in the figure (Ps > 0.05).

Supplementary Table 2.1. Abbreviated study site information with coordinates, region, country (BE = Belgium, NL = the Netherlands, DE = Germany, PL = Poland and UK = United Kingdom), current drainage status, vegetation type, and approximate time since rewetting. For vegetation, only plant species with > 10% cover are reported (adapted from Supplementary Table1; Emsens et al., 2020).

Site ID	Region	Country λ	Drainage status	Longitude; Latitude	Vegetation type – Dominant vascular plant and moss species	Rewetting year
1	Arlon	BE	Undrained	5.71758; 49.68723	**Fen** – *Carex appropinquata, Comarum palustre, Calliergonella cuspidata*	NA
2	Arlon	BE	Drained	5.66434; 49.65910	**Fen** – *Filipendula ulmaria, Juncus acutiflorus, Persicaria bistorta, Calliergonella cuspidata, Brachythecium spec*.	NA
3	Arlon	BE	Rewetted	5.69653; 49.67478	**Fen** – *Carex acutiformis, Sphagnum subnitens*	Gradually since 1963
4	Zwarte Beek	BE	Undrained	5.28580; 51.08014	**Fen** – *Carex rostrata, Equisetum fluviatile, Juncus acutiflorus, Lotus uliginosus, Calliergonella cuspidata, Calliergon cordifolium*	NA
5	Zwarte Beek	BE	Drained	5.27309; 51.07441	**Wet grassland** – *Anthoxanthum odoratum, Carex nigra, Holcus lanatus, Brachythecium rutabulum*	NA
6	Zwarte Beek	BE	Rewetted	5.32251; 51.09108	**Fen** – *Caltha palustris, Carex rostrata, Juncus acutiflorus*	1990
7	Binnenveld	NL	Undrained	5.57093; 52.01230	**Fen** – *Calliergonella cuspidata, Plagiomnium species, Sphagnum subnitens*	NA
8	Binnenveld	NL	Drained	5.60049; 51.99292	**Wet grassland** – *Carex acuta, Holcus lanatus, Phalaris arundinacea, Poa pratensis, Poa trivialis*	NA
9	Binnenveld	NL	Rewetted	5.58189; 52.01083	**Fen** – *Carex rostrata, Camarum palustre*	2003

10	Drentse Aa	NL	Undrained	6.66381; 53.04981	**Fen** – *Menyanthes trifoliata, Calliergonella cuspidata*	NA
11	Drentse Aa	NL	Drained	6.66665; 53.00443	**Wet grassland** – *Agrostis stolonifera, Poa trivialis, Ranunculus repens*	NA
12	Drentse Aa	NL	Rewetted	6.66862; 53.02187	**Fen** – *Carex rostrata, Calliergonella cuspidata, Fontinalis spec*.	Gradually since 1995
13	Gützkow	DE	Undrained	13.40780; 53.96960	**Fen** – *Carex appropinquata, Carex nigra, Carex panicea, Juncus subnodulosus, Calliergonella cuspidata*	NA
14	Gützkow	DE	Drained	13.43210; 53.97860	**Wet grassland** – *Carex nigra, Holcus lanatus, Phalaris arundinacea, Poa pratensis, Rhinanthus angustifolius*	NA
15	Gützkow	DE	Rewetted	13.57510; 53.80040	**Fen** – *Carex acuta, Juncus subnodulosus*	1994
16	Peene mouth	DE	Undrained	13.64870; 53.88340	**Fen** – *Agrostis stolonifera, Carex appropinquata, Carex nigra, Juncus subnodulosus, Calliergonella cuspidata, Drepanocladus aduncus*	NA
17	Peene mouth	DE	Drained	13.71730; 53.87010	**Wet grassland** – *Carex acutiformis, Juncus effusus, Scirpus sylvaticus*	NA
18	Peene mouth	DE	Rewetted	13.70720; 53.83700	**Fen** – *Caltha palustris, Carex acuta, Carex disticha, Carex nigra*	Before 2007
19	Kiel	DE	Undrained	10.34016; 54.20532	**Fen** – *Filipendula ulmaria, Calliergonella cuspidata, Rhytidiadelphus squarrosus*	NA
20	Kiel	DE	Drained	10.08809; 54.27470	**Wet grassland** – *Agrostis stolonifera, Alopecurus geniculatus, Poa trivialis, Ranunculus repens*	NA
21	Kiel	DE	Rewetted	10.02990; 54.22730	**Wet grassland** – *Ranunculus repens, Rhinanthus angustifolius, Calliergonella cuspidata, Rhytidiadelphus squarrosus*	Before 2009
22	Recknitz	DE	Undrained	12.51030; 54.18460	**Fen** – *Carex nigra, Equisetum fluviatile, Lysimachia thyrsiflora, Menyanthes trifoliata, Comarum palustre*	NA

23	Recknitz	DE	Drained	12.62869; 54.13185	**Wet grassland** – *Poa pratensis, Ranunculus repens*	NA
24	Recknitz	DE	Rewetted	12.73950; 54.10105	**Fen** – *Carex acutiformis*	Before 2007
25	Biebrza	PL	Undrained	23.32948; 53.73428	**Fen** – *Carex diandra, Menyanthes trifoliata, Hamatocaulis vernicosus*	NA
26	Biebrza	PL	Drained	23.23166; 53.75858	**Wet grassland** – *Festuca rubra, Poa trivialis, Ranunculus repens, Rumex acetosa, Brachythecium rutabulum*	NA
27	Biebrza	PL	Rewetted	23.23310; 53.75875	**Fen** – *Carex acuta, Carex nigra, Drepanocladus aduncus*	Between 2011-2014
28	Rospuda	PL	Undrained	22.95370; 53.90399	**Fen** – *Carex rostrata, Festuca rubra, Menyanthes trifoliata, Aulacomnium palustre, Hamatocaulis vernicosus, Tomentypnum nitens*	NA
29	Rospuda	PL	Drained	22.68317; 53.81010	**Wet grassland** – *Carex cespitosa, Filipendula ulmaria, Holcus lanatus*	NA
30	Rospuda	PL	Rewetted	22.69392; 53.80973	**Fen** – *Carex paniculata, Carex rostrata, Equisetum fluviatile, Calliergonella cuspidata*	Before 1983
31	Suwalszczyzna	PL	Undrained	22.82706; 54.21241	**Fen**– *Carex rostrata, Eriophorum angustifolium, Aulacomnium palustre, Calliergonella cuspidata, Drepanocladus aduncus, Helodium blandowii, Marchantia polymorpha, Plagiomnium ellipticum*	NA
32	Suwalszczyzna	PL	Drained	22.66418; 54.31710	**Wet grassland**– *Anthoxanthum odorarum, Helictotrichon pubescens, Carex cespitosa, Cirsium rivulare, Filipendula ulmaria, Geum rivale, Climacium dendroides*	NA
33	Suwalszczyzna	PL	Rewetted	22.66035; 54.32749	**Wet grassland** – *Carex acutiformis, Cirsium rivulare, Deschampsia cespitosa, Festuca rubra, Filipendula ulmaria, Galium rivale, Geum rivale, Ranunculus repens*	2016
34	Mazury	PL	Undrained	21.23354; 53.68418	**Fen** – *Menyanthes trifoliata, Calliergon giganteum, Calliergonella cuspidata, Hamatocaulis vernicosus, Plagiomnium spec.*	NA
35	Mazury	PL	Drained	21.52789; 53.77411	**Wet grassland** – *Anthoxanthum odoratum, Festuca rubra, Geum rivale, Poa trivialis, Ranunculus repens*	NA

36	Mazury	PL	Rewetted	21.52884; 53.77382	**Fen** – *Carex appropinquata, Carex rostrata, Epilobium palustre, Calliergonella cuspidata, Drepanocladus aduncus*	Before 2013
37	Anglesey	UK	Undrained	-4.26600; 53.30528	**Fen** – *Menyanthes trifoliata, Calliergon giganteum, Calliergonella cuspidata*	NA
38	Anglesey	UK	Drained	-4.30639; 53.31783	**Wet grassland** – *Carex acuta, Holcus lanatus, Juncus acutiflorus, Calliergonella cuspidata*	NA
39	Anglesey	UK	Rewetted	-4.29388; 53.32041	**Fen/Wet grassland** – *Juncus subnodulosus, Molinia caerula, Myrica gale*	between 1982-1993

Supplementary Table 2.2. Pyrolysis products and their code, compounds names, group, characteristic fragment ions and retention time (RT). Grouped according to probable origin and chemical characteristics.

Code	Group	Name	RT	m/z
Al1	Aliphatics	unspecified aliphatic	9.37	55, 69
Al2	Aliphatics	unspecified aliphatic	12.52	57, 69
Al3	Aliphatics	unspecified aliphatic	33.28	55, 83
16	Alkanes	C16 n-alkane	21.33	57, 71
24	Alkanes	C24 n-alkane	32.39	57, 71
25	Alkanes	C25 n-alkane	33.52	57, 71
29	Alkanes	C29 n-alkane	37.69	57, 71
31	Alkanes	C31 n-alkane	39.56	57, 71
11:1	Alkenes	C11 n-alkene	11.55	55, 97
26:1	Alkenes	C26 n-alkene	34.55	55, 97
B1	Benzenes	benzene	3.02	78
B2	Benzenes	toluene	4.47	91, 92
B3	Benzenes	C2 benzene	6.27	91, 106
B4	Benzenes	C2 benzene	6.35	91, 106
B5	Benzenes	styrene	6.82	78, 104
B6	Benzenes	C2 benzene	6.93	91, 106
B7	Benzenes	indene	10.21	115, 116
C1	Carbohydrates	(2H)-furan-3-one	4.52	55, 84
C2	Carbohydrates	3-furaldehyde	4.88	95, 96
C3	Carbohydrates	2-cyclopenten-1-one	5.21	67, 82
C4	Carbohydrates	2-furaldehyde	5.27	95, 96
C5	Carbohydrates	unspecified carbohydrate	6.44	55, 84
C6	Carbohydrates	2-cyclopenten-1-one, 2-methyl-	6.8	67, 82
C7	Carbohydrates	2,3-dihydro-5-methylfuran-2-one	7.13	55, 98
C8	Carbohydrates	5-methyl-2-furaldehyde	7.99	109, 110
C9	Carbohydrates	4-hydroxy-5,6-dihydro(2H)-pyran-2 one	8.64	58, 114
C10	Carbohydrates	3-hydroxy-2-methyl-2-cyclopenten· one	9.02	55, 112
C11	Carbohydrates	2-hydroxy-3-methyl-2-cyclopenten· one	9.45	55, 112
C12	Carbohydrates	3-hydroxy-2-methyl-4(H)pyran-4-o	11.29	55, 126
C13	Carbohydrates	unspecified carbohydrate	14.21	57, 73
C14	Carbohydrates	levoglucosan	18.8	60, 73

C15	Carbohydrates	unspecified carbohydrate	19.52	100
Lg1	Lignins	guaiacol	10.96	109, 124
Lg2	Lignins	4-methylguaiacol	13.25	123, 138
Lg3	Lignins	4-vinylphenol	13.7	91, 120
Lg4	Lignins	4-ethylguaiacol	15.05	137, 152
Lg5	Lignins	4-vinylguaiacol	15.69	135, 150
Lg6	Lignins	syringol	16.21	139, 154
Lg7	Lignins	4-formylguaiacol	17.04	151, 152
Lg8	Lignins	4-acetylphenol	17.85	121, 136
Lg9	Lignins	C3 guaiacol	18.28	77, 164
Lg10	Lignins	4-acetylguaiacol	18.7	151, 166
Lg11	Lignins	4-vinylsyringol	20.14	165, 180
Lg12	Lignins	C3 syringol	22.41	91, 194
Lg13	Lignins	4-acetylsyringol	22.74	181, 196
Lg14	Lignins	unspecified lignin	22.91	137, 180
Lg15	Lignins	4-(Propan-2-one) syringol	23.29	167, 210
Mk1	Methyl ketones	C19 n-methyl ketone	28.57	58, 59
Mk2	Methyl ketones	C21 n-methyl ketone	31.13	58, 59
N1	N compounds	unspecified N	3.86	80, 81
N2	N compounds	pyridine	3.92	52, 79
N3	N compounds	pyrrole	4.04	67
N4	N compounds	acetamide	4.06	59
N5	N compounds	C1 pyridine	5.18	66, 93
N6	N compounds	C1 pyrrole	5.5	80, 81
N7	N compounds	C1 pyrrole	5.71	80, 81
N8	N compounds	C1 pyridine	6.01	66, 93
N9	N compounds	benzonitrile	8.42	76, 103
N10	N compounds	unspecified N	8.94	95, 94,
N11	N compounds	benzonitrile	11.63	90, 117
N12	N compounds	3-acetamidofuran	13.6	83, 125
N13	N compounds	indole	15.1	90, 117
N14	N compounds	unspecified N	15.24	97, 139
N15	N compounds	unspecified N	18.05	94, 67
N16	N compounds	diketodipyrrole	22.45	93, 186
N17	N compounds	alkyl amide	36.08	59, 72
Ph1	Phenols	phenol	8.6	66, 94
Ph2	Phenols	C1 phenol	10.24	107, 108

Ph3	Phenols	C1 phenol	10.69	107, 108
Ph4	Phenols	C2 phenol	12.67	107, 122
Ph5	Phenols	catechol	13.39	64, 110
Ph6	Phenols	C3 phenol	16.16	133, 134
Unidentifed1	Unidentified	Unidentified	7	70
Unidentifed2	Unidentified	Unidentified	11.34	81,124
Unidentifed3	Unidentified	Unidentified	14.81	110, 98

References: Schellekens et al., 2009; Schellekens et al., 2015; Vancampenhout et al., 2016; Klein et al., 2022

Supplementary Table 2.3. Proportion of peat molecular composition as a function of drainage status (DS; undrained, rewetted, and drained) and depth (0−5 cm, 15−20 cm, and 45−50 cm).

	Unspecified aliphatic	Alkanes	Alkenes	Benzenes	Carbohydrates	Lignins	Methyl ketones	N compounds	Phenols	Unidentified
Undrained	1.3 ± 0⁋	2.4 ± 0.2 a	0.6 ± 0 a	10.6 ± 0.6 a	33.7 ± 1.6 b	18.1 ± 0.6 b	0.8 ± 0.1	13 ± 0.7 a	17.9 ± 0.6	1.5 ± 0.1 b
Drained	1.4 ± 0.1	3.8 ± 0.4 b	0.8 ± 0.1 b	14 ± 0.9 b	27.7 ± 1.6 a	15.5 ± 1.1 a	0.6 ± 0.1	17.6 ± 0.9 b	17.3 ± 0.7	1.4 ± 0.1 ab
Rewetted	1.4 ± 0.1	3.3 ± 0.3 ab	0.7 ± 0.1 ab	13.6 ± 0.8 b	28.4 ± 1.6 a	17.1 ± 0.8 ab	0.7 ± 0.1	15.7 ± 0.8 b	17.9 ± 0.7	1.3 ± 0.1 a
0-5 cm	1.4 ± 0	2.3 ± 0.2 a	0.5 ± 0 a	10.8 ± 0.7 a	38.8 ± 1.2 c	16.9 ± 0.8 b	0.3 ± 0.1 a	13 ± 0.8 a	14.1 ± 0.3 a	1.8 ± 0.1 b
15-20 cm	1.3 ± 0.1	3.6 ± 0.4 b	0.8 ± 0.1 b	14.5 ± 0.9 b	28.4 ± 1.4 b	14 ± 0.8 a	0.7 ± 0.1 b	18 ± 0.9 c	17.4 ± 0.5 b	1.2 ± 0.1 a
45-50 cm	1.4 ± 0.1	3.6 ± 0.3 b	0.8 ± 0.1 b	12.9 ± 0.7 b	22.6 ± 1.2 a	19.8 ± 0.7 c	1 ± 0.1 b	15.3 ± 0.6 b	21.5 ± 0.5 c	1.1 ± 0.1 a
DS	0.8535	0.0027	0.0036	<0.0001	<0.0001	0.0181	0.5399	<0.0001	0.5757	0.0404
Depth	0.0641	<0.0001	<0.0001	<0.0001	<0.0001	<0.0001	<0.0001	<0.0001	<0.0001	<0.0001
DS : Depth	0.5831	0.1610	0.0369	0.0105	0.2999	0.0001	0.2613	0.0095	0.4834	0.1528

⁋ Mean ± standard error

Different lowercase letters indicate significant differences between experimental treatments based on two-way ANOVA (n=13).

Supplementary Table 2.4. Correlation between ordination axes (scores) and peat physicochemical properties as paralleled to Fig.3.

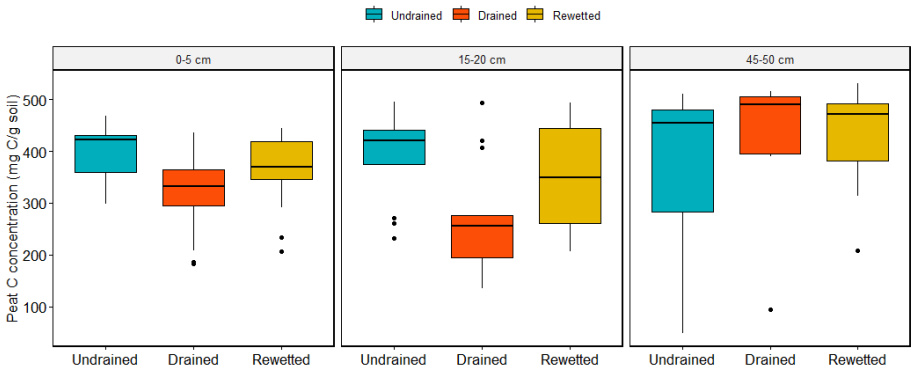
	NMDS1¶	NMDS2¶	R^2Φ	P-value
C	-0.2923	-0.4334	0.5228	0.01*
N	-0.0181	-0.1048	0.1064	0.01*
CN	-0.2956	-0.1615	0.3369	0.01*
$\delta^{13}C$	0.0478	-0.1877	0.1937	0.01*
$\delta^{15}N$	0.1249	0.0874	0.1525	0.01*
BD	0.5188	0.0660	0.5230	0.01*

¶ Pearson's correlation coefficient (r) are given between the physiochemical properties and ordination axis.

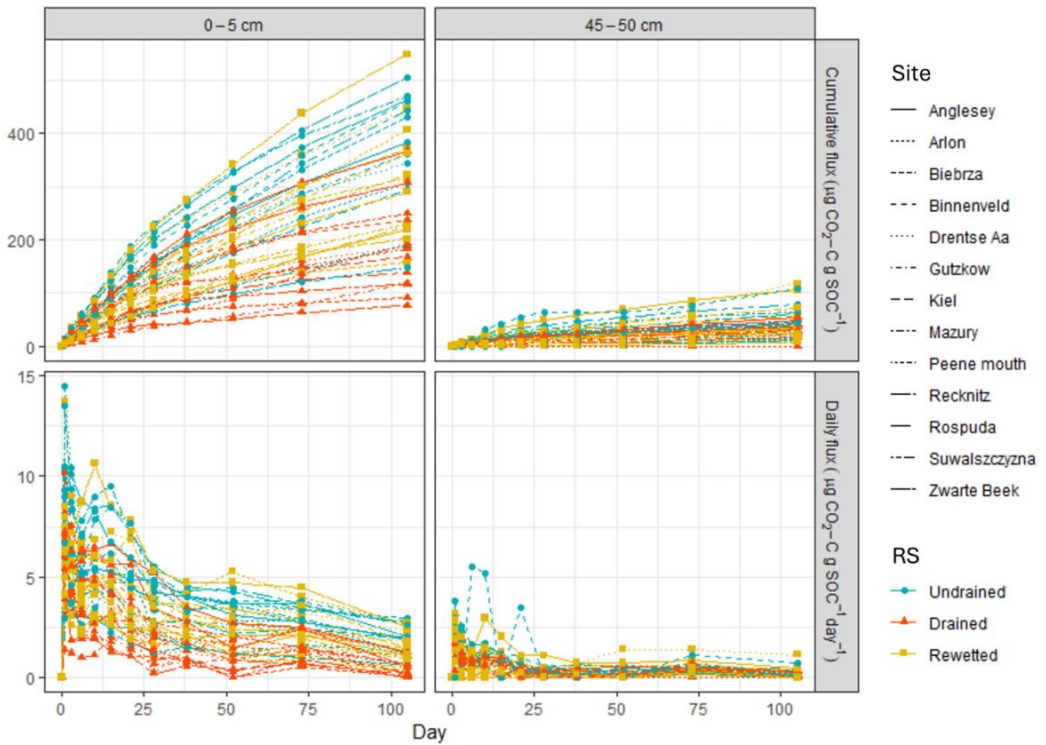
Φ Variation explained by the regression model.

Significance was tested by permutation test, P-value was adjusted by Bonferroni's method; number of permutations: 999.

Appendix B

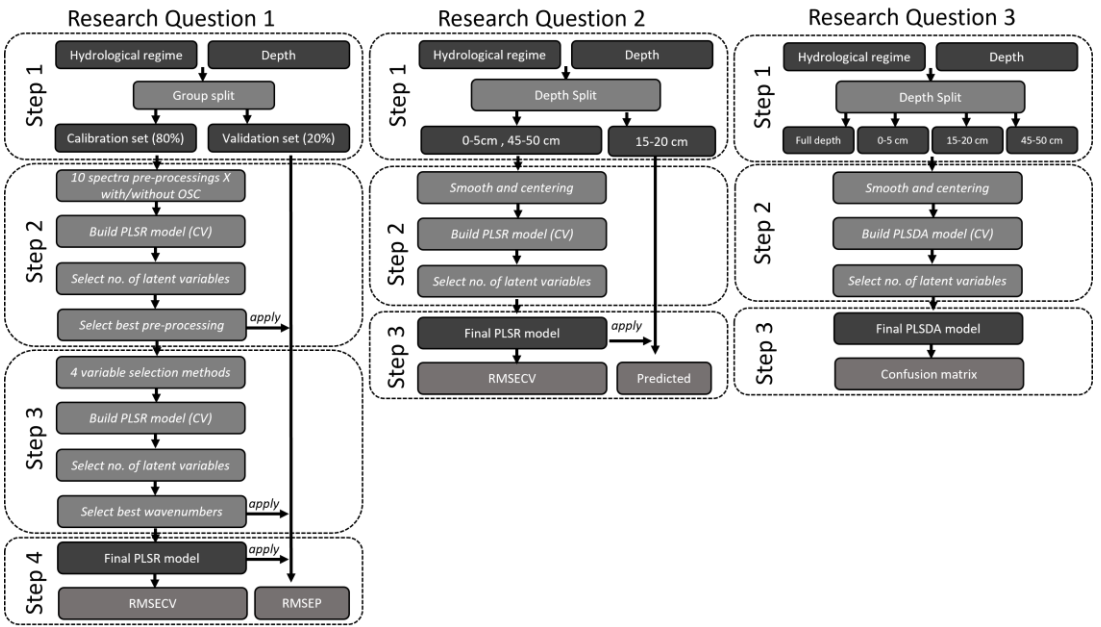


Supplementary Fig. 3.1. Peat C concentration across restoration status and depths (P <0.05).

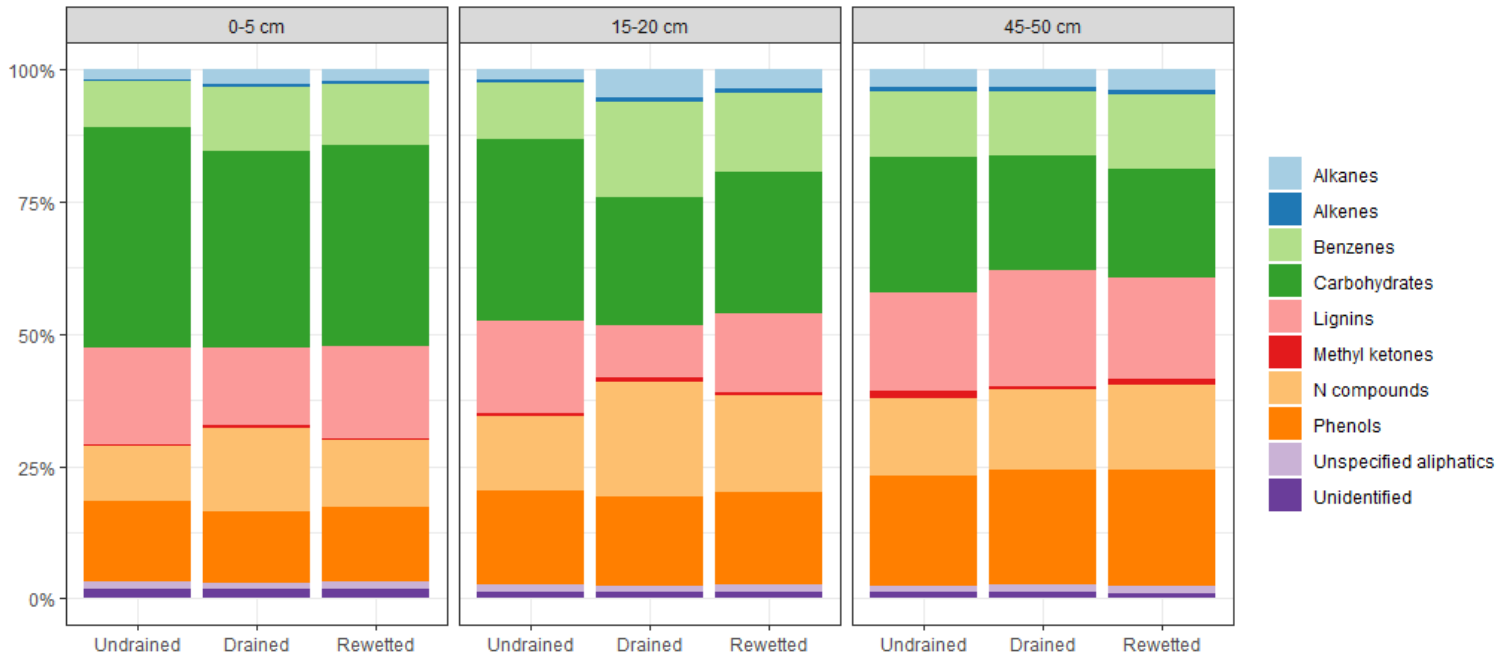


Supplementary Fig. 3.2. Cumulative and daily basal respiration per SOC across restoration status (RS; undrained, drained and rewetted) at two peat layers (0-5 cm and 45-50 cm) at the 39 sites.

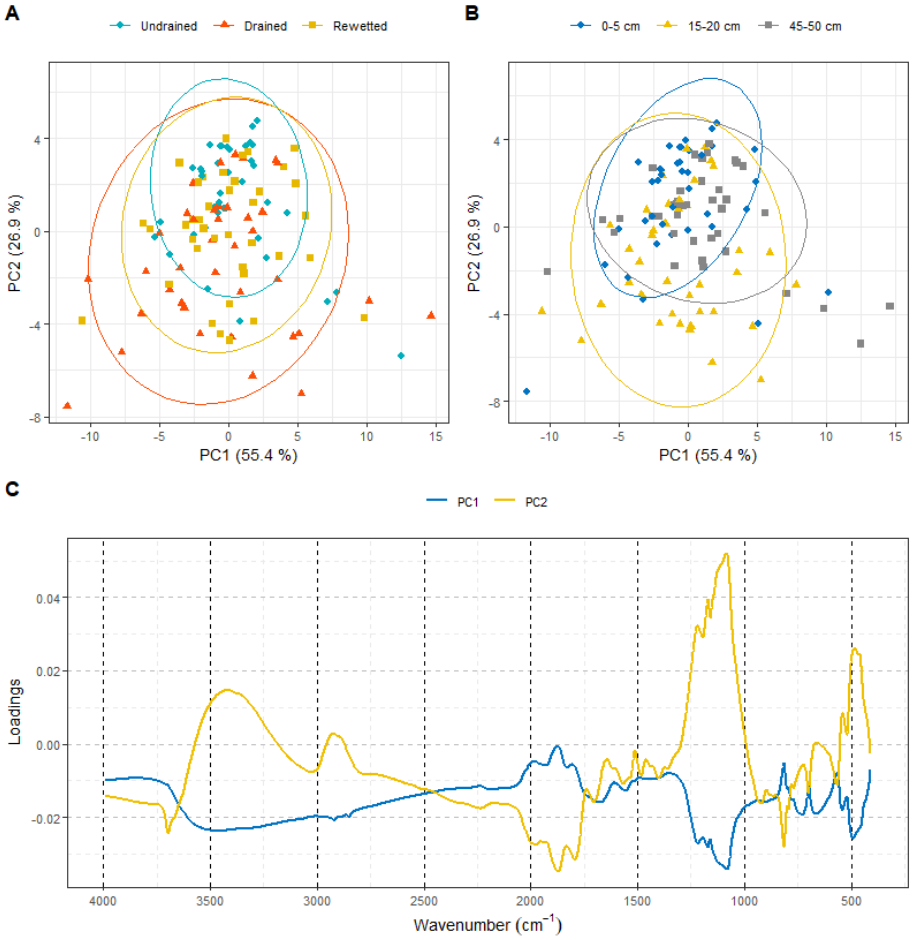
Research questions: (1) Can mid infrared (MIR) spectra reproduce the percentage of chemical groups derived from pyrolysis gas chromatography mass spectroscopy (py-GC/MS)? (2) Can MIR spectra estimate soil organic carbon (SOC) decomposability? (3) Can MIR spectra differentiate SOC variation across three restoration status?



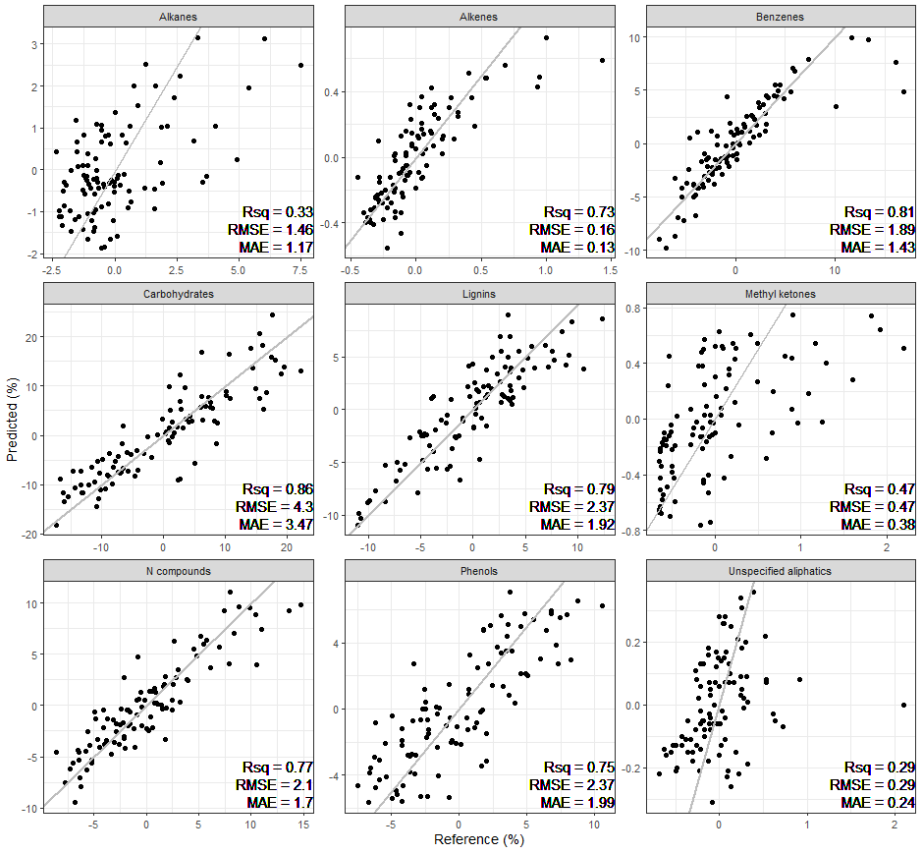
Supplementary Fig. 3.3. Schematic overview of the workflow to address our research questions, utilizing both partial least squares regression (PLSR) models and partial least squares discriminate analysis (PLS-DA) model. OSC = orthogonal signal correction, CV = cross-validation, RMSECV = root mean square error of cross-validation, RMSEP = root mean square error of prediction (Aernouts et al., 2020).



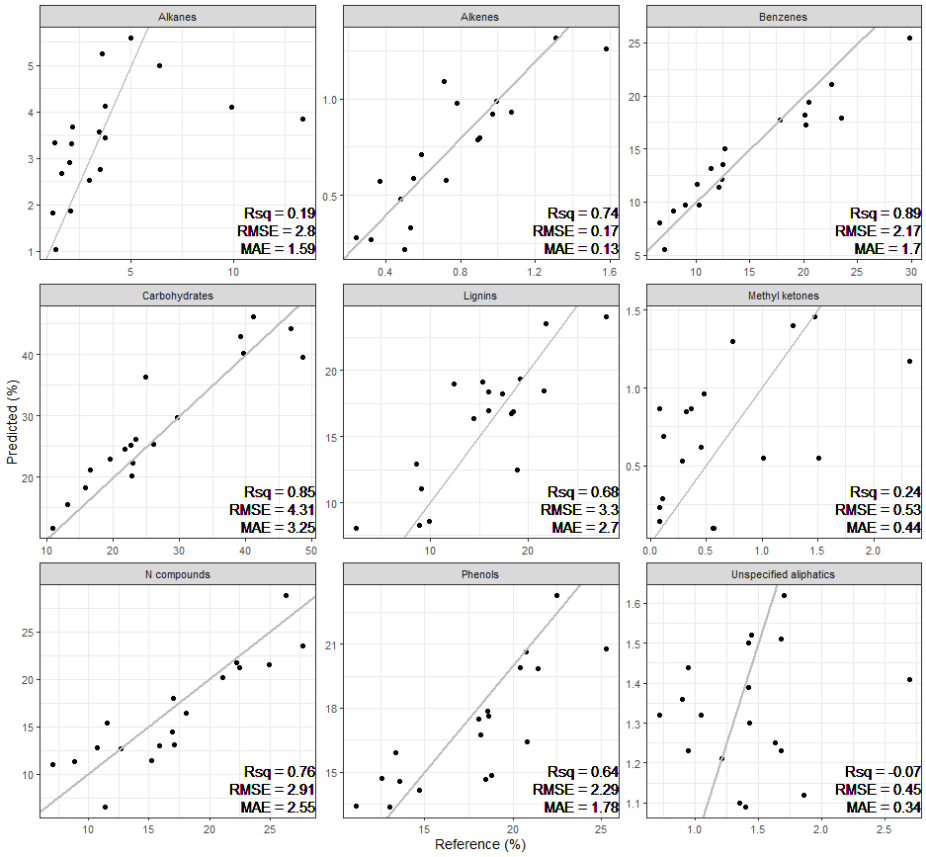
Supplementary Fig. 3.4. SOM chemical groups at three restoration status (undrained, drained, and rewetted) in three peat layers (0−5 cm, 15−20 cm, and 45−50 cm) as determined by pyrolysis GC-MS.



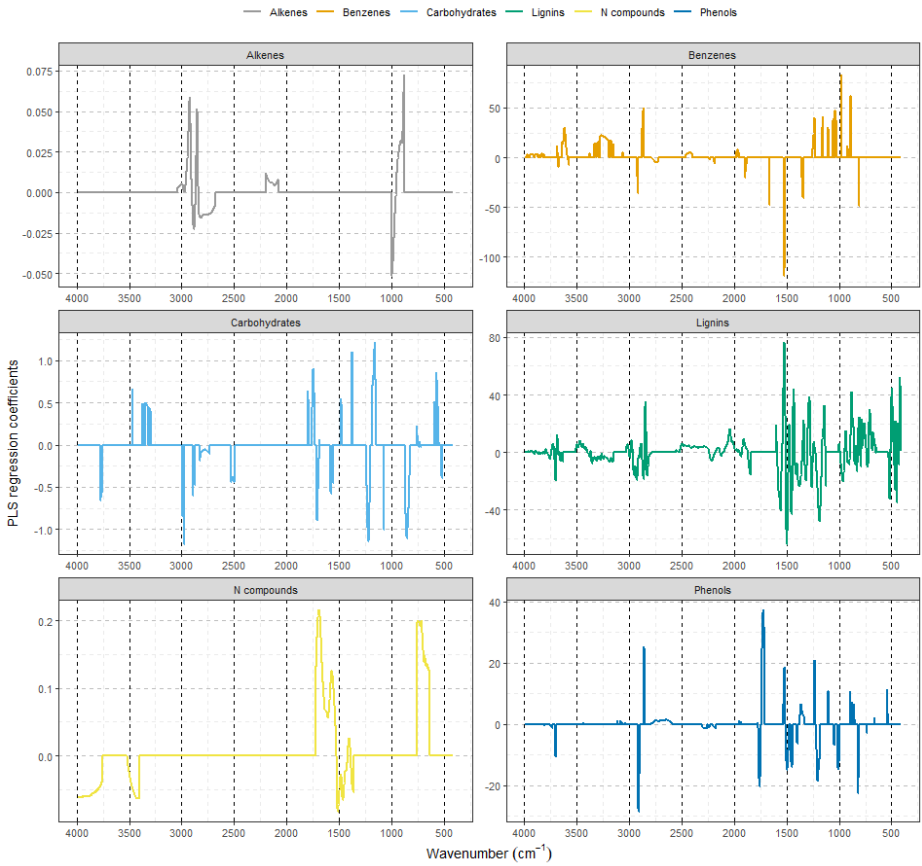
Supplementary Fig. 3.5. Scores and loadings of principal component analysis (PCA) based on mid-infrared spectra, illustrating the partitioning of 117 samples by two principal components. Scores are clustered into three levels of restoration status (A; undrained, rewetted, and drained) and depth (B; 0−5 cm, 15−20 cm, and 45−50 cm). PC loadings are shown in plot C.



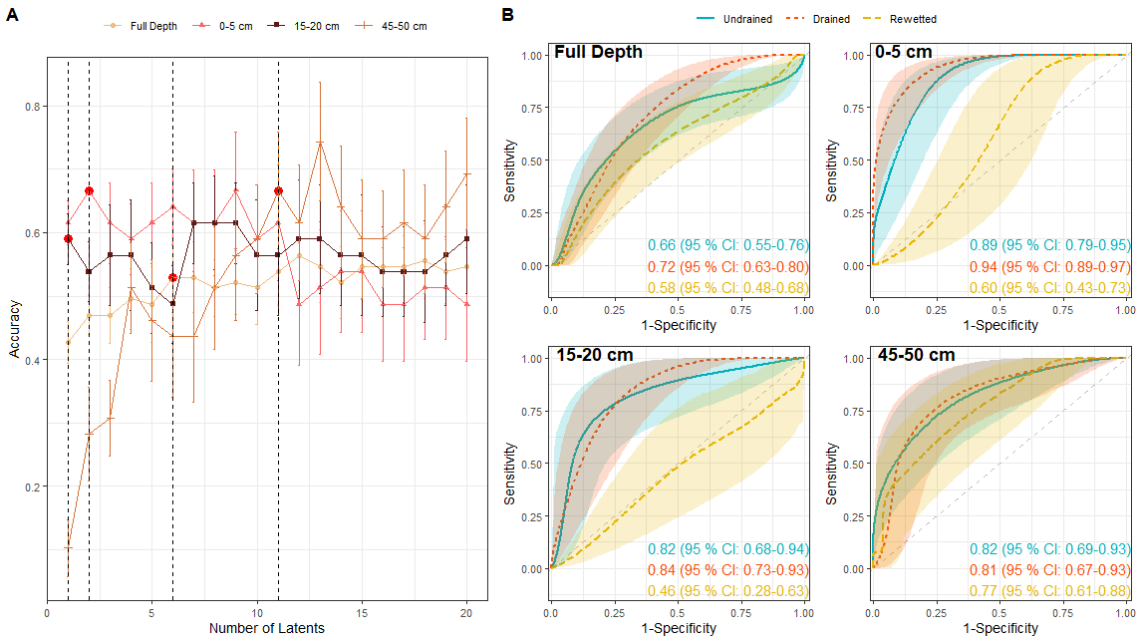
Supplementary Fig. 3.6. Cross-validation results of the 91 peat samples in the calibration set, with proportions of chemical group measured by pyrolysis GC/MS as reference. These proportions were obtained using MIR spectra in combination with partial least squares regression models.



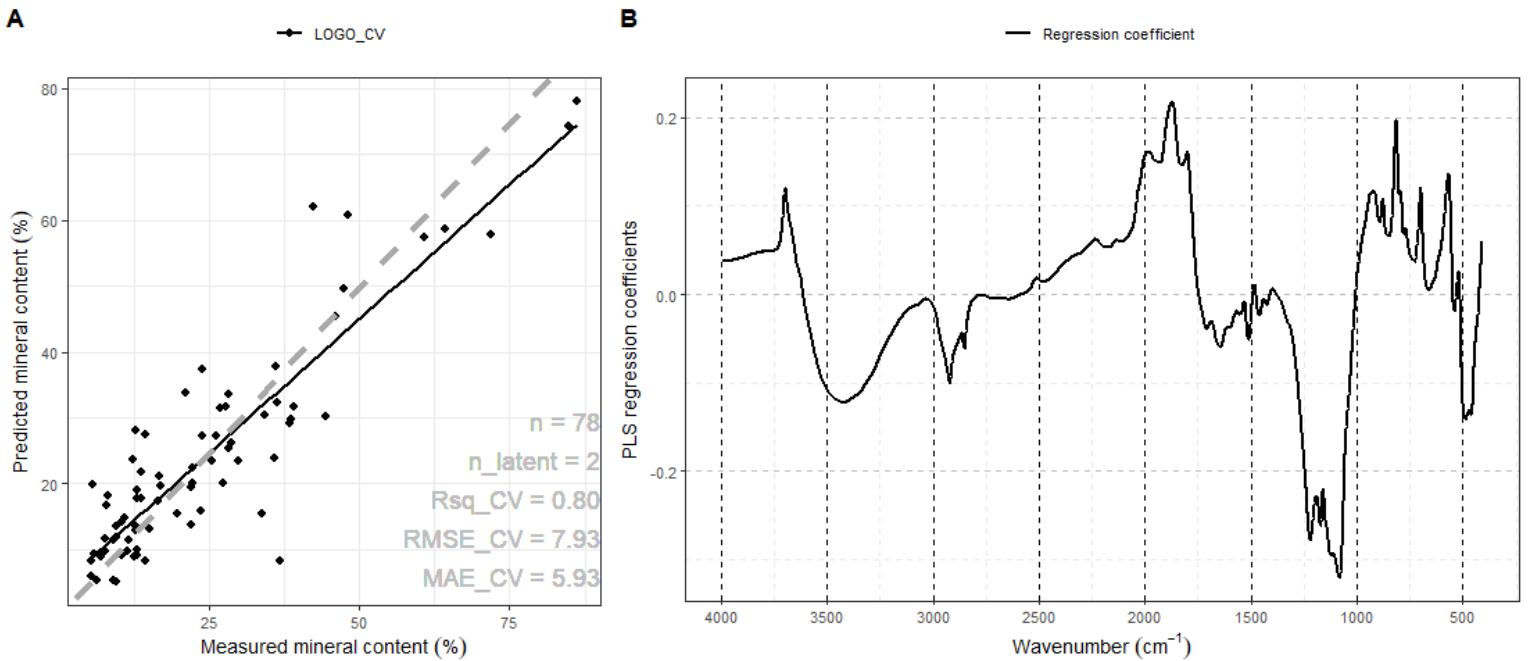
Supplementary Fig. 3.7. Validation results of the 26 peat samples in the validation set, with proportions of chemical group measured by pyrolysis GC/MS as reference. These proportions were obtained using MIR spectra in combination with partial least squares regression models.



Supplementary Fig. 3.8. Coefficients of the final partial least squares regression model, showing the contribution of each chemical group across the mid infrared spectra range.



Supplementary Fig. 3.9. Partial least square discriminate analysis (PLS-DA) model tuning and accuracy metrics. Left panel (A): Accuracy of the PLS-DA trained on the full depth dataset versus individual depth dataset of mid-infrared spectroscopy of peat samples in cross-validation, in relation to the number of latent variables of the model. Points represent the mean values, and bars indicate standard errors, with red points marking the optimal number of latent variables determined by a one-tailed paired T-test. Right panel (B): Smoothed receiver operating characteristic (ROC) curves and area under curve (AUC) showing the classification performance for restoration status based on each model. The smoothed ROC curves (lines), AUC annotations, and 95% confidence intervals (shaded areas) are shown for the cross-validation dataset results.



Supplementary Fig. 3.10 Performance and coefficients of partial least square regression (PLSR) model for mineral content. (A): Measured versus predicted mineral content for the cross-validation predictions (black regression line, and black dots) and for the calibration (grey regression line, and grey dots), n denotes the number of samples and n_latent the number of PLS latent variable. (B): Regression coefficients obtained for the PLS regression model based on mid-infrared spectroscopy for mineral content.

Supplementary Table 3.1. Permutational multivariate analysis of variance (PERMANOVA) of peat molecular composition across restoration status and depth, based on MIR spectra, including pairwise comparisons between groups.

	Drainage × Depth		
	R^2	F.model	*P* value
Drainage	0.047	3.079	0.005**
Depth	0.082	5.345	0.001***
Drainage: Depth	0.034	1.110	0.231
	Pairwise comparison (P value)		
	Undrained	Drained	
Drained	0.006*		
Rewetted	0.141	0.141	
	0-5 cm	15-20 cm	
15-20 cm	0.003**		
45-50 cm	0.008**	0.008**	
	Drainage effects along the depth		
	R^2	F.model	*P* value
0-5 cm	0.139	2.913	0.024*
15-20 cm	0.134	2.773	0.017*
45-50 cm	0.008	0.153	0.971
	Pairwise comparison (P value) for each depth		
0-5 cm	Undrained	Drained	
Drained	0.030*		
Rewetted	0.166	0.166	
15-20 cm			
Drained	0.018*		
Rewetted	0.214	0.214	
45-50 cm			
Drained	0.962		
Rewetted	0.962	0.962	

Signifiant codes : $P < 0.05$,* ; $P < 0.01$,** ; $P < 0.001$,***.

P value is adjusted by false discovery rate (FDR), the number of permutations with 999 iterations.

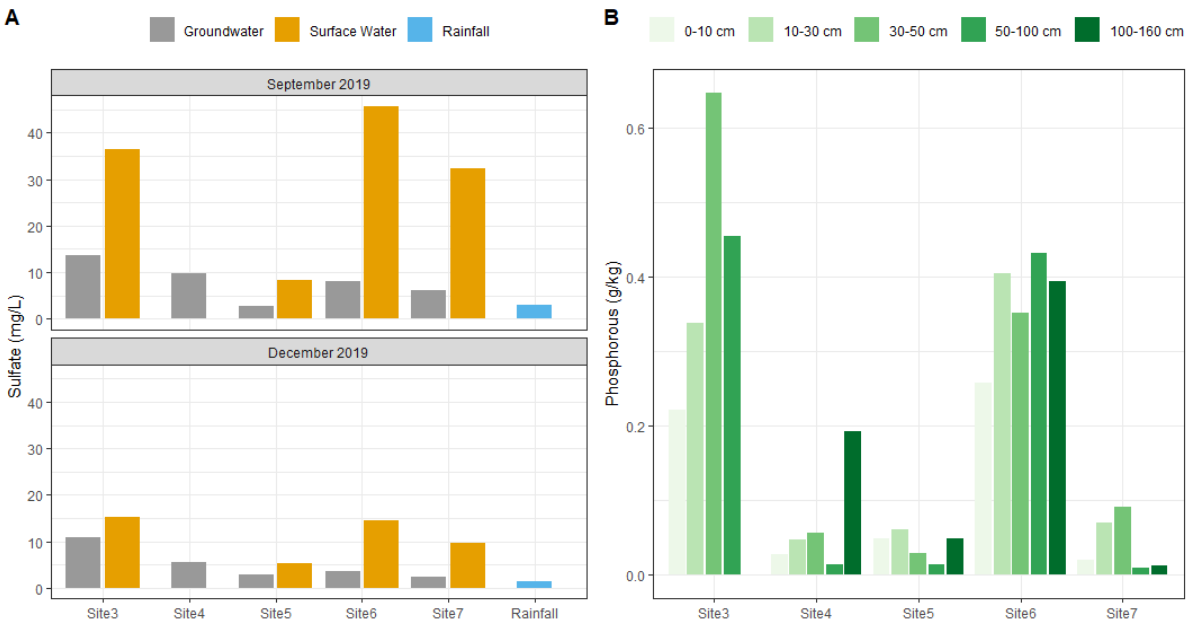
Supplementary Table 3.2. Confusion matrix of a group-wise cross validation from each depth model (Full depth, 0−5 cm, 15−20 cm, and 45−50 cm) from partial least squares discriminated analysis.

Confusion matrix				Class-wise metrics				
Full Depth								
	Reference							
Prediction	Undrained	Drained	Rewetted	Class	Precision	Recall	F1	Macro_F1δ
Undrained	25	6	12	Undrained	0.58	0.64	0.61	0.53
Drained	4	20	10	Drained	0.59	0.51	0.54	
Rewetted	10	13	17	Rewetted	0.42	0.44	0.43	
0−5 cm								
Prediction	Undrained	Drained	Rewetted	Class	Precision	Recall	F1	Macro_F1
Undrained	13	0	8	Undrained	0.62	1	0.77	0.53
Drained	0	13	5	Drained	0.72	1	0.84	
Rewetted	0	0	0	Rewetted	NaN±	0	NaN	
15−20 cm								
Prediction	Undrained	Drained	Rewetted	Class	Precision	Recall	F1	Macro_F1
Undrained	11	1	7	Undrained	0.58	0.85	0.69	0.47
Drained	2	12	6	Drained	0.60	0.92	0.72	
Rewetted	0	0	0	Rewetted	NaN	0	NaN	
45−50 cm								
Prediction	Undrained	Drained	Rewetted	Class	Precision	Recall	F1	Macro_F1
Undrained	8	3	2	Undrained	0.61	0.62	0.62	0.67
Drained	3	8	1	Drained	0.67	0.62	0.64	
Rewetted	2	2	10	Rewetted	0.71	0.77	0.74	

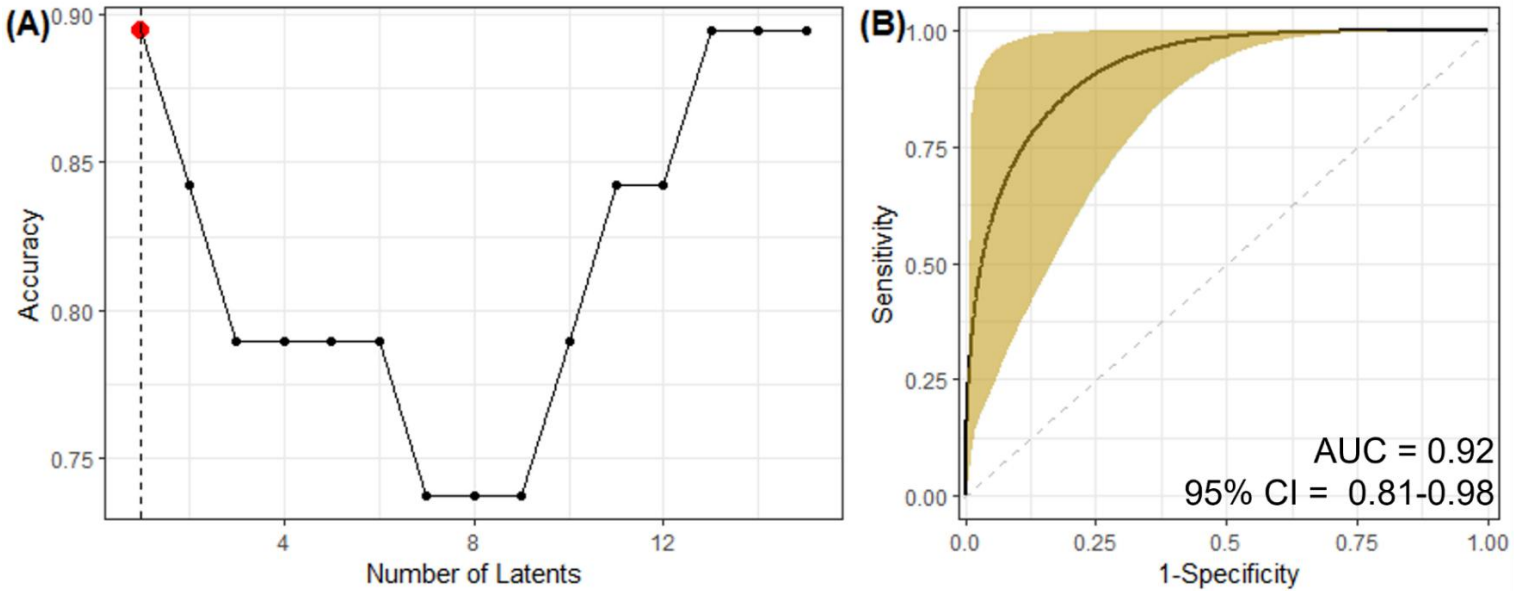
± Model fails to predict that class (False Positive + True Positive = 0).

δ When calculating Macro-F1, missing class penalizes the model by replacing NaN with 0.

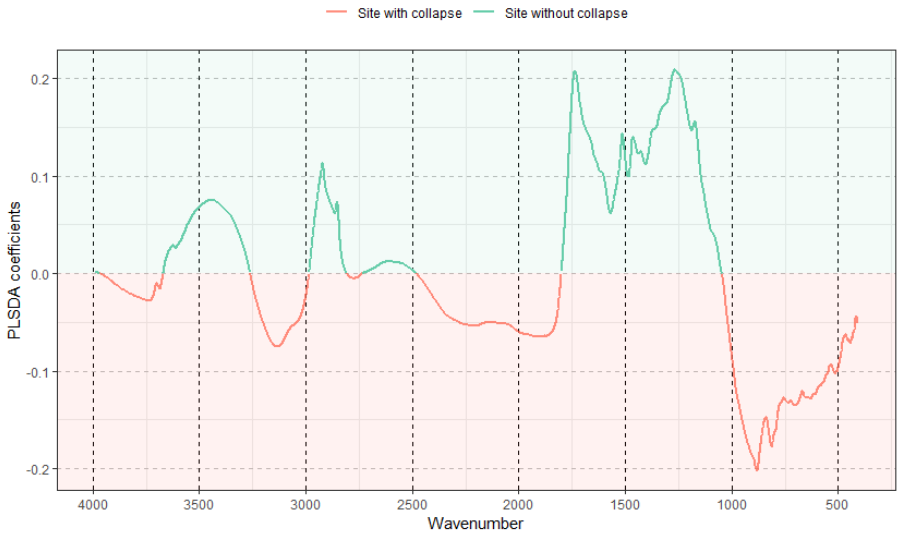
Appendix C



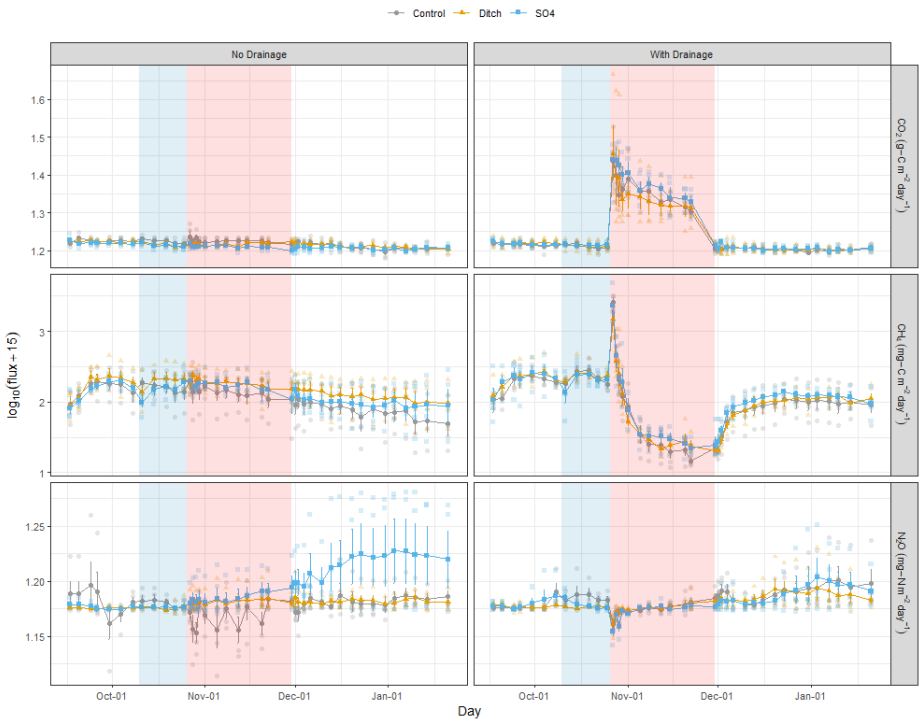
Supplementary Fig. 4.1. Sulfate concentration in water samples (A) and phosphorous concentration in peat samples (B) from non-collapsed sites sampled in 2019, as reported in Moris (2020). Sites 3,6, and 7 −located near peat collapsed area – exhibited high sulfate levels in surface water, which may have been linked to increased soil phosphorus concentrations via redox-mediated mobilization along the redox chain.



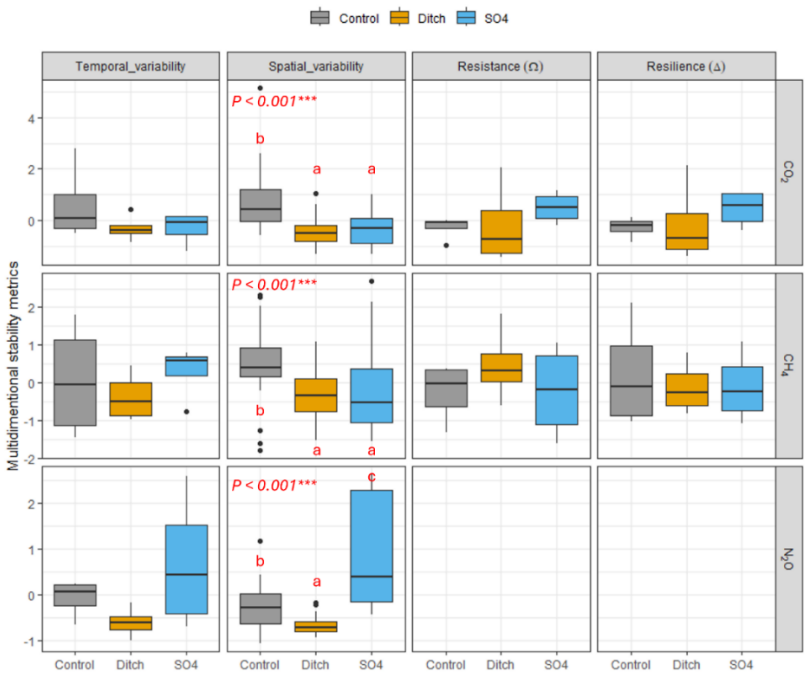
Supplementary Fig. 4.2. Optimal latent variable selection in partial least squares discriminate analyses (PLS-DA) and model performance as receiver operating characteristic (ROC) curve. The area under the curve (AUC) indicates the classification performance with 95 % Confidence Intervals (CI) representing the uncertainty around the AUC estimates.



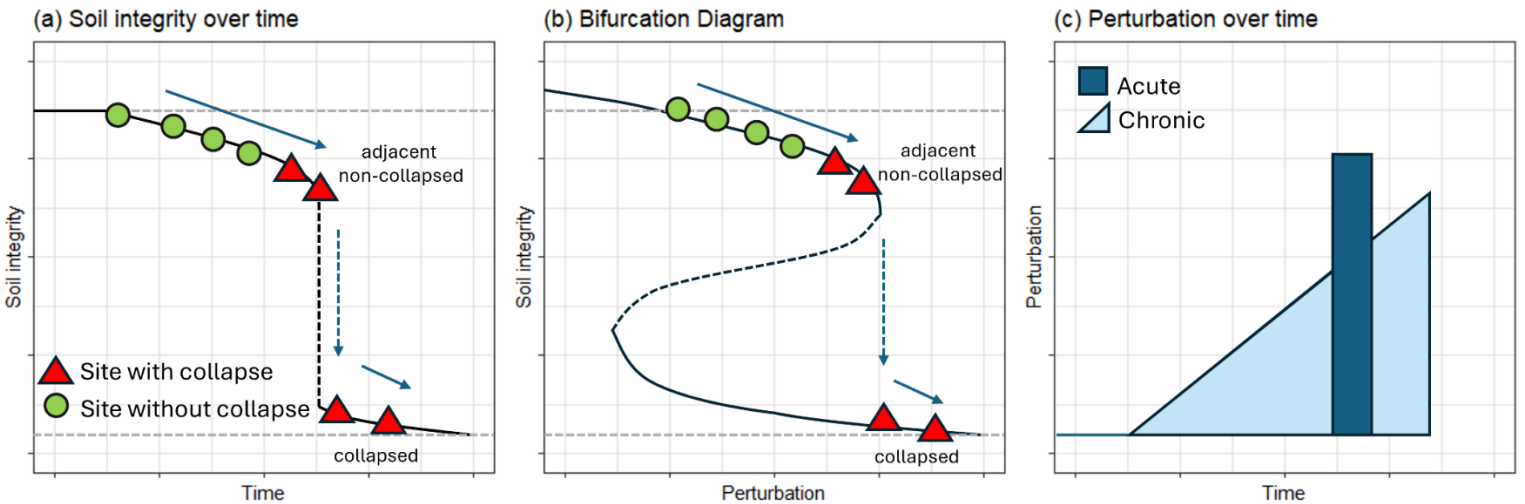
Supplementary Fig. 4.3. Coefficients from partial least squared discriminate analysis (PLS-DA) for classifying site with collapse (collapsed + non-collapsed adjacent plots) verse site without collapse (non-collapsed distant plots) based on soil organic matter (SOM) molecular compositions from mid infrared spectra. Peaks represent molecular vibration and bending, allowing inference of the relative abundance of functional group in SOM molecular composition. Intact peat is likely associated with peaks with positive coefficients, whereas degraded peat is likely associated with peaks with negative coefficients.



Supplementary Fig. 4.4. Responses of daily CO_2, CH_4, and N_2O fluxes to a consecutive deep water table drawdown (n=4). Responses in CO_2, CH_4, and N_2O fluxes are shown for the three treatments: control (i.e., demineralized water), ditch water, and SO_4^{2-} addition. The blue panel indicates a period of post-treatment, and red panel indicate a period of deep-water table drawdown. Solid dots indicate means and faint dots suggests data point, and error bars show standard error of the means.



Supplementary Fig. 4.5. Multidimensional stability metrics of greenhouse gas fluxes (CO_2, CH_4, and N_2O) across solution addition treatments (control, ditch, and SO_4^{2-} addition). Temporal and spatial variability were calculated for unperturbed (continuously waterlogged) mesocosm cores, while resistance and resilience were derived from log response ratio (Fig. 5) based on flux responses to hydrological perturbation over time.



Supplementary Fig. 4.6. Conceptual representation of pedogenic regime shift in temperate fen peatlands in response to acute hydrological and chronic geochemical stressors. This composite diagram illustrates the rationale behind the experimental design, which considers three peat conditions: collapsed, adjacent non-collapsed, distant non-collapsed status.

Supplementary Table 4.1. Permutational multivariate analysis of variance (PERMANOVA) on different ecological datasets (mesofauna, vegetation community composition, physiochemistry, and soil organic matter molecular composition) across collapsed, non-collapsed adjacent, non-collapsed distant plots.

Mesofauna			
	R^2	F.model	P value
Model	0.37	10.233	<0.001***
Pairwise comparison (P value)			
	collapsed	non-collapsed (adjacent)	
non-collapsed (adjacent)	<0.001***		
non-collapsed (distant)	<0.001***	0.191	
Vegetation community composition			
	R^2	F.model	P value
Model	0.23	2.878	0.022*
Physiochemistry			
	R^2	F.model	P value
Model	0.23	2.344	0.008**
Pairwise comparison (P value)			
	collapsed	non-collapsed (adjacent)	
non-collapsed (adjacent)	0.343		
non-collapsed (distant)	0.007 **	0.046*	
Soil organic matter			
	R^2	F.model	P value
Model	0.30	3.576	0.005**
Pairwise comparison (P value)			
	collapsed	non-collapsed (adjacent)	
non-collapsed (adjacent)	0.8		
non-collapsed (distant)	0.006**	0.009**	

Significance levels : P <0.05,* ; P<0.01,** ; *P* <0.001,***.

P value is adjusted by false discovery rate (FDR), the number of permutations with 999 iterations.

Supplementary Table 4.2. Least squares means of electrical conductivity (EC), pH and alkalinity under different solution addition treatments and drainage condition during four consecutive experimental phases.

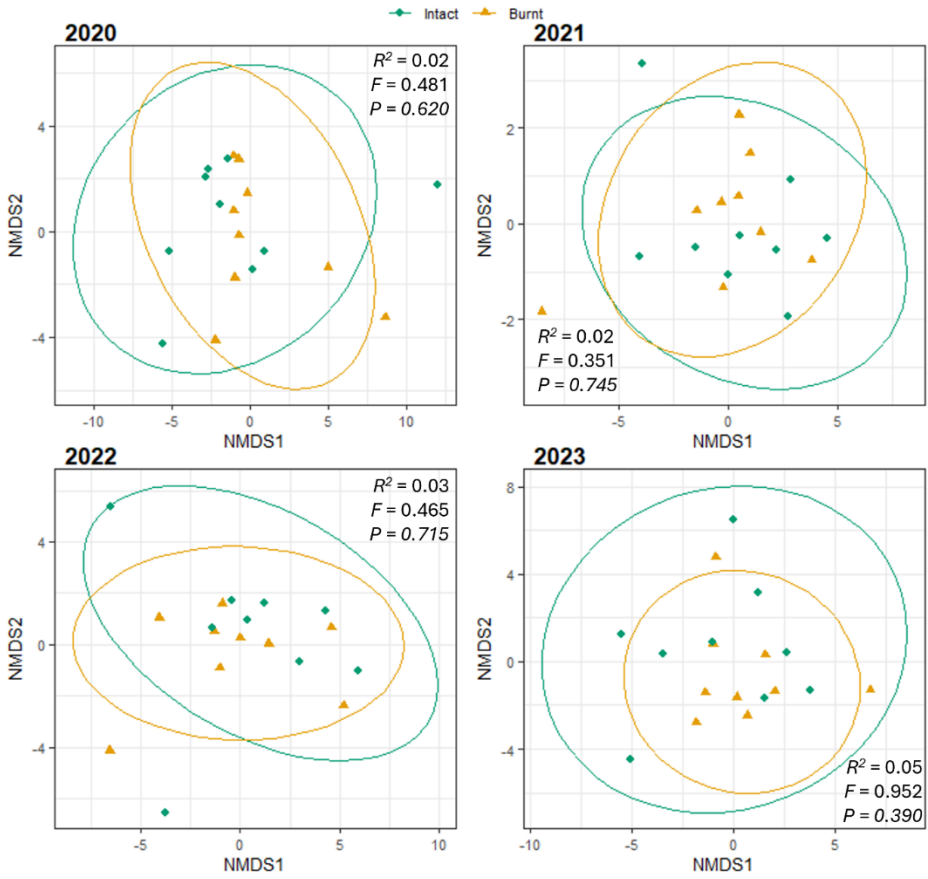
	Baseline	Treatment-loading	Drawdown	Re-saturation
		EC (µS/cm)		
Control	654	561	361	467
Ditch	501	454	333	522
SO_4	569	485	345	554
No_Drainage	542	464	458b	544
Drainage	601	535	235a	485
Treatment	0.1188	0.2078	0.8067	0.0909
Drainage	0.3085	0.1513	<0.0001***	0.0676
Treatment: Drainage	0.7161	0.6682	0.8756	0.9520
		Alkalinity (meq/L)		
Control	3.24	4.20b	1.95	2.51a
Ditch	2.71	2.45a	1.35	2.81a
SO_4	2.99	2.76ab	1.44	3.42b
No_Drainage	2.92	3.47	2.76	3.08
Drainage	3.05	2.81	0.40	2.75
Treatment	0.6593	<0.05*	0.1356	<0.01**
Drainage	0.7933	0.2371	<0.0001***	0.0632
Treatment: Drainage	0.5547	0.6044	0.9990	0.6856
		pH		
Control	6.34	6.45	6.21a	6.59a
Ditch	6.30	6.60	6.08a	6.63a
SO_4	6.38	6.54	7.06b	6.92b
No_Drainage	6.29	6.48	6.87b	6.70
Drainage	6.39	6.59	6.03a	6.73
Treatment	0.3761	0.2073	<0.01**	<0.0001***
Drainage	0.0501	0.1087	<0.01**	0.5256
Treatment: Drainage	0.1862	0.3868	0.8777	0.0502
		NH_4^+(µmol/L)		
Control	-	-	198.7	268
Ditch	-	-	98.4	197
SO_4	-	-	77.2	244
No_Drainage	-	-	161.0.	237
Drainage	-	-	88.5	236
Treatment	-	-	0.1225	0.5030
Drainage	-	-	0.1533	0.9813
Treatment: Drainage	-	-	0.8809	0.6056
		NO_3^+(µmol/L)		
Control	-	-	12.12b	2.25
Ditch	-	-	4.14a	8.25
SO_4	-	-	4.02a	5.39
No_Drainage	-	-	7.99	3.25
Drainage	-	-	5.52	6.74
Treatment	-	-	<0.01**	0.2624
Drainage	-	-	0.1109	0.2618

Treatment: Drainage	-	-	0.3560	<0.05*
		Total P (mg/ L)		
Control	-	-	0.414	1.40
Ditch	-	-	0.218	1.31
SO_4	-	-	0.303	1.92
No_Drainage	-	-	1.280b	1.60
Drainage	-	-	0.056a	1.49
Treatment	-	-	0.4148	0.0718
Drainage	-	-	<0.0001***	0.6180
Treatment: Drainage	-	-	0.3028	<0.05*

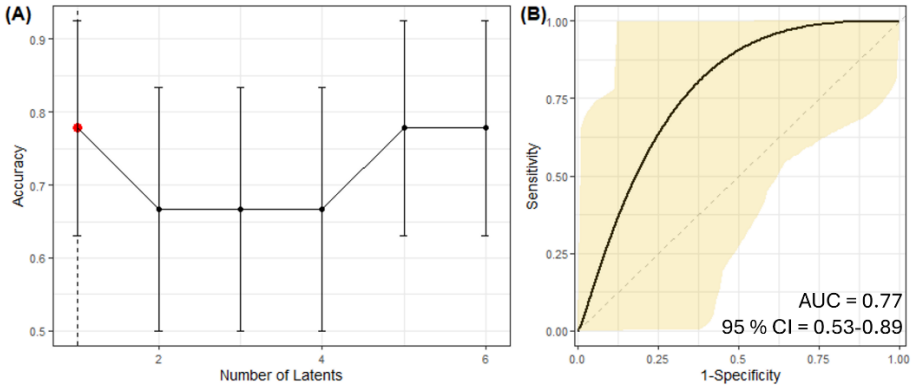
*, **, and *** indicates statistical significance at $P < 0.05$, $P < 0.01$, $P < 0.001$.

Different lowercase letters indicate significant differences between treatments based upon post hoc analysis after two-way ANOVA ($\alpha = 0.05$).

Appendix D



Supplementary Fig. 5.1. Non-metric multidimensional scaling (NMDS) of mid-infrared spectra from intact and burnt plots over four consecutive years following the fire. Permutational multivariate analysis of variance (PERMANOVA) with its respective R2, F, and P values provided in the figures. Dissimilarity is measured as Euclidean distance for mid infrared spectra. Each point represents an independent peat sample, connected to the centroid of its respective same group. None of the yearly comparison between intact and burnt plots revealed statistically significant differences (Ps > 0.05).



Supplementary Fig. 5.2. Partial least square discriminate analysis (PLS-DA) model tuning and accuracy metrics. Left panel (A): Accuracy of the PLS-DA trained on mid-infrared spectra of peat samples in cross-validation, in relation to the number of latent variables of the model. Points represent the mean values, and bars indicate standard errors, with red points marking the optimal number of latent variables determined by a one-tailed paired T-test. Right panel (B): Smoothed receiver operating characteristic (ROC) curves and area under curve (AUC) showing the classification performance between intact and burnt plot. The smoothed ROC curves (lines), AUC annotations, and 95% confidence intervals (shaded areas) are shown for the cross-validation dataset results.

Statement on the use of Generative AI

I did not use generative AI assistance tools such as ChatGPT and Copilot for research and writing of this thesis. These tools were used solely for language assistance and the generation of icons images and thesis cover. The text, code, other images in this thesis are my own (unless otherwise specified) and generative AI has only been used in accordance with the KU Leuven guidelines and appropriate references have been added. I have reviewed and edited the content as needed and I take full responsibility for the content of the thesis.

List of publications

Peer-revied articles in international journals

Kim, K., Aernouts, B., Emsens, W.-J., Schellekens, J., Van Diggelen, R., Aggenbach, C., Verbruggen, E., Jansen, B., Briones, M.J.I., Vancampenhout, K., 2026a. Mid-infrared spectroscopy as a tool to monitor molecular changes in fens upon restoration. Organic Geochemistry 214, 105154. https://doi.org/10.1016/j.orggeochem.2026.105154

Kim, K., Schellekens, J., Emsens, W.-J., van Diggelen, R., Aggenbach, C., Verbruggen, E., Liczner, Y., Klimkowska, A., Tanneberger, F., Kotowski, W., Iglesias Briones, M.J., Jansen, B., Vancampenhout, K., 2026b. Limited recovery of soil organic matter composition in fen peatlands after rewetting. Geoderma 465, 117646. https://doi.org/10.1016/j.geoderma.2025.117646